Improved flood modelling for the built environment and infrastructure - Achieving urban flood resilience through hydrodynamic models

Christos Iliadis

A Thesis submitted to Newcastle University in partial fulfilment of the requirements for the degree of Doctor of Philosophy (PhD) in the School of Engineering – Faculty of Science, Agriculture and Engineering

September 2023

Abstract

This thesis explores and develops methods for the simulation and analysis of flood risk for urban environments, using an advanced hydrodynamic model (CityCAT). Focused on bolstering urban flood resilience, the research is aimed at the need for better representation of urban features and blue green adaptations within hydrodynamic models. A number of aspects of urban flood modelling, exposure analysis and adaptation are addressed using novel methods and detailed applications to city case-studies in Newcastle-upon-Tyne, Greater London (both UK) and Thessaloniki (Greece). Accurately representing buildings is addressed by critically comparing the *'Building Hole'* method with the prevalent *'Stubby Building'* approach, demonstrating superior performance using a detailed flood validation dataset. Efficient flood risk management in urban areas necessitates interventions that modify surface flow pathways and introduce storage, so a novel cost-benefit *'source-receptor'* framework is developed to identify flood sources, vulnerable receptors, and optimal locations for implementing Blue-Green Infrastructure (BGI). The framework integrates economic considerations, surpassing conventional hydraulic analyses. High-resolution flood risk and property-level exposure modelling for whole megacities has previously not been achievable, so here a case study of London is carried out, showcasing cloud-based flood modelling as a transformative tool for insurance and flood resilience strategies worldwide. In addition to extending the scale and accuracy of flood risk and exposure modelling practice, a number of conclusions are drawn and advice presented on practical aspects, such as : assessment of the superiority of the *"Building Hole"* method, alongside advice on improving the alternative *"Stubby Building"* method; firm guidelines for minimum DEM resolution and building representation in the model domain, considering both cases where high quality datasets are available and absent; an improved benefit-cost method for optimising placement of blue-green infrastructure, alongside proposals for further development through automation.

Acknowledgements

I would like to express my deepest gratitude to my supervisors Vassilis Glenis & Chris Kilsby, for their excellent support, invaluable guidance, and continuous encouragement throughout this journey. Their expertise, patience, and insightful feedback have been instrumental in shaping this research project. The time we have spent working together was amazing and I would like to thank you for the exciting opportunities you have offered me.

Special thanks to Dr. Panagiota Galiatsatou for her guidance and support for Chapter 6 of this thesis.

I also have to express my gratitude to EPSRC for funding this project, and especially thanks to Peter Jarvis and Luca Alibardi from Cranfield University.

I extend my heartfelt appreciation to Justine Easten for all her help and support during the last four years.

My gratitude to Sven and Asid for their invaluable contributions during moments of intellectual challenge. Their insightful brainstorming sessions were instrumental in overcoming difficulties and moving this research forward.

Moreover, I would like to thank Willis Research Network for their encouragement in modelling flood risk in London and special thanks goes to Ferg Kilsby for his assistance with identifying the locations of the social media flood reports.

Special thanks are due to my family for their love and encouragement throughout this journey. Their belief in me has been a constant source of motivation.

Lastly, I want to express my deepest thanks to my late grandparents, who raised me and played a monumental role in shaping the person I am today. This thesis is dedicated to you. I hope to carry on your legacy in a way that would make you proud.

Contents

List of Figures

List of Tables

List of Abbreviations

1D	one-dimensional
1D/2D	1D simulation of sub-surface domain and 2D simulation of surface domain
2D	two-dimensional
AOI	Area of Interest
AUTh	Aristotle University of Thessaloniki
BB	The *'Building block'* method
BH	The *'Building Hole'* method
CityCAT	City Catchment Analysis Tool
CPU	Central processing unit
DDC	Depth-Damage-Curve
DDF	Depth-Duration-Frequency
DEM	Digital Elevation Model
DSM	Digital Surface Model
DTM	Digital Terrain Model
FD	Flood Damages
FE	Flood Exposure
GB	Gigabyte
GEV	Generalised Extreme Value
GPD	Generalised Pareto distribution
IDF	Intensity-Duration-Frequency
LiDAR	Light Detection and Ranging
POT	Peaks-Over-Threshold
QGIS	Quantum GIS
RAM	Random-access memory
rc	Rainfall cell
RP	Return period
SB	Stubby building
SB100	The *'Stubby Building'* method with 100 cm threshold
SB20	The *'Stubby Building'* method with 20 cm threshold
SB30	The *'Stubby Building'* method with 30 cm threshold
SB30 FR	The *'cleaned Stubby'* method with flat roofs and 30 cm threshold
SB40	The *'Stubby Building'* method with 40 cm threshold
SB60	The *'Stubby Building'* method with 60 cm threshold
SB80	The *'Stubby Building'* method with 80 cm threshold
SWE	Shallow Water Equation
TB	Terabyte
UK	United Kingdom

Chapter 1. Introduction

1.1 Background

Floods are a physical phenomenon characterised by the temporal covering of land by water, which is followed by negative consequences for humans (Galiatsatou, 2009). The extent and severity of the damage caused by urban floods is a product of both the intensity and duration of the rainfall (variable in space and time) and its interaction with the complex flowpaths of a city, on the surface and below ground. Nowadays, the impact of pluvial flooding is a major problem due to frequent natural disasters in the urban fabric (Teng et al., 2017). Detailed hydrodynamic modelling can be used to test a range of mitigation strategies to reduce urban flooding (Kilsby et al., 2020). There is, therefore, a great need to improve flood modelling and analysis tools to understand the impacts of floods and water flowpaths in an urban area. Computational hydraulics is one field of science for which computers opened a new way of working to researchers and engineers to determine what is happening in reality and to predict what may happen in the future (Popescu, 2014). Flood inundation models are valuable resources that enable researchers to model the hydrodynamics of past flood events and anticipate future occurrences that may cause damage in urban areas (Willis et al., 2019). Given the global climate change and the uncertainties it brings, studies in this field are of utmost importance. Enhancing hydraulic models is crucial to accurately predict the direction and magnitude of flooding. Buildings act as barriers to water flow, influencing its path, and therefore, they should be considered in hydraulic models (Rak et al., 2018). Numerous studies have utilised 2D hydraulic models to address complex urban challenges, encompassing numerical solutions of the 2D shallow water equations (Leandro et al., 2009; Mignot et al., 2006) and the analysis of surface water movement around buildings and underground urban drainage systems.

In recent years, the UK has experienced multiple severe flood events causing significant damage to people, infrastructure, and the economy. The increase in urbanisation has heightened the risk of urban flooding, making it a pressing issue. Pluvial floods, which are triggered by intense but short-duration rainfall events, are a major cause of flooding in urban areas (Bruwier et al., 2020). With the effects of climate change, the exposure to floods in urban areas is expected to rise, putting more lives at risk. Flood risk management has shifted towards resilience thinking, emphasizing the importance of designing cities that can absorb water and provide protection against floods (Potter & Vilcan, 2020). Hydraulic models are crucial in simulating urban flooding, considering the complex topography with buildings, drainage networks, and critical infrastructure (K. Guo et al., 2021). Accurate and high-resolution data such as Digital Elevation Models (DEM), Digital Surface Models (DSM), and Digital Terrain Models (DTM) play a significant role in defining flood pathways within cities (McClean et al., 2020). Hydrodynamic models are rapidly evolving with the introduction of new simulation methods and increased computational power. The growing demand for detailed and reliable estimates of surface water flood risk, as well as inundated risk protection for assets, infrastructure, and urban constructions, drives the development of hydraulic models with more realistic results (Kilsby et al., 2020). However, there are challenges in accurately representing urban features and incorporating effective blue-green interventions into these models. Currently, there is a lack of detailed and innovative techniques hindering the improvement of pluvial flood modelling, making it a priority area of focus.

1.2 Aim and Objectives

This thesis centres around urban flood modelling, with a specific emphasis on investigating and better defining the water flowpaths within urban areas, contributing to a better understanding of flood dynamics and aiding in the development of effective flood mitigation strategies.

1.2.1 Aim

The thesis aims to enhance the representation of urban features within hydrodynamic models and utilise novel methodologies to achieve flood resilience in urban areas and catchments. The thesis will focus on applying these methods to real storm events in cities and analysing the urban features that are exposed to flood risk. By improving the representation of buildings and assessing their vulnerability to flooding, the research aims to contribute to the development of more accurate and effective flood management strategies in urban environments.

1.2.2 Objectives

The following objectives were primarily identified during the work of the thesis, but they will be discussed in detail at the end of the literature review in Chapter 2:

1. Review the current methods for representing urban features in hydrodynamic models;
2. Assess how simulated flowpaths and flood depths in cities are affected by building representation and develop advice for best practice in modelling;
3. Develop a new methodology to locate areas and buildings at high risk of flooding and then provide solutions to reduce damages from flooding by adding Blue-Green infrastructure in critical locations;
4. Demonstrate improved model representations in practical applications covering hazard (inundated areas and depths) and exposure (number and type of buildings and assets);
5. Explore the significance of the Digital Elevation Model resolution in urban flood modelling;
6. Application of the CityCAT model to a range of different cases for pluvial flooding (e.g. Newcastle, London etc);

1.3 Research contribution

The project was funded by the EPSRC Centre for Doctoral Training in Water Infrastructure and Resilience (CDT-WIRe) as its aims align very closely with those of the CDT, with potential applications for CDT partners in industry, local authorities and the insurance sector. Data for various applications and the modelling software, in CityCAT, were primarily provided by Newcastle University, in some cases building on previous research. Outputs of this thesis were presented at various national and international conferences and have been published or are in review in international journals:

- Chapter 3 - Flood Risk Management Journal (published on the 19/09/2023, Iliadis et al. (2023b))
- Chapter 4 – Journal of Hydrology (in review)
- Chapter 5 – Water (received reviewers' comments and - corrections under way)
- Chapter 6 – Hydrology (published on the 17/08/2023, Iliadis, Galiatsatou, et al. (2023))

1.4 Thesis structure

This thesis comprises seven chapters. The schematic workflow can be seen in Figure 1.1. To make the thesis more readable, chapters three to six have their own introduction, methodologies and conclusions.

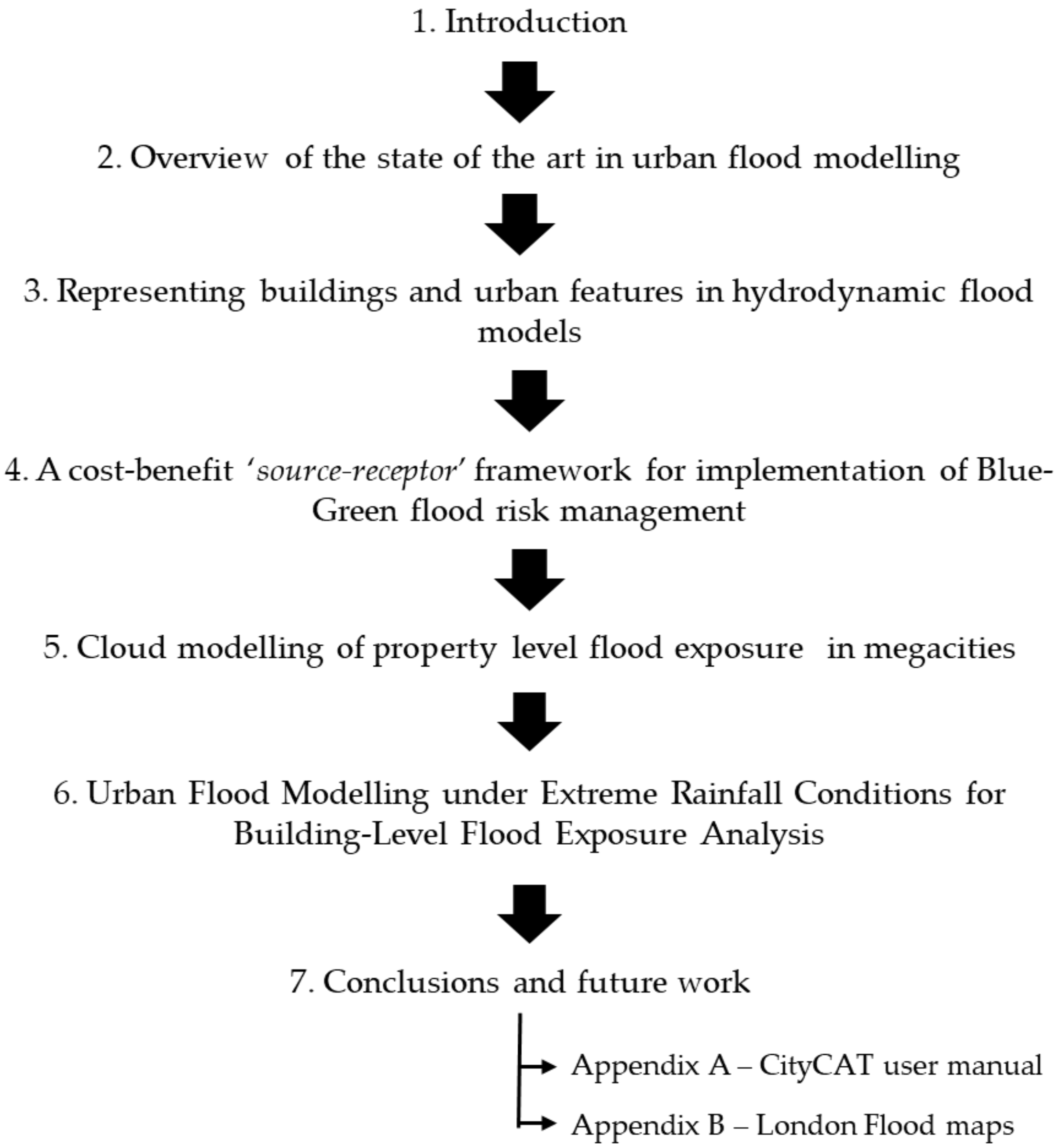

Figure 1.1 Schematic workflow of the thesis.

Chapter 2. Overview of the state of the art in urban flood modelling

2.1 Modelling the Urban System

Flooding is a significant natural hazard that poses substantial threats to urban areas worldwide. As urbanisation continues to increase and climate change intensifies, the vulnerability of cities to flooding has become a pressing concern (Suriya & Mudgal, 2012). Integrated flood risk assessment methodologies, nature-based solutions, community engagement, and adaptive strategies are pivotal in building urban resilience against flooding. While significant progress has been made in understanding and addressing this issue, ongoing research is essential to adapt to evolving circumstances and ensure the sustainability and safety of urban systems in the face of increasing flood risks. Flood modelling within the context of urban systems plays a pivotal role in understanding the impact of floods on cities and their inhabitants (Rosenzweig et al., 2018). Hydrodynamic models are able to combine topographic data, urban features and hydrological data, to simulate overland flow in urban settings. These models are often used to simulate flood wave propagation, inundation extents, and potential damages to buildings, roads, and critical infrastructure. Moreover, by incorporating climate change projections and historical flood data, hydrodynamic models can help city planners devise effective strategies for flood risk mitigation, early warning systems, and emergency response. The accuracy of flood modelling in urban systems is paramount for fostering disaster preparedness and minimize the economic and social repercussions of flooding events. In this chapter, a range of approaches for modelling urban flooding (starting with 1D modelling and moving on to 2D modelling) are presented and evaluated.

2.1.1 Drainage models

Urban stormwater management relies heavily on an effective drainage network. When the network capacity is inadequate to handle the volume of stormwater runoff, urban surfaces are susceptible to flooding. To combat analyse this challenge, drainage network models are frequently employed, particularly when detailed data for the pipe network is available (Lee & An, 2019). Typically, flow within enclosed channels or pipes is analysed in a one-dimensional manner. These 1D models enable the simulation of stormwater dynamics within urban settings, aiding in the assessment of potential flood risks and the development of strategies to mitigate them. The primary objective of the 1D models is to replicate the movement of water within the sub-surface drainage network, producing flow hydrographs at the discharge points of urban catchments or sub-catchments. Most of the drainage network models are based on the 1D Saint-Venant equations for shallow free surface flow (K. Guo et al., 2021). However, within urban drainage systems, the flow inside the pipes is able to undergo a dynamic transition between open-channel flow and pressurised flow, depending on variations in discharge. Open-channel flow manifests when a free surface exists, permitting pressure approximation through hydrostatic variables. In contrast, pressurised flow lacks a free surface and diverges from the hydrostatic pressure variables. Open-channel drainage flow is simulated using the open-channel flow 1D St. Venant equations, whereas pressurised flow demands a distinct modelling approach (Néelz & Pender, 2013) which introduces significant computational expense, known as the Preissman slot (Preissmann & Cunge, 1961) to retaining a free surface. Unfortunately, this method introduces inaccuracies and numerical instabilities during trans-critical flow, see for example Malekpour and Karney (2016); Meselhe and Holly (1997). To assess overall surface flooding in urban areas, it is common practice to integrate drainage network models with hydrological or hydraulic models. Widely used commercial models like the Urban Drainage and Sewer Model (MOUSE), EPA SWMM, InfoWorks ICM, HEC-RASS, as well as various research models (Djordjević et al., 1999; Maksimović et al., 2009; Schmitt et al., 2004; Simões et al., 2010), are often employed or customised to simulate urban rainfall-runoff dynamics and flooding events within drainage networks and for flood mapping. These 1D models may not fully capture the intricacies of urban inundation processes due to the limitations of the extracted information from the surface elevation in cities, and the sewer network. Moreover, the main issue with 1D models is that complex flow dynamics are not captured and this leads to inaccuracies as lateral flow is neglected. Acknowledging the critical role of surface connectivity and the resolution of both Digital Terrain Models (DTMs) and buildings is paramount. In pursuit of a physically based representation, these 1D models involve preprocessing the surface DTM data to delineate 1D surface flow pathways. These pathways are subsequently integrated into a 1D-1D dual drainage model (Chen et al., 2016; Djordjević et al., 2005; Simões et al., 2010). However, this process, while retaining a physical basis for representing the flow on the major pathways, loses accuracy across the whole domain through not retaining the full DEM information, which may be critical for flood exposure to individual buildings. The approach also makes it difficult to introduce blue green infrastructure features into the model to test flood risk management designs. Leitão et al. (2017) highlighted the critical role of inlet capacity in shaping the effectiveness of storm sewer systems. Understanding the interplay between the hydraulic components is paramount, and this is where the 1D-2D surface pathway method, as introduced by Maksimović et al. (2009), comes into play. It is now routine to integrate 2D surface pathway models with 1D modelling capabilities, e.g. the Infoworks sewer model, at least for relatively small urban areas. While such modelling strategies can provide useful understanding of the overall dynamics of stormwater systems, it should be noted that the limitations of the Preissman slot approach (Preissmann & Cunge, 1961) pose serious issues when modelling surcharged pipes in drainage networks. What Leitão et al. (2017) findings reaffirm, and which is further validated by the research conducted by Bertsch et al. (2017), is that regardless of the modelling nuances and the capacity of the pipe network itself, the significance of inlet drains remains consistently central. Their efficiency directly impacts how well the drainage system can handle and manage heavy rainfall events. These inlets act as the first line of defence against flooding, making their proper functioning essential in urban environments during intense storm events.

In the context of modelling sewer systems, whether as standalone entities or in conjunction with surface data, it is essential to have accurate data for the pipe network. However, in situations where data regarding the drainage system is unavailable, flood modellers are faced with various approaches. These include making assumptions, such as removing a specific percentage of rainfall from the modelling domain (Iliadis, Galiatsatou, et al., 2023) or generating synthetic storm inlets (Bertsch et al., 2017). In some countries, like the UK, guidelines may suggest subtracting 6mm to 15mm from the model to represent the drainage system (Guiding principles for drainage and wastewater management plans - GOV.UK (www.gov.uk)). A recent development in the UK presented in a recent study of the city of Leeds by Singh et al. (2023) uses spatially variable drainage capacity datasets estimated from water company pipe network data. This approach makes the assumption that this network capacity is all available and requires extra assumptions to include limitations due to the inlet capacity.

2.1.2 Surface models

Surface (or 2D) hydrodynamic models utilising a DEM over the whole domain, rather than identifying 1-D flow paths, represent a significant advance in our ability to understand and manage flood risks. This added detail, especially if coupled with sub-surface models, allows for a more accurate and realistic depiction of flood water dynamics in complex urban landscapes. These models are crucial for assessing flood extents, depths, velocities, and the upcoming climate change, by helping authorities make informed decisions about flood risk mitigation and improving resilience in the urban environment.

The evolution of urban flood modelling that solve the full 2D Shallow-Water equations has ushered in a new era of precision and insight into the complex dynamics of flooding within urban areas. These models are transformative in their approach. One of the cornerstones of these advanced urban flood models is the use of high-resolution data, such as DTMs and urban fabric data. DTMs, which capture terrain elevation at a fine scale, are instrumental in simulating how floodwaters flow across the urban landscape. This high level of detail allows the models to consider even subtle variations in ground elevation, ensuring a more precise depiction of flood extents and depths. In tandem, urban fabric data, which includes information on buildings, roads, and other infrastructure, helps in replicating the intricate layout of urban areas. By factoring in the presence of structures, these hydrodynamic models can assess how flood waters interact with and are influenced by the built environment, improving the accuracy of flood predictions (K. Guo et al., 2021; Teng et al., 2017). The practical applications of these advanced flood models are diverse and far-reaching. Nowadays, urban planners and engineers use them to design resilient stormwater management systems, optimising drainage systems and flood defences to protect urban communities from inundation. Many research hydrodynamic models are applied in different fluvial and urban areas studies (Bates et al., 2010; Ghimire et al., 2013; Glenis et al., 2018; Guidolin et al., 2016; Xia et al., 2019) to understand the flood dynamics and to plan adaptation solutions with the collaboration of local authorities and the industry. Nonetheless, conducting modelling with such intricate detail, often down to the street or meter scale, inevitably leads to a substantial increase in the number of computational grids required. This heightened level of granularity necessitates the implementation of parallel algorithms and acceleration methods to effectively manage and mitigate the associated computational overhead. GPU-based parallel algorithms have proven to be a game-changer, delivering substantial speed enhancements in flood simulations. Meanwhile, when it comes to flood modelling, GPUs can encounter several challenges. Firstly, while GPUs excel at parallel processing, some hydrodynamic models may not be inherently parallelisable, limiting the potential speedup that GPU can offer. Note here that not all hydrodynamic models are optimised for GPU utilisation, which can lead to inefficiencies and underutilisation of the hardware. Another notable challenge with GPU is that due to limited overall memory, the expansive domains must be divided for effective flood modelling.

Research has documented remarkable improvements, with some studies reporting simulations speeds over ten times faster than traditional methods. This progress has been particularly evident in the application of GPU acceleration to tackle diverse scenarios, from catchment-scale flooding to urban flood modelling, even in instances involving grids numbering well beyond 100 million (as demonstrated by Smith and Liang (2013); Vacondio et al. (2014)). Meanwhile, in cases where urban flood models are employed, the computational demands are met through the utilization of GPU or cloud computing resources, as exemplified by Glenis et al. (2013) and Hou et al. (2018). These advancements in computational techniques not only empower researchers and practitioners to conduct more intricate flood simulations but also significantly enhance our preparedness and responsiveness in managing flood risks in urban environments.

Commercial and other research flood models have been used in recent studies (Apel et al., 2009; Bisht et al., 2016; Fewtrell et al., 2011a; Hunter et al., 2008a; Syme, 2008; Thrysøe et al., 2021; Zhao et al., 2021). Some of the most commonly used models are:

- HEC-RAS 2D: developed by the U.S. Army Corps of Engineers, the Hydrologic Engineering Centre’s River Analysis System (HEC-RAS) includes a 2D modeling component. It's widely used for river and floodplain modeling and is particularly valuable for analysing complex hydraulic conditions (HEC-RAS (army.mil));
- FLO-2D is a comprehensive flood modeling software used for simulating rainfall-runoff and open-channel hydraulics. It's employed in a variety of applications, including urban flood analysis and dam breach modeling (Homepage - FLO-2D Software);
- TUFLOW is a hydrodynamic simulation software used for 2D flood modeling. It's known for its ability to handle complex topographies and is commonly used for flood risk assessments and urban drainage planning (TUFLOW, 2018);
- MIKE Flood which is part of the MIKE software suite by DHI, MIKE Flood provides a range of tools for 2D flood modeling, enabling users to simulate

flood scenarios, assess flood risks, and design flood mitigation measures (MIKE FLOOD (mikepoweredbydhi.com));

- InfoWorks ICM is used for integrated urban drainage and flood modeling. It combines 1D and 2D modeling to simulate the entire urban water cycle, making it valuable for urban flood management;
- Flood Modeller Pro is a 1D and 2D flood modelling software that's used globally for flood risk assessments, river modelling, and urban flood management (Flood Modeller | Industry leading flood modelling software);
- LISFLOOD-FP is a distributed hydrological model designed for floodplain inundation modeling. It has been influential in simulating flood events and understanding the interactions between river flow and floodplain dynamics. The model has seen developments and improvements in recent years (LISFLOOD-FP | School of Geographical Sciences | University of Bristol);
- The TELEMAC system, developed by EDF (Electricité de France), is a suite of numerical models for hydrodynamic and sediment transport simulations in rivers, estuaries, and coastal zones. It has been essential in studying complex water flow phenomena and flood dynamics (Galland et al., 1991);
- The Caddies Framework, originating by the University of Exeter, has been engineered to expedite large-scale flood modelling by harnessing the advanced processing capabilities of contemporary hardware equipped with parallel computing capabilities (Caddies framework | Centre for Water Systems | University of Exeter);

In many instances, these models encounter challenges in accurately capturing shocks and flood wave propagation. Furthermore, when striving for high-speed simulations over expansive geographical areas, concerns about the precision and reliability of the results frequently arise (Bentivoglio et al., 2022; Mokarram & Khosravi, 2021). To achieve high-speed processing, hydrodynamic models resort to approximations and coarser resolutions, potentially sacrificing precision and reliability in predicting crucial flood parameters like extents, depths, and velocities. Balancing these factors is critical for producing trustworthy results in expansive geographical analyses. The intricate dynamics of flood waves, often characterised by abrupt changes and complex interactions, pose difficulties for these models in effectively capturing and representing these phenomena (Hunter et al., 2008b; Néelz & Pender, 2013). This limitation can impact the fidelity of the simulations, particularly in scenarios where precise and detailed flood wave behaviour is crucial for informed decision-making, such as in densely populated urban areas or regions prone to flash floods. Finally, there is a delicate balance to be struck between computational speed and the accuracy of results. Striving to achieve both remains a priority to ensure that flood modelling tools not only run efficiently but also produce accurately results in the urban fabric.

2.1.2.1 Hydrodynamic modelling with CityCAT

In this thesis, the fully coupled 1D/2D hydrodynamic City Catchment Analysis Tool – CityCAT developed at Newcastle University by Glenis et al. (2018) was employed to develop innovative and resilient methodologies for reducing flooding in urban areas and catchments. CityCAT is an advanced urban flood modelling tool that can simulate both surface and pipe network flows, explicitly representing buildings, surface and sub-surface drainage systems, and various types of Blue-Green Infrastructure (BGI) within built-up areas. This capability allows to assess different flood alleviation measures and comprehensively evaluate flood risk mitigation strategies. Moreover, it offers advanced capabilities for modelling, analysing, and visualising surface water flooding and urban drainage (Bertsch et al., 2017).

CityCAT's architecture is based on the object-oriented method, offering flexibility in development and rapid extension of functionalities (Glenis et al., 2018; Kutija & Murray, 2007). The 2D Shallow Water Equations (SWEs) solved by finite volumes with high order shock capturing schemes for propagation of flood wave for flows with discontinuities (Tan, 1992; Toro, 2001; Toro, 2013). New Riemann solvers have been developed which can handle free surface, pressurised and mixed flows. Moreover, the model is based on the St Venant equations and a conservative form of the Alievi equations based on the compressible Euler equations (Bourdarias et al., 2012). Infiltration in permeable spaces is calculating using the Green-Ampt method (Warrick, 2003), allowing for 1D vertical water transfer (a part of the equations can be seen in section 5.2.1 and for full description see Glenis et al. (2018)).

The model uses Digital Terrain Models (DTMs) for topography, which are crucial for hydrodynamic models, and for the representation of buildings, the *'Building Hole'* approach is used (see Iliadis et al. (2023b)). Excluding the buildings from the computational grid by generating a no-flow boundary around them and re-distribute the rainfall from the roof to the nearest grid square improves the accuracy of flow path representation constrained by buildings, the simulation time is reduced, and making the model more efficient. CityCAT provides water depth and velocity flow time series, flood maps, and volume calculations for various components such as manholes, gully drains, and buildings. The required inputs for the model include are: the DTM, the buildings footprint, the green areas, and rainfall intensity information.

CityCAT stands out as one of the most advanced and comprehensive hydrodynamic models available, enabling effective flood risk assessment and evaluation of flood mitigation strategies in the urban fabric. CityCAT has been used in all four of the following chapters in this thesis in a varied range of applications. To facilitate this use, and to provide background to the reader, a user manual of CityCAT was produced and can be found in Appendix A. The manual provides step-by-step instructions on how to utilize CityCAT effectively, making it a valuable resource for researchers, engineers, and policymakers seeking to employ advanced flood modelling techniques in urban settings.

2.1.3 DEM resolution

Digital Terrain Models (DTMs) or Digital Elevation Models (DEMs) play a crucial role in hydrodynamic modelling, aiding the accurate simulation and prediction of water flow, flooding, and other hydraulic processes. DTMs are essential for various applications, including flood risk assessment and urban drainage design (McClean et al., 2020). These models, are derived from digital elevation data such as LiDAR or satellite imagery, represent the topography of the terrain with high precision. In flood models, a DTM is used to define the spatial characteristics of the land surface, including elevation and slope. Roughness can be estimated if the type of surface is known, e.g. grass, roads. This information is vital for simulating the movement of water and the interactions between water and the terrain. Several studies explored the influence of DTMs in resolving the water flowpaths in pluvial flooding (Apel et al., 2009; Fewtrell et al., 2011b; Leitão et al., 2009; Noh et al., 2018; Pappenberger et al., 2008) and in fluvial flooding (Muthusamy et al., 2021; Ngo et al., 2022; Xafoulis et al., 2023). A study by Bates et al. (2010) addresses the importance of accurate terrain representation in hydrodynamic models. They conducted simulations of flooding events by using a flood model and found that the accuracy of the DTM significantly influenced the model's ability to predict flood extents and depths accurately. This highlights the need for high quality DTM data in flood models. Another study by Leitão et al. (2009) shows that at least a 5m DTM resolution is required to represent buildings and roads adequately in flood models by testing the 1D-1D generated flow pathway model initially developed by Maksimović et al. (2009) with different DTM resolutions. Moreover, Leitão et al. (2016) conducted a comparative analysis between unmanned aerial vehicles (UAVs) DEM data with a resolution of 0.05 m and LiDAR data with a resolution of 2m. Their findings indicated that a 2m resolution DEM was mostly sufficient to resolve the water flowpaths. The significance of highly accurate DTMs in flood modelling for effective urban flood management has been presented in studies by Wang et al. (2018) and Jamali et al. (2018). In both studies 1m resolution DTMs were used to demonstrate the critical role of precision in flood modelling for informed decision-making in urban flood management scenarios. Escobar-Silva et al. (2023) delved into the impact of spatial resolution on flood modelling. Their case study involved a comparative assessment of three distinct rainfall events with spatial resolutions of 0.50m and 5m. They concluded that when it comes to flood simulations, a DTM with an ultrafine spatial resolution of less than 0.50m, derived from spatial imagery, may not necessarily yield superior results compared to a DTM with a coarser spatial resolution of 5m, derived from orthoimages. The use of neural networks based on DTM to rapidly generate flood maps proposed and demonstrated by Z. Guo et al. (2021). This perspective is rooted in the argument that physically based models remain unsuitable for regions exceeding 1,000km^2 when employing a raster grid size smaller than 10m, which is clearly not valid if sufficient computational resource is deployed. They proposed that in urban environments, the optimal raster grid size should fall within the range of 1m to 5m to adequately capture the complex urban characteristics. Note here that the natural network approach when combined with a DTM presents limitations in accurately representing the sewer systems and accommodating necessary adaptations within the modelling and design process for risk management and adaptation solutions. Some attempts have been made to simulate water flow in large urban areas more than 1000km^2, a study introduced by Guerreiro et al. (2017) to model the flood impacts in 571 cities in Europe with a 25m DTM resolution and another study by Xu et al. (2023) to evaluate the flood risk in Shanghai with a 30m DTM resolution. The limitations of flood modelling in large urban areas can be significantly reduced by combining cloud computing with efficient hydrodynamic models (Glenis et al., 2013). By harnessing the power of cloud computing, flood modelling can tap into vast computational resources, enabling the processing of extensive datasets and the execution of complex simulations.

2.1.4 Representation of urban features in hydrodynamic models

In hydrodynamic models, multiple approaches are used to represent features such as bridges, embankments, leaky barriers, and buildings as obstacles within the model. These approaches aim to simplify the simulations for computational efficiency.

Buildings, in particular, are challenging to represent accurately in 2D flood models, and several techniques are commonly used (CH2M, 2019; SEPA, 2018; TUFLOW, 2018):

i. The *'Building Block'* (BB) approach involves raising the local topography to the height of the buildings' roof level. This approach prevents floodwater from flowing into cells unless the water level reaches the roof. However, this method is not widely used due to the significant difference in water surface elevation between the roof and the ground level, which can cause instabilities in most numerical schemes.

ii. The *'Building Hole'* (BH) approach consists of removing the cells with buildings from the DEM/DTM, effectively excluding them from the simulation as by default no flow is allowed across the boundary between the domain and the "hole".

iii. The *'Stubby Building'* (SB) method entails raising the DEM/DTM within the footprint of the buildings, typically by around 30cm. This approach avoids large elevation differences between neighboring cells caused by buildings.

iv. Replace buildings with grid squares characterised by high roughness values, such as Manning's coefficients ranging from 0.5 to 10. The purpose of this approach is to slow down and store water on the building footprint, reducing downstream flow, which can lead to significant ponding in some cases.

In industry models the most commonly employed approaches to represent buildings are: the "*Building Hole*" (BH) and the "*Stubby Building*" (SB) techniques. Both of these methods are popular due to their computational efficiency and straightforward implementation. When deciding which approach to use, it is essential to consider the specific modelling objectives and the desired level of accuracy for the flood simulations.

2.1.5 Extreme rainfall information

Extreme rainfall events are a significant concern in hydrologic risk analysis, critical infrastructure design, and management worldwide. They can lead to destructive floods, necessitating the estimation of extreme rainfall for specific timeframes and selected return periods. The emergence of a climate change has brought more frequent and intense storm events, escalating the vulnerability and exposure of urban environments to flooding (Galiatsatou & Iliadis, 2022). Intensity-Duration-Frequency (IDF) curves serve as a valuable tool for summarising the interplay between rainfall intensity, duration, and the likelihood of an event occurring within a specified return period. Currently these curves find widespread applications in the fields of hydrodynamic infrastructure design and management, flood risk assessment for assets and infrastructure, as well as flood mitigation projects (Da Silva et al., 2018; Norbiato et al., 2007; Yan et al., 2020). IDF curves are essentially graphical representations that capture how rainfall intensity changes with varying durations, each associated with a specific return period. These curves are typically constructed by fitting theoretical probability distribution functions to the annual maximum rainfall intensities, which cover a range of durations, from brief sub-hourly events to daily and even longer-duration rainfall occurrences (Galiatsatou & Iliadis, 2022). In hydrodynamic models, IDF curves play a pivotal role in simulating and predicting the behaviour of water systems during extreme rainfall events. These curves provide critical input data that help these models recreate realistic scenarios of rainfall intensity and duration, which are essential for accurately assessing flood risks, designing resilient hydraulic structures, and planning effective flood mitigation strategies. Incorporating IDF curves into hydrodynamic models raises two fundamental questions. Firstly, there is the choice between these curves uniformly across the entire modelling domain or generating storm profiles using the rainfall-runoff method pioneered by Kjeldsen (2007b) and Kjeldsen (2007a) followed by their uniform application over the entire domain, as demonstrated by Iliadis, Galiatsatou, et al. (2023). Secondly, the decision on whether to utilise stochastic or recorded rainfall data as model inputs is pivotal.

Typically, when researchers seek to analyse flood dynamics within an urban area comprehensively, the application of recorded rainfall data proves essential. This data provides a more accurate representation of real-world conditions, shedding light on the intricate flowpaths and immediate impacts of flooding on urban features. There is a greater need for the construction of accurate IDF curves to improve flood resilient solutions in urban environments.

2.2 Exposure and risk mapping

Due to the growth of urbanisation and the upcoming climate change more pluvial floods result from localised storm events characterised by exceptionally heavy rainfall concentrated within a brief timeframe and a relatively limited geographical area. These intense rainfalls generate substantial surface runoff, which can lead to direct damage to people, assets, and infrastructure (Cea & Costabile, 2022b). There is a great need for efficient exposure tools to analysing and identifying flooding in every structure of the urban fabric rather than generating flood risk zones to categorise areas based on their vulnerability to flooding (Lazaridis & Latinopoulos, 2023; Oppenheimer et al., 2014; Pham et al., 2022) or applied the Depth-Damage curves to buildings (Huizinga et al., 2017; Paulik et al., 2022; Velasco et al., 2015). Flood risk zones are areas prone to potential inundation during heavy storm events or rising water levels from the rivers or the sea. Flood risk zones categorised by buildings pertain to geographical areas vulnerable to flooding, often as a whole, rather than assessing individual building level risk. In some cases, despite a high zone categorisation, not all buildings within face immediate flood risk.

A more quantitative approach aiming to estimate losses and damages to properties and contents uses Depth-Damage curves, which are graphical representations of the relationship between flood depth and the extent of damage to structures or properties. Nowadays, both flood risk zones and Depth-Damage curves are effective tools for assessing the flood risks, aiding in disaster planning, and determining the potential economic impacts of flooding events (Huizinga et al., 2017; Martínez-Gomariz et al., 2020). With the increased power of urban flood models, these studies should focus on a more detailed analysis of the flood exposure to individual properties by categorising them according to the water depth around them or inside them, depending on the preferred representation of buildings in the hydrodynamic models (BH, SB etc). The last decade a few studies have focussed on flood risk to buildings with different approaches. Fuchs et al. (2015) presented a national multi-hazard exposure assessment in Austria, focusing on properties exposed to both pluvial and fluvial flooding. Their approach involved representing hazard information as polygons surrounding buildings, extending 15m from each structure. Note here that their methodology did not account for flooded roads and the flooded perimeter of buildings. Torgersen et al. (2017) and Szewrański et al. (2018) proposed a combination of hydrological modelling with drainage models and ArcGIS software to develop flood risk frameworks to analyse and calculate the exposure to individual buildings in newly developed areas. Both frameworks don't count the flood dynamics on the surface as they extract flood information from the sewer system and historical rainfall events, and they did not validate their methodologies against real storm events. Zischg et al. (2018) applied an exposure analysis in Switzerland, utilising a flood model (BASEMENT) to validate model predictions against insurance data. This validation was carried out across four distinct areas of the country, and the assessment was performed at the scale of river reaches.

Bertsch et al. (2022) developed a tool for urban-scale analysis that evaluates building-level exposure to flooding. They assessed the tool's accuracy by comparing its predictions to actual flood data from a storm event in Newcastle upon Tyne, UK. The validation dataset was gathered through surveys conducted by the local authority of residents affected by the storm, with a reasonably high level of coverage. The study showed model accuracy between 67% to 75%, which was impressive given that sub-surface drainage was not included in the modelling. In this thesis, the flood exposure calculator originally created by Bertsch et al. (2022) was used and further developed to assess the likelihood of exposure to urban features. The calculator's application and findings are discussed in detail in each chapter of the thesis.

2.3 Blue-Green Infrastructure

Blue-Green Infrastructure (BGI) plays a pivotal role in transforming urban environments into more sustainable and resilient spaces, addressing the complex challenges posed by rapid urbanisation and climate changes (O'Donnell et al., 2020). The representation of BGI in hydrodynamic models is a critical component of contemporary flood risk assessment and the designing of resilient management solutions. BGI refers to use of natural or nature-based systems, such as green and blue roofs, permeable pavements, swales and ponds, to manage and reduce flood risks (Woods Ballard et al., 2015). Integrating BGI into flood models involves capturing the dynamic interactions between these features and the urban environments (Sörensen & Emilsson, 2019). Hydrodynamic models can simulate how BGI features absorb, store, and slow down excess rainfall and flood waves, reducing the impact of floods on urban areas (Fenner et al., 2019). The accuracy of the BGI representation in hydrodynamic models is crucial for urban planners and local authorities to make informed decisions about where and how to implement green infrastructure to improve flood resilience, in some cases the water quality, and promote sustainable urban development in the face of changing climate conditions. The most common BGI representation in hydrodynamic models as mentioned earlier are (Fletcher et al., 2015; Woods Ballard et al., 2015):

- Green roofs are installations of live vegetation positioned atop buildings by serving various purposes such as improved building functionality and the mitigation of water runoff;
- Blue roofs are a specially designed roofing system with the primary purpose of actively storing and managing flood water;

- Permeable pavements are designed to accommodate both pedestrian and vehicular traffic while facilitating the infiltration of rainwater through the surface and into the underlying structural layers;
- Swales serve as channels for managing low-flow waters;
- Ponds are landscape elements featuring a consistently present body of water, offering simultaneous functions of reducing and treating surface water runoff;

In various studies addressing adaptation strategies at both local scales using Sustainable Urban Drainage Systems (SuDS) as seen in Fletcher et al. (2015) and Hörnschemeyer et al. (2023), and at larger scales, exemplified by Li et al. (2018), a common thread of non-adaptive efficiency becomes evident. This inefficiency is attributed to the limited information and uncertainties surrounding the capacity, performance, and optimal placement of these systems, as discussed in Ernst and Preston (2017), Kuller et al. (2017), and Preston et al. (2015). A recent research by Oladunjoye (2022) highlights the potential significance of SuDS in flood mitigation. These systems have the capacity to reduce runoff volume and mitigate flood risks by effectively managing flow through natural infiltration mechanisms. Although, there is a growing recognition of the potential of practical and cost-effective solutions like BGI, significant barriers hinder their widespread adoption (O'Donnell et al., 2021). To be effective on a city-wide scale, BGI adaptation solutions require substantial investments in multiple locations, rather than relying on opportunistic and fragmented initiatives tied to redevelopment projects. Consequently, a more systematic, city-wide strategy is imperative. This approach should include a comprehensive assessment of the overall costs and benefits before city planning authorities commit to such investments. Achieving this necessitates an urban flow simulation with sufficient precision, capable of not only assessing exposure and risk reduction at the property level but also identifying localised sources of runoff and the specific flow paths where BGI can be effectively implemented. An effective approach for pinpointing areas contributing to the overall flood extent in a simulated event involves a *'source-to-impact'* flood analysis method, as presented by Vercruysse et al. (2019) and Dawson et al. (2020) in a city-scale and by Ewen et al. (2013) in a river-scale. Vercruysse et al. (2019) introduced a four-step methodology designed to trace flow paths and identify locations at high flood risk. This methodology involved assessing variations in modelled maximum water depths by comparing the baseline scenario with cells in the catchment that lacked rainfall. Additionally, four spatial prioritization criteria were employed to locate the most suitable cells for implementing flood adaptation interventions. Note here that by using maximum values of water depth is not ideal for this objective due to inaccuracies in elevation data in the DTM that could lead to overestimation of flood levels, especially in areas with relatively low flood hazard. Finally, a more systematic approach is required to manage the evaluation of interventions. This entails not only identifying the optimal locations for implementing effective adaptation solutions but also estimating potential damages to buildings and assessing how many buildings may be affected by flood waves.

2.4 Real world and bigger applications

Hydrodynamic models play a crucial role in assessing flood risk, particularly in densely populated urban areas facing the challenges of urbanisation and anticipated climate change impacts, as mentioned earlier. However, the progress in designing optimal and efficient flood risk management solutions has been hindered by the limitations in integrating cloud computing with flood models. Recent advancements in cloud-based flood modelling have expanded the capabilities for processing and storing data. This evolution in technology has opened up a wide array of possibilities for comprehensively understanding and addressing flood risk management in large urban areas and expansive catchments areas (Glenis et al., 2013). Nowadays, cloud services offer flexible payment arrangements based on resource rental duration and the necessary Random-Access-Memory (RAM) specifications. Conversely, there are situations where a local compute server must be deployed, incurring costs that align with the specific usage demands. Frequently, researchers shy away from simulating surface flow in large urban areas. This reluctance can stem from either a lack of understanding in connecting their flood models with cloud resources or concerns about the reliability of these models. Additionally, many of the current flood models exhibit inefficiencies when utilising high-resolution DTMs as input data resulting in frequent crashes. Numerous research studies have focused on small urban catchments (Chen et al., 2009; Fewtrell et al., 2008; Huang et al., 2022; Iliadis, Galiatsatou, et al., 2023; Rak et al., 2018; Xu et al., 2023) with a range of DTM resolutions from 1m to 10m by using several flood models such as HEC-RAS, TUFLOW, CityCAT etc. As mentioned in section 2.1.3, Guerreiro et al. (2017) simulated the surface flow across over 500 European cities using a 25m DTM resolution. The limitations in accurately representing water flow pathways were clear in their conclusions. Furthermore, Al-Suhili et al. (2019) developed an urban flood alert system tailored for big cities, focusing particularly on Manhattan, New York City, USA. They achieved this by subdividing the Manhattan area into 140 sub-basins, by using a DTM resolution of 0.30m, and coupling a drainage model with a database of flood level maps. In a recent study by Escobar-Silva et al. (2023), an evaluation has been made to determine the scope of flooding in São Caetano do Sul, situated in the southern region of São Paulo, Brazil. Their research focused on a modelling domain encompassing 15.33km^2 and examined the impact and effectiveness of two distinct DTMs. The DTMs, with resolutions of 0.50m and 5m, were employed in conjunction with real rainfall data for analysis and validation. The precision and accuracy of the outcomes have now reached a level where they can apply to evaluations in critical urban areas, especially megacities with the highest levels of flood risk and vulnerability. In closing, it is imperative to further strengthen the link between cloud computing and flood modelling in future endeavours to achieve flood resilience across cities of varying sizes worldwide.

2.5 Problems and research gaps addressed

The literature review in this chapter provided a comprehensive overview of the state of the art in urban flood modelling. This chapter explored the intricacies of modelling urban systems, including drainage models and surface models, with a particular focus on hydrodynamic modelling using CityCAT. The significance of Digital Terrain Model (DTM) resolution and the representation of urban features within hydrodynamic models are discussed in detail. The incorporation of extreme rainfall information, the vital role of flood exposure and risk mapping, and the growing importance of Blue-Green Infrastructure in flood management are discussed too. Real-world and large-scale applications of flood models are explored, offering insights into their practical utility. Finally, this chapter identifies key research problems and gaps that will be addressed in the chapters of this thesis as summarised in Table 2.1.

Table 2.1 Summary of the identified gaps in the literature review, the description, the action, and the referred chapter.

A/A	Research Gap	Description and Actions	Chapter
1	Representation of buildings (BH or SB?)	• Industry uses two approaches for the representations of buildings, the BH and the SB techniques. • Need to compare these two approaches and identify the advances and disadvantages.	**3**
2	Improvement of the SB approach	• Many modellers use this approach but, in most cases, there is noise in the DTM within the building's footprints. • A new improved method for SB.	**3**
3	Identification of buildings and locations at high risk of flooding	• Need to analyse how many buildings contribute to flooding during a storm event. • Estimation of the likelihood of exposure at building level.	**4**
4	Cost-benefit nexus between the *'source'* and the *'receptor'*	• Flood damages are important in urban areas. • Calculation of damages based on the type of building	**4**

5	Identification of high priority areas to mitigate flooding by adding Blue-Green Infrastructure (BGI)	• High priority locations to add BGI are crucial. • Develop a methodology to identify locations at high flood risk and add interventions to reduce flooding and achieve resilience.	**4**
6	Comparison of different resolution DTMs in cities	• There is a great need for urban flood risk management, especially in megacities. • Comparison of different DTM resolutions and analyse the flood exposure of urban features.	**5**
7	Use of high-resolution of DTM in large urban areas	• Megacities need to improve their resilience against flooding. • Link cloud computing with hydrodynamic models, with a high-resolution DTM, to understand the flood dynamics and estimating the buildings exposed.	**5**
8	Construction of accurate IDF/DDF	• The IDF/DDF are an important input to hydrodynamic models. • Construct accurate IDF curves with a POT threshold.	**6**
9	Data scarcity	• In countries like the UK or U.S. the data for flood modelling is available almost to everyone, in other countries there are limitations in the available data. • Model a city outside of the UK with limited access to data.	**6**

After identifying the gaps in the literature review and the actions that need to be taken, an abstract of every chapter is presented below.

Gaps [1 & 2]: The literature review highlights that two widely used approaches for the representation of buildings and urban features in hydrodynamic models, the approximate *'Stubby Building'* approach and the more accurate *'Building Hole'* approach. A direct comparison of the two approaches is carried out allowing quantification of the errors incurred, a validation of these two approaches by using real storm data from the *'Toon Monsoon'* event, and an improved method for the '*Stubby Building*' approach which corrects for common errors in DTM generation is presented in Chapter 3. Moreover, the outcomes of this chapter have been published in Journal of Flood Risk Management – “Iliadis, C., Glenis, V., & Kilsby, C. (2023). Representing buildings and urban features in hydrodynamic flood models. *Journal of Flood Risk Management*, *n/a*(n/a), e12950. https://doi.org/https://doi.org/10.1111/jfr3.12950”.

Gaps [3-5]: A novel framework is presented in Chapter 4 to identify locations at high flood risk regarding the cost-benefit from the flood damages during multiple storm events, priority options to mitigate flooding by adding Blue-Green Infrastructure in critical locations, and a combination of rainfall information with flood dynamics and the cost benefits. This chapter was submitted in Journal of Hydrology , and it is under review – “Iliadis, C., Glenis, V., & Kilsby, C. (2023). *A cost-benefit 'source-receptor' framework for implementation of Blue-Green flood risk management*. Journal of Hydrology (*under review*). arXiv:2311.00420 ”.

Gaps [6 & 7]: Chapter 5 highlights the crucial importance of DTMs in hydrodynamic models, incorporating multiple storm scenarios and including a validation with observations from a real storm event that happened on the 12th of July 2021. Thus, a novel demonstration is presented of how cloud-based flood modelling can be used to inform exposure insurance and achieve flood resilience. The outcomes of this chapter has been submitted in MPDI Water, and it is currently under review – “Iliadis, C., Glenis, V., & Kilsby, C. (2023). *Cloud Modelling of Property-Level Flood Exposure in Megacities*. Water, 15(19), 3395. https://www.mdpi.com/2073-4441/15/19/3395”.

Gaps [8 & 9]: A methodological framework for combining hydrological with hydrodynamic modelling in the city of Thessaloniki to understand the impacts of urban floods, the water flowpaths in the city centre, and the urban features exposed at high flood risk are presented on Chapter 6. It is the first time that CityCAT is applied in a country with limited access to data and this combination can significantly assist reliable assessment of infrastructure exposure to flooding, as well as contribute to flood damage mitigation and flood risk reduction. The outcomes of this chapter have been published in MODI Hydrology – "Iliadis, C., Galiatsatou, P., Glenis, V., Prinos, P., & Kilsby, C. (2023). *Urban Flood Modelling under Extreme Rainfall Conditions for Building-Level Flood Exposure Analysis*. Hydrology, 10(8), 172. https://www.mdpi.com/2306-5338/10/8/172".

To address the existing gap in accurately representing the drainage systems within urban environments, a planned initiative for future work is outlined in Chapter 7.

Chapter 3. Representing buildings and urban features in hydrodynamic flood models

3.1 Introduction

3.1.1 Background

Flood inundation models have become an essential tool in understanding flood events, assessing flood risk, and predicting future risk to urban fabric (Willis et al., 2019). The latest generation of hydrodynamic models is capable of simulating flooding in the urban environment where the topography with buildings, drainage networks, and critical infrastructure are complex (K. Guo et al., 2021). High-resolution Digital Elevation Models (DEMs), Digital Surface Models (DSMs), and Digital Terrain Models (DTMs) play a key role in hydraulic models in defining the pathways of flood into cities (McClean et al., 2020). Hydrodynamic models have undergone rapid development exploiting new numerical schemes, more powerful computational implementation, as well as higher resolution data and a major leap in predictive capabilities is possible. The increasing demand of accurate and reliable estimates of surface water flood risk and flood risk protection of the assets, infrastructure, and man-made constructions for flood insurance purposes and for urban planning by local authorities, drives this development of hydraulic models with more realistic results (Kilsby et al., 2020). Such studies are important due to global change and the possible *'unknowns'* to be faced. Several studies have been conducted applying 2D hydrodynamic models to complex urban problems, including numerical solutions of the 2D shallow water equations (Choley et al., 2021; Leandro et al., 2009; Mignot et al., 2006; Paquier et al., 2015), the surface water movement around buildings and the underground drainage system. A few of these studies have focused on the demanding issue of how to represent buildings within 2D hydraulic models as obstacles to water flow (Bellos & Tsakiris, 2015; Beretta et al., 2018; Bisht et al., 2016; Glenis et al., 2013; Maksimović et al., 2009; Néelz & Pender, 2013; Rak et al., 2018; Schubert & Sanders, 2012; Schubert et al., 2008; Syme, 2008; Zhou et al., 2016) for pluvial flooding applied in urban areas.

A large proportion of urban areas is covered by buildings and during flood events they exert significant influence on flow paths as water will only flow through them in cases when the main entrance or windows are open or the flood water exceeds the threshold of the entrance (Fewtrell et al., 2008; Wang et al., 2010). Alcrudo (2004) presented different approaches for the representation of buildings including (a) vertical walls to exclude buildings from the computational grid; (b) the bottom elevation approach, i.e. raising the elevation of the building to reach the rooftop; and (c) the local friction based representation of buildings, increase the friction coefficient (values between 0.50 to 1.00) where buildings exist; he concluded that removing buildings from the computational grid is the most accurate representation. Hunter et al. (2008b) presented a test study to compare the performance of six 2D hydraulic models to simulate surface flooding of an urban catchment in the city of Glasgow, UK which showed an effective approach is to represent a building in hydrodynamic models by raising its elevation up to 12 m (high buildings) or 6m (small houses) to allow water flow around it, the so-called *'island method'*. Chen et al. (2012) proposed another approximation by abstracting the buildings from a coarse grid and using the building coverage ratio and a conveyance reduction factor. Glenis et al. (2018) showed how the buildings' footprint can be excluded from the computational grid and replaced by no-flow boundaries to improve the ability of the model to capture realistic flow paths in the built environment. In their method the buildings are retained as objects which can support other process representation (e.g. storage and/or flow of rainfall from roof surfaces, and ingress of flood water).

In this chapter the two most widely used approaches for representation of urban features in hydrodynamic are assessed by validation against a real flood event: (a) the exclusion of buildings from the computational grid (*'Building Hole'*), and (b) the raising of the buildings' footprint by 30 cm (*'Stubby Building'*). Moreover, a detailed analysis of multiple *'stubby'* models is presented and an improved version of the *"Stubby Building"* technique is proposed.

3.2 Modelling system

Among the many hydraulic models developed for surface flows, one of the most advanced and fully featured is CityCAT – City Catchment Analysis Tool, a fully coupled 1D/2D urban flood modelling tool, developed at Newcastle University for surface flow, representation of buildings, sewer network, and blue-green infrastructure with interventions (Glenis et al., 2018; Glenis et al., 2013). It also enables the assessment of benefits of different flood alleviation measures. CityCAT can produce maps and time series for given rainfall inputs of flood depth, flow velocity and volume in and out of manholes, gully drains, buildings etc (Kilsby et al., 2020). The software architecture in CityCAT is based on the object-oriented method which offers flexibility in development and rapid function extension (Glenis et al., 2018; Kutija & Murray, 2007). The DTMs for the topography and the UK Ordnance Survey Mastermap© (Lidar, 2016; MasterMap, 2020; Ordnance Survey, 2020) data for urban features such as roads, permeable surfaces, and buildings, are standard datasets used by CityCAT.

The building footprint is excluded from the computational grid with no-flow conditions implemented along the building walls, which improves the ability to capture the flowpaths where they are constrained by buildings.

In general, exclusion of buildings also delivers a reduced simulation time due to the reduction in the number of computational cells of some 29% in this application, which will be greater in other more densely built areas. The concentration of flow between buildings and consequent increased flow velocity may require a reduction in time step to ensure stability resulting in longer computational time, but this is limited to a small proportion of the simulation at the flood peak when high flows occur. This is also counteracted by a further reduction in computational time, as the more concentrated flows resulting from no-flow building walls transfer the flood wave more rapidly than the more dispersed wave in the stubby building case, so requiring shortened timesteps for a reduced duration. Timings of equivalent simulations using Building Hole and Stubby Building methods show a reduction of some 28% in computational times, therefore confirming that the dominant effect is the reduction of the number of computational cells.

To simulate the free surface flow, the 2D shallow water equations are used in their conservative form and the solution is obtained by using a high-resolution finite volume method with shock-capturing schemes (Glenis et al., 2018). The infiltration for green areas is calculated with the Green-Ampt method (Warrick, 2003) allowing 1-D, vertical, transfer of water.

3.3 Representation of urban features into hydrodynamic models

3.3.1 State of the art

Hydraulic models generally approach the representation of features like bridges, embankments, leaky barriers and buildings as an obstacle inside the model, so the simulations are much quicker and easier to run but often deliver incorrect and unrealistic results. The most common techniques to represent buildings in 2D hydraulic models are: (*a*) the '*Building Block*' (BB) method where the buildings are modelled by raising the local topography to the roof level, so the flood cannot flow into cells unless the water levels reaches the roof. This method is not often used as the large water surface elevation difference between roof and ground level causes instabilities in most numerical schemes; (*b*) '*Building Hole*' (BH) where the cells with buildings will be clipped from the DEM/DTM and they are not involve in the simulation; (*c*) '*Stubby Building*' (SB) where the buildings are represented by raising the DEM/DTM within the buildings' footprint by (typically) 30 cm, thus avoiding large elevation differences between neighbouring cells; (CH2M, 2019; Kilsby et al., 2020; SEPA, 2018; Shen et al., 2018; Syme, 2008; TUFLOW, 2018).

Furthermore some studies (Bach et al., 2014; Beretta et al., 2018; Hunter et al., 2008b; Schubert et al., 2008; SEPA, 2018; Syme, 2008; Teng et al., 2017) replaced buildings by a flat area with high roughness, e.g. Manning coefficient between 0.50 to 10, which is intended to slow and store water on the building footprint to reduce downstream transfer. With sufficient calibration, such models can deliver plausible large-scale results for some situations, but at a local street or building scale methods such as SB or enhanced roughness introduce un-realistic flow paths and systematic under-estimation of *'blocking'* of flow which may in some situations cause significant ponding.

3.3.2 Aim of this chapter

In this chapter, we will assess the performance and identify the differences between the *'Building Hole'* and the *'Stubby Building'* approaches. These two techniques are widely used in industry to estimate flood risk in cities, where the hazard is higher, due to human lives, assets etc, and depth damage calculations are applied to buildings (SEPA, 2018). The other technique identified earlier, using increased roughness is less widely used and presents major issues with non-realistic flow pathways, so is not assessed here.

The BH approach represents buildings as void space where the cells within the building are removed from the computational grid. The surface water cannot flow into the building voids, so the water flows around the building boundary (Bertsch, 2019). In addition, reduction of the simulation time from a smaller number of computational cells is an advantage, especially for dense built-up areas. In this chapter the BH numerical grid has 29% fewer cells than the SB numerical grid. With the SB approach, the threshold (h) of the building entrance height is used for the representation of buildings into the model. However, due to the variable entrance height of the buildings and to avoid instabilities in the model with large elevation differences, the most common values are 30 cm to 40 cm. Typically, buildings are assumed to be constant 30 cm above the local ground level elevation of the DEM/DTM which prevents water from flowing into buildings until the water depth exceeds 30 cm and can then flow over the building (Pettit, 2014; SEPA, 2018).

3.3.3 Study Area

Having outlined the principles behind the techniques to represent urban features in hydrodynamic models, a case is conducted in the city centre of Newcastle upon Tyne, UK. The domain has complex topography due to some substantial slopes and a range of roads of different widths, as well as green areas, and a variety of buildings of different plan areas and heights. This diversity provides a substantial opportunity to explore the behaviour of the urban features in the model with some 5422 buildings present. An additional advantage is that the area was subject to a major pluvial flood on June 28, 2012, and documentation of the flow paths and damage to exposed buildings is available for validation (see section 3.3.4.). Figure 3.1 shows the area of the case study with the general downslope flow direction is to the bottom, right (south-east) corner into the river Tyne.

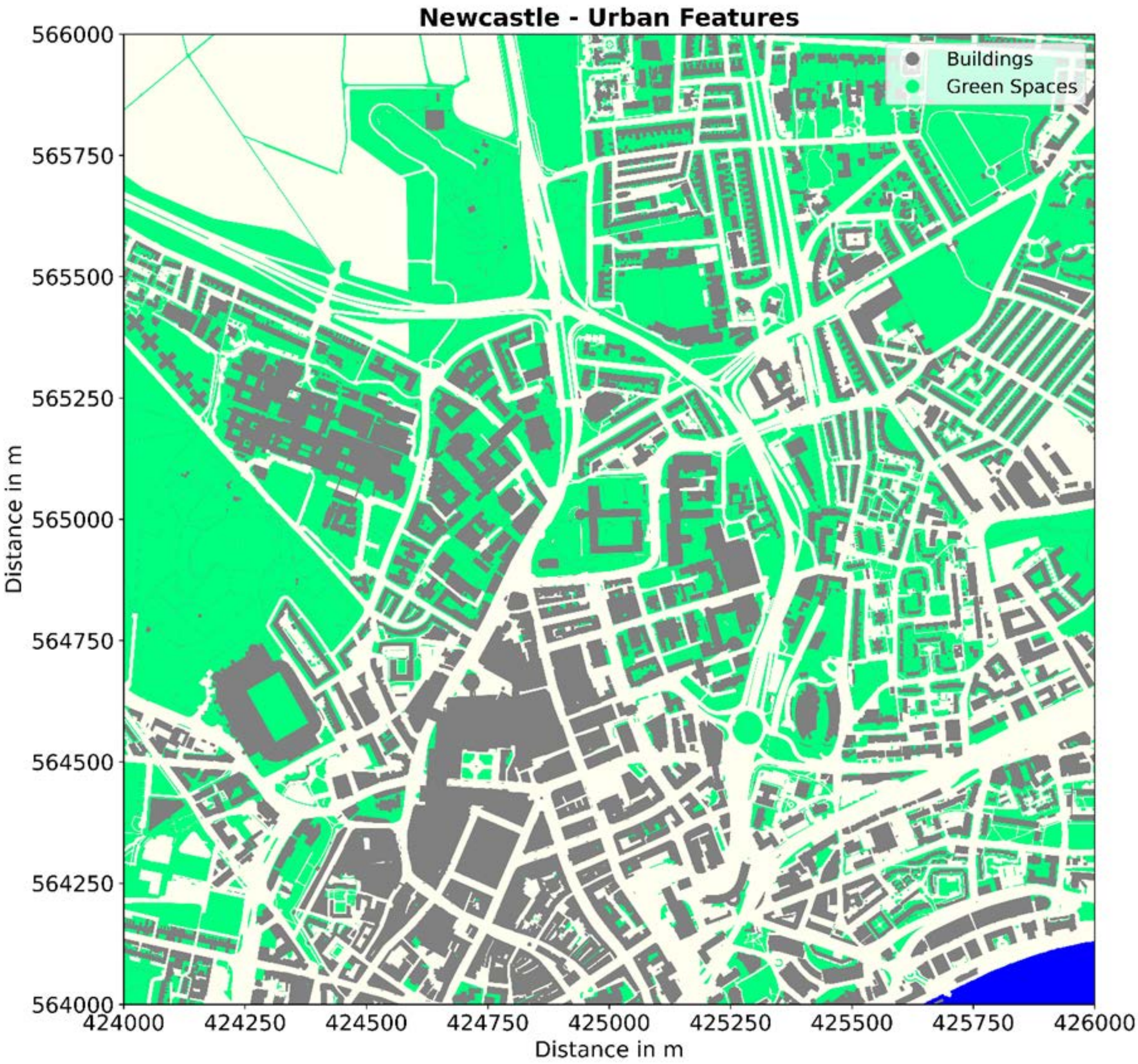

Figure 3.1 Urban features in the study area of Newcastle city centre, UK. Grey represents the buildings, green the permeable spaces, yellow the impermeable surfaces, and blue the main river.

3.3.4 Model Set up

CityCAT (Glenis et al., 2018) was used to simulate flooding and urban features in this chapter for all models. The flow domain was constructed using LiDAR (Light Detection And Ranging) terrain data at resolution of 1m (area of each cell is 1 m^2), while the building footprints and the green spaces were extracted from Edina Digimap (Lidar, 2016; Ordnance Survey, 2020). The catchment comprises 4,000,000 cells resulting in a total area of 4.0 km^2 (2,842,209 cells for the BH as the buildings footprint is excluded from the computational grid and 4,000,000 cells for the SB). The infiltration of water in pervious areas is estimated using the Green-Ampt method (Warrick, 2003) and the outer boundaries of the domain are transmissive. MasterMap data are used to delineate urban features such as roads, permeable areas, and impermeable areas. The centroid of each computational cell and the polygons for the urban features are used to classify each cell and assign friction coefficients and soil properties.

For the SB approach, an algorithm was developed to prepare the DEM for CityCAT starting from the DTM (i.e., the lidar coverage with the buildings removed) and adding 30 cm to cells identified within the building footprint shapefiles. This process replicates the standard procedure in the flood modelling industry (CH2M, 2019). Furthermore, we identified some *'errors'* (see section 3.4) affecting DTMs inside the building footprints in specific locations in the Area of Interest (AOI), where a new algorithm was developed to identify anomalous depressions within a building footprint and restore the elevation of these areas to ground level, adding 30 cm for the *'stubby platform'* approach.

For the BH approach, a custom mesh generation procedure is used which removes any cell of which more than half falls within the building shapefile (see Glenis et al. (2018) for full description, Figure 3.3). A spatially uniform rainfall series is used to drive all the simulations, based on the depth of the historical storm of June 28, 2012 (45 mm in two hours, see Figure 3.2). The rainfall falling onto roofs is redistributed to the neighbouring cells of the computational grid. A range of simulations with storm events of 1 hour duration and return periods of 50 and 100 years (2% and 1 % Annual Exceedance Probability respectively) are used to compare the two approaches and identify the differences in flow paths. The primary aim is to validate and better understand the techniques for the representation of buildings, so we excluded the sub-surface drainage network system from the simulations reported here. While model results with and without the sub-surface network show differences in some locations, the main features of flooding are similar for this very large event, and acceptably close to the observed impacts (Glenis et al., 2018).

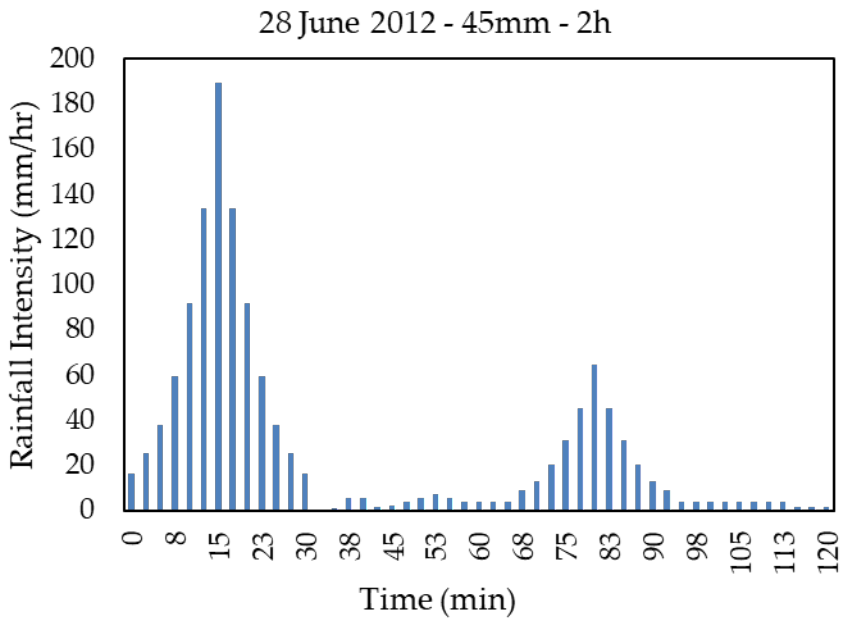

Figure 3.2 Storm profile corresponding to the historical storm on June 28, 2012, at Newcastle Upon Tyne.

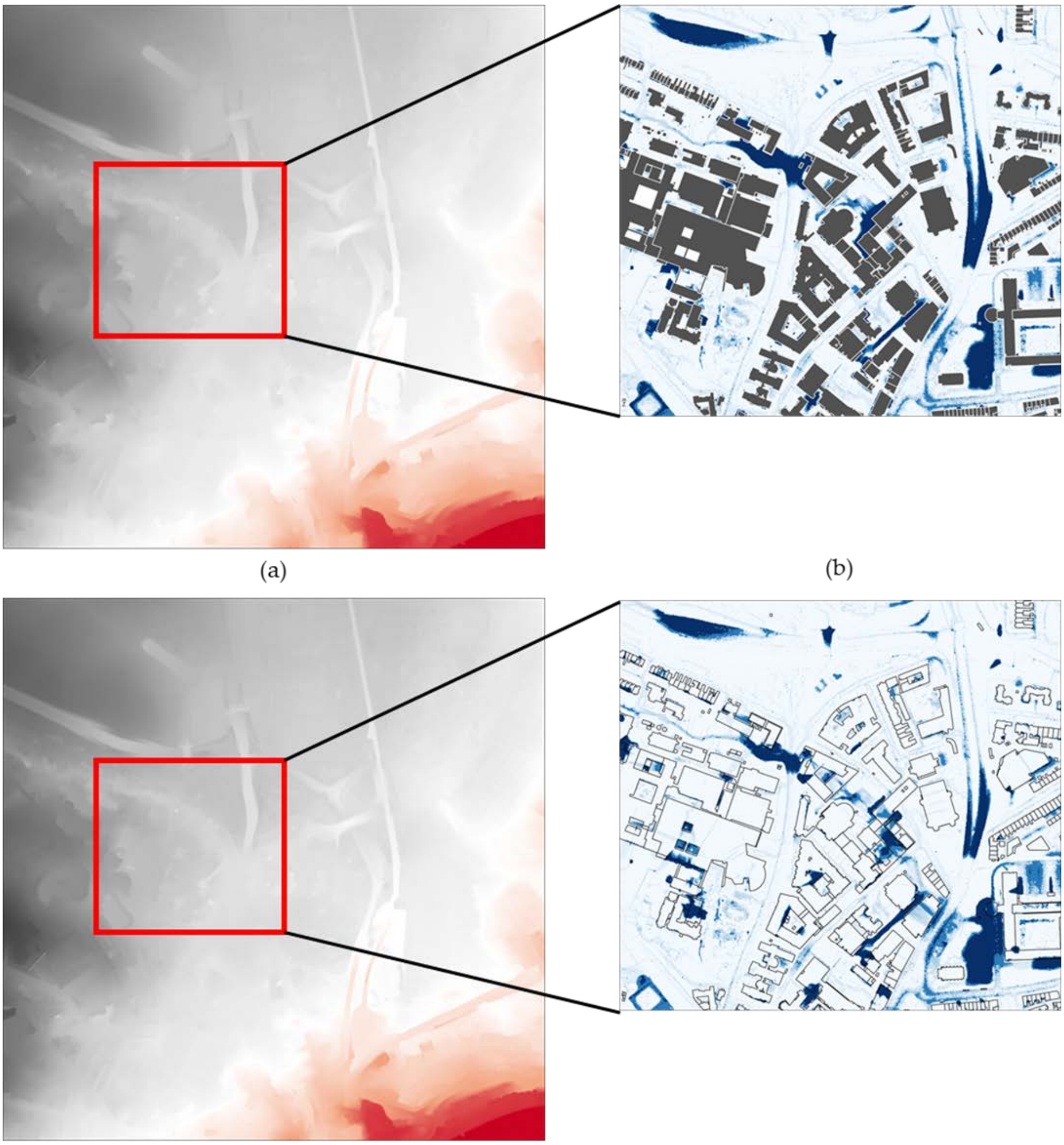

(a) (b)

(c) (d)

Figure 3.3 The DEM and the extracted results from CityCAT of the study area (a & b) with the *'Building Hole'*; (c & d) with the *'Stubby Building'*.

3.3.5 Flood exposure analysis

Building outlines from OS (MasterMap, 2020; Ordnance Survey, 2020) were used to estimate the flood risk to buildings by analysing each model's maximum flood depth output in a one-cell wide buffer around the building outline. Buildings were classified as flooded if the flood water is above a typical property threshold of 30 cm (Bertsch, 2019; Bertsch et al., 2022; Environment Agency, 2021).

Table 3.1 Classification scheme for calculating flood exposure likelihood for buildings (Bertsch, 2019; Bertsch et al., 2022).

Exposure Class	Mean depth (m)	Max depth (m)
Low	<0.10	<0.30
Medium	<0.10	≥0.30
	≥0.10 - <0.30	<0.30
High	≥0.10	≥0.30

3.4 Results and Discussion

The performance of each simulation was compared in terms of the flood depth, the number of buildings inundated, and the water flowpaths. The complex topography and the high slopes around the city centre allow examining detailed water flowpaths and the direct influence on buildings. Figure 3.4(a) presents the study area with the *'Building Hole'* technique for the storm of June 28, 2012, and it can be seen that the flowpaths change direction or stop when there are buildings in the way, which is physically realistic. Thus, Figure 3.4(b) shows, for the same storm event, that with the *'Stubby'* approach, while the broad distribution of flood water is similar, the flood flowpaths frequently traverse the buildings where the water depth outside them exceeds the 30 cm threshold, which is not physically realistic. Proponents of the SB approach suggest that this process represents ingress to the building and subsequent egress, but this is very speculative, and the number of instances in this simulation show that there is a major mis-representation of flow pathways due to the approximation of 30 cm roof elevation of the buildings.

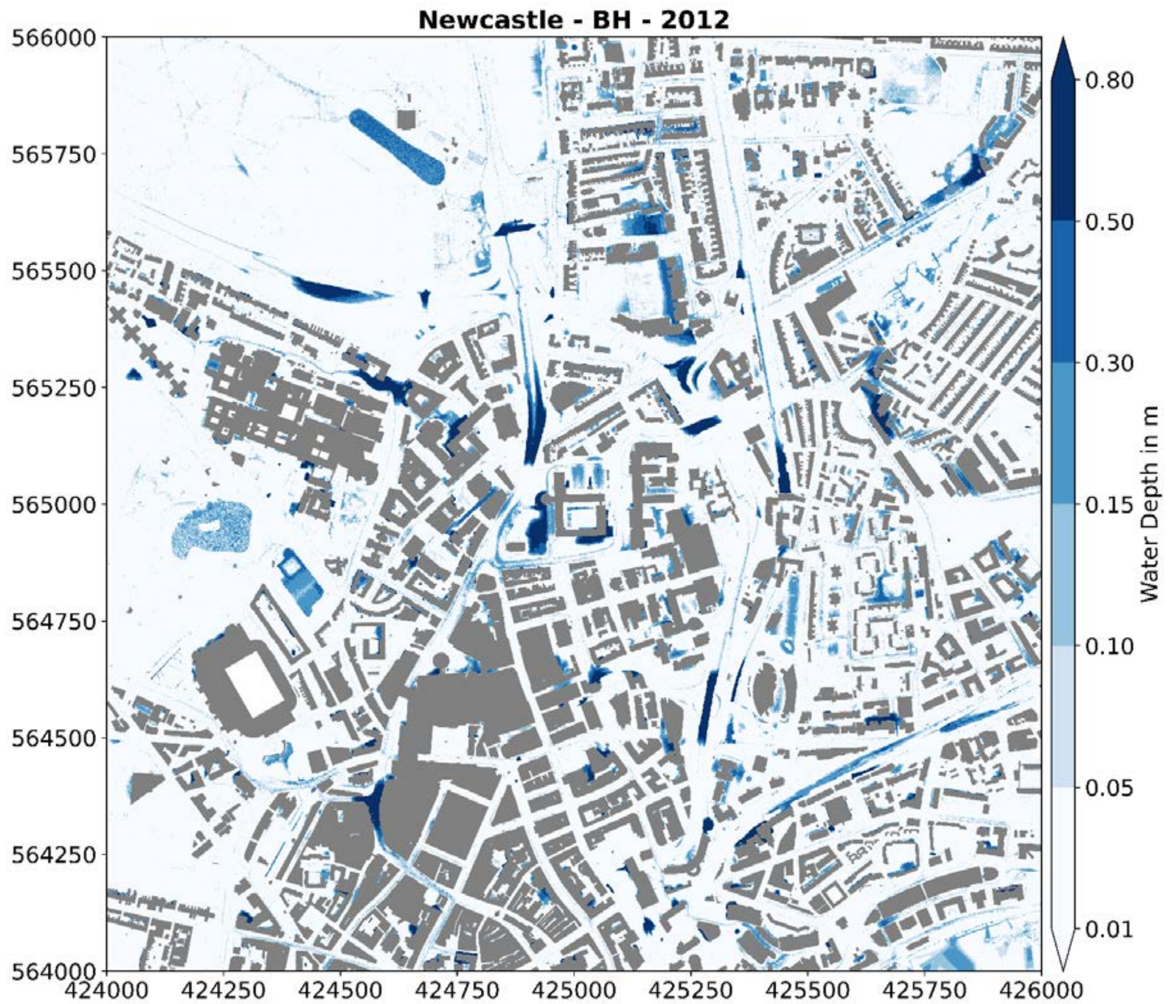

Figure 3.4(a) Water depths from CityCAT for the storm on 28th June 2012 with the *'Building Hole'* approach for Newcastle city centre.

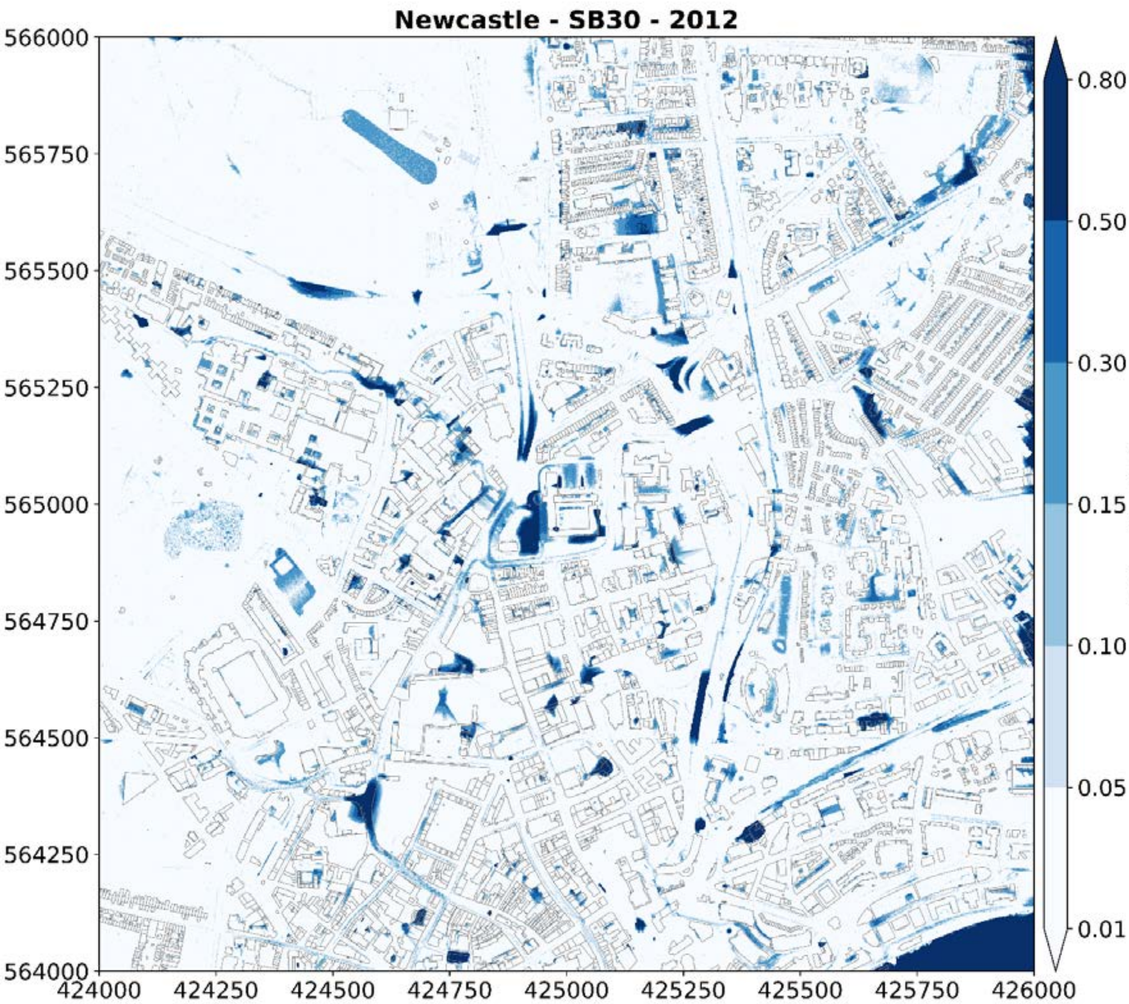

Figure 3.4(b) Water depths from CityCAT for the storm on 28th June 2012 with the *'Stubby Building'* approach for Newcastle city centre.

Table 3.2 Summary of mean water flood depth for each model in different storm scenarios; BH denotes the *'Building Hole'* method; SB30 denotes the *'Stubby Building'* method with a 30 cm threshold; Final code denotes either observed event rainfall used, or depth corresponding to an estimated return period.

Models	Mean flood depth (m)
BH - 2012	0.044
SB30 - 2012	0.042
BH - 50y rp	0.038

SB30 - 50y rp	0.033
BH - 100y rp	0.046
SB30 - 100y rp	0.041

Table 3.2 presents the water mean depths between the two techniques in different storm events, and it is clear that the mean depths are higher with the BH approach than with SB, which is plausible due to the exclusion of buildings from the computational grid and increased number of cases of flow blocking.

3.4.1 Velocity comparison

Furthermore, a useful extension of flood modelling in dense cities is to capture the correct direction of water flow paths and velocity considering the roads, pavements, all types of buildings, topography etc. A detailed comparison of velocity of flows is presented in this section between the *'Building Hole'* and the *'Stubby Building'* approach.

Figure 3.5(a) presents the mean velocity of flow averaged over all grid squares in the domain for the two approaches. It can be seen that the velocity of flow with the BH approach is somewhat higher than with the SB which is consistent with the higher friction in the SB domain due to lower water depths overall, relative to the BH case where flows are channelled between buildings. Figure 3.5(b) shows that the differences in percentiles of the velocity of flow for the 70 min of the storm event are minor until the 70th, where the BH values are larger. The differences are largest for the 90th and the 99th percentiles, i.e. the deepest flood waters.

A detailed comparison of modelled flows is presented in Figure 3.6, near the Merz Court building on Newcastle University campus which was severely flooded. It is clear that in graphs (a) and (c) with the BH approach, the flood water changes direction on reaching the building and flows around it, as observed during the storm event. In contrast, with the SB approach the flood water flows over the building, generating unrealistic flowpaths.

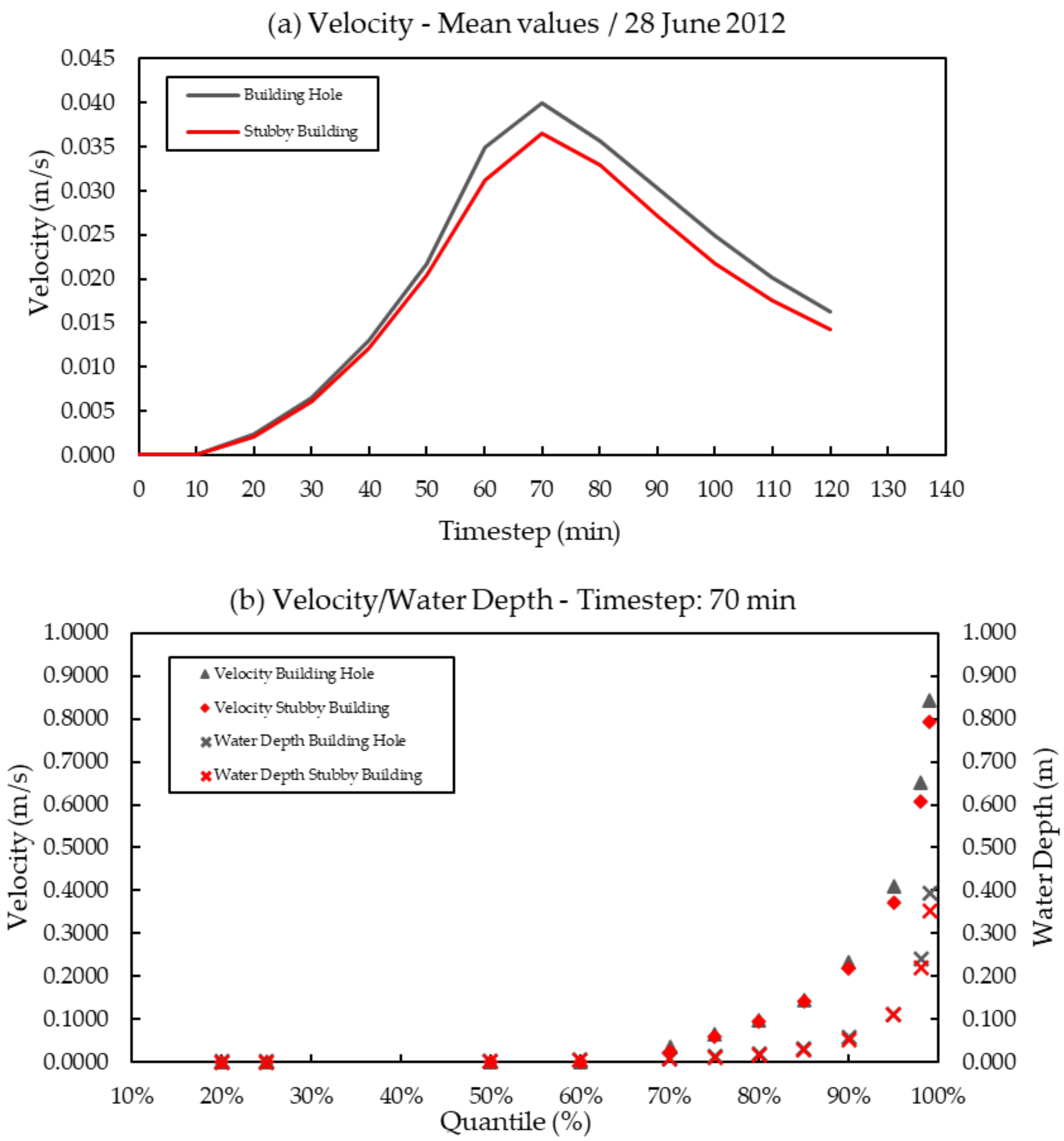

Figure 3.5 (a) The domain average flow velocity for the BH and the SB approaches during the 2012 storm; (b) the distribution of flow velocity (left axis) and water depth (right axis) for the 70 minutes for the storm event plotted against its quantile.

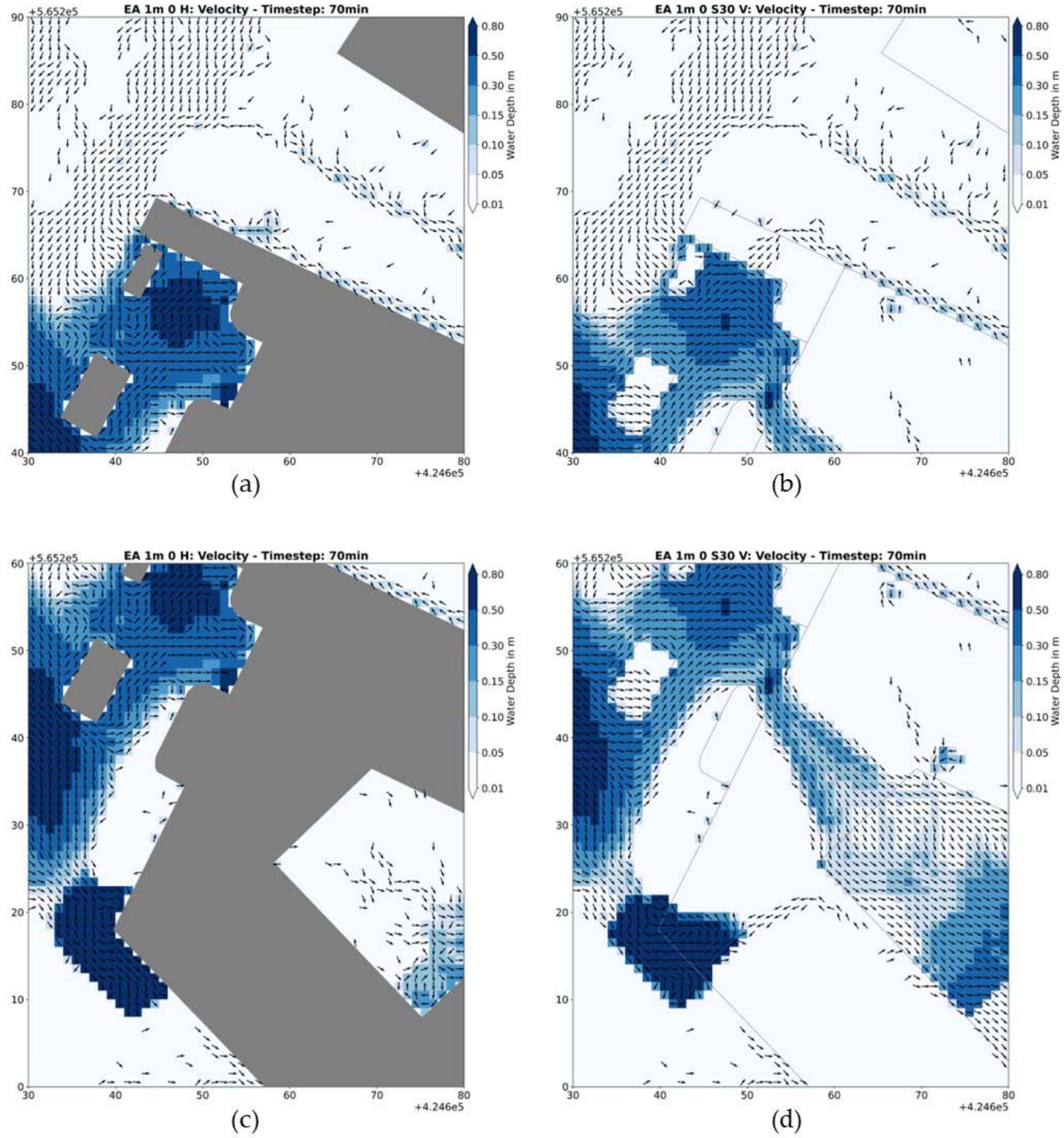

Figure 3.6 (a), (c) Water depths and flow velocity (black arrows) for the BH approach and (b), (d) for the SB approach for two frontages of the Merz Court building – north (a, b) and west (c, d).

3.4.2 Comparison of modelled flow depths

To examine the differences between generated flow paths from the two approaches, two small areas of the domain were extracted. Firstly, Figure 3.7 illustrates the flood depth maps with the two techniques around Newcastle University main campus for a storm event of 60min with 100 years return period. On the left-hand map, a major surface flow path from the (mostly culverted) Pandon Burn can be seen which is blocked by the Merz Court building (distinctive trapezoidal shape with central open space) and subsequent buildings, whereas the flow overtops every building in the SB model in the right-hand map. Figure 3.8 shows photographs taken during the storm event which provide detailed validation of the modelled depths upstream of Merz Court.

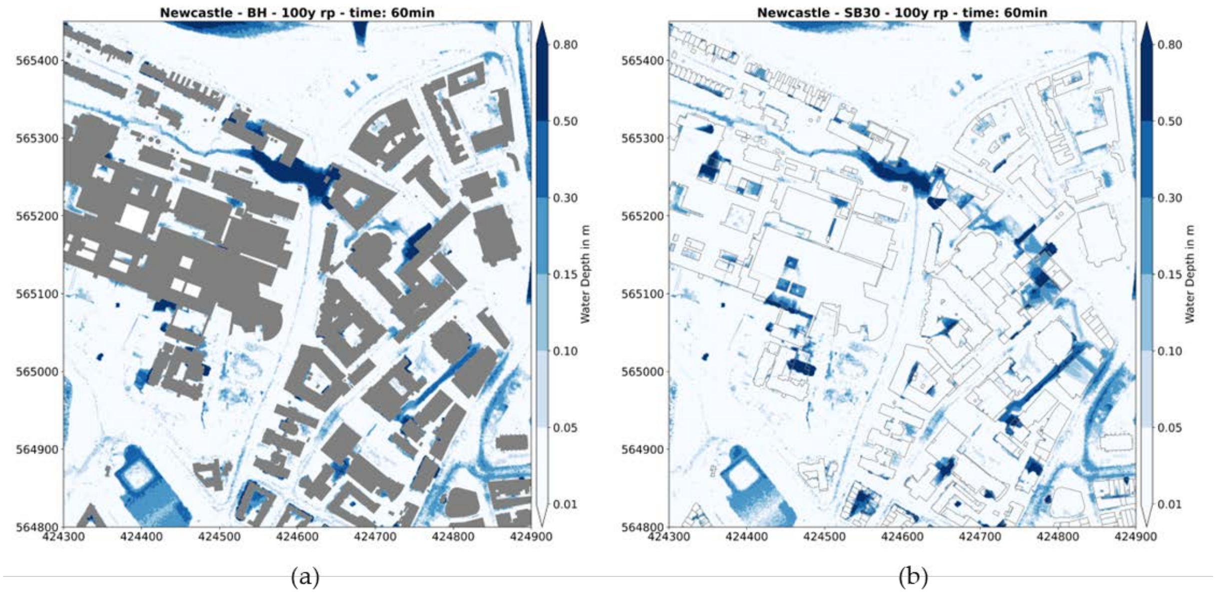

Figure 3.7 Flood depth from CityCAT simulations around Newcastle University main campus. Left graph (a) is with BH and the right graph (b) with SB approach.

Figure 3.8 Observation points upstream of Merz Court building for the validation of flood paths with BH & SB approaches.

Figure 3.9 shows results from CityCAT simulations with BH and the SB approaches and it is apparent that with the SB the flood water flows over/through the Merz Court building, and a deep pond was created in the roof on that building. While the building is documented as having suffered major flood ingress in the 2012 event, the observed flooding closely corresponds to that generated by the BH method, including the deep upstream ponding (see Figure 3.8).

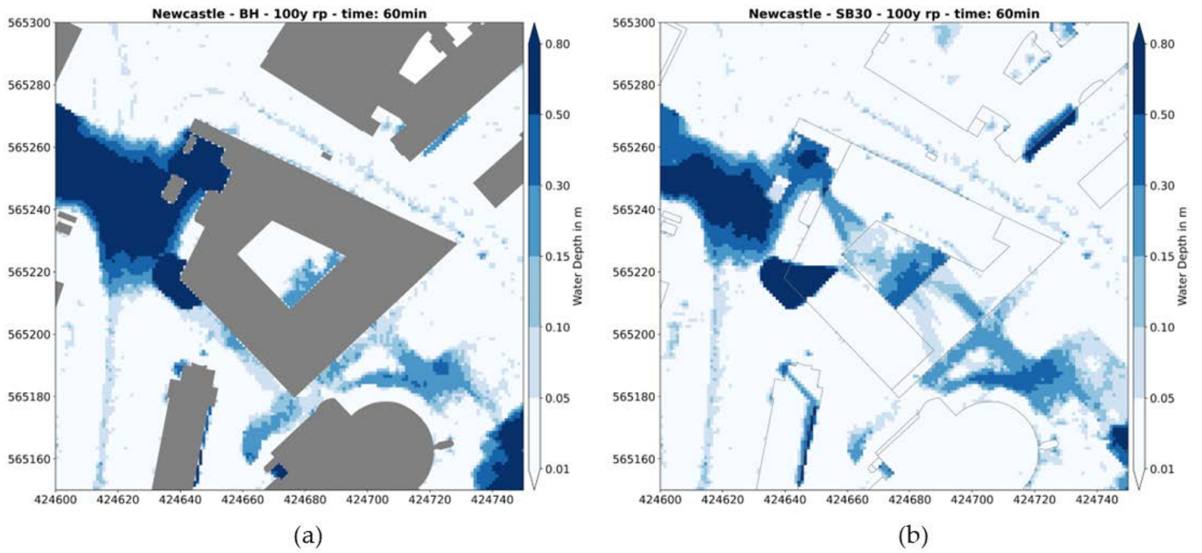

Figure 3.9 Flooding in Merz Court building at Newcastle University for a storm event of 60 min duration and 100 years return period with (a) *'Building Hole'* and (b) *'Stubby Building'* approaches.

Results from a second area on the city centre which was subject to severe flooding are shown in Figures 3.10 & 3.11 where it can be seen that the SB model again generates flood flows which overtop and flow *'through'* buildings. This creates small *'ponds'* on buildings due to *'errors'* in the DTMs, as discussed in Section 3.4., which are then characterised as high flood risk, which is not physically realistic. These *'errors'* in the DEM are likely to be associated with buildings located on sloping ground (around 1 in 5, 20% gradient in this instance) due to poor identification of a mean *'ground level'* for the area to allow interpolation within the building outline.

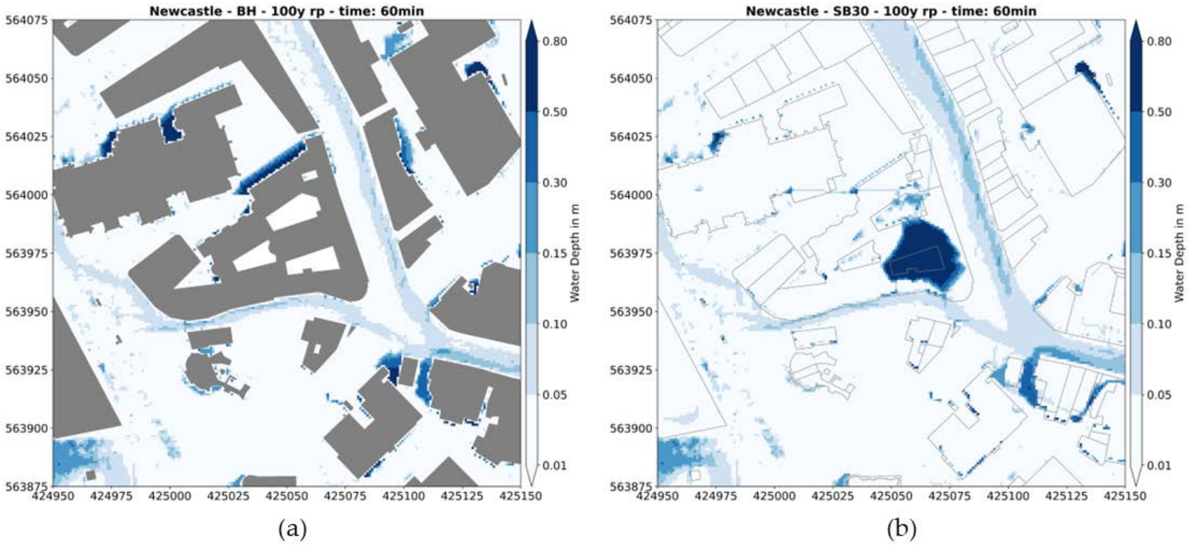

Figure 3.10 Flooding in a steep location of the city, Dean Street, with (a) BH and (b) SB approaches.

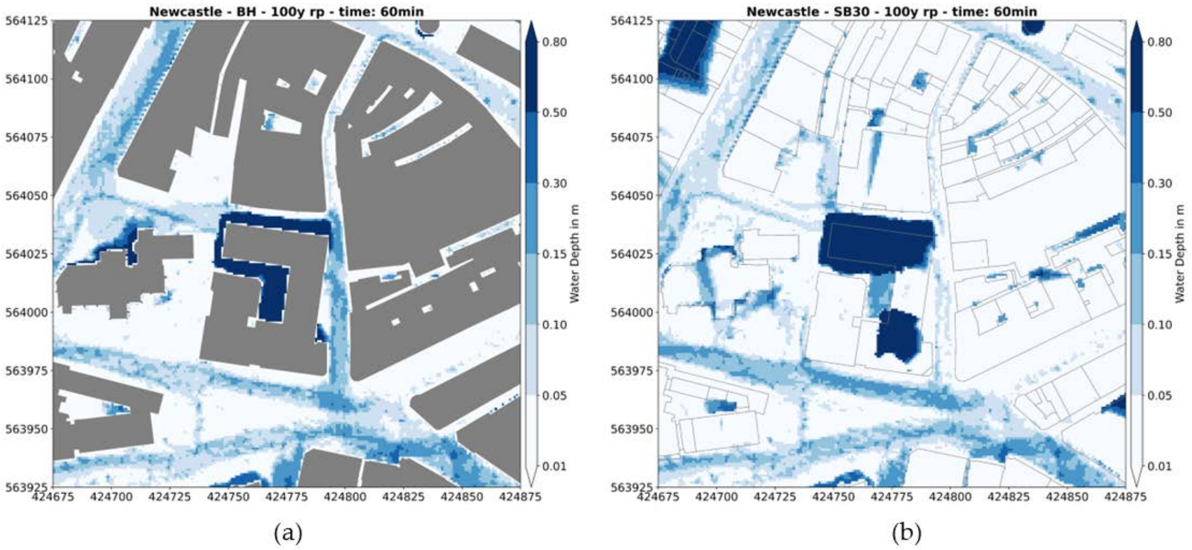

Figure 3.11 Flooding at a second location with steep slopes, Westgate Street, with (a) BH and (b) SB approaches.

3.4.3 Flood hazard to urban features

In order to identify the critical differences to water flowpaths between the two approaches, flood depth maps simulated with the *'Building Hole'* were subtracted from those with *'Stubby Building'* and are shown in Figure 3.12. It can be seen that, systematically, blue grid squares (positive depth difference) are where BH approach depths are greater than corresponding SB depths (e.g. on roads), (BH depths > SB) and red grids are generally on buildings where SB flowpaths exist and BH are absent (SB depths > BH). With the *'Building Hole'* the flood water is forced to flow around the buildings, whereas with *'Stubby Building'* the flow paths are different, as the flood water overtops almost 35% of the buildings in this area.

The total number of flooded buildings for each model is shown in Table 3.3. The BH models present the largest number of inundated buildings (high flood risk) in the AOI in contrast with the SB30 models where the buildings in the high-risk class are around one third less of the totals due to the flood water which spreads more frequently onto buildings. Thus, SB30 models underestimate the flood risk to buildings due to the widespread ingress of water.

Table 3.3 Number of buildings inundated per scenario by each model.

Models	Low	Medium	High
BH - 2012	3941	646	835
SB30 - 2012	4122	928	372
BH - 50y rp	4102	638	682
SB30 - 50y rp	4194	939	289
BH - 100y rp	3945	674	803
SB30 - 100y rp	4079	993	350

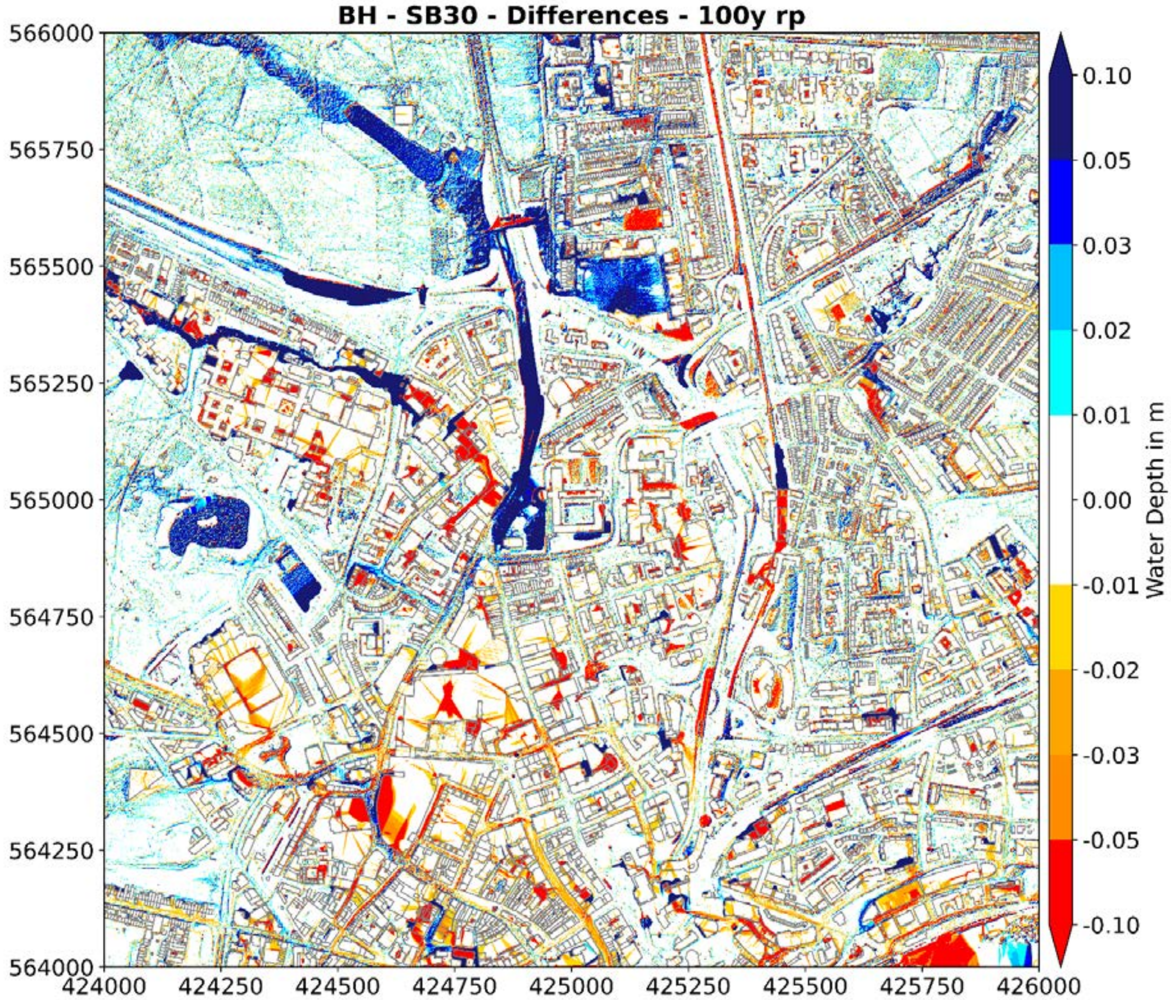

Figure 3.12 Differences in water depth between the BH and the SB models at Newcastle City Centre. Red is where SB predicts larger water depths than the BH and blue is vice versa.

An artefact of the SB approach is that systematic differences in ground level across the domain are introduced, so generating increased gradients (at building outlines). Figure 3.13 shows the distribution of local slope calculated as the maximum elevation differences between a grid square and its four neighbours. It can be seen that the initial DEM is smoother in contrast with the generated DEM for the *'Stubby Building'* approach, where a variation in elevation has been introduced between 0.20 to 0.40 m.

This is further evidence that water flow will be modified in the simulations, with consequent change in flow paths and velocities.

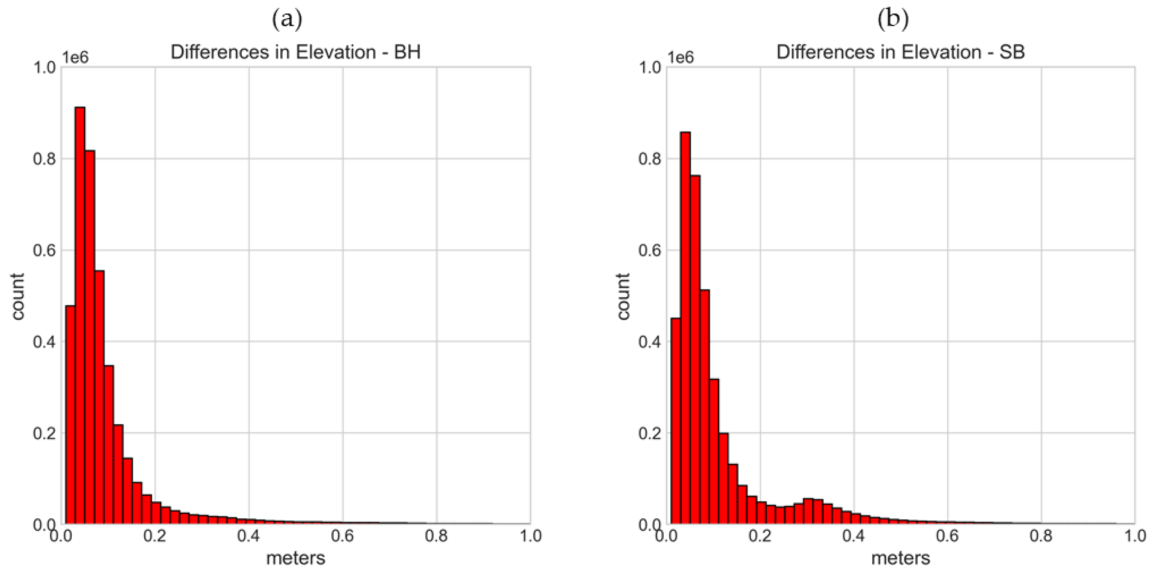

Figure 3.13 Distribution in grid-by-grid elevation differences for (a) BH approach (original DEM); (b) the generated DEM for SB approach.

3.4.4 Validation of the '*Building Hole*' and the '*Stubby Building*' against a real storm event

The approach taken here to validation of the models is to estimate the flood exposure of each building and compare it with flooding in areal observed event. In a recent study by Bertsch et al. (2022), a new tool was developed to assess exposure of buildings to flooding and validate against a real flood event in Newcastle upon Tyne, UK. The '*Building Hole*' approach was used for the representation of buildings and the model successfully predicted between 68% and 75% of the surveyed buildings that suffered from flooding.

In this section, a validation between the BH and the SB approaches will be presented for the buildings of the Newcastle University campus that suffered from different causes of flooding (from the surface and from the drainage system) during the storm event on the 28th of June 2012, also called the '*Toon Monsoon*'. Of 100 buildings on the campus 20 were flooded and are presented in Table 3.4 with a description of the flooding mechanism. The location of the buildings and the dominant flooding mechanism are shown in Figure 3.14.

Additionally Figure 3.15 shows the water depth modelled with the BH approach in four different locations where observed data existed. The CityCAT model correctly identified 80% (16 of the 20 buildings) of the affected buildings. Exposure calculated with water depths modelled with the *'stubby'* approach is presented in Figure 3.16 showing an underestimation of flood impact as the model was able to identify only 15% (3 of the 20 buildings) of the exposed buildings.

Table 3.4 Flooded buildings at Newcastle University campus during the 2012 flood event.

A/A	Buildings	Description of damages.
1	Bio-Medical Research Building (BRB)	Flood water travelled through building from central Courtyard area at CAV to Car Park next to NHS Estates.
2	Merz Court	Significant flooding. Flood water travelled through building from Queen Victoria Road to Claremont Walk.
3	Philip Robinson Library	Significant flooding to basement areas from surcharging drains and direct water ingress from external areas.
4	Ridley 1	Significant water ingress to entrance area adjacent to Lovers Lane.
5	Agriculture	Flooding to lift pit at basement level.
6	Claremont Sports Hall	Entrance area only. On route of Pandon Burn.
7	Hadrian Building	Flooding to lift shaft and basement level. Significant surface water flooding to service road.
8	Herschel	Flooding to lift shaft.
9	Herschel Annex	Flooding at basement level from duct.
10	King's Gate	Minor flooding to plant rooms adjacent to service road. Considerable surface water flooding on service road/outside entrance door.

11	Music	Water ingress from service road to basement areas.
12	Students' Union	Surface water flooding to lane outside and lift pit and basement areas.
13	Armstrong Building	Significant flooding to basement area of Music Practise Rooms. Drains back flowed into area, also unusual drainage layout.
14	Windsor Terrace 19/20	Drainage could not cope and flooded basement areas.
15	Windsor Terrace 21/24	Drainage could not cope and flooded basement areas.
16	Claremont Building	Some basement flooding from drains / groundwater?
17	Claremont Tower	Backflow from drainage causing minimal damage.
18	Grand Hotel and Commercials	Basement level of Blackwell's Bookshop and residential accommodation from back flowing drains.
19	Old Library	Drains back flowed into building, causing considerable damage to ground floor area.
20	Percy Building	Basement area flooded due to surcharging drains.

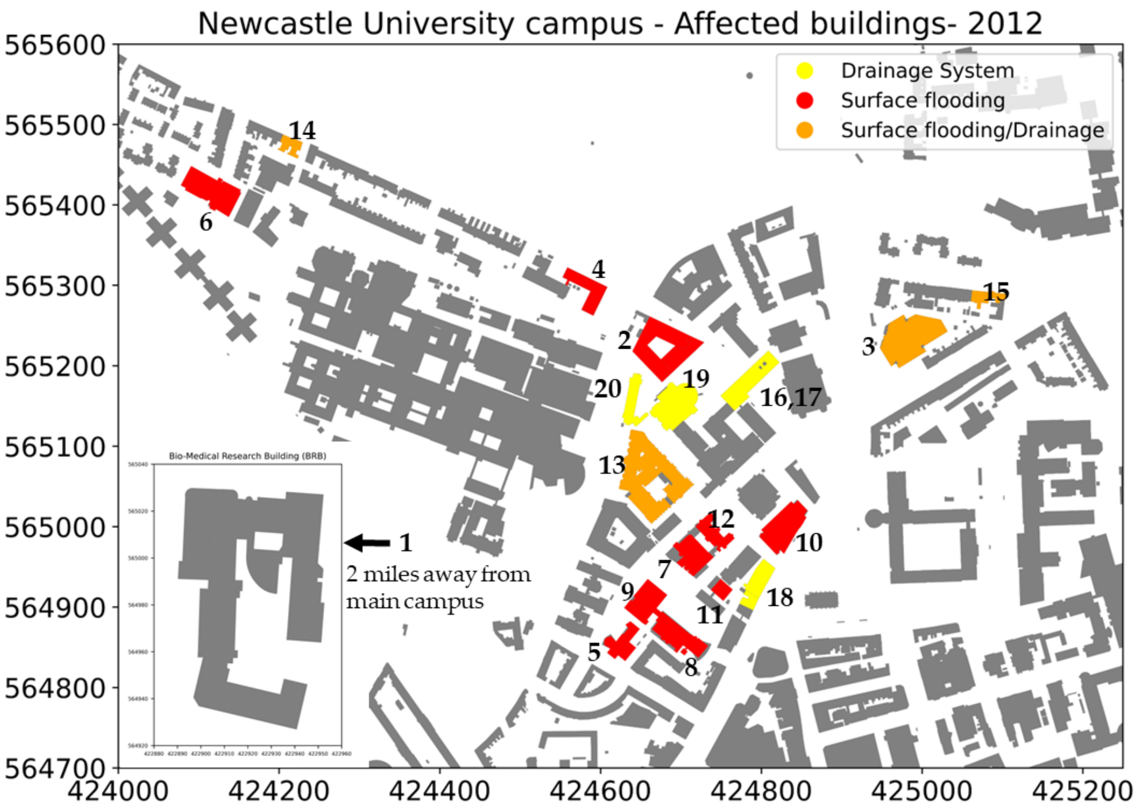

Figure 3.14 The flooded buildings from the *'Toon Monsoon'* storm event and dominant mechanism of flooding.

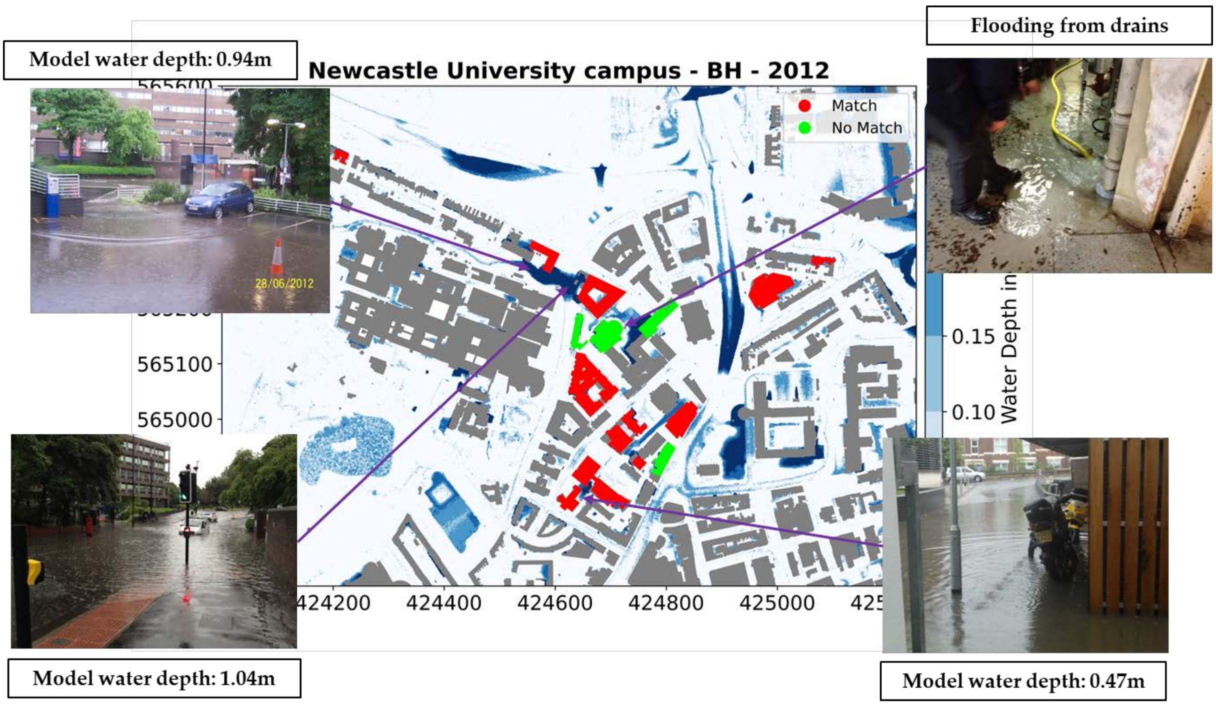

Figure 3.15 Validation for the *'Building Hole'* approach.

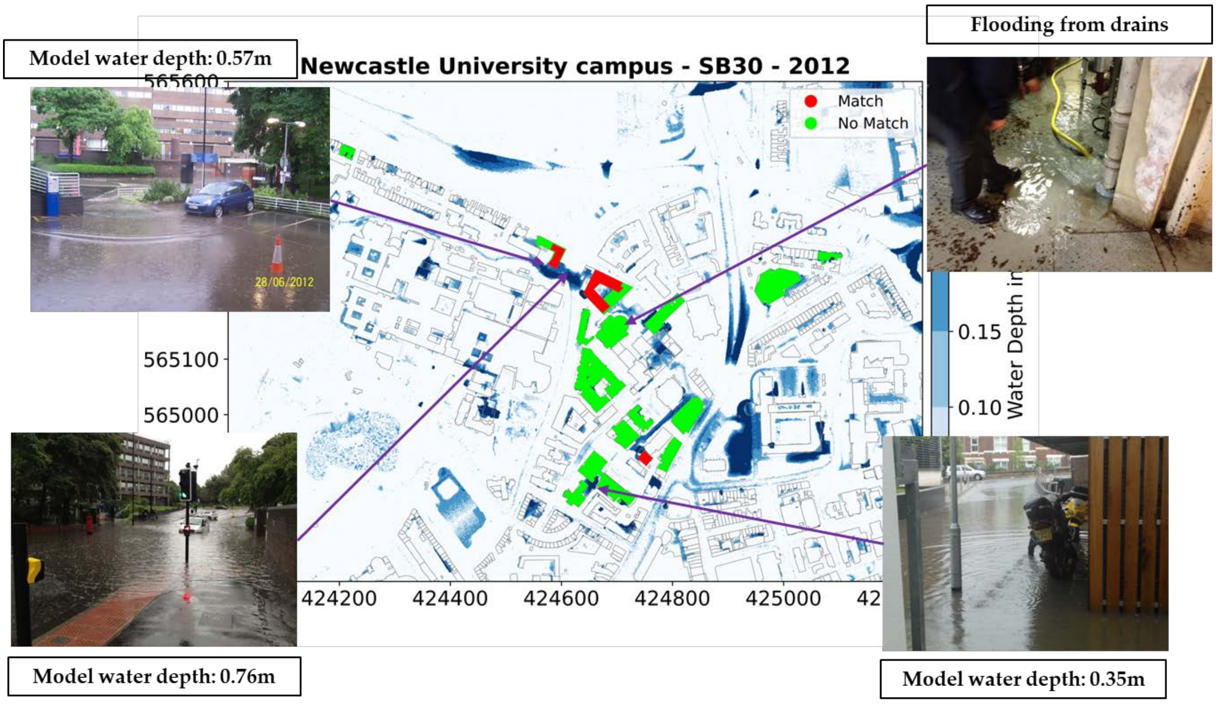

Figure 3.16 Validation for the *'Stubby Building'* approach.

3.5 Improved application of the '*Stubby Building*' approach

An important question in modelling practice is why a value of 30 cm is used to represent building heights in flood models, and how this could be improved in order to obtain more realistic results. The *'Stubby Building'* (as described in section 3.2.2.) approach increases the building threshold, usually by 30 cm, and in some cases, an increased hydraulic roughness to the building footprint (Environment Agency, 2021; SEPA, 2018; TUFLOW, 2018). The schematic framework in Figure 3.17 highlights the issues of the modeller and the actions that could be taken before using the *'Stubby Building'* approach. DEMs are mostly used in pluvial flood modelling but according to McClean et al. (2020) there are instabilities in the accuracy of the elevation (*'errors'*), where a modeller should first think of an effective way to identify them and correct them inside the model to avoid the overprediction of flooding in places with minor hazards.

Furthermore, there is a range of actions that could improve the model using the *'stubby'* approach. An obvious action is to increase the elevation of the building from 30 cm, if the model numerical stability allows this. Otherwise, the modeller could avoid using this approach, or to flag the results as low confidence, in areas with steep slopes, as these are more likely to create conditions for overtopping the *'stubby'* platforms due to interpolation *'errors'* within the building footprint. A further option is to generate a uniformly flat roof in every building in the study area, thus avoiding relative low points for water to overtop. Section 3.4.2. will describe methods to *'clean'* the DEM and thus improve the *'Stubby Building'* approach.

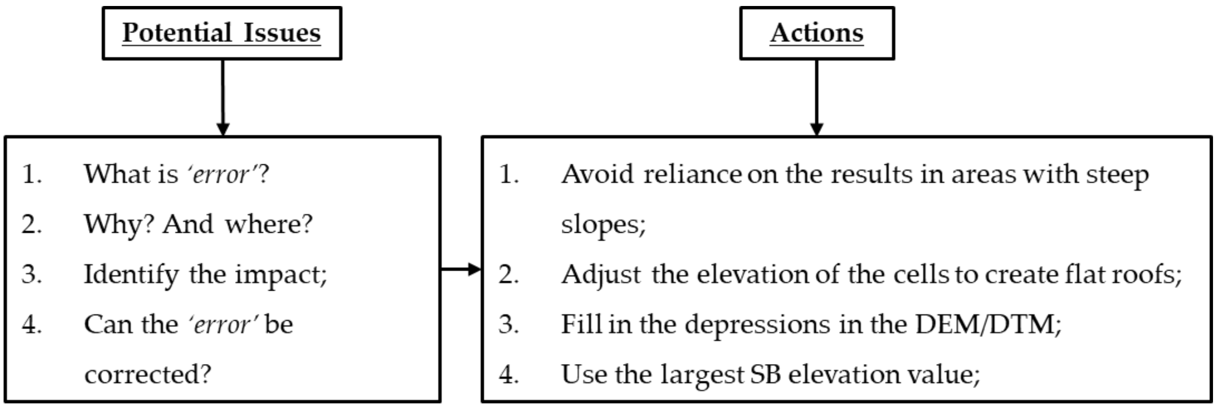

Figure 3.17 A framework with suggested steps to improve the *'Stubby Building'* approach.

3.5.1 *'Stubby'* models

To assess the magnitude of the DEM errors in using the SB approach, and to attempt to identify a good choice of platform height as a trade-off with DEM error, a range of scenarios was generated with different platform heights. While this height is essentially selected in industry models to maintain numerical stability, it can also be considered as representing an ingress threshold. The variant models have been set up as in Section 3.2.4. but as well as 30 cm, the ground elevation of the DEMs was raised in the buildings' footprints by 20, 40, 60, 80, and 100 cm. Figure 3.18 presents the generated variants of SB, and it can be seen in Figures (a – SB20), (b – SB40) & (c – SB60) that the water more frequently spreads over the buildings, while in Figures (d – SB80) & (e – SB100) there is as expected a reduction of spread to flood water in buildings which is more realistic. Newgate Street in Newcastle city centre was selected to validate the behaviour of the different thresholds for the *'stubby'* models due to the complexity of the topography and the high slopes of the ground.

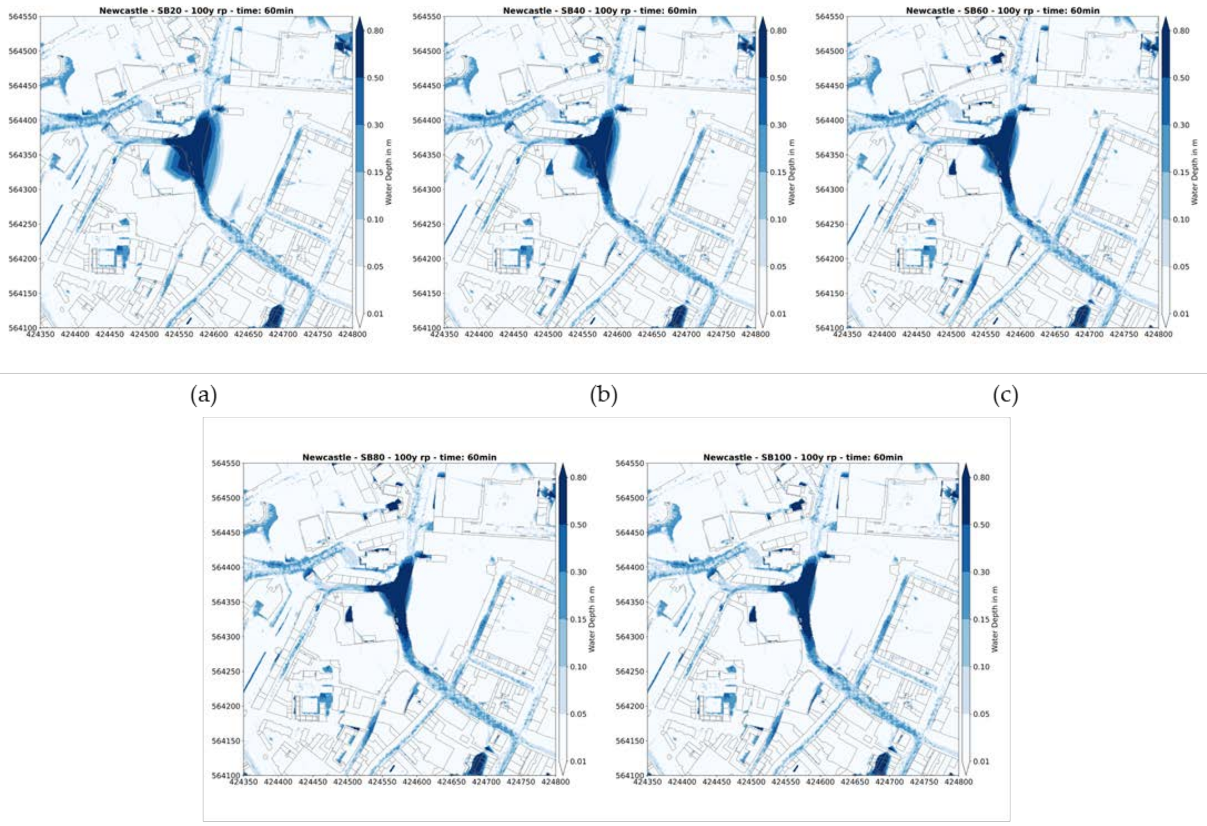

(a) (b) (c)

(d) (e)

Figure 3.18 Water depths at Newgate Street, Newcastle city centre, for a storm event of 60 min and 100 years return period with the generated *'stubby'* scenarios. a) model refers to *'stubby'* approach with a raised platform of 20 cm; b) 40 cm; c) 60 cm; d) 80 cm; e) 100 cm.

3.5.2 A *'cleaned Stubby'* approach

In this section, a new corrected version of *'Stubby Building'* is discussed. After the first simulation with the *'stubby'* approach, the results have shown that there are anomalous depressions on some building footprints, with resultant flood depths above 1 m. These anomalies are assumed to arise from lack of robustness in the interpolation algorithm used to assign a *'ground elevation'* to building footprints when converting from DTM to DEM in areas with high gradient. In order to develop a corrected DEM accounting for this systematic error source, the buildings with 1 m (or more) of inundated depth within the footprint were first identified. A total of 191 urban features in the AOI were found (highlighted in red in Figure 3.19). Next the elevation of the DEMs was raised to the 95 percentile values of the elevations around the building perimeter to create flat roofs to these buildings. Then, a step of 30 cm was added to all buildings in the AOI, including the *'cleaned'* buildings with the flat roofs, and the CityCAT model was run again with these new variants. This correction or cleaning of the DEM can be an important step in the modelling, as it removes spurious occurrences of potentially large flood depths and avoid overestimating flood risk in a complex urban area with elevation instabilities.

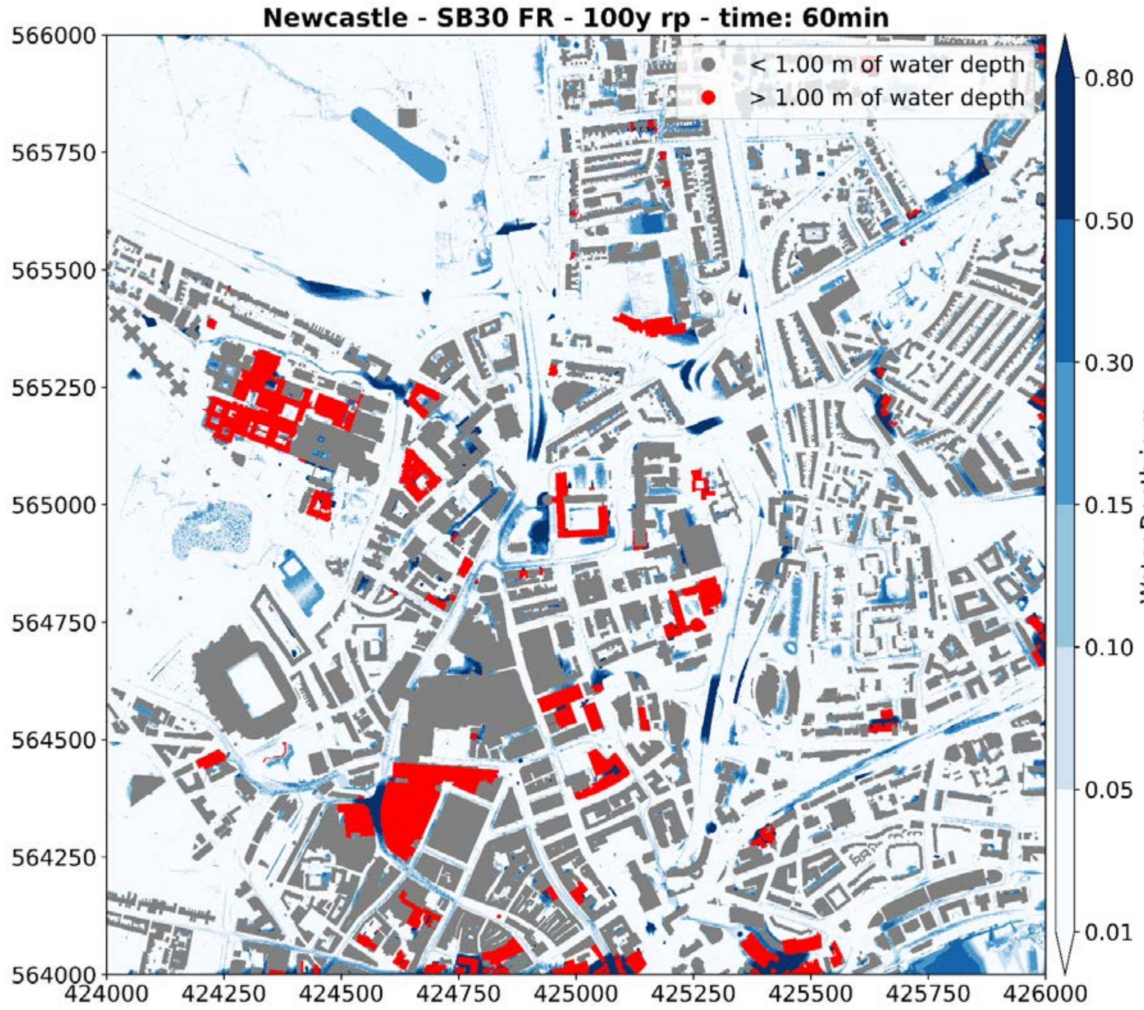

Figure 3.19 The identified buildings with depressions in the AOI.

To illustrate the effect of the various modified *'stubby'* treatments, the case of the Merz Court building is examined again in detail. Figure 3.20 shows flood depths in the area around the flooded Merz Court building at Newcastle University with the three different approaches: BH, SB and *'cleaned'* SB with flat roofs. It can be seen the *'cleaned'* variant model SB30 FR – 100y rp (Figure 3.20(c)), shows a more realistic condition, closer to the BH – 100y rp (BH) model – *'Building Hole'*, (Figure 3.20(a)) due to the generation of a flat roof and the correction of the elevation.

Table 3.5 List of codes for the modified *'stubby'* models.

SB20	The *'Stubby Building'* method with 20 cm threshold
SB30	The *'Stubby Building'* method with 30 cm threshold
SB40	The *'Stubby Building'* method with 40 cm threshold
SB60	The *'Stubby Building'* method with 60 cm threshold
SB80	The *'Stubby Building'* method with 80 cm threshold
SB100	The *'Stubby Building'* method with 100 cm threshold
BH	The *'Building Hole'* method
SB30 FR	The *'cleaned Stubby'* method with flat roofs and 30 cm threshold

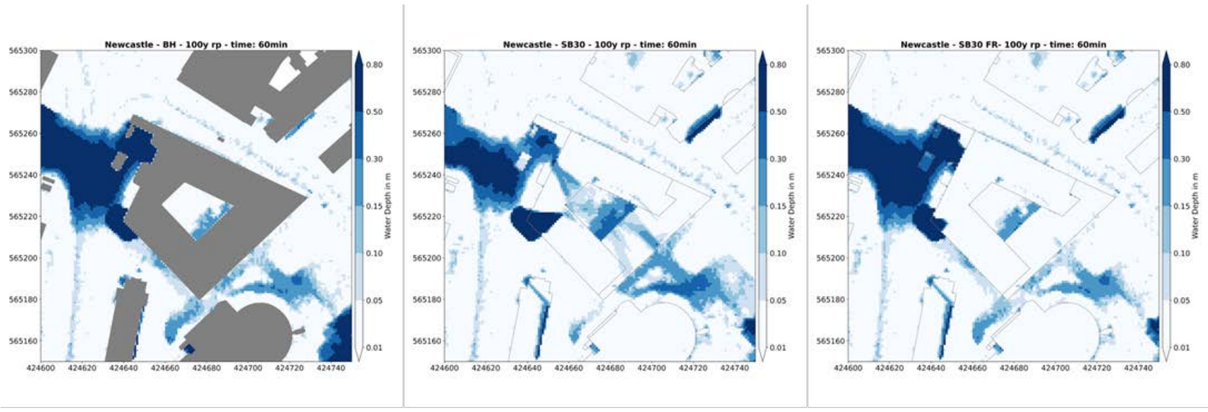

(a) (b) (c)

Figure 3.20 Flooding in Merz Court Building for a storm event of 60 min and 100 years return period with (a) BH approach; (b) SB approach; (c) the *'fixed'* version of *'Stubby Building'*.

While looking at individual buildings is helpful to understand the effects of different model treatments, most exposure analysis will be for larger areas with many buildings, so the total number of flooded buildings for all the *'stubby'* variant models has been calculated and is shown in Table 3.6. The models SB20 – 100y rp (20 cm threshold) and SB30 – 100y rp (30 cm threshold) generate the highest number of buildings at high flood risk due to the low threshold, while the total appears to reach a steady limit value above 60 cm threshold. While these total numbers are not closer to the BH benchmark value, the number of *'high risk'* is still a factor of two larger.

A comparison of the SB results with the more physically realistic BH approach shows that for the widely used 30 cm platform, an underestimation of some 34% in the identification of high flood risk buildings is evident, as shown in Figure 3.21 which highlights the buildings according to flood risk with BH and SB approaches. This difference is reduced by raising the platform height, but of course at the expense of introducing numerical instabilities into codes less robust than CityCAT.

Table 3.6 A total number of flooded buildings per scenario for each *'stubby'* model, and for the *'Building Hole'* approach for reference.

Models	Low	Medium	High
BH - 100y rp	3945	674	803
SB20 - 100y rp	4410	662	350
SB30 - 100y rp	4079	993	350
SB40 - 100y rp	3791	1291	340
SB60 - 100y rp	3649	1427	346
SB80 - 100y rp	3612	1465	345
SB100 - 100y rp	3612	1465	345
SB30 FR - 100y rp	4014	1053	355

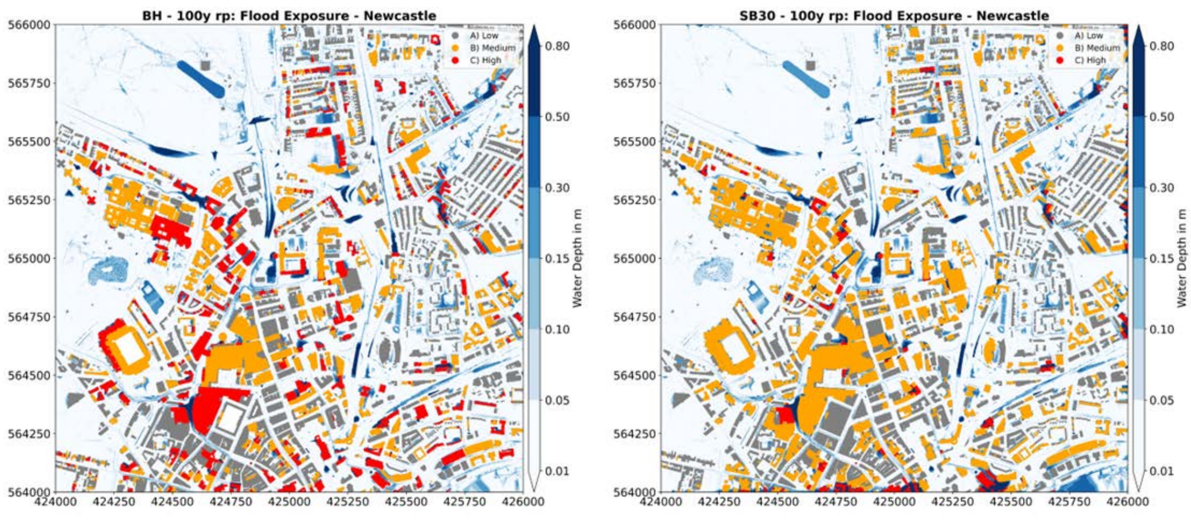

(a) (b)

Figure 3.21 Flood exposure maps with the (a) BH (model BH – 100y rp); (b) SB (model SB30 - 100y rp) approaches for the city centre of Newcastle, UK. Red is high risk, orange medium.

3.6 Conclusions

This chapter presents an analysis of the performance of two widely used approaches for the representation of buildings in hydrodynamic flood models and presents an improved method for the *'Stubby Building'* approach which corrects for common errors in DEM generation. For the first time, a direct comparison of the SB approach with the more realistic BH approach has been carried out and shows that the BH approach generates larger flood depths, as is to be expected since the SB approach allows re-distribution of deep water over building footprints and presents fewer flow blocking situations. The flood paths with the SB approach are more dispersed, resulting in more buildings being affected.

The velocity of flood water is also somewhat higher with the BH approach due primarily to larger flow depths (see Figure 3.6(a),(c) with *'Building Hole'*). The SB allows the water to flow more frequently over the buildings, and the direction of the water can be seen very clearly over and on top of them (see Figure 3.6(b),(d) with *'Stubby Building'*).

Furthermore, on some buildings, a *'pond'* is generated on roofs with the SB approach due to *'errors'* in the DEM which the modeller should check and correct before the simulations. An advantage of the *'Building Hole'* approach is that this task of checking and correcting the DEM is not required, as the area within the building footprint is simply removed from the model domain and does not require an interpolated elevation to be assigned.

Aside from *'errors'* caused by artefacts in the DEM, in general, the SB approximation underestimates water depths, and the highest category of flood risk in the urban fabric, due to unrealistic flow paths over-riding the building forms. The validation of the affected buildings on the Newcastle University campus showed that the difference between the two approaches for the classification of building flood risk is very large (80% for the BH and 15% for the SB). This large difference suggests that a modified version of the exposure tool is needed to correctly identify high risk buildings.

In conclusion, the *'Building Hole'* approach offers more realistic results which validate well against observed flooding where flow paths and flood depths are well captured by the model. The computational time and cost, especially in big urban areas with high resolution, to run a simulation is an important factor that favours the BH, due to fewer computational cells in the model (29% fewer cells). Additionally, it is simple and easy to identify buildings at high flood risk according to the water depth around their perimeter. An important advantage of this approach is that is suitable in any area, and especially for dense built-up areas, regardless of with the presence of steep slopes, in contrast to the *'Stubby Building'* approach which is suggested in this chapter to be more suitable for use in flatter areas.

Chapter 4. A cost-benefit *'source-receptor'* framework for implementation of Blue-Green flood risk management

4.1 Introduction

Surface water flooding is a major and increasing hazard in cities, where assets, properties, and humans are directly affected. The extent and severity of the damage caused by urban floods, around $40 billion per year according to OECD (2016), is a product of both the intensity and the duration of a storm and its interaction with the complex flow paths of a city on the surface and below ground. Extreme storm events are expected to increase worldwide and therefore constitute a critical issue in flood risk analysis and the design or management of critical adaptation solutions is a necessity to reduce and, in some cases, control the flow and the volume of flood water in the urban fabric (Galiatsatou & Iliadis, 2022).

It is expected that by 2050 almost 75% of the world's population will live in urban areas (Liu et al., 2014). The combination of climate change and the increasing urbanisation with the frequency of storms will lead dense areas to improve the current flood mitigation strategies and the drainage system to create resilience cities against future floods and protect humans, assets, infrastructure, and properties from damages (Bertilsson et al., 2019; Carter et al., 2015; Vercruysse et al., 2019). Nowadays, drainage systems in cities are under pressure due to urbanisation and are not able to withstand higher intensity and frequency of storm events (Eulogi et al., 2021; Rosenzweig et al., 2018). As a result, flood risk management adaptation solutions are currently blocked by the lack of affordable and feasible strategies. In some studies of adaptation strategies at local scales with Sustainable Urban Drainage Systems (SuDS) (Fletcher et al., 2015) and larger scales (Li et al., 2018) there is a non-adaptation efficiency apparent between them (Ernst & Preston, 2017; Kuller et al., 2017; Preston et al., 2015) due to the lack of information and uncertainty of the capacity, the performance and the location of these systems (Hoang & Fenner, 2016; Mailhot & Duchesne, 2010; O'Donnell et al., 2017; Schuch et al., 2017). A recent study by Oladunjoye (2022) asserts that SuDS could be a crucial component of flood mitigation due to the capacity to decrease runoff volume and lower the danger of floods by controlling the flow in natural infiltration systems.

While the potential of more realistic and affordable solutions such as Blue-Green Infrastructure (BGI) or Natural Flood Management (NFM) is increasingly recognised, the barriers to their uptake are formidable, as effective city-wide schemes require significant investment in implementation in multiple locations if they are to be effective, rather than opportunist and piecemeal schemes where re-development permits. A more systematic city-wide approach is therefore required, with a clear demonstration of the overall cost and benefits, before a city planning authority will be prepared to invest. Such an approach requires an urban flow simulation with sufficient detail to resolve not only the exposure (and subsequent benefit form risk reduction) at property level, but also the highly localised runoff sources and flow paths where BGI can be implemented. This chapter therefore sets out to advance a new and systematic methodology combining an advanced high-resolution hydrodynamic flood model with a source-receptor benefit cost methodology.

Urban flood models have been developed over the last decade (Glenis et al., 2018; Guo et al., 2020; Sanders, 2017; Teng et al., 2017; TUFLOW, 2018) to better understand the flood dynamics, better estimate the water flow paths and the flood depths around cities, and can increasingly be used to investigate the connectivity of flood management options and interventions with the characteristics of a city (impermeable surfaces, topography, storms etc). If applied at high resolution and large enough scales, these hydrodynamic models can provide accurate analysis of future flood risk, and with the collaboration of local authorities can be used to design flood mitigation solutions by locating areas at high flood risk and adding interventions in critical areas to reduce pluvial or fluvial flooding (Alves et al., 2016; Casal-Campos et al., 2015; Dawson et al., 2020; Hewett et al., 2020; McKenna et al., 2023; Morgan & Fenner, 2019). This chapter demonstrates the use of such an advanced high resolution system, the CityCAT hydrodynamic model (Glenis et al., 2018), in a systematic framework to locate optimal areas where interventions can be made, accounting not only for their cost, but also their benefit in reduction of damages to properties from flooding in a city scale catchment. Recent studies have begun to explore methods of optimising location of BGI interventions, such as Birkinshaw and Krivtsov (2022) who established that for a particular urban setting locating a retention pond further upstream was most effective, and that storage in the lower part of the catchment could actually increase flood risk. There is however a need to more systematically manage the assessment of such options, so a cost-benefit driven *'source-receptor'* analysis is developed here to locate areas at high flood risk, how many buildings are impacted by flooding, what information we extract from the model and where critical interventions should be added to the model to most efficiently reduce cost and flood damages.

4.2 Methodology

4.2.1 Case study

The novelty of the cost-benefit driven *'source-receptor'* flood risk framework offers the flexibility for designs to be developed in every urban area or catchment with any suitable resolution of the Digital Terrain Model (DTM) (according to Iliadis et al. (2023a), a DTM resolution of less than 5m is required to capture all the required information for this framework) to any commercial or research flood model. The required information and inputs of the methodology are: a) the Digital Elevation Model or Digital Terrain Model (DEM/DTM) of the study area; b) the buildings (classification, e.g. commercial or residential) and green spaces; c) rainfall data - the construction of IDF/DDF curves or storm profiles are needed to specify a range of flood hazards and d) flood damage estimates for commercial and residential buildings of the study area. In this chapter, the campus of Newcastle University and the adjacent city centre are subject to a major flood risk from upstream and suffered major damages during the 2012 *'Toon Monsoon'* thunderstorm event (Kutija et al., 2014). The area is characterised by historic and commercial buildings, residential properties, and green space with the most important being parkland areas, primarily the Town Moor and Leazes Park, which cover a significant extent of the study area. Previous studies have been made in relation to pluvial flooding after the historic storm, on the 28th of June 2012, to add BGI in critical places in order to protect the assets (Fenner et al., 2019; Kilsby et al., 2020; O'Donnell et al., 2020; Wright & Thorne, 2014).

The catchment has been modelled using CityCAT (Glenis et al., 2018) for storm events spanning 1 in 10-year to 1 in 100-year return period with a duration of 60 min. Figure 4.1 shows the study catchment with buildings colour coded according to use, and land use. The resolution of the DEM and computational grid is two metres (area of each grid square is $4m^2$) and was derived from Lidar (2016). The total number of computational cells in the domain is 1,005,904 covering an area of 5.30 km^2. The numerical grid was generated following the *'Building Hole'* approach where building footprints are removed from the computational domain by generating a non-flow boundary around them, which is more realistic than widely used approximations such as the so-called stubby-building approach. Rainfall on to the building is retained by re-distribution to the nearest surface grid square (for a full description, see Iliadis et al. (2023b)).

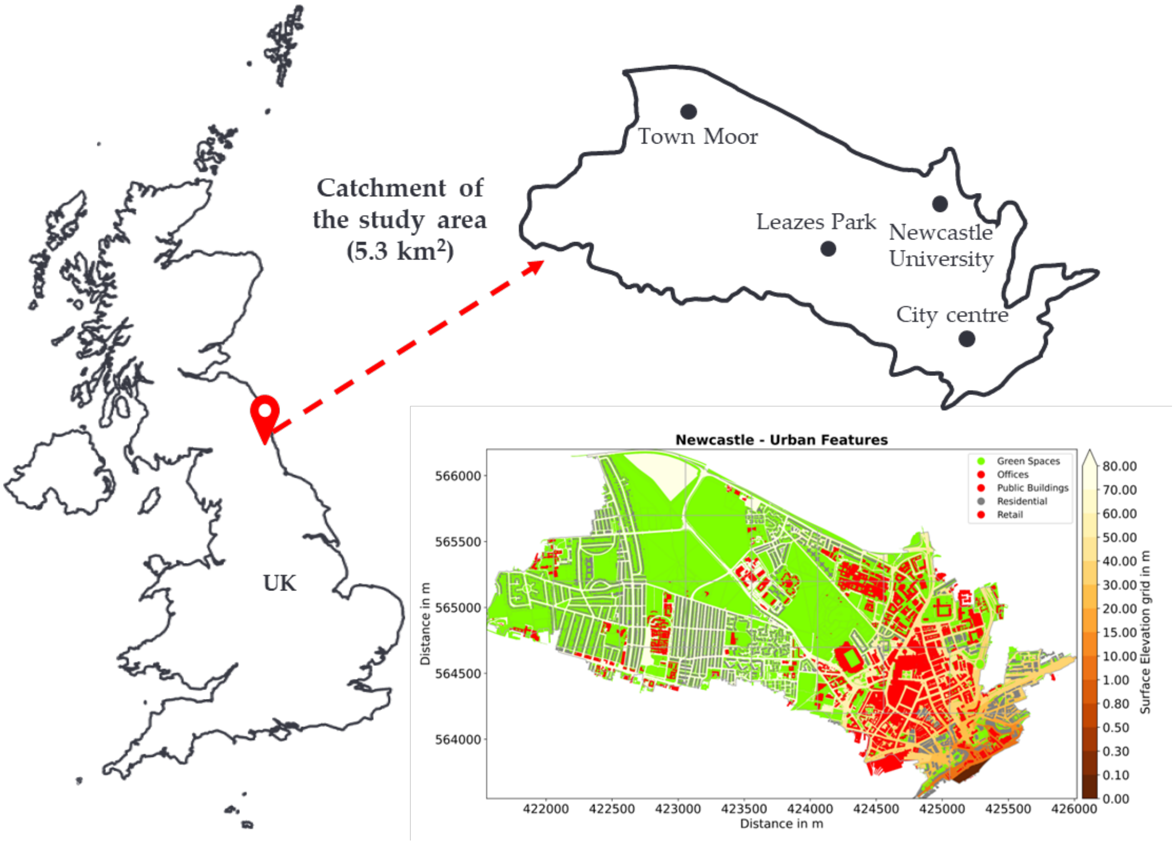

Figure 4.1 Overview of the study area in Newcastle upon Tyne, UK. Grey represents residential buildings, red commercial (offices, public buildings, retail), green is permeable areas, and brown to yellow shading the ground surface elevation.

4.2.2 A cost-benefit '*source-receptor*' flood risk framework

A powerful way to identify areas contributing to the total flood extent during a simulated event is the *'source-to-impact'* flood analysis based on a systematic cell dependency applied by Vercruysse et al. (2019) and Dawson et al. (2020) for the urban core of Newcastle upon Tyne and by Ewen et al. (2013) for the river Hodder catchment in the northwest England. The analysis of Vercruysse et al. (2019) presented a four step methodology to capture the flow paths and identify the location at high flood risk. They considered the differences of modelled maximum water depths generated by subtracting the baseline scenario with the cells without rainfall of the catchment, and four spatial prioritisation criteria to identify the best cells in which to add interventions. In many cases, maximum values are not suitable for this purpose due to the instabilities in the accuracy of elevation (*'errors'* in the DEM/DTM) which can result in the overestimation of flood values in places with minor hazard (Huang et al., 2022; Iliadis, Glenis, et al., 2023b; McClean et al., 2020).

The framework developed in this chapter combines extreme rainfall information, flood dynamics and the cost-benefits of flood risk management in an urban area. The methodology consists of five steps to (i) identify the water flow paths; (ii) capture the rainfall for a range of different magnitude storm events; (iii) categorise buildings at significant flood risk; (iv) calculate the damages from flooding; and (v) add interventions in critical high-risk locations upstream or downstream prioritised according to their cost-benefit. The steps of the cost-benefit *'source-receptor'* framework are detailed below:

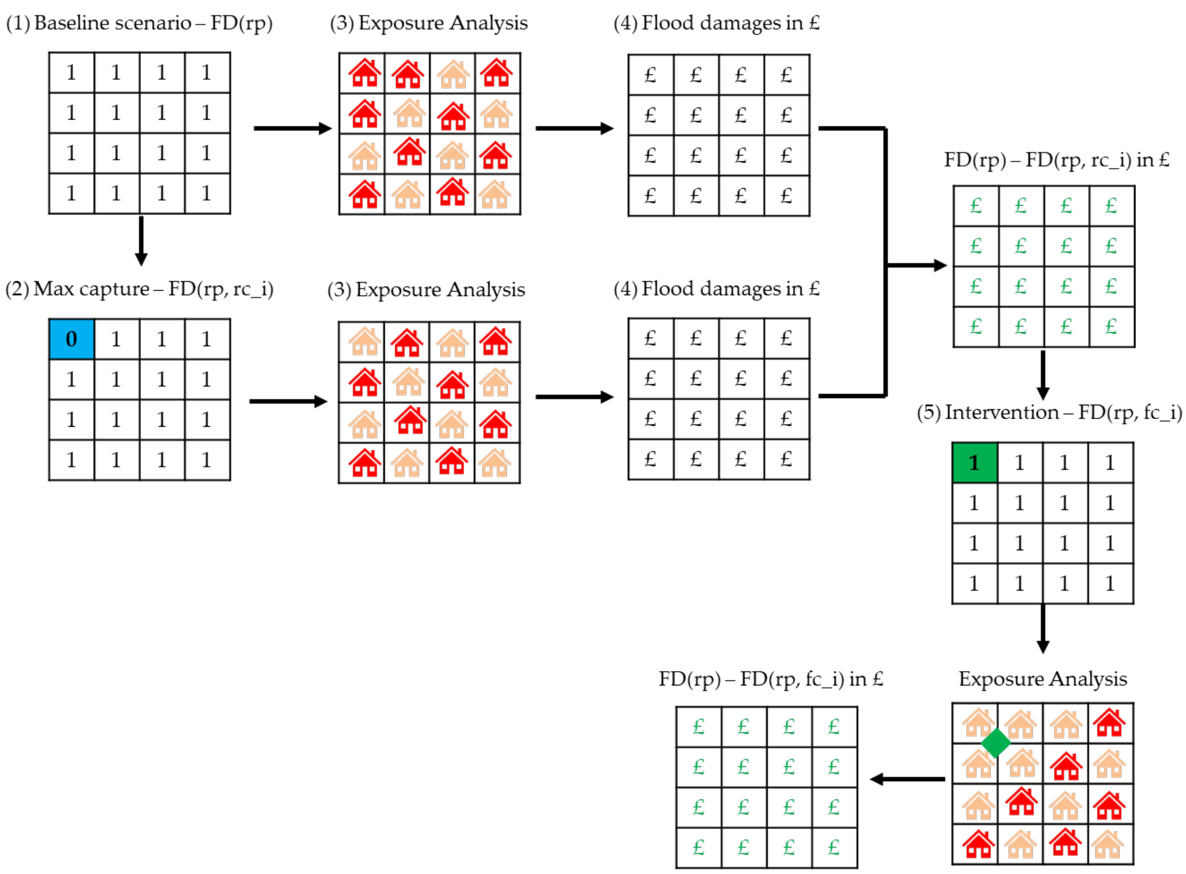

Figure 4.2 Schematic workflow of the cost-benefit '*source-receptor*' flood risk methodology.

1. *Divide the study area into approximately equal size cells and classify the type of buildings;*

2. *Run the CityCAT model to generate flood depths for equal rainfall across all cells for the four different storms – Baseline Scenario FD(rp), where FD is the flood damages and rp is the return period of the storm;*
3. *Turn off rainfall in individual cells – we refer to this as Max Capture FD(rp, rc_i), where rc_i is a rainfall cell and i = 1..Total number of rainfall cells;*
4. *Classify the buildings according to their flood risk (exposure analysis) and calculate the flood damages for the baseline scenarios and the max capture scenarios;*
5. *Calculate the benefit by subtracting the max capture scenarios damages from the baseline scenarios flood damages FD(rp) – FD(rp, rc_i);*
6. *Add interventions to cells (such as permeable pavements, water butts, green roofs, storage ponds etc) FD(rp, fc_i), where fc_i is an intervention (or "feature") cell and i = 1..Total number of intervention cells;*
7. *Classify the buildings according to their flood risk (exposure analysis) and calculate the damages;*
8. *Compare the baseline scenarios with the intervention scenarios to identify the best cost-benefit solution to reduce flooding FD(rp) – FD(rp, fc_i);*

The outcomes of the analysis are of course dependent on the size of the cells within the grid, the spatial resolution of the DEM/DTM, the type of buildings and the available green space in the study area. The first step is to divide the catchment into equal cells, twenty-three, with an area of 500m × 500m approximately which would be considered as *'source area'* for the surface runoff and classify the type of buildings (commercial and residential) in the study area. The second step is to run the CityCAT model to generate the baseline scenario (*FD(rp)*) for multiple storm events: here four different storm magnitudes were used, which cover the range of storms required to estimate the flood exposure of the buildings, and the damages from flooding in the study area. We use storms corresponding to 1 in 10-year, 1 in 20-year, 1 in 50-year and 1 in 100-year (similar to the historic storm *'Toon Monsoon'*) return period with a duration of 60 minutes. The third step is to one-by-one switch off the rainfall in every cell of the study area (*FD(rp, rc_i)*) and then run the CityCAT model multiple times (i.e. one run per cell per storm scenario, a total of 92 runs). This represents a total *'capture'* of the rainfall which means that there is no runoff from that cell. Moreover, the fourth step is to estimate the flood exposure to buildings and the flood damages per max capture scenario. In addition, the next step is to compare the baseline flood damages with the max capture damages by subtracting both for every cell (*FD(rp) – FD(rp, rc_i)*). Then, this cost-benefit step and the available green space in every cell allows ranking the areas from high-priority to low-priority cells to add adaptation solutions to mitigate runoff.

A range of interventions such as permeable pavements, water butts, green roofs, and storage ponds (SuDS) can be explicitly represented in CityCAT. Hence, the next step is to locate the areas at high flood risk through the provided information from steps 1 to 5 and the connectivity between the damages, the available green space and flood source areas where interventions can be implemented (see section 4.3.3.) in order to add interventions to these cells/areas (*FD(rp, fc_i)*), and run again the model equal times as the added interventions for different storms, in this chapter permeable pavements and ponds in critical locations were used. Then, the new flood exposure to buildings and the damages are calculated to check the behaviour of interventions against multiple storms. Finally, the baseline scenarios are compared with the intervention scenarios (*FD(rp) – FD(rp, fc_i)*) to identify the best cost-benefit solution to reduce flood damages, and explore if the proposed adaptation options for their building are acceptable to local authorities and insurance companies to reduce damages, content the properties and increase their resilience against the direct contact of flood water (Priest et al., 2022).

4.2.3 Assessing flood risk – flood exposure to buildings caused by each grid square

The most important criterion of the cost-benefit *'source-receptor'* flood risk framework to locate areas at high flood risk is a novel flood exposure analysis (Bertsch et al., 2022) to estimate the flood risk likelihood to buildings by analysing the water depths adjacent to the building (i.e. a one grid square buffer). These depths could be analysed as the mean depth in a buffer zone around the building, or the maximum depth, or more robustly the 90th percentile depth (used in this chapter) to avoid undue influence of a single erroneous depth value. The buffer zone depends on the computational grid resolution, 2m here. If the depths exceed a threshold of 30 cm (see Table 4.1) then buildings can be classified as high, medium, and low risk. In addition, the buildings at low flood risk have been excluded here by assuming that the damages from flooding are minor in comparison to damages to buildings at high and medium risk.

Table 4.1 The criteria for calculating flood exposure likelihood for buildings.

Exposure Class	Mean depth (m)	90th percentile (m)
Low	<0.10	<0.30
Medium	<0.10	≥0.30
	≥0.10 - <0.30	<0.30
High	≥0.10	≥0.30

4.2.4 Flood damages to properties

In the UK, flooding causes average damages of £1.3 billion per year, the cost for flood defence is around £4.4 billion the last decade, and the properties at flood risk are more than 5.2 million in England alone (Craig, 2021; Environment Agency, 2022; UK Government, 2016). Hence, residential and commercial flood damage is a crucial case that the researchers, the local authorities, and insurance companies collaborate with each other to propose efficient and innovative solutions against flooding. The available buildings in the study area are commercial (retail, public buildings, offices) and residential. The cost-benefit *'source-receptor'* flood risk framework took values (corresponding to 2022 prices) to calculate the damages to commercial and residential buildings from the Handbook for Economic Appraisal (Multi-Coloured Handbook, 2022) by Priest et al. (2022) (Figure 4.3). Note that prices may differ for other parts of the UK and definitely for other countries.

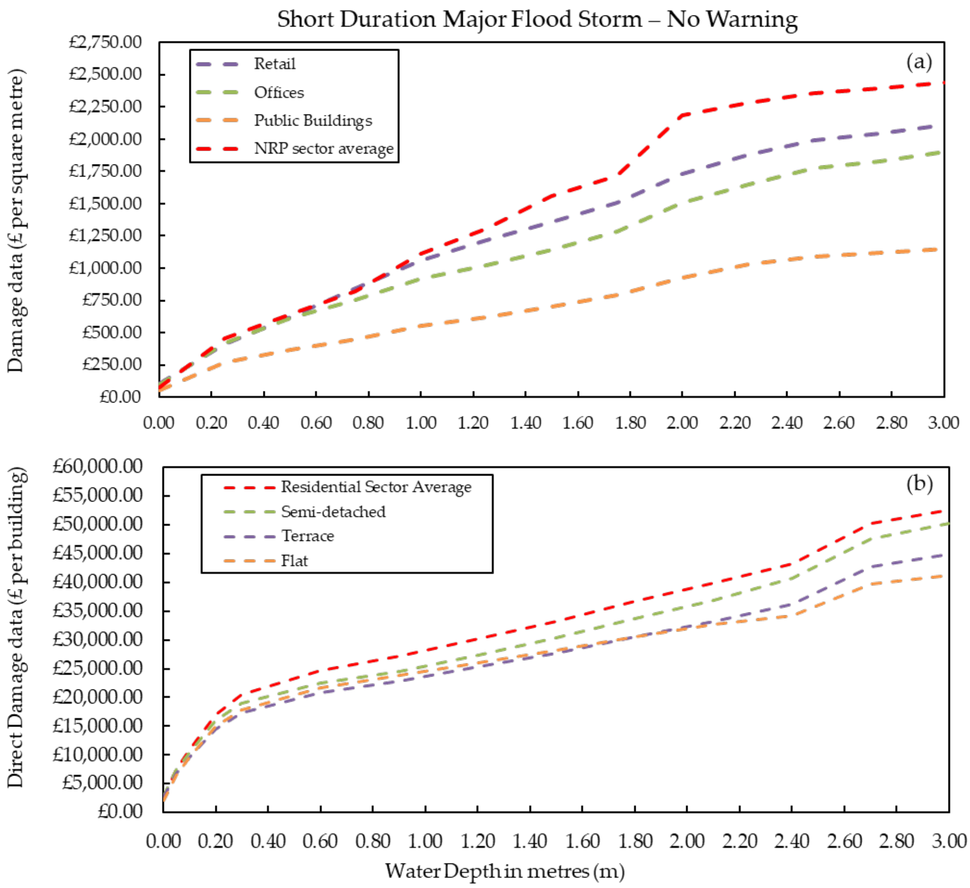

Figure 4.3 Direct damage from different water depths for: (a) commercial buildings; (b) residential buildings (Priest et al., 2022).

4.2.5 Land in green spaces in cells

The only spatial criterion in this framework covers the percentage of land use in the study area (Figure 4.4) where flooded green spaces may be considered as the areas most suitable to add efficient interventions such as ponds or swales to protect assets downstream or to guide the researcher to add other types of interventions such as permeable pavements, water butts etc. to other parts of the catchment.

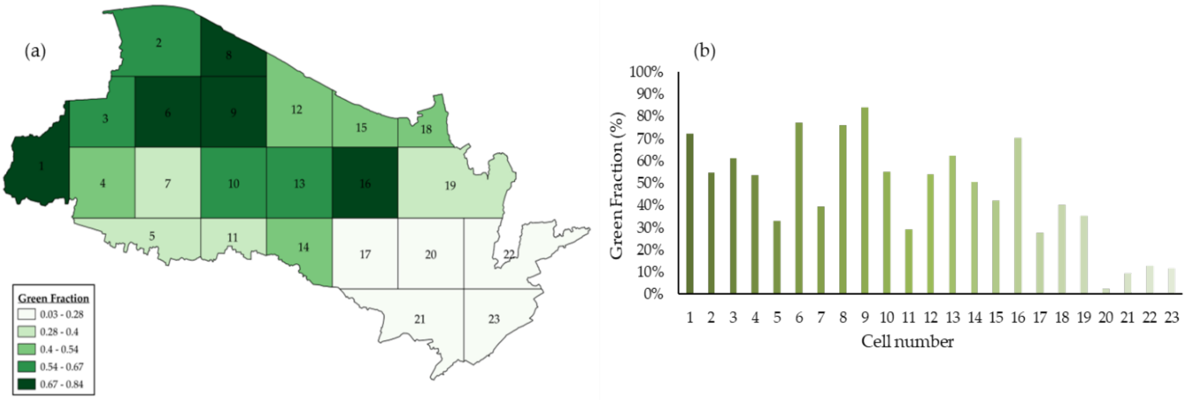

Figure 4.4 The percentage of green spaces on the cells of the study area: (a) model green spaces; (b) the summary statistics.

4.3 Results

4.3.1 Baseline

The modelled flood depths for the baseline scenarios (*FD(rp)*) shows us that in the catchment there are two main flow paths, the first from the west side of the catchment to the east (cells 1, 4, 6, 7, 9, 12, 15, 18 and 19) through Newcastle University campus and the second through the city centre in the lower catchment (cells 6, 9, 10, 13, 14, 17, 20 and 21), see Figure 4.5. The flood exposure to buildings was calculated for the baseline scenarios to identify the number of buildings at high and medium flood risk and the cells that caused flooding to them (Table 4.2, Figure 4.5). Most of the buildings at high flood risk are located in the west, central, and downstream of the catchment, which is to be expected due to the generated flow paths in cells of the study area and the different characteristics of the ground, e.g. impermeable pavements, in the study area.

Table 4.2 Number of inundated buildings per baseline scenario for different storm events.

FD(rp)	Medium	High	Total
FD(10y)	206	258	464

FD(20y)	272	396	668
FD(50y)	411	627	1038
FD(100y)	518	809	1327

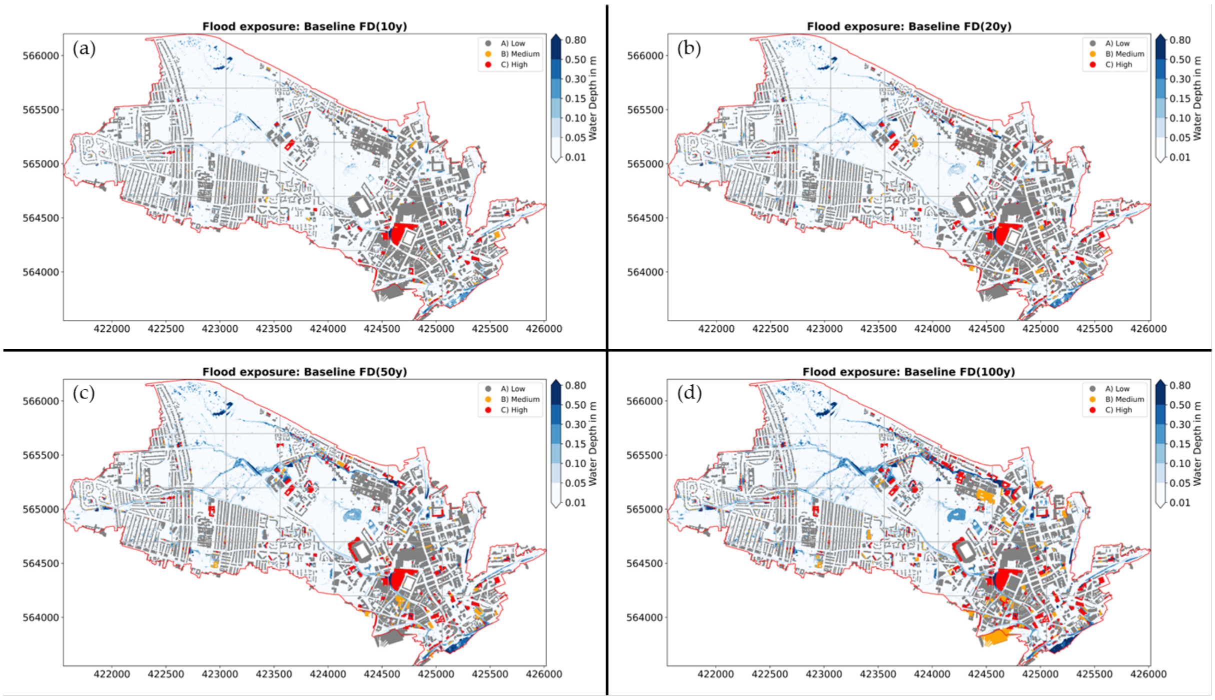

Figure 4.5 Flood depth from CityCAT simulation and flood exposure to buildings for the baseline scenarios - *FD(rp)* for: (a) a 1 in 10-year storm event; (b) a 1 in 20-year storm event; (c) a 1 in 50-year storm event; and (d) a 1 in 100-year storm event with a duration of 60 min, the red colour defines the building at high risk, the orange at medium risk and the grey at low risk for Newcastle city centre.

The estimated total flood damages per baseline scenario can be seen in Table 4.3 and in Figure 4.6, where the total damages even for the *'small'* storm events (1 in 10-year and 1 in 20-year return period) are high. This is consistent with the significant commercial buildings which are impacted in the centre of the catchment. Note here that from the exposure analysis for the baseline scenarios some buildings are classified at high and medium flood risk but after turning off the rainfall to cells the classification scheme changes to some buildings from high to medium and low further downstream as expected (see Figure 4.7).

Table 4.3 The total flood damages for the baseline scenarios – *FD(rp)*.

FD(rp)	Commercial (£)	Residential (£)	Total Damages (£)
FD(10y)	£40.8M	£6.1M	£47.0M
FD(20y)	£59.5M	£8.9M	£68.5M
FD(50y)	£92.3M	£14.3M	£106.7M
FD(100y)	£147.9M	£18.4M	£166.5M

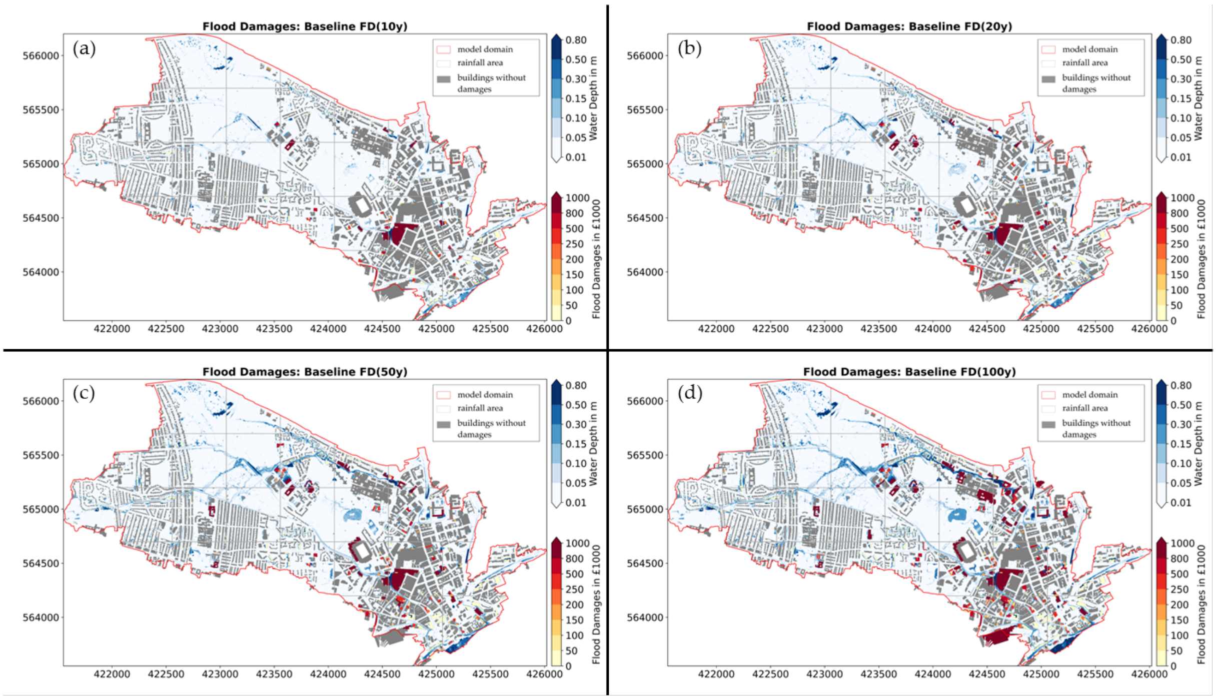

Figure 4.6 Examples of flood damages and water depth maps for the baseline scenarios – *FD(rp)* for: (a) a 1 in 10-year storm event; (b) 1 in 20-year storm event; (c) 1 in 50-year storm event; and (d) 1 in 100-year storm event with a duration of 60 min, yellow to dark red defines the cost per buildings from flooding.

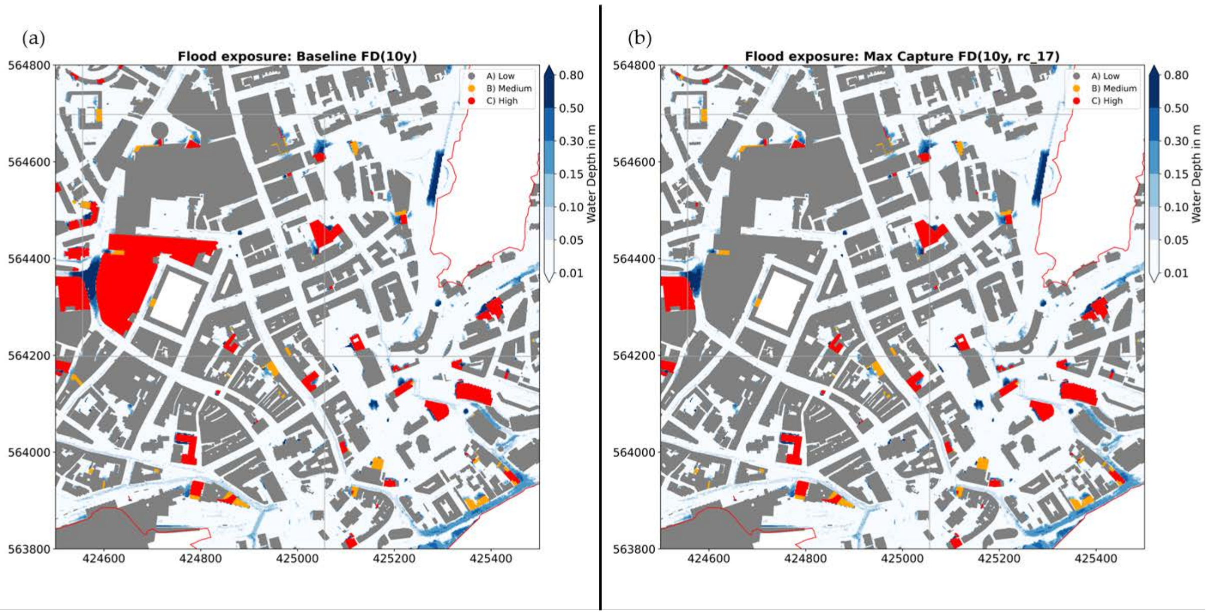

Figure 4.7 Example of flood exposure map, before (left) and after (right) turning off rainfall in cell 17 *(FD(10y, rc_17))*, the red colour defines the buildings at high risk, orange at medium risk and the grey at low risk.

4.3.2 Rainfall capture

The cost-benefit *'source-receptor'* flood risk framework was developed to assess the impact of certain cells on surface flooding by analysing the exposure to buildings and calculating the flood damages to properties on a local/large scale and further downstream. The simulated flood depths from the baseline scenarios (*FD(rp)*) for the multiple storm events allow us to identify the flow paths in the study area. Next the exposure analysis allows us to locate the buildings (commercial & residential) at high/medium flood risk and then the difference in flood damages to buildings from (a) the baseline scenarios (*FD(rp)*) and (b) the max capture scenarios (*FD(rp, rc_i)*) represents the cost-benefit (damage reduction) to buildings by switching-off the rainfall to cells (i.e. capturing all the rainfall in the cell – the ideal maximum intervention). The matching of cells identified in this way with the available green space offers the capability to identify high-priority cells to add adaptation solutions (Table 4.4, Figure 4.8 and 4.9) in a straightforward way. The highest value in the final column (Cost-Benefit * Green Fraction (GF)) of Table 4.4 corresponds to the highest priority location and this is used to select the location and type of intervention most suitable to build: this is discussed further in section 4.3.3. Moreover, due to simulating for multiple storm scenarios, it can be seen in Figure 4.9 that the prioritisation of cells varies for different magnitudes of storm (*FD(rp, rc_i)*) which is to be expected due to the different flow paths in the catchment and the different extent of rainfall capture in cells.

Table 4.4 The ranking system to prioritise cells with a high need of intervention for the different storm events, the five high-priority cells for all the max capture scenario per storm event, damages in £ million.

10-year return period						
Cells	**Green Fraction (GF - %)**	**Commercial (£)**	**Residential (£)**	**Total Damages (£)**	**Cost-Benefit (FD(10y) – FD(10y, rc_i)) in £**	**Cost-Benefit * GF**
FD(10y, rc_13)	62.20%	£35.7M	£5.8M	£41.5M	£5.5M	3.38
FD(10y, rc_17)	27.71%	£29.2M	£6.1M	£35.3M	£11.7M	3.24
FD(10y, rc_14)	50.70%	£36.2M	£6.1M	£42.3M	£4.7M	2.37
FD(10y, rc_15)	42.30%	£39.7M	£5.7M	£45.4M	£1.6M	0.69
FD(10y, rc_16)	70.29%	£40.6M	£5.7M	£46.3M	£0.7M	0.46
20-year return period						
Cells	**Green Fraction (GF - %)**	**Commercial (£)**	**Residential (£)**	**Total Damages (£)**	**Cost-Benefit (FD(20y) – FD(20y, rc_i)) in £**	**Cost-Benefit * GF**
FD(20y, rc_13)	62.20%	£52.1M	£8.6M	£60.9M	£7.6M	4.79
FD(20y, rc_17)	27.71%	£48.4M	£8.9M	£57.3M	£11.2M	3.08
FD(20y, rc_12)	53.82%	£55.7M	£8.2M	£63.9M	£4.6M	2.47
FD(20y, rc_14)	50.70%	£55.3M	£8.9M	£64.2M	£4.3M	2.21
FD(20y, rc_10)	55.28%	£56.5M	£8.3M	£64.8M	£3.7M	2.05
50-year return period						
Cells	**Green Fraction (GF - %)**	**Commercial (£)**	**Residential (£)**	**Total Damages (£)**	**Cost-Benefit (FD(50y) – FD(50y, rc_i)) in £**	**Cost-Benefit * GF**
FD(50y, rc_13)	62.20%	£82.2M	£14.0M	£96.2M	£10.5M	6.53
FD(50y, rc_16)	70.29%	£86.3M	£13.8M	£100.1M	£6.6M	4.64

FD(50y, rc_17)	27.71%	£76.4M	£14.2M	£90.6M	£16.1M	4.45
FD(50y, rc_12)	53.82%	£85.3M	£13.6M	£98.9M	£7.8M	4.21
FD(50y, rc_14)	50.70%	£85.2M	£14.1M	£99.3M	£7.4M	3.76
100-year return period						
Cells	**Green Fraction (GF - %)**	**Commercial (£)**	**Residential (£)**	**Total Damages (£)**	**Cost-Benefit (FD(100y) – FD(100y, rc_i)) in £**	**Cost-Benefit * GF**
FD(100y, rc_16)	70.29%	£135.0M	£17.8M	£152.8M	£13.7M	9.56
FD(100y, rc_9)	84.13%	£138.9M	£18.1M	£157.0M	£9.5M	7.98
FD(100y rc_13)	62.20%	£137.9M	£18.1M	£156.0M	£10.5M	6.50
FD(100y, rc_19)	35.24%	£132.6M	£18.3M	£150.9M	£15.6M	5.49
FD(100y, rc_12)	53.82%	£138.7M	£17.8M	£156.5M	£10.0M	5.33

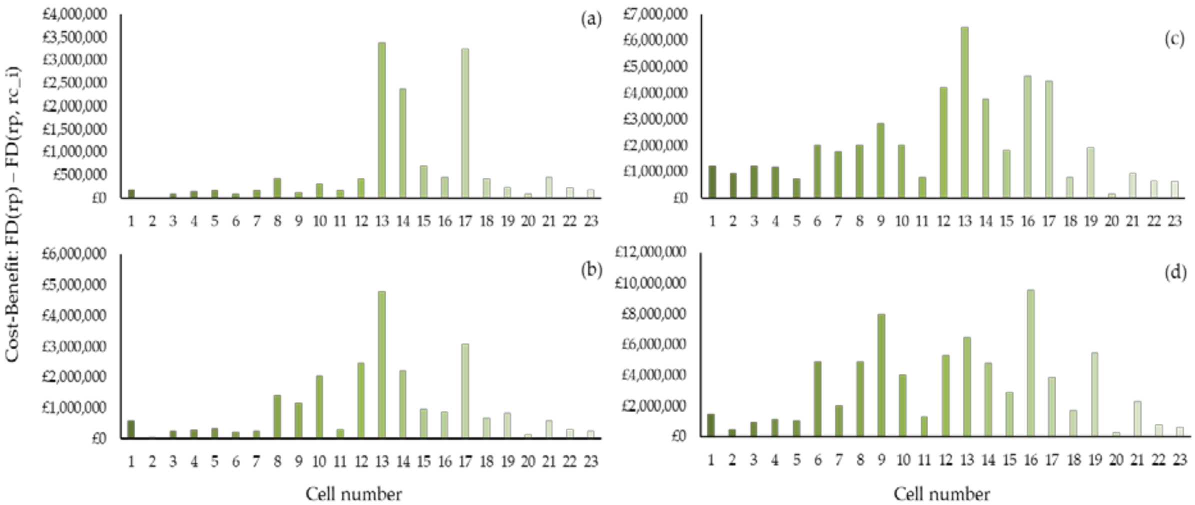

Figure 4.8 Summary statistics of the cost-benefit *'source-receptor'* for the max capture scenarios for all the storm events: (a) 1 in 10-year return period; (b) 1 in 20-year return period; (c) 1 in 50-year return period; and (d) 1 in 100-year return period with a duration of 60 min.

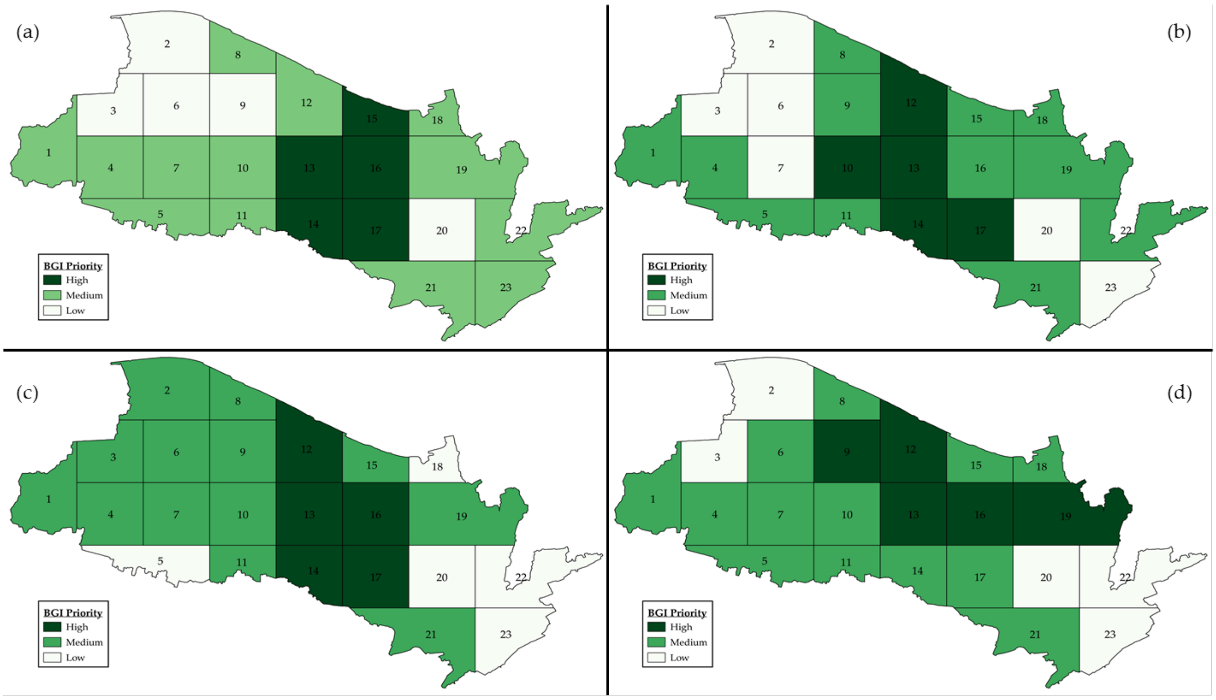

Figure 4.9 Classification of cells as priority areas for BGI in the study area: (a) 1 in 10-year return period; (b) 1 in 20-year return period; (c) 1 in 50-year return period; and (d) 1 in 100-year return period with a duration of 60 min.

4.3.3 Adding Blue-Green Infrastructure to urban areas and catchments

The previous section has examined the use of BGI to capture rainfall directly on receipt at the ground, but the cost-benefit *'source-receptor'* flood risk framework can equally well be used with BGI interventions to capture runoff, for example with permeable pavements or detention ponds.

4.3.3.1 Runoff Capture – permeable pavements

Firstly permeable pavements are introduced to capture runoff for storm events at 1 in 10-year and 1 in 20-year return period with a duration of 60 min. The results from the exposure, the cost-benefit analysis of buildings and the ranking system for the small events (see supplementary material for the tables and the flood maps) suggest location of adaptation in cells 13, 17, 14, 15 and 16 for a 1 in 10-year storm event and to cells 13, 17, 12, 14 and 10 for a 1 in 20-year storm event. Following identification, permeable pavements (*FD(rp, fc_i)*) were introduced in these cells to estimate the benefit reducing damages to buildings downstream. The installation cost for permeable pavements is around £30 per square metre of pavement according to SNIFFER (2006) and Woods Ballard et al. (2015). Table 4.5 below describes the cost-benefit in cells classified as high priority with the area of pavements in these cells and the installation cost to identify the most economic cell to add the proposed BGI. It can be seen that for cell 17 the reduction in damages is almost £1.60M by adding permeable pavements with a cost of £0.65M (Figure 4.10).

Table 4.5 The flood damages for the intervention scenarios, add permeable pavements in cells 13, 14, 15, 16 & 17, the cost-benefit, and the installation cost.

Intervention Scenarios 10-year return period						
Cells	**Commercial (£)**	**Residential (£)**	**Total Damages (£)**	**Cost-Benefit (FD(10y) – FD(10y, fc_i)) in £**	**Area (m²)**	**Installation cost (£)**
FD(10y, fc_13)	£40.7M	£6.1M	£46.8M	£0.24M	15,396.718	£0.46M
FD(10y, fc_14)	£40.3M	£6.1M	£46.4M	£0.64M	21,468.389	£0.64M
FD(10y, fc_15)	£40.8M	£6.0M	£46.8M	£0.24M	7,143.89	£0.21M
FD(10y, fc_16)	£40.8M	£6.1M	£46.9M	£0.14M	9,429.084	£0.28M
FD(10y, fc_17)	£39.3M	£6.1M	£45.4M	£1.64M	21,726.375	£0.65M

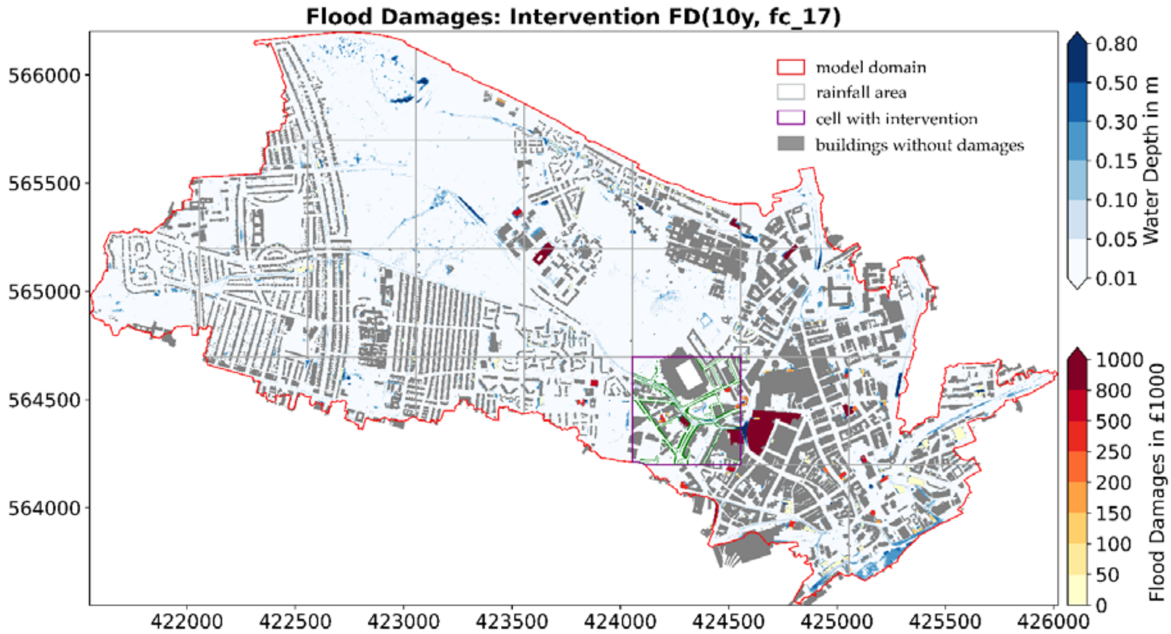

Figure 4.10 Example of flood damages and water depth map, add an intervention in cell 17, green denotes the permeable pavements, yellow to dark red defines the cost per buildings from flooding.

4.3.3.2 *Runoff Capture – detention ponds*

A second method of runoff capture, installing detention ponds, has been examined targeted at expendable green spaces. This builds on previous work (Birkinshaw & Krivtsov, 2022) which assessed the optimal location for ponds. Two cells (9 and 12, see Figure 4.11) were chosen for further investigation as they are classified as high-priority cells with a high percentage of available green space (84% and 54% respectively) and a detention pond (*FD(rp, fc_i)*) was proposed to be built in each cell. The first step is to choose manually the best place in these cells to add the pond and re-run the model to estimate the reduction in flood damages. In cell 12 the total area of the proposed pond is 510 m^2 with corresponding volume of 765 m^3 and in cell 9 the area of the detention pond is 8,000 m^2 with a volume of 10,000 m^3. The estimated flood damages, the cost-benefit, and the installation cost by simulating the ponds in cells 9 and 12 for multiple storm events can be seen in Table 4.6. An average cost to construct a pond is £80,000 per 5,000 m^3 water volume, so the estimated cost to build the two detention ponds in cells 9 and 12 is around £0.16M with the economic benefit being more than £8.5M for the high storm events and more than £0.50M for small events (SNIFFER, 2006; Woods Ballard et al., 2015). Finally, a combination of interventions could be proposed to model in areas where the intensity of rainfall is extremely high (e.g. > 100 mm of rainfall).

Table 4.6 The flood damage costs for the intervention scenarios, add storage pond in cells 9 and 12 for multiple storm events, the cost-benefit, and the installation cost, see Table 4.3 for the baseline scenario damages *FD(rp)*.

Cells	Commercial (£)	Residential (£)	Total Damages (£)	Cost-Benefit (FD(rp) – FD(rp, fc_i)) in £	Installation cost (£)
FD(20y, fc_9_12)	£59.1M	£8.9M	£68.0M	£0.55M	≈ £0.16M
FD(50y, fc_9_12)	£90.3M	£13.7M	£104.0M	£2.75M	≈ £0.16M
FD(100y, fc_9_12)	£140.0M	£17.7M	£157.7M	£8.78M	≈ £0.16M

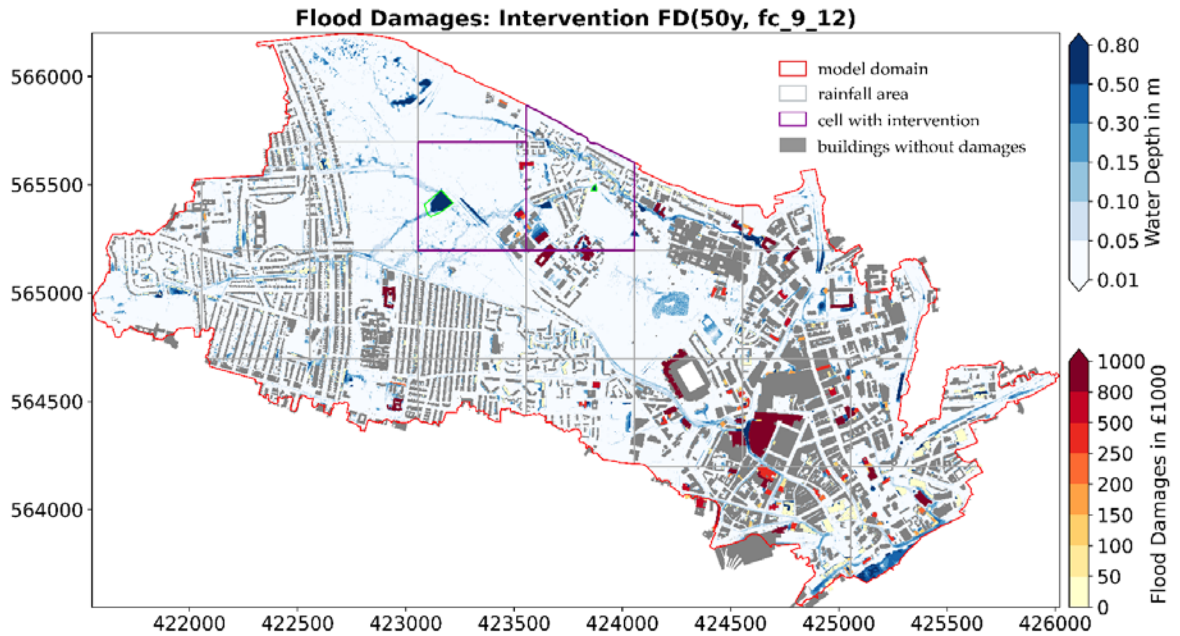

Figure 4.11 Example of flood damages and water depth map, with intervention in cells 9 and 12 (*FD(50y, fc_9_12)*, storage ponds), green denotes the ponds, yellow to dark red defines the damages per buildings from flooding.

4.4 Discussion

It is crucial to recognise the constraints that define the scope of the outcomes. A framework such as the cost-benefit *'source-receptor'* often encounters practical challenges in real-world complexities, such as fragmented land and property ownership, which could present significant obstacles to coordinating and implementing comprehensive adaptation solutions across diverse stakeholders. Achieving a balance between the theoretical effectiveness of risk reduction measures and their practical feasibility requires addressing these intricate challenges, streamlining procedures, and fostering collaborative efforts among stakeholders, insurance companies, and local authorities to ensure long-term success of risk mitigation strategies.

This study has prioritised economic considerations, but it must be recognised that other aspects may be equally important. Restricting aspects include not only land ownership as outlined above, but also acceptance by communities and stakeholders on aesthetic, access or safety grounds. Positive aspects to increase benefit are increasingly found to be helpful in building cases for BGI and these include measures to improve bio-diversity, reduce pollution, increase carbon sequestration and combat urban heating.

Moreover, representing drainage systems in flood models is a challenging task, especially when data is unavailable. Future work is planned to improve the accuracy of the cost-benefit *'source-receptor'* framework by incorporating the sub-surface system into the model or developing new novel methodologies to accurately represent the sewer drainage network by generating synthetic inlets according to the study area and the design standards worldwide. These approaches will provide modellers with flexibility in cases where access to data is limited (Bertsch et al., 2017; Costabile et al., 2023; Dasallas et al., 2023; Iliadis, Galiatsatou, et al., 2023; Singh et al., 2023).

4.5 Conclusions

This chapter demonstrates a novel approach to link surface water flooding information with the exposure and the flood damages to buildings in urban fabric and catchments. It uses a detailed hydrodynamic model to identify how many buildings are impacted by flooding during multiple magnitude storm events, the incurred damages and the potential locations to add the most effective type of BGI. The combination of hydrological data, flood dynamics and cost-benefits could guide spatial prioritisation for intervention in critical locations. Furthermore, the proposed framework has all the necessary principles to become a standard planning tool for flood risk management due to the simplicity of every step in the proposed methodology and the quantitative exposure outputs from flood models at individual building level.

The systematic procedure of classifying the buildings at high and medium flood risk and calculating the damages by switching-off the rainfall in every cell for multiple storm events allows identification of areas and properties with high contribution and high direct flood impact. The proposed combination and comparison between the cost-benefit and the available green spaces provides information to choose different types of interventions according to the intensity of the storm, e.g. permeable pavements, water butts and green roofs for storms with low intensity and ponds and swales for storms with high intensity or even a combination of interventions according to flood results in the study area. Furthermore, this framework offers the flexibility to be applied in larger dense cities and catchments where the results offer more options for flood management intervention. For example, a target percentage of rainfall could be removed in every cell, for example 5% of the total storm, instead of unrealistic total capture when the rainfall is extremely high (e.g. more than 100 mm per hour).

Finally, much further work is planned to extend the capability of this cost-benefit *'source-receptor'* flood risk framework, such as automating the procedure to add BGI instead of manually investigating the best location in every cell (Rehman et al., 2023), and considering combinations of larger number of interventions with smaller footprints and lower unit cost to improve feasibility and flexibility of implementation.

Chapter 5. Cloud modelling of property level flood exposure in megacities

5.1 Introduction

Surface water flooding is emerging as a major natural hazard due to the growth of urbanisation and the upcoming climate change that leads to more frequent flash floods from severe rainfall events in urban areas and catchments resulting in economic damages to infrastructure, assets, properties, and people worldwide (Barredo et al., 2012; Di Paola et al., 2014; IPCC, 2014; Yang et al., 2016). In megacities, there is an especially notable increase in risk through anthropogenic activities increasing vulnerability (Guan et al., 2015; Sillanpää & Koivusalo, 2014). The capacity of the current drainage system to most of the cities is overwhelmed during intense rainfall (Falconer et al., 2009) with subsequent damages to properties, critical infrastructure and population.

In the face of climate change and urbanisation, flood risk management is pivotal to offering adaptation solutions and flood models are crucial to informing resilience planning in urban areas. Over the years, many research models have been developed to model the drainage system (Djordjević et al., 1999; Simões et al., 2010) and to solve the full shallow water equations (SWEs) (Bates et al., 2010; Glenis et al., 2018; Xia et al., 2019). Many reviews have been written to evaluate the advantages and the limitations of hydrodynamic models (Bach et al., 2014; K. Guo et al., 2021; Karim et al., 2023; Mignot et al., 2019; Singh et al., 2021; Teng et al., 2017). Among the many hydrodynamic models developed to solve the full 2D - SWEs, City Catchment Analysis Tool (CityCAT) was employed in this study. CityCAT has undergone testing in various real flood events in the past (Bertsch et al., 2017; Bertsch et al., 2022; Glenis et al., 2013; Iliadis, Glenis, et al., 2023a, 2023b; Jenkins et al., 2018; Kutija et al., 2014; Vercruysse et al., 2019), encompassing different cities within the UK. Additionally, it has been applied in studies conducted in the USA, with a particular focus on urban flooding

(Rosenzweig et al., 2021). Furthermore, the model was employed in a recent study in Greece by Iliadis, Galiatsatou, et al. (2023). The accuracy and the quality of the results is now sufficient to take on assessments of the most important locations such as megacities where the greatest risk and vulnerabilities are found. Such large-scale modelling requires correspondingly large computational resources and as the power of cloud computing has increased, a few attempts have been made to assess flood risk in larger cities using hydrodynamic models. Many studies to simulate surface flow have been applied to small urban catchments (Bisht et al., 2016; Chen et al., 2009; Fewtrell et al., 2008; Fewtrell et al., 2011a; Huang et al., 2022; Hunter et al., 2008b; Neal et al., 2009; Paquier et al., 2015; Syme, 2008; Xu et al., 2023). Other larger scale studies have focused on the flood risk from rivers (fluvial flooding) (Bellos & Tsakiris, 2016; Lamb et al., 2010; Ngo et al., 2022; Papaioannou et al., 2021). The first attempt to simulate the flood impacts in European cities was presented by Guerreiro et al. (2017), where they calculated the percentage of urban areas flooded for 571 cities in Europe with a spatial resolution DTM of 25x25m for nine different rainfall events, but concluded that the low resolution of the DTM imposed major limitations through not representing flow paths accurately. Another study evaluated the flood risk by simulating the pluvial flood distribution caused during three extreme rainfall events in Shanghai with a DEM of similar (30m) resolution (Hu et al., 2023).

Digital Elevation Models (DEM) and Digital Terrain Models (DTM) play a key role in hydrodynamic models to produce accurate results by defining the water flowpaths and the flood risk in urban areas where the topography is complex due to the dense buildings and roads (McClean et al., 2020). Xafoulis et al. (2023) investigated the influence of different spatial resolutions in DEMs on flood risk assessment, focussing specifically on fluvial flooding in an agricultural region located in Greece. In terms of urban environments, recent studies by Wang et al. (2018) and Jamali et al. (2018) highlight the importance of the high accuracy of DEMs in flood modelling for urban flood management options through two different case studies with the use of 1m resolution DEM. Escobar-Silva et al. (2023) explored the influence of spatial resolution in flood modelling by comparing three different rainfall events in São Caetano do Sul, São Paulo, Brazil, and validated the results with field measurements provided from the local civil defence agents of the area.

This chapter therefore aims to investigate the limits of the ability of a high-resolution cloud-based hydrodynamic model to estimate the flood risk and exposure at individual building level for a large city. The critical role of the DTM resolution on accuracy and run-time is established using four different grid resolutions for multiple storm depths. While performance is mostly assessed through model inter-comparison, the underlying model fidelity is established with a validation against field measurements from a real storm event. The demonstration of large area, high resolution modelling and exposure analysis provides timings and costs of Cloud simulations which can guide and set new standards for industry practice to achieve.

5.2 Methodology

5.2.1 Hydrodynamic modelling with CityCAT

The City Catchment Analysis Tool – CityCAT is a fully 1D/2D coupled hydrodynamic model, developed at Newcastle University, that can be used for modelling, analysis and visualisation of surface water flooding (Glenis et al., 2018) and urban drainage (Bertsch et al., 2017). The architecture of the model is based on the object-orient approach which offers rapid extension of functionality and flexibility in development (Kutija & Murray, 2007). CityCAT contains explicit solutions to the full Shallow Water Equations (SWE) (Tan, 1992) solved by finite volumes with high order shock-capturing schemes for propagation of flood wave for flows with discontinuities (Toro, 2013). New Riemann solvers have been developed which can handle free surface, pressurised and mixed flows (Erduran & Kutija, 2003). The model is based on the St Venant equations and a conservative form of the Alievi equations based on the compressible Euler equations, which can be written as:

$$\partial_t A + \partial_x Q = 0$$
$$\partial_t Q + \partial_x \left(\frac{Q^2}{A} + p(x, A, T) \right) = gA(S_o - S_f) \tag{5.1}$$

Where: Q is the discharge, A is the cross-sectional area, p is the pressure, S_o is the slope, S_f is the friction term; T denotes the flow state: FS (free surface) or Pr (pressurised) (Glenis et al., 2018).

$$p(x, A, T) = \begin{cases} gI_1, & if\ T = FS \\ gI_1 + c^2(A_{Pr} - A_{max}), & if\ T = Pr \end{cases}$$
$$I_1 = \int_0^{h(x)} (h(x) - \eta)\sigma(x, \eta)\, d\eta;\ c^2 = \frac{1}{\rho_o \beta};\ A_{Pr} = \frac{\rho}{\rho_o} A_{max} \tag{5.2}$$

Where: η is the depth integration variable along the vertical axis; $h(x)$ is the water depth; $\sigma(x, \eta)$ is the width of the cross-section; ρ_o is the density of the water at atmospheric pressure; ρ is the density of the water; β is the water compressibility coefficient.

An example of the shallow water equations used in CityCAT and solved by Finite Volumes shock-capturing methods can be written as follows:

$$\partial_t \boldsymbol{Q} + \partial_x \boldsymbol{F}(\boldsymbol{Q}) + \partial_y \boldsymbol{G}(\boldsymbol{Q}) = \boldsymbol{S}(\boldsymbol{Q}), \quad \boldsymbol{Q} = \boldsymbol{Q}(\boldsymbol{x}, t) \in \mathcal{D},\ \boldsymbol{x} = (x, y) \in \Omega \subset \mathbb{R}^2,\ \ t > 0 \tag{5.3}$$

Where: $\mathcal{D}$ is an open convex subset of $\mathbb{R}^p$; p is the number of conservation laws; $\boldsymbol{Q}$ is the conserved quantities vector; $\boldsymbol{F}, \boldsymbol{G}$: $\mathcal{D} \rightarrow \mathbb{R}^p$ are the flux vectors; and $\mathbf{S}$: $\mathcal{D} \rightarrow \mathbb{R}^p$ is the source terms vector. With initial conditions: $\mathbf{Q}(\mathbf{x},0) = \mathbf{Q}_0(\mathbf{x})$, $\mathbf{x} \in \Omega$; and boundary conditions: $\mathbf{Q}(\mathbf{x},t) = \mathbf{Q}_{BC}(\mathbf{x},t)$, $\mathbf{x} \in \partial\Omega$, $t>0$.

The vectors are given as follows:

$$\boldsymbol{Q} \equiv [q_1,\ q_2, q_3]^T = \left[h,\ hv_x, hv_y\right]^T; \boldsymbol{F}(\boldsymbol{Q}) \equiv [f_1,\ f_2, f_3]^T = \left[hv_x,\ hv_x^2 + gh^2/2, hv_x v_y\right]^T$$
$$\boldsymbol{G}(\boldsymbol{Q}) \equiv [g_1,\ g_2, g_3]^T = \left[hv_y,\ hv_x v_y, hv_y^2 + gh^2/2\right]^T; \boldsymbol{S}(\boldsymbol{Q}) = \boldsymbol{R} - \boldsymbol{L} + \boldsymbol{S_o} - \boldsymbol{S_f} \tag{5.4}$$

Where v_x and v_y represent the depth-averaged velocity components in the x and y directions respectively; h is the water depth; g is the gravity acceleration.

$\boldsymbol{R} = [R,\ 0{,}0]^T$ is the rainfall intensity; $\boldsymbol{L} = [L,\ 0{,}0]^T$ is the infiltration rate;

$\boldsymbol{S_o} = \left[0, gh\partial_x z_b, gh\partial_y z_b\right]^T$ is the bed slope source term and z_b denotes the bed elevation;

$\boldsymbol{S_f} = \left[0, ghSf_x, ghSf_y\right]^T$ is the friction term; (see full description of the equations in Glenis et al. (2018)).

The model represents built-up areas with explicit representation of buildings by using the *'Building Hole'* approach (Iliadis et al., 2023b), bridges (McKenna et al., 2023) and different types of Blue-Green Adaptation solutions (Iliadis, Glenis, et al., 2023a). The produced outputs of CityCAT are time series of water depth, velocity flow, flood maps and volume in and out of manholes, gully drains, buildings etc (Kilsby et al., 2020). The required inputs to simulate a study area with CityCAT are: a) Digital Terrain Models (DTM); b) the buildings' footprint; c) the permeable areas; and d) the rainfall intensity; Figure 5.1 highlights the steps to set-up a simple simulation in an urban area.

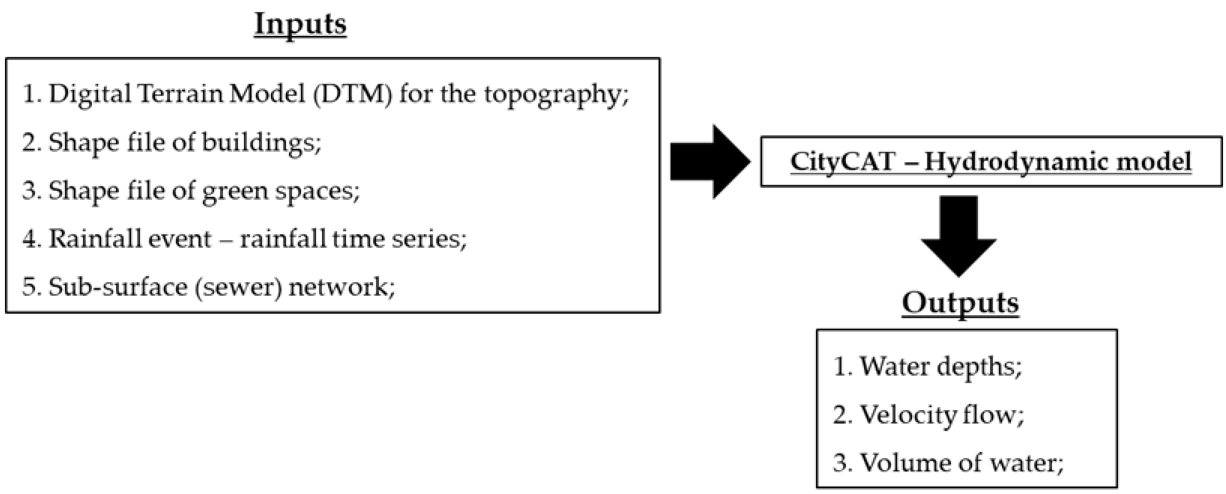

Figure 5.1 Schematic workflow to set-up a simulation with CityCAT in an urban area.

5.2.2 Cloud computing

The design of optimal and efficient solutions for flood risk management is restricted due to the limitations of combining high performance computing with flood models.

The evolution of cloud flood modelling in the last years has offered a range of options to process and store data to understand and explore flood risk management in big urban areas and catchments (Glenis et al., 2013). In most cases, the use of the cloud meets specific payment options for the time of renting the resources and the required Random-Access-Memory (RAM). Alternatives to the Cloud usually involve a dedicated compute server, with a proportional cost.

Many studies have explored and reviewed the use of the cloud for different cases, such as flood modelling, flood mapping, etc (Alonso et al., 2023; Bentivoglio et al., 2022; Cea & Costabile, 2022a; Karim et al., 2023; Liu et al., 2017; Mignot et al., 2019; Teng et al., 2019; Thrysøe et al., 2021). A '*blade*' server installed and located at Newcastle University for research purposes is presented here and compared with the use of the Cloud with extra payment options, like the Microsoft Azure platform.

5.2.3 LiDAR data

Digital Terrain Models (DTMs) are the most fundamental input for a hydrodynamic model as they define the computational grid and main flow characteristics. The key consideration for selection of DEM resolution is the trade-off between accuracy of flow path representation, affected by buildings as well as slopes, and speed of simulation as a doubling of grid resolution (e.g. from 2 to 1m) may increase run times by a factor of eight due to reduction of time step as well as increasing the number of calculations, as well as increasing memory requirements. Validation against historic storms in the past shows that 1m and 2m grid squares satisfactorily resolve streets and other flow paths between buildings while grid squares of size > 5m may close flow paths between buildings, resulting in unrealistic flood depths (Iliadis et al., 2023b; Kutija et al., 2014). For the UK, LiDAR derived DEM data is available from Digimap (Digimap (edina.ac.uk)) in different resolutions with unit pixels in metres. This study will explore the influence of high-resolution DTMs in flood modelling of megacities, and the required RAM to achieve that. The resolutions of the DTMs used in this case study are 1m, 2m, 5m, and 10m. Table 5.1 shows an example of computational grid squares with the RAM required to run a simulation with CityCAT.

Table 5.1 Number of cells in a computational grid and required memory to run CityCAT model.

Number of cells in a computational grid	Required RAM in GB
500,000	≈16
1,500,000	≈20
10,000,000	≈40
15,000,000	≈60
50,000,000	≈200

5.2.4 Estimating flood exposure to buildings

The flood exposure tool, initially developed by Bertsch et al. (2022), was used in this work to estimate the flood risk to buildings and classify them according to the water depth in a buffer zone with a simple scheme (see Table 5.2). The mean and the 90th percentile of water depth were extracted for each building of the study areas in multiple buffer zones around the building perimeter. Note that, the buffer zone depends on the DTM resolution (the proposed buffer zones are: 1.50m for the DTM with a 1m resolution, 3m for the DTM with a 2m resolution, 5m for the DTM with a 5m resolution, and 10m for the DTM with a 10m resolution). These depths can be used for damage estimation using depth-damage curves as well as a classification. The threshold of 30cm was used to classify the buildings according to the flood risk.

Table 5.2 Classification criteria to calculate the flood risk likelihood to buildings.

Exposure Class	Mean depth (m)	90th percentile (m)
Low	<0.10	<0.30

Medium	<0.10	≥0.30
	≥0.10 - <0.30	<0.30
High	≥0.10	≥0.30

5.2.5 Rainfall data

The FEH22 Rainfall Depth-Duration-Frequency (DDF) model is used with the latest rainfall estimation for the area of central London – Piccadilly Circus (Vesuviano, 2022). UK Centre for Ecology & Hydrology (2022). The storm profiles were generated following the FEH Rainfall-Runoff method (Kjeldsen, 2007a, 2007b). Table 5.3 presents the storm events for multiple return periods for a 1-hour duration, among them is the historic storm event which hit London on the 12th of July 2021 with 76.20 mm of rainfall in a 90 min duration. This extreme event corresponds to a 1 in 484-year return period and is used to validate the observed data with the modelled output. Hence, the intensity of precipitation for this event is more than twice the average July total rainfall for London in less than two hours. Figure 5.2 shows the generated storm profiles for the range of return periods. A full risk assessment should consider storms of multiple durations as well as multiple return periods (depths) to establish the overall risk which may vary across the domain as different areas will have different catchment sizes and therefore different critical durations. A comprehensive coverage of durations and return periods was not possible within this study due to computational and time constraints, so a single duration was selected for ease of analysis and comparisons with other studies. Storm events of one hour were used for this initial study as the effective average catchment size for London is relatively small (of order 10 km2) and the majority of flooding in recent years is caused by events of around one hour duration.

Table 5.3 Storm event depths for multiple return periods.

Return Period	Rainfall (mm)
2	11.7

5	20.4
10	26.7
20	32.9
50	41.5
100	48.4

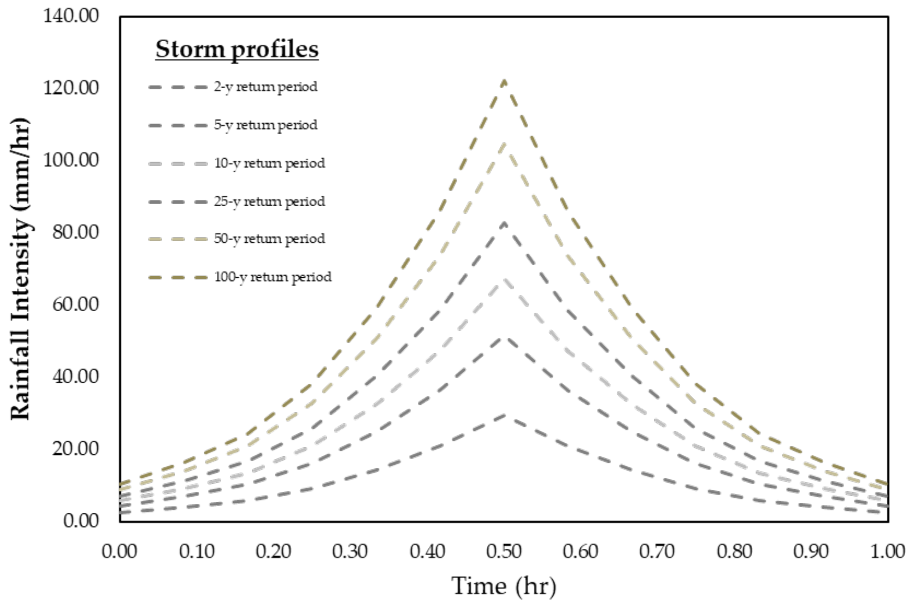

Figure 5.2 Storm profiles for multiple return periods with a 1hr duration for the area of London.

5.3 Area of interest and modelling set-up

5.3.1 Case study

The primary analysis focuses on a part of the Lea catchment, Central London, UK, with an area of 37.6 km^2, which is subject to major flood risk. This catchment was hit by severe storm events in the last decade, twice recently in July 2021, resulting in damages from surface flooding to many houses, basements, businesses, and underground stations as reported by the Mayor of London (Great London Authority, 2022). Moreover, this study examined the flood risk during multiple storm events and a range of DTM resolutions for the City of London, Westminster, Kensington, and Chelsea where historic buildings are located such as Westminster Abbey, Big Ben, the British

Museum, residential properties, commercial places and large green spaces such as Hyde Park, Green Park, and Regent's Park. Hence, this part of London is highly exposed, with Oxford Street having more than 500,000 pedestrians per day (LONDON ASSEMBLY, 2016), and ageing underground stations (Piccadilly Circus, Baker Street, Covent Garden, etc). Figure 5.3 illustrates the study catchment for the first part of the analysis where the locations are highlighted. Moreover, a larger part of London, which covers an area of 687 km^2 and includes more than 1,700,000 buildings, was selected to explore the usage and the cost of the Cloud for flood modelling with the CityCAT model, more details will be discussed in section 5.4.4.

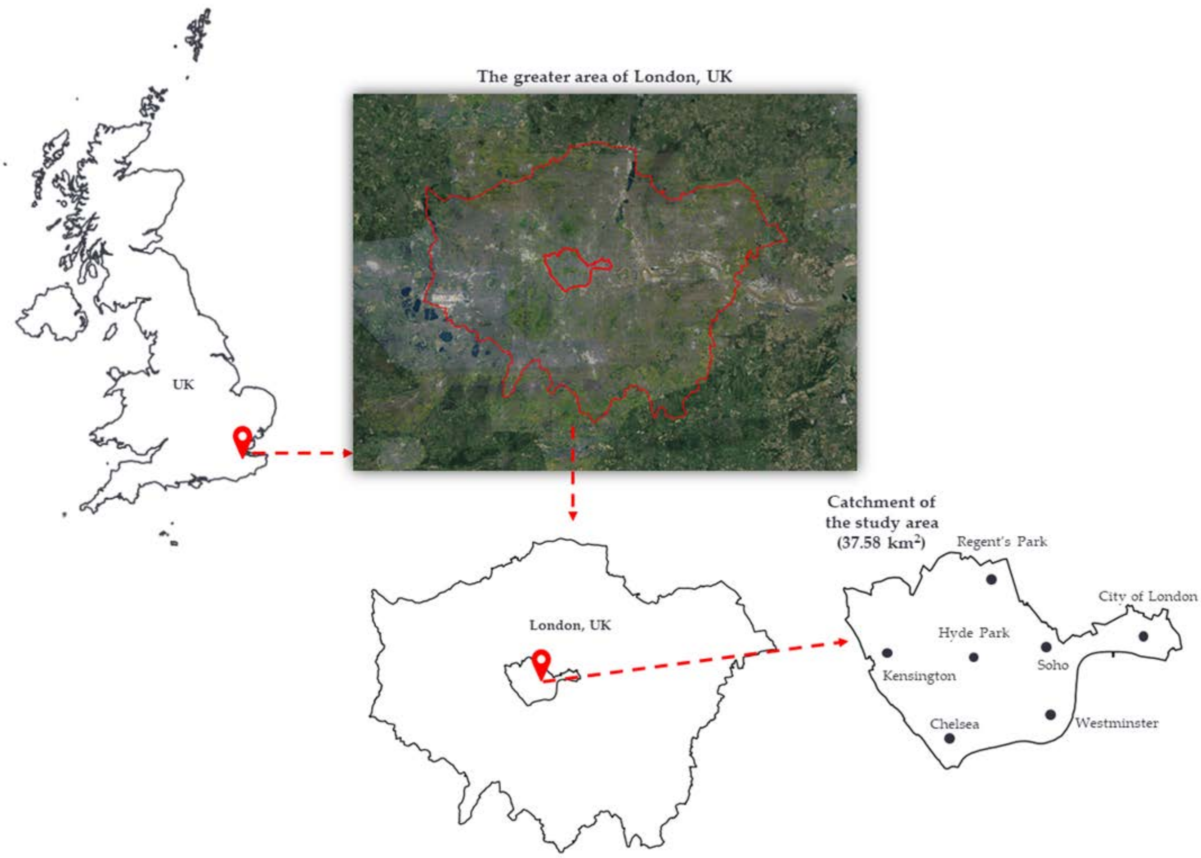

Figure 5.3 Overview of the study area in London, UK.

5.3.2 CityCAT set-up

The overland flow over and around urban features (buildings, green spaces) has been simulated using the hydrodynamic model CityCAT (Glenis et al., 2018) for storm events of 60 minute duration and return periods of 2, 5, 10, 20, 50 and 100 years Additionally, the historic storm of July 2021 was simulated with a 1 in 484-year return period design storm with a duration of 90 min. Simulations were carried out for multiple spatial resolutions of the DTMs, e.g. grid squares of area $1m^2$, $4m^2$, $25m^2$ and $100m^2$. The buildings and the permeable areas were extracted from OS Mastermap Topography (Ordnance Survey, 2020). The *'Building Hole'* technique was used to all models for the representation of the urban features, where the buildings' footprints are removed from the computational grid and the rainfall on every roof is re-distributed to the nearest surface grid square (Iliadis et al., 2023b) The total number of buildings in the study area is 95,976. The advantage of this approach is that offers more realistic results which validate well against observed data from real storm events, and it is easy and simple to categorise buildings according to their flood risk as well as to calculate the damages from surface flooding. For the sake of simplicity and ease of use, the catchment boundary conditions were kept open.

The total computational grid squares in the domain comprise 25,199,282 cells, 6,299,585 cells, 1,007,735 cells, and 255,786 for the DTMs with a resolution of 1m, 2m, 5m, and 10 respectively. The Green-Ampt method is used to calculate the infiltration of water in permeable areas (Warrick, 2003). A significant limitation to this study is that the sewer network was excluded from all simulations due to the limited available data. While some practitioners make an allowance for this by reducing the input rainfall by e.g. 20mm (see Iliadis, Galiatsatou, et al. (2023)), for transparency and inter-comparison we have not made any correction. An alternative option is to decrease the rainfall intensity to match the intensity associated with the concentration-time derived from the Intensity-Duration-Frequency curve corresponding to the design frequency, as per standards in place when the sewage system was originally commisioned. For the largest storms simulated here the storm sewer system would be expected to be overwhelmed in any case as in principle it is designed to drain only up to 20 or so years return period storm event. All the simulations were performed on the Newcastle University blade server with a 767GB RAM memory, except the simulation for Greater London where the Microsoft Azure platform was used. Table 5.4 shows the required memory and run time for every simulation per rainfall scenario.

Table 5.4 Number of grid squares, required RAM and simulation time per storm scenario.

Number of cells in computational grids	Cell size	Required RAM (GB)	Simulation time per storm scenario (min)
255,786	10 m	≈16	10
1,007,735	5 m	≈20	30
6,299,585	2 m	≈40	300
25,199,282	1 m	≈122	1200

5.4 Flood risk in London

Flood risk management in megacities, like London, is a critical aspect of urban planning and is exacerbated from the case of normal cities by the extra vulnerabilities of large (underground and overground) mass transit networks for their larger populations. Flood modelling is also crucial to these large cities in terms of insurance exposure as very large risk portfolios for residential and business properties are built up requiring re-insurance to spread the risk.

5.4.1 Modelled flow depth

In this section, the flood depth, the number of buildings exposed to flooding, the water flow paths, and the estimated inundated damages of each model were compared for the 1 in 100-year storm event with a 60min duration. The complex topography, roads, and the low gradient of the surface elevation in this part of London allow the examination of the direct influence of flooding on urban features and the detailed changes to flood flowpaths.

For models with lower spatial resolution (i.e. 5 and 10 m) significant underestimation of water depths, the buildings exposed to flooding and the changes to water flow paths can be seen in Figure 5.4. The differences between the 1m and the 2m resolution are minor, and resolution of the main flow paths in the domain can clearly be seen. The 5m resolution model outputs show blocking of the main roads in the catchment, and only the major flow paths associated with natural channels are satisfactorily captured. The use of a 10m resolution in the study area results in the underestimation of water depth and the occurrence of unrealistic concentrations of water in certain locations. This leads to the formation of unrealistic ponding upstream without posing a severe flood risk. An artefact of the low spatial resolution across the computational domain is the systematic differences in water depths. Figure 5.5 shows the distribution of modelled water depths among the different spatial resolution of the DTMs, which shows that low resolution modelling cannot produce the full range of flooding observed. Note here that the very high depths in these tables correspond to the Thames river and several ponds of the study area.

To achieve reliable results for flood risk management in large catchments in urban areas, it is advisable to avoid a square grid size larger than 5m in flood modelling. The sensitivity and the high accuracy of the Digital Terrain Models in flood models are crucial for designing effective flood defences in densely populated urban areas. This is especially important considering the projected urbanisation growth by 2050 and the anticipated increase in intense and frequent storm events due to climate change (United Nations Department of Economic and Social Affairs, 2019).

In general, considering the critical importance of accurate flood modelling in densely populated urban areas, the high-resolution of the DTMs is crucial in achieving reliable results for flood risk management. The findings presented in this study highlight the limitations of lower spatial resolution DTMs (5m and 10m) in accurately simulating flood depths, identifying buildings exposed to flooding, and capturing the water flowpaths in the urban fabric. Such underestimations and inaccuracies in flood modelling could have serious implications for designing effective flood defences. As megacities, such as London, continue to experience rapid urbanisation and face challenges of climate change, including more intense and frequent storm events, it becomes paramount the use of high-resolution DTMs (1m or 2m) to improve: a) accurate flood modelling; b) achieve flood resilience against intense storms.

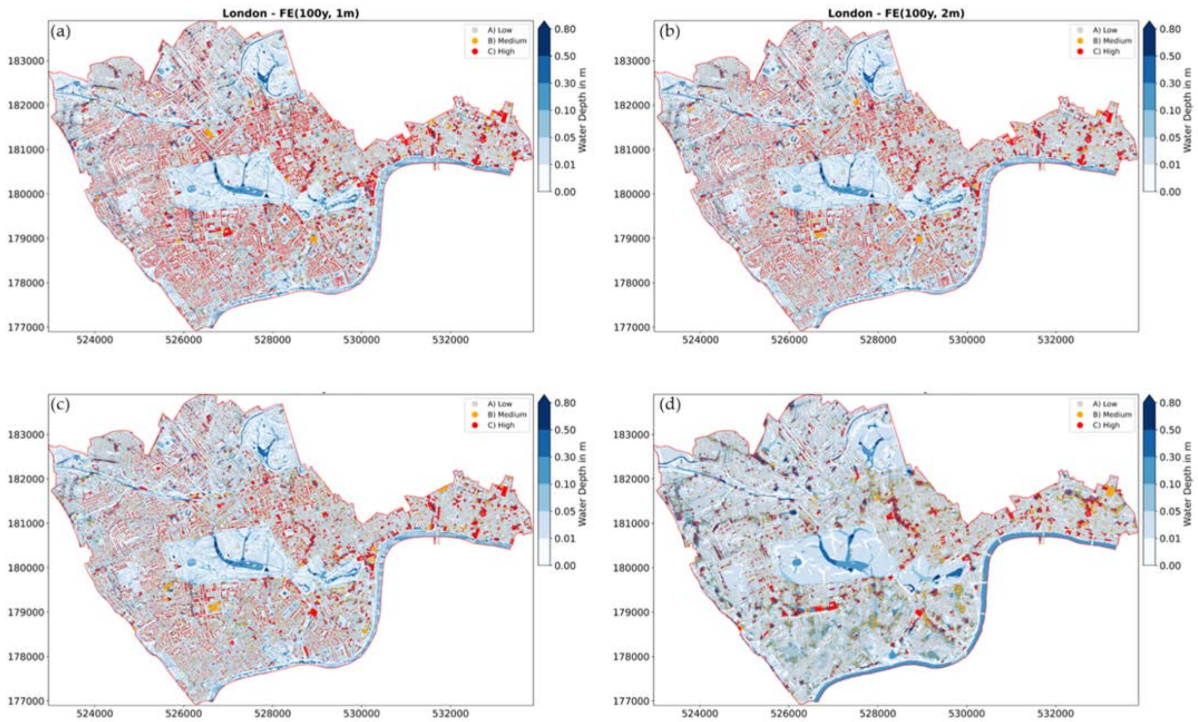

Figure 5.4 Example of flood exposure and modelled water depth for a 1 in 100-year storm event for grid resolutions of: (a) 1m ; (b) 2m ; (c) 5m ; and (d) 10m resolution.

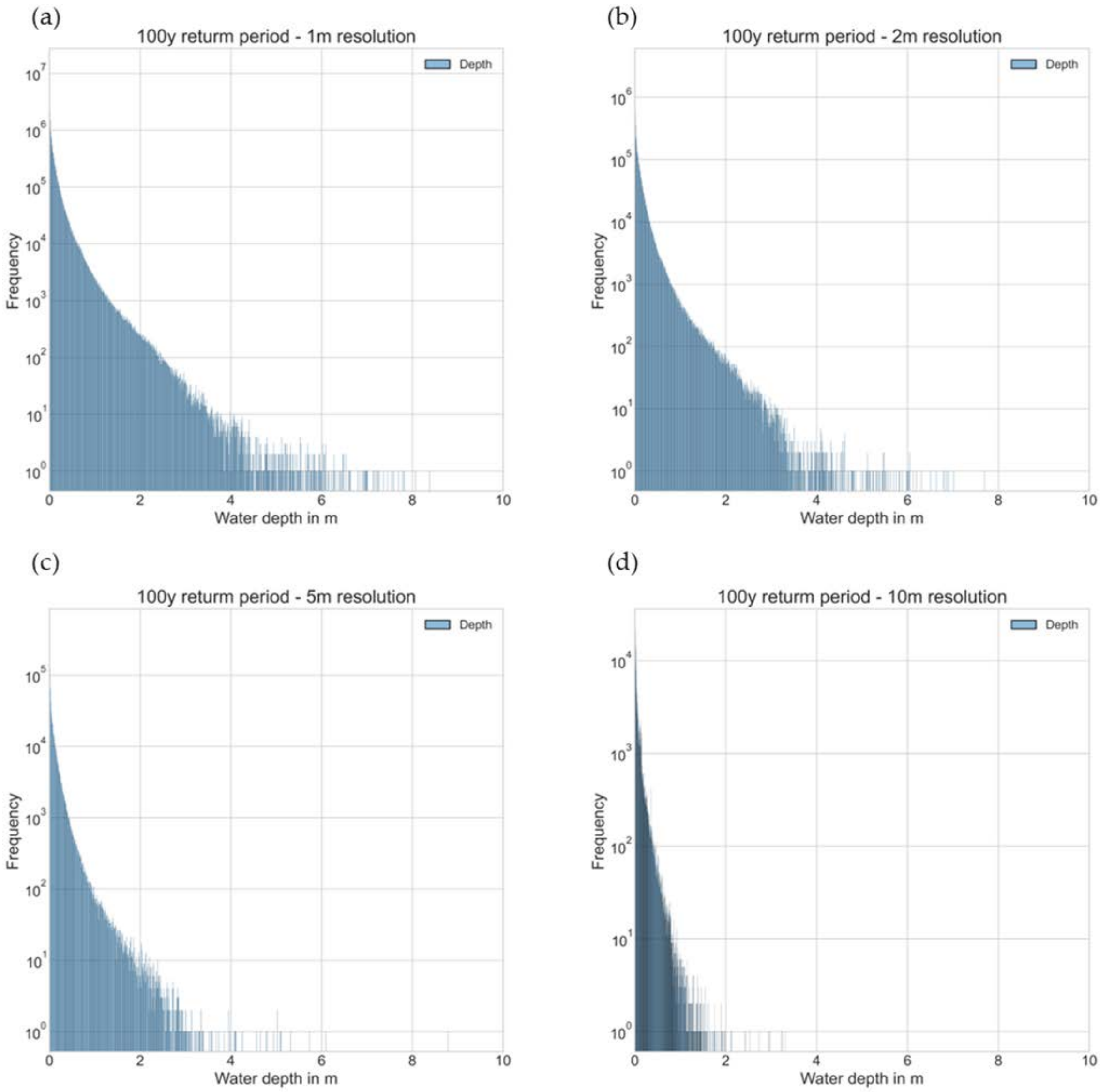

Figure 5.5 Distribution in water depth for: (a) 1m resolution; (b) 2m resolution; (c) 5m resolution; and (d) 10m resolution.

5.4.2 Exposure and flood damages to urban features

To identify and compare the urban features exposed to flood risk for multiple storm scenarios and resolutions of the DTMs, the flood exposure calculator was used (see section 5.2.4.) developed by Bertsch et al. (2022). There are 95,976 separate unique buildings identified by the MasterMap coverage in the domain. Figure 5.6a highlights the exposed buildings to surface flooding per storm scenario and different resolutions of the computational grid. The model with a 1m resolution estimates the largest number of buildings at flood risk for all the intensities of rainfall and the 10m the smallest, which is consistent with the correct capture of the water flow paths in the domain. Figure 5.6b presents the percentage of buildings at flood risk in the study area, where again the 1m resolution DTM shows the highest affected buildings from inundated depth. Figure 5.7 displays the buildings identified as being at high flood risk for multiple DTM resolutions. It is evident from the table that there is a noticeable decrease in the number of buildings at high risk estimated by the 10m resolution model compared with the 1m model. Figure 5.8 illustrates water depths and exposed buildings to flooding in a selected area of London, Mayfair, with a total of 3430 buildings. It can be seen that for lower spatial resolution, e.g. 5m and 10m, this shows a similar under-estimation as was seen in the larger domain. It can be seen that the use of a low resolution DTM (e.g. 10m) introduces erroneous obstructions to the flowpath, resulting in an increased flood risk upstream while simultaneously reducing the flood risk downstream. The disparity in building assessments is shown in Table 5.5, which illustrates the differences in the count of buildings exposed to elevated flood risks between the 1m DTM resolution and the 10m DTM resolution. While the classification scheme is unchanged for 2029 buildings, substantial shifts are seen for the remainder, such as transition from low to high risk (e.g., 575 buildings, constituting 16.8% of the total urban features) and vice versa (e.g., 826 buildings, accounting for 24.1% of the total), rather than gradual shifts between medium and high or high and medium risk. While the total number of buildings classified as high flood risk at the 10m DTM resolution is reduced to around half that at the 1m DTM resolution, this change is actually the net result of 826 buildings at reduced risk (mostly downstream of blockages to the flow pathways) and 575 at increased risk (mostly upstream of blockages).

The conventional approach was followed here of calculating the estimated damages from flooding with a Depth-Damage-Curve (DDC), with the simplification that the buildings in the study area are either all residential or all commercial. In megacities it is a very challenging task to categorise buildings[1] according to their type or to find proper data with all these useful pieces of information. The proposed prices from the Handbook for Economic Appraisal (Multi-Coloured Handbook, Priest et al. (2022)) were used to calculate the damages to residential and commercial properties. Average damages for residential and commercial buildings are given in Figure 5.9. For clarity, the buildings at low risk have been excluded from the damage calculation by assuming that the damages are only significant for buildings identified at medium and high risk.

The estimated total flood damages per storm scenario and per different resolution of the computational grid are presented in Figure 5.10. It can clearly be seen that improving the model resolution increases the total damages successively, with a factor of three increase from 10m to 1m resolution, and even around 25% from 2m to 1m. The modelled water depth, the exposed buildings, and the total estimated damages in the Mayfair area of London are shown in Figure 5.11. Major differences can again be seen between coarse resolution (10m) model estimates and the higher resolution estimates (1m and 2m). This example shows that coarse models (10 m or worse) can substantially misidentify areas of flood risk, in this case by severely under-estimating the risk in the centre of the map and over-estimating the risk in the north west sector.

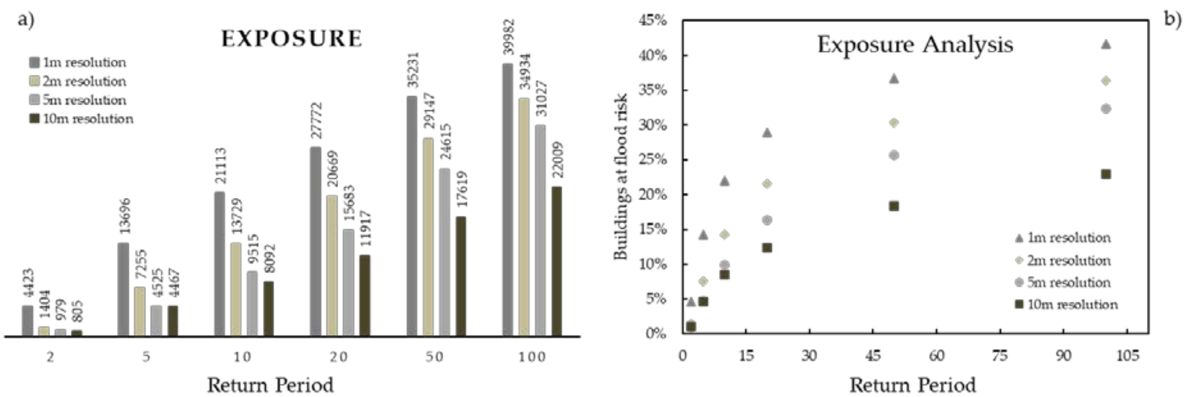

Figure 5.6 a) Total numbers and b) Percentage of inundated buildings per storm scenario and per DTM resolution.

[1] The GeoInformation Group (2014): UK building classes. NERC Earth Observation Data Centre, 07/07/2023.

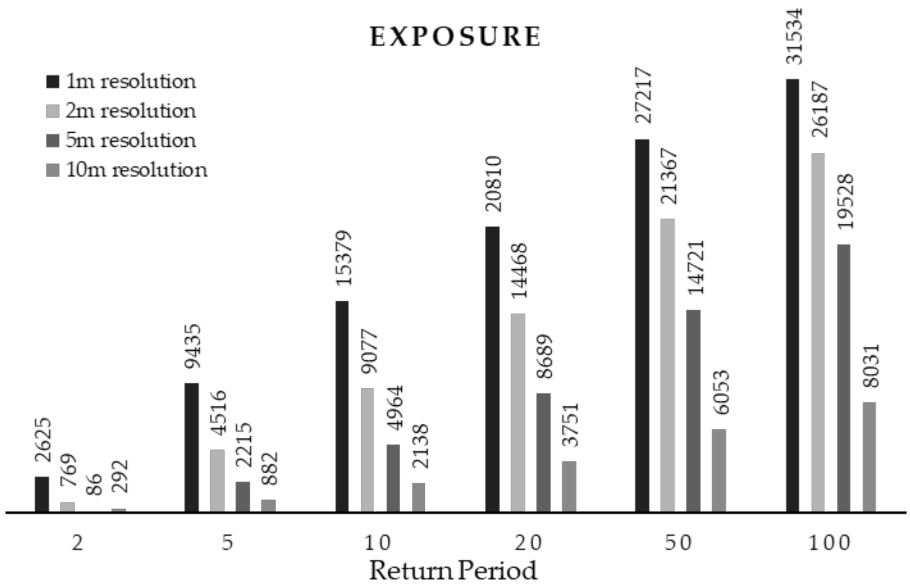

Figure 5.7 Number of buildings at high flood risk per rainfall scenarios and per DTM resolution.

Table 5.5 Analysis of changes in numbers of buildings with flood risk for 1m and 10m DTM resolution models, for a 1 in 100-year storm event

	Number of buildings (total 3430)	**Percentage of total**
High Flood Risk – 1m model	695	20.3%
High Flood Risk – 10m model	363	10.6%
No change from 1m and 10 m models	2029	59.2%
Change: Zero/Low/Medium to High	575	16.8%
Change: High to Zero/Low/Medium	826	24.1%
Net change : High to Zero/Low/Medium	251	7.3%

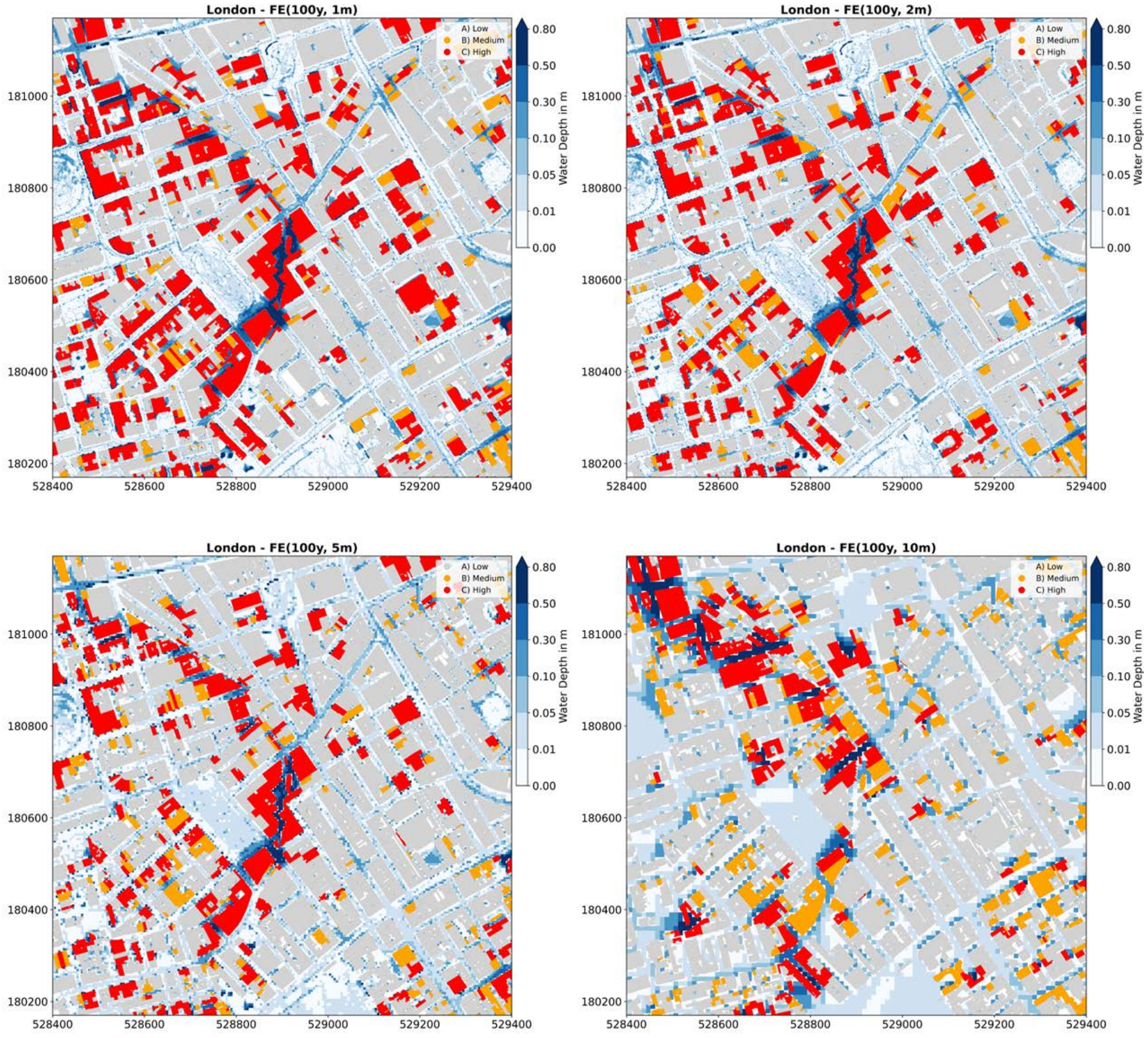

Figure 5.8 Examples of water depth and flood exposure to buildings, inundation maps for a 1 in 100-year storm event for: (a) 1m resolution; (b) 2m resolution; (c) 5m resolution; and (d) 10m resolution of the computational flow domain. *FE* refers to flood exposure. Red, orange, and light grey colours define buildings at high, medium, and low risk respectively, while blue shades are water depths.

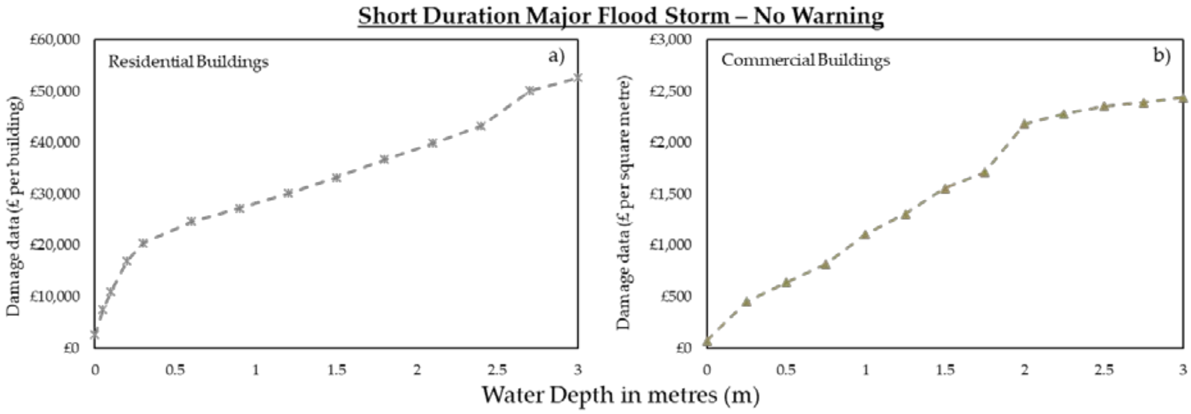

Figure 5.9 Depth damage curves for direct damage from different water depths for: (a) residential buildings; (b) commercial buildings (Priest et al., 2022).

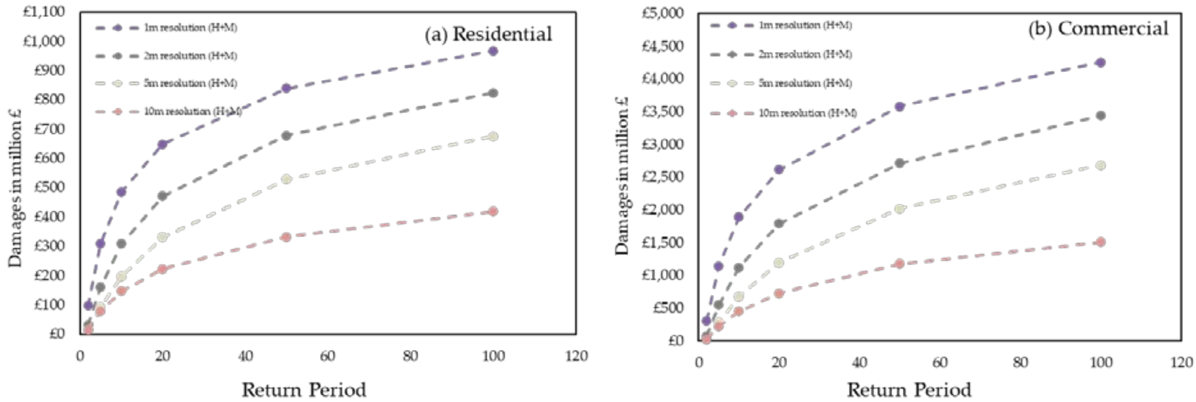

Figure 5.10 Estimated total damages per storm scenario and per spatial resolution.

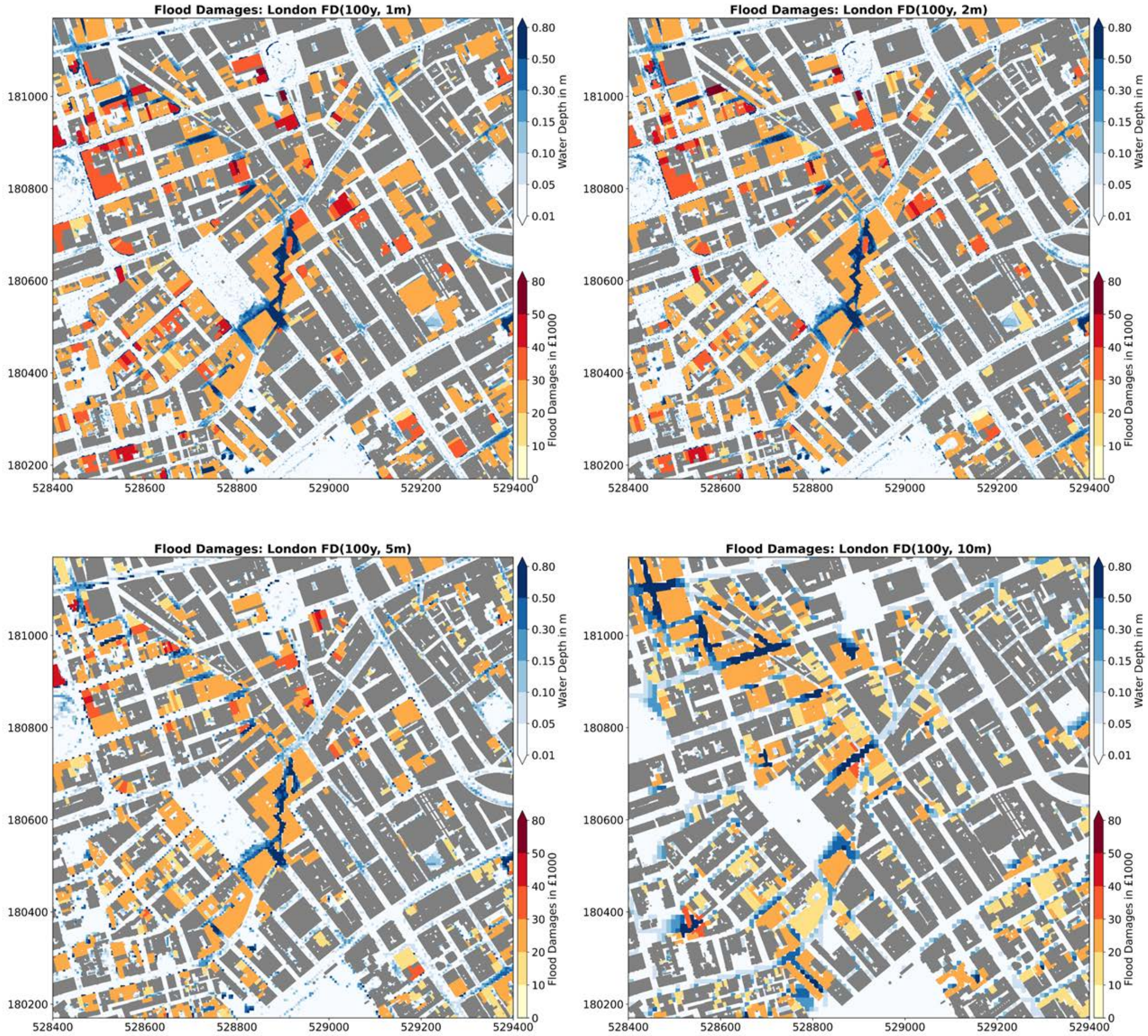

Figure 5.11 Examples of water depth, flood exposure and damages to building maps for a 1 in 100-year storm event for: (a) 1m resolution; (b) 2m resolution; (c) 5m resolution; and (d) 10m resolution of the computational flow domain. *FD* refers to flood damages, and yellow to red defines the cost per building from flooding.

5.4.3 Validation against real storm event

Validation against real events is a fundamental step in assessing the reliability and accuracy of hydrodynamic models by comparing observed data from actual storm events with the model predictions to increase planning and designing flood resilience in cities. This process builds confidence in the model's ability to accurately simulate flood events and has largely been absent from commercial modelling of urban floods to date, but there is potential due to increased availability of flood depth data from social media and citizen science, e.g. Loftis et al. (2017) and See (2019). In this section, a validation between affected locations during a real rainfall event and the outputs from CityCAT will be compared. Following the extreme storm event on the 12th of July 2021, fourteen flood points in the whole area of London have been selected (the flood points correspond to roads with buildings) where the observed depth was estimated from flood pictures downloaded from the Twitter platform during the day of this extreme event and from statements of people affected (Table 5.6). This comparison aims to ensure that the modelled water depth from CityCAT corresponds to the observed data. The resolution of the DTM for the validation has been chosen at 2m, as it resolves the water flowpaths quite well in large catchments as discussed in section 5.4.1. Table 5.6 presents the affected sites with the observed (Dobs refers to observed depth) and the modelled data (Dmin refers to minimum model water depth and Dmax to maximum model water depth), while Figure 5.12 is the graphical comparison of the results. To ascertain the range of estimated water depths (Simulated range) at the observed points, a 12-metre buffer zone was generated to encompass the neighboring computational cells. Both the model and the observed values are associated with the nearest grid square location. It can be seen that there is some overestimation of the depths by the model, which is consistent with the exclusion of the drainage system from the simulations (see point 12). The largest difference (at point 4) between the observed and the modelled water depth is most likely because the observed depth is measured inside the property (see Figure 5.13 for the fourteen flood points with the flood picture) while CityCAT has excluded the buildings from the computational flow (see section 5.3.2.) and estimates the depth in the nearest surface grid of the building. In the other flood points, the modelled inundated depth is satisfactorily close to the observed depth. Figure 5.14 illustrates the likelihood of inundation exposure to buildings in the study area during this historic storm event.

The CityCAT model has demonstrated acceptable accuracy in predicting depths at affected areas during validation. This highlights the model's effectiveness in detecting areas that may be impacted by various factors, such as floods. It is worth noting that the modelled water depths, on average, show an overestimation of around 23%. This overestimation can be attributed to the exclusion of the drainage system from the simulations, and that there is a systematic bias due to the observed data being carried out by eye at the deepest point due to the limited access to flood survey data. This validation has been carried out with opportunist reports of flood depths, focussed on areas where flooding was severe. A more balance and substantive approach in addition to comparing these "*true hits*" would consider more systematically areas where actual depths were low and model depths were high (i.e. "*false hits*") as in, for example at Bertsch et al. (2022). Such an approach requires a systematic survey of property owners and residents, and this was not available at the time of writing.

Table 5.6 Flood validation points in London during the 2021 storm event with observed and model estimated water depth.

A/A	Flood Points	Dops	Dmin	Dmax	Model depth in m
1	Horse Guards Road	0.07	0.034	0.49	0.10
2	Leicester Square	0.01	0.002	0.16	0.02
3	Piccadilly Circus	0.10	0.002	0.22	0.13
4	Ladbrook Grove	0.60	0.001	0.82	0.82
5	Maida Vale	0.65	0.001	0.75	0.75
6	Portobello Road	0.38	0.110	0.46	0.46
7	Dorset Square	0.25	0.133	0.34	0.34
8	Maida Vale	0.07	0.116	0.27	0.08
9	TFC Camberwell	0.23	0.204	0.42	0.29
10	Hackney Wick DLR Station	0.22	0.400	0.61	0.25
11	New Covent Garden Market	0.30	0.002	0.34	0.34
12	Brookfield Rd	0.35	0.510	0.99	0.40
13	Lea Bridge road	0.90	0.002	0.96	0.96
14	Idea Store Whitechapel	0.22	0.002	0.84	0.25

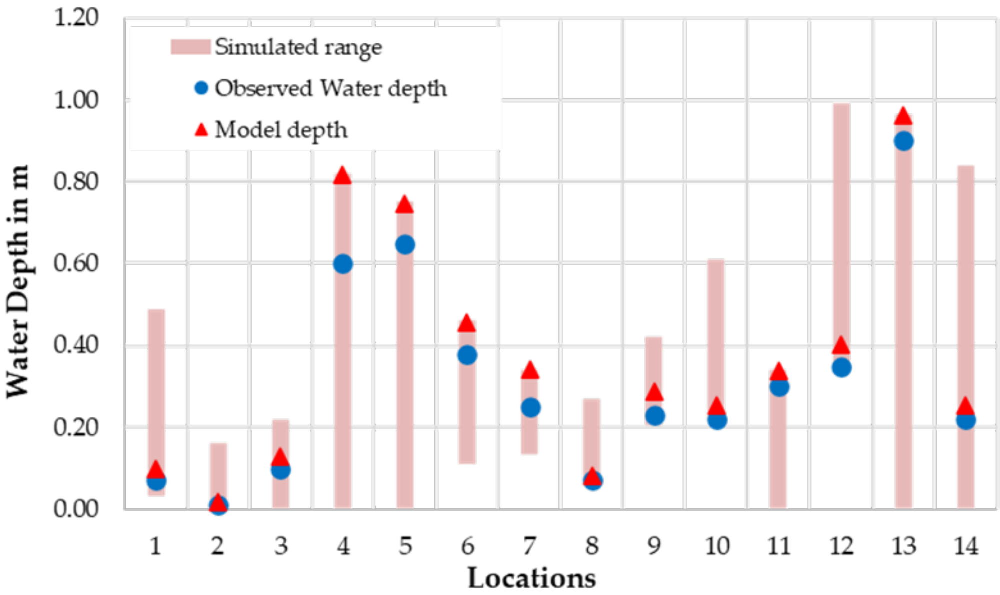

Figure 5.12 Comparison of the modelled and the observed water depths.

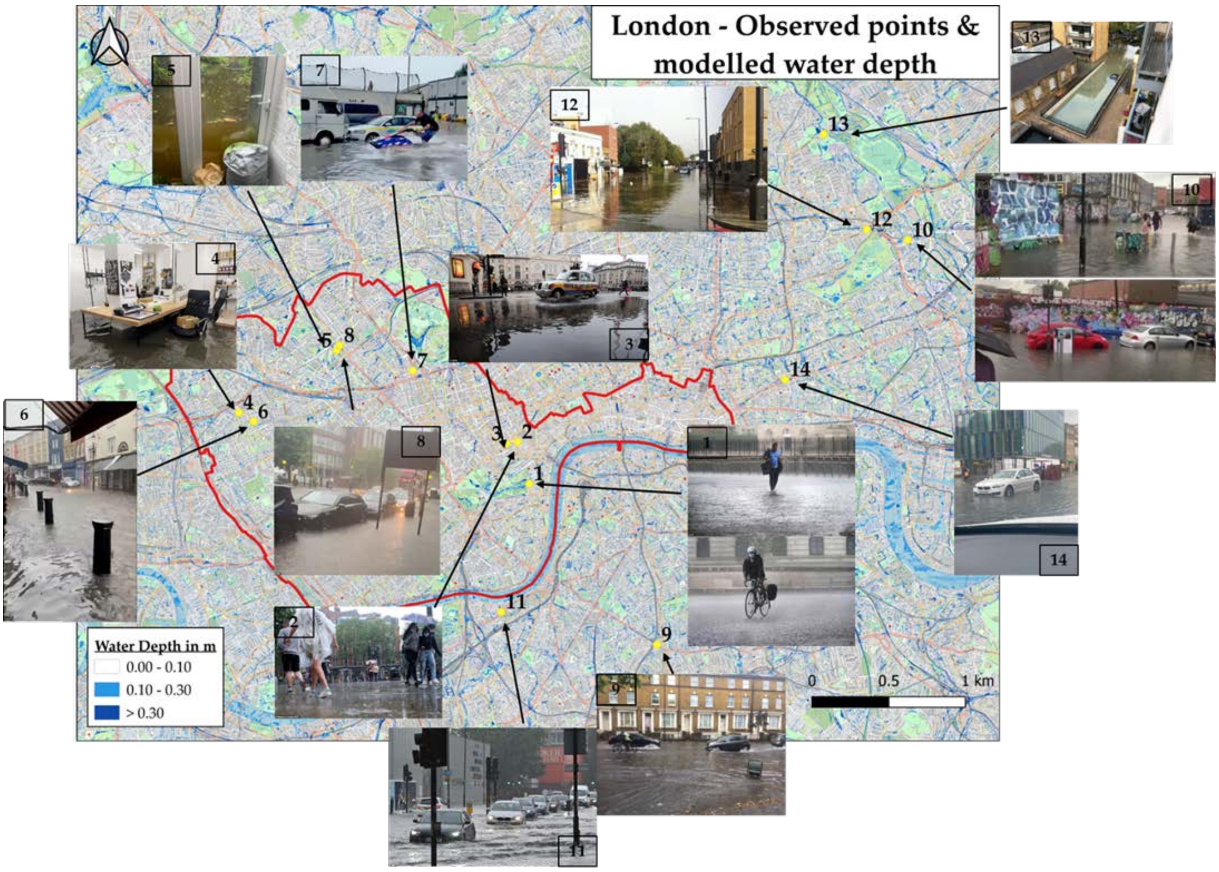

Figure 5.13 Overview of the study area with the validation locations and the modelled inundation depth for the whole domain.

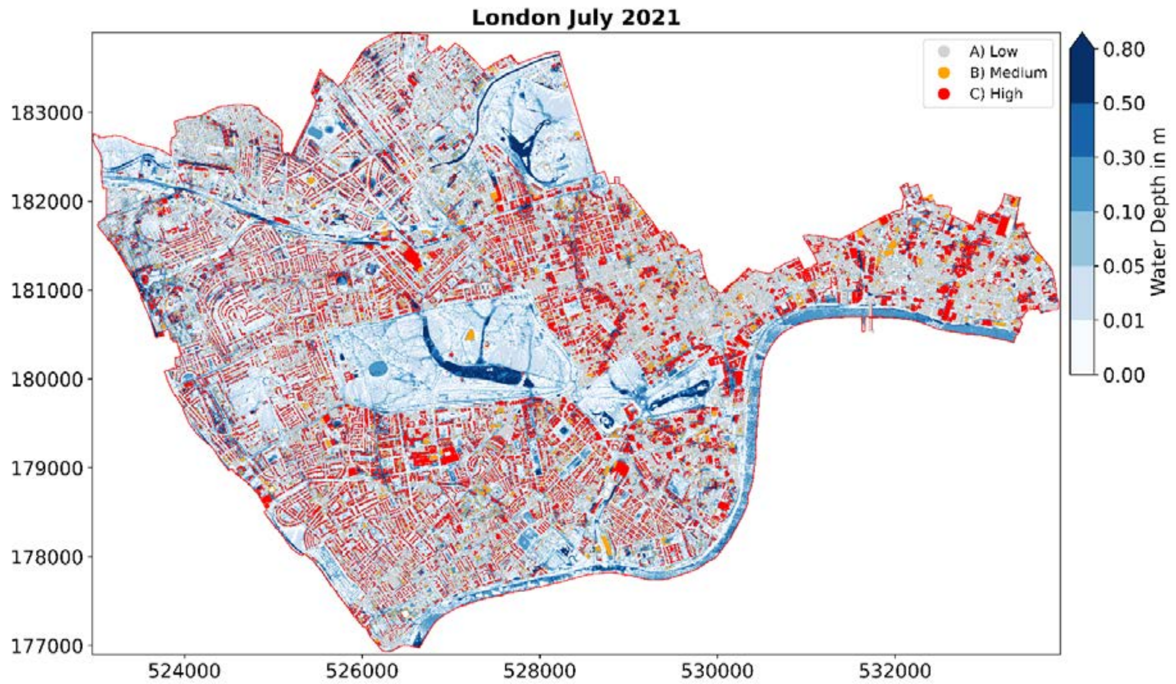

Figure 5.14 Water depth and flood exposure to buildings during the storm event in July 2021 for the central London (first part of validation).

5.4.4 Cloud flood modelling – The Greater area of London

Assessing flood risk in megacities, like London, is always a challenging task due to the limitation of computer power and the possible high cost of using the cloud. In this section, a flood risk analysis with a DTM at a high spatial resolution of 4m^2 (grid square is 2m) for all individual properties in Greater London is presented for a range of intense rainfall events by using the power of the cloud to model an area of 687 km^2 which comprises 132,857,544 computational cells in the flow domain and 1,750,914 buildings approximately. Thus, this approach is suitable for a densely built-up area such as London. The outputs of this analysis are at property level, so in principle, and with appropriate validation, could be appropriate for detailed insurance portfolio assessment, as well as large scale strategic planning, resilience, and climate change stress tests.

Microsoft Azure platform (Microsoft, 2022) was used to perform all the simulations of this area with 700GB RAM memory and almost 20 hours of CPU time for each storm event with a one-hour duration. The advantage of the Azure platform is that it provides the same simulation cost per hour for all the instance types of resources and for that reason has been chosen (Glenis et al., 2013), with different configurations ranging from 1 core with 1 GB RAM to 96 cores with 1 TB RAM. The final cost of every simulation was around £12 per hour. Calculating the likelihood of exposure to urban features for each storm event required an additional four hours per storm scenario on the Newcastle University blade server. Table 5.7 shows the buildings estimated to be exposed to flooding for multiple storm events for a storm with a 1 in a 100-year return period where the total urban features correspond to the 16% buildings of in the study area. Figure 5.15 illustrates the estimated model water depth and the buildings exposed to flooding in the Greater London area (more flood exposure maps are available on Appendix B).

This is the first time that such a large urban area has been modelled with a hydrodynamic model at such a high spatial resolution and for a range of storm events. The industry standard until now for large areas typically uses a DTM at 5m resolution and the *'stubby'* platform for the representation of buildings where this approach according to Iliadis et al. (2023b) causes unrealistic water flowpaths in the domain and systematically underestimates flood risk. This study is a clear demonstration that modern, efficient codes like CityCAT, coupled with Cloud-based computing, obviate the need for simulating large domains at either inadequately low resolutions, or with inefficient sub-divisions of the domain.

Table 5.7 Total number of inundated buildings per storm event for the Greater London area.

RP	Medium	High	Total
2	5,159	5,447	10,606
5	13,458	15,274	28,732
10	37,553	48,948	86,501
20	50,414	68,337	118,751
50	63,189	89,885	153,074
100	105,381	163,516	268,897

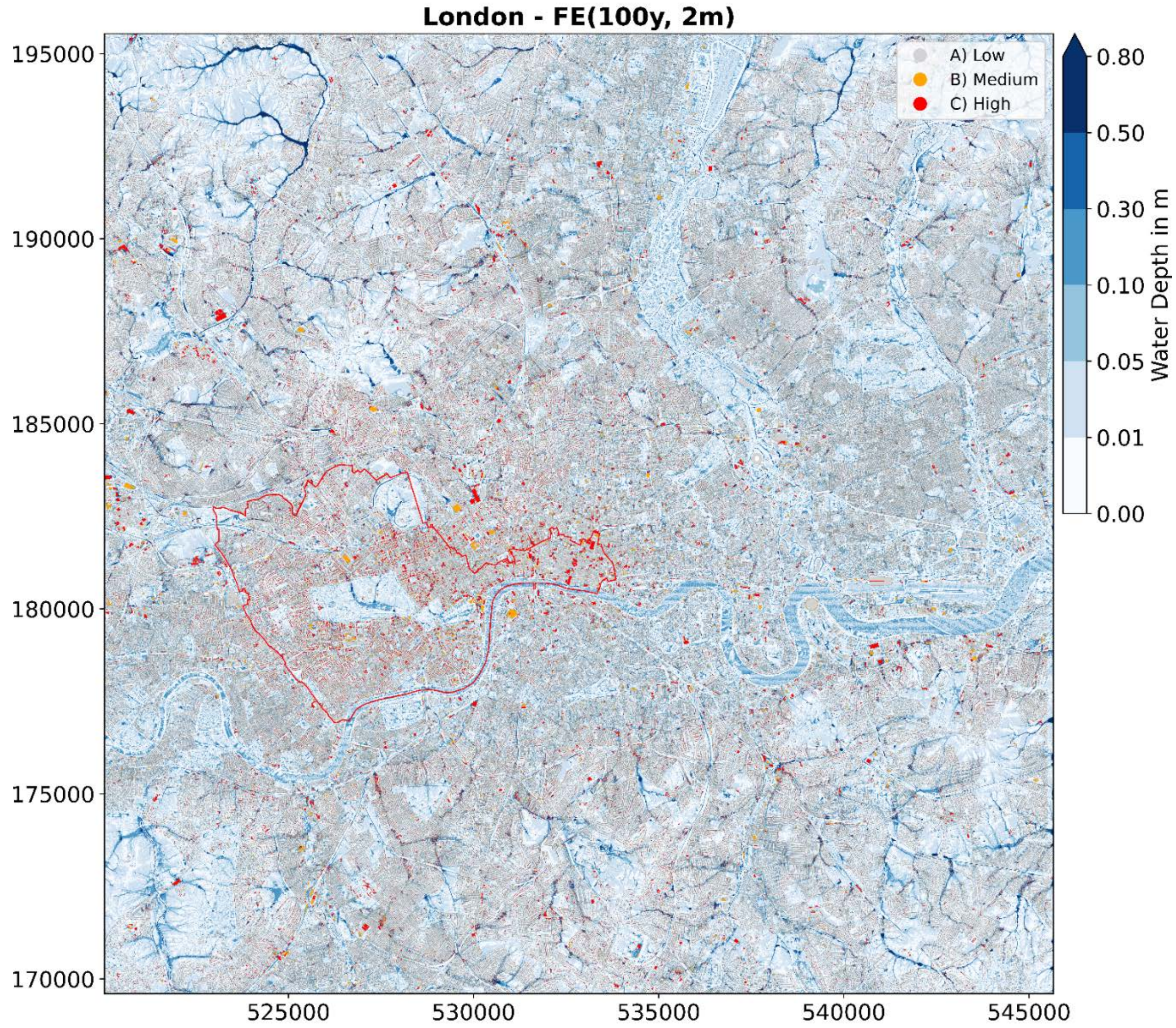

Figure 5.15 Example of the modelled domain of Greater London. Flood depths from CityCAT simulation and flood exposure to buildings for a storm event for a 1 in 100-year return period with one hour duration. The red colour defines the buildings at high risk, the orange at medium risk and the light grey at low risk.

5.5 Discussion & Conclusions

This study illustrates the critical role of DTM resolution in large scale hydrodynamic flood modelling, using an application which evaluates the flood exposure to individual buildings in a large city. The high resolution hydrodynamic model CityCAT operating on the Azure platform (cloud) is presented to assess the flood risk in megacities which provides a template and guide for modellers engaged by insurers, local authorities, and other risk managers and planners to define modern assessment strategies and workflows.

Water flowpaths and flood depths are well captured with a high spatial resolution DTM, such as 1m and 2m resolution, while with a lower resolution DTM (5m or more), many flowpaths are systematically blocked due to buildings. In many cases with low resolution DTM models, blocked flowpaths lead to some overestimation of water depths upstream, while downstream widespread under-estimation occurs, leading to unrealistic results by falsely highlighting areas as high risk. Moreover, assessing the exposure flooding likelihood of urban features with a high-resolution offers more accuracy in identifying and locating all the exposed buildings, in contrast with the low-resolution modelling where there is overall a manifest underestimation.

A validation of model estimates of water depth during a real storm event in multiple places in London showed that the use of a 2m resolution DTM in CityCAT successfully predicts the water depth, with an overestimation of 23% consistent with the exclusion of the sewer system from the simulations, and the systematic bias via eye. A more comprehensive and systematic validation is planned when flood survey data are available. Overall, the model results have a good correlation with observed flood data from a major pluvial flood on the 12th of July 2021.

Finally, cloud computing has enabled higher resolution of pluvial flood modeling and access to enough resources to allow simulations for multiple storm events in larger areas than before with the hydrodynamic model CityCAT. This novel city-wide scale application in London demonstrated here can be replicated for other megacities globally to cover the needs of urban flood risk management assessments. An efficient collaboration between the insurance industry and other hazard management agencies could offer verification of the results to validate and test the estimated model depths for real rainfall events.

Further work is in hand to improve simulations in megacities by adding the storm drainage or combined sewer network. This is a major challenge, since the network data and properties are rarely available, forcing modellers to use approximations such as the UK practice of subtracting 12mm/hr from the observed rainfall. While this approach can be improved using spatially variable pipe capacity datasets (e.g. Singh et al. (2023)), the high resolution approach demonstrated here demands a similarly high resolution and accurate representation of pressurised flows in storm drainage networks (see e.g. CityCAT capability in Bertsch et al. (2017)) to account for potentially important interactions between the surface and network flows. An urgent need is evident to establish a standardized and straightforward methodology for accurately representing sewer systems, particularly in cities where datasets are scarce. This can be achieved by generating synthetic storm drains that mirror the prevailing conditions and comply with the design regulations of every country. A pioneering effort in this direction was made by Bertsch et al. (2017) in a Scottish city, where they successfully calibrated and validated a systematic approach for simulating synthetic storm inlets against the existing drainage system. This approach holds promise in addressing the challenges posed by limited data availability and can significantly contribute to improving the representation of sewer systems.

Chapter 6. Urban Flood Modelling under Extreme Rainfall Conditions for Building-Level Exposure Analysis

The collaboration of this chapter involved Newcastle University and Aristotle University of Thessaloniki, Greece. In terms of my contribution, I played a significant role in analysing the extreme rainfall information, modelling the storms in the study area and calculating the likelihood of exposure to buildings. The editing of this chapter was a joint effort between me and Dr. Panagiota Galiatsatou from Aristotle University, who supervised the part of the extreme rainfall.

6.1 Introduction

Urban surface water floods are amongst the most widely distributed natural hazards, endangering lives and causing damage to properties worldwide. The extent and severity of the damage is a product of both the intensity and duration of extreme rainfall events (variable in space and time), and their interaction with the complex flowpaths in a city on the ground surface and below it (Iliadis et al., 2023b). Impermeable surfaces in urban areas, impeding infiltration and creating overland flow which exceeds the drainage capacity of the existing infrastructure, renders cities vulnerable to flash floods. Climate change and urbanisation are expected to increase urban flood risk, contributing to different components of the flooding system. Climate change, associated with global warming and an increase in the frequency and severity of extreme weather events, is anticipated to intensify flooding hazards. Urbanisation will contribute to the increase in flooding hazards, caused by a decrease in infiltration, baseflow and lag times and an increase in runoff volumes and peak discharges (Ogden et al., 2011; Suriya & Mudgal, 2012), but also to the increasing impacts of urban floods (increase in potential flood damages) caused by the growth of settlements and assets in flood-prone areas followed by a rise in property value in such areas (Cabrera & Lee, 2019; Park et al., 2021).

Nowadays, urban floods affect both developing and developed countries, with the impacts of pluvial flooding being a major problem due to frequent natural disasters in urban areas (Teng et al., 2017). Flood damage mitigation in urban areas includes both structural and non-structural measures. Structural measures involve urban flood defences and flood control structures or designing or upgrading stormwater and drainage networks. Non-structural measures mainly focus on flood early warning systems and preventive actions (Andjelkovic, 2001; Park et al., 2021). Urban flood modelling combined with exposure assessment of the buildings and population affected represents a principal non-structural measure to effectively manage urban flooding events and their adverse effects, as well as a prerequisite for disaster prevention and mitigation.

Flood modelling is a powerful tool in understanding the hydrodynamics of historic flood events, and in some cases, the construction of accurate IDF (intensity–duration–frequency)/DDF (depth–duration–frequency) curves can be used to predict future events that will cause damage to the urban fabric (Willis et al., 2019). There exist several studies combining flood inundation modelling with hydrological modelling and the unit hydrograph theory, mainly focusing on fluvial flooding in small or larger catchments (Bellos & Tsakiris, 2016; Hdeib et al., 2018; Papaioannou et al., 2018; Papaioannou et al., 2019; Papaioannou et al., 2021; Xafoulis et al., 2023), using DEMs (Digital Elevation Models) or DTMs (Digital Terrain Models) with a computational grid resolution ranging between 5 m and 100 m. However, it should be noted that the combination of an incorrect representation of urban features in the flood model such as buildings, bridges, infrastructure, etc., and the resampling of the DEM/DTM multiple times might cause large inconsistencies (Alcrudo, 2004; Iliadis, Glenis, et al., 2023b; McClean et al., 2020) and overestimation of the flooding hazard in areas with minor inundation issues and vice versa. Unlike studies modelling fluvial flood inundation in urban areas, studies focusing on the exposure assessment of urban areas to pluvial floods are rather limited, and started receiving significant interest quite recently. Zhu et al. (2020) used the LISFLOOD-FP hydrodynamic model to simulate flooding in Lishui City, China, and employed the building-scale population distribution map to assess the population affected. Park et al. (2021) evaluated flood risk for different building types, conducting vulnerability and exposure analysis in five regions of Ulsan City, South Korea. Their analysis resulted in a classification of each building type into five risk-related classes. Stefanidis et al. (2022) presented a coupling of hydrological and hydraulic modelling on a national scale to produce flood hazard maps regarding flooding exposure in residential areas and infrastructure in Greece. Bertsch et al. (2022) presented a sensitivity analysis and validation of a generic flood exposure analysis following a large storm event in Newcastle upon Tyne, UK, where more than 70% of the inundated buildings in the area were correctly identified during the storm event.

Pluvial flood risk assessment in urban areas, associated with estimating the hazard, exposure, and vulnerability components for the affected system, is therefore a major challenge for future societies. There is a great need to combine hydrological and hydrodynamic modelling to understand the impacts of urban floods, the water flowpaths in a city, and the urban features exposed to high flood risk. This study combines a detailed analysis and modelling of extreme rainfall events in the centre of Thessaloniki, Greece, with an advanced hydrodynamic model, CityCAT, to simulate pluvial flooding, significantly assisting a reliable assessment of exposure to flooding. The results of this study can aid in the planning and design of resilient solutions against urban flash floods, as well as contributing to targeted flood damage mitigation and flood risk reduction.

CityCAT has previously been applied in studies in the UK (Bertsch et al., 2017; Bertsch et al., 2022; Glenis et al., 2018; Iliadis, Glenis, et al., 2023a, 2023b) and the USA (Rosenzweig et al., 2021) (Environmental Justice of Urban Flood Risk and Green Infrastructure Solutions-Urban Systems Lab, Urban Flooding, Equity, and Green Infrastructure (https://storymaps.arcgis.com/stories/3d982b40189c42aa9af56d52548caaf0, accessed on 10 July 2023)), where detailed and reliable spatial datasets were available, such as

DTMs, building footprints, green spaces, and roads. This chapter also aims to demonstrate and assess the universal applicability of CityCAT, even in regions where comparable datasets may not be readily available, emphasising the value of integrating the model with extreme rainfall data to enhance flood resilience in urban areas. The practical implementation of the model in this study will assist local authorities and engineers in improving their future flood adaptation strategies. This chapter also marks the first published implementation of a flood exposure analysis calculator at the building level in a large Greek city, as opposed to conventional assessments limited to flood zoning.

6.2 Materials and Methods

6.2.1 Study area and available datasets

The historic centre of Thessaloniki city in Greece was the study area of the present work, located in the northern part of Greece. Thessaloniki is part of the municipality of Central Macedonia, and it is the second largest city in Greece with a population of around 814,000 (Thessaloniki Population 2023: worldpopulationreview.com, accessed on 5 June 2023). The dense city centre facing the coastal front is characterised by historic buildings, residential properties, marketplaces, and a few green open spaces (see Figure 6.1). This part of Thessaloniki has suffered from severe storms and flash floods in the last decade, causing significant damage to roads, basements, local stores, etc. It should be noted that, during storm events, the roads are seen to become the main flowpaths for floodwater.

Two different datasets are available in the study area for the analysis of extreme rainfall events. The first dataset consists of daily rainfall data at AUTh (Aristotle University of Thessaloniki) station located in the centre of the city and covering 64 years (1958–2021) of measurements (no missing data are present), obtained from the database of the School of Geology, AUTh. The second dataset includes monthly maximum rainfall depths for rainfall durations of 5 min, 10 min, 15 min, 30 min, 1 h, 2 h, 6 h, 12 h and 24 h at Mikra station, located in the eastern part of the city. This dataset was made available by the Hellenic National Meteorological Service (HNMS) and covers a period of 25 years (1963–1987). It is therefore evident that the second dataset includes rainfall measurements of finer temporal scales than the first one, but it contains only monthly maximum values, and its length is significantly shorter than that of the daily rainfall series available at AUTh. It should also be noted that the second dataset contains missing values. To proceed with the extreme value analysis of all available datasets, annual maxima were first extracted for both the daily and the sub-daily series, and each dataset was tested for stationarity and trends (Coles et al., 2001). The datasets examined satisfy the hypothesis of stationarity, while no statistically significant trends were detected.

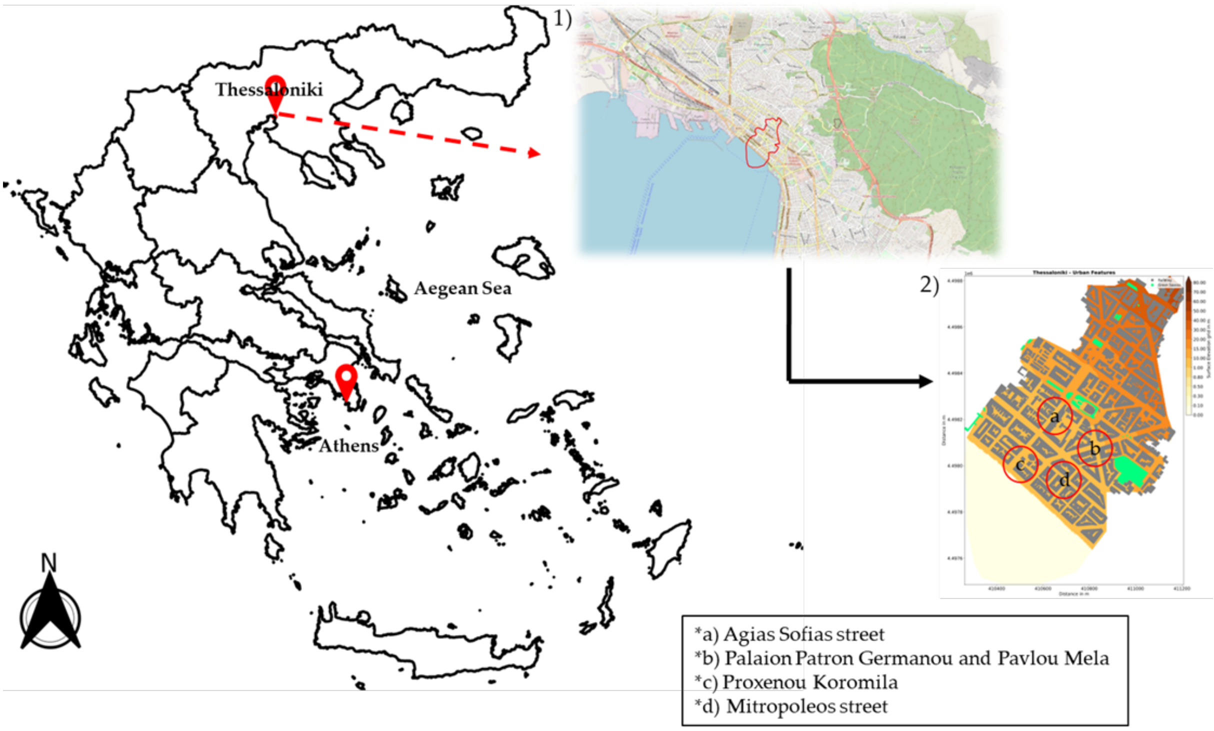

Figure 6.1 An overview of the study area in Thessaloniki, Greece: a) the computational domain; b) the urban features, where grey denotes the buildings, green the permeable areas and yellow to brown shading the surface elevation of the area.

6.2.2 Extreme rainfall assessment

Extreme value theory includes two main approaches for identifying and modelling the extreme values of a random process, namely the block-maxima approach where the extremes follow a generalised extreme value (GEV) distribution, and the peaks-over-threshold (POT) approach that fits the extremes using a generalized Pareto distribution (GPD). In the former approach, the observation period is divided into nonoverlapping equal intervals (of length usually equal to one year) and block maxima are selected to be fitted according to a GEV distribution (Coles et al., 2001)

$$G(x;\mu,\sigma,\xi)=\begin{cases}\exp\left\{-\left[1+\xi\left(\frac{x-\mu}{\sigma}\right)\right]^{-1/\xi}\right\},\ \xi\neq 0\\ \exp\left[-\exp\left(\frac{x-\mu}{\sigma}\right)\right],\ \xi=0\end{cases} \tag{6.1}$$

where μ, σ and ξ are the location, scale and shape parameters of the distribution, respectively. The POT approach employs two probability distribution functions: one for the intensity of exceedances over an appropriately defined threshold, typically a GPD, and another for the number of events per year (typically a Poisson distribution, or alternatively a constant number is used). The cumulative distribution function of the GPD is given by (Coles et al., 2001):

$$G(x;\sigma,\xi,u)=\begin{cases}1-\left[1+\xi\left(\frac{x-u}{\sigma}\right)\right]^{-1/\xi},\ \xi\neq 0\\ 1-\exp\left(-\frac{x-u}{\sigma}\right),\ \xi=0\end{cases} \tag{6.2}$$

where σ and ξ are the scale and shape parameters of the GPD, respectively, while u is the defined threshold value. The scale parameter of the GPD, sometimes referred to as the modified scale parameter, is expressed as a function of the respective GEV scale parameter as:

$$\sigma_{GPD} = \sigma_{GEV} + \xi(u - \mu) \tag{6.3}$$

considering that the shape parameter, ξ, of the GPD is equal to that of the corresponding GEV. The GPD-Poisson, which employs the Poisson distribution to model the number of exceedances over the threshold value per year, is characterized by three parameters, the exceedance rate, λ, the scale, σ, and the shape, ξ, parameters. Considering the threshold of the POT approach, a high value improves the validity of the asymptotic approximation of the GPD, but at the same time increases the variance of parameter estimates because of the reducing dimensions of the excess sample. In contrast, a very low threshold may increase bias from model misspecification (Mackay & Jonathan, 2020; Northrop & Coleman, 2014). Finding a trade-off between these two issues is critical in fitting an extreme value distribution and producing reliable estimates of extremes. The parameters of the extreme value distributions were assessed using both maximum likelihood estimation (MLE) and the L-moments (Galiatsatou & Prinos, 2011) approach.

6.2.2.1 POT threshold selection

When the POT approach is used to model rainfall extremes, an appropriate threshold should be selected to detect exceedances and define the extreme sample. Various threshold selection methods have been proposed in the literature, such as empirical methods, distance measure approaches, or diagnostic plots such as the mean residual life plot and GPD parameter estimates stability plots (Alonso et al., 2014). However, these approaches have a significant level of subjectivity in the threshold selection process. This chapter uses two methodologies, which aid a more automatic threshold selection (Radfar & Galiatsatou, 2023). These threshold selection methods are proposed by Bader et al. (2018) and Silva Lomba and Fraga Alves (2020) assisting a less ambiguous and more objective selection of daily extreme rainfall events.

Bader et al. (2018) consider a set of candidate thresholds $u_1 < \ldots < u_l$, each having n_i exceedances, $i = 1, \ldots, l$. Let $H_0^{(i)}$ denote the null hypothesis that the distribution of n_i exceedances above the threshold u_i follow the GPD. Following the Forward stop rule of G'Sell et al. (2016) a rejection rule is constructed by returning a cutoff level $\hat{k}$, such that H_1 to $H_{\hat{k}}$ are rejected:

$$\hat{k} = max\left\{k \in \{1, \ldots, l\}: -\frac{1}{k}\sum_{i=1}^{k} log(1 - p_i) \leq a\right\} \tag{6.4}$$

where a is a prespecified significance level and p_i $i= 1, \ldots, l$ are the corresponding p-values of the l hypotheses. If there is no $\hat{k} \in [1, \ldots, l]$, there is no rejection of the null hypothesis.

The p-values in Eq. (6.4) are assessed using the Anderson-Darling (AD) test for each candidate threshold, with the respective statistic assessed as:

$$A_n^2 = -n - \frac{1}{n}\sum_{i=1}^{n}(2i - 1)\left[log\left(z_{(i)}\right) + log\left(1 - z_{(n+1-i)}\right)\right] \tag{6.5}$$

where $z_{(i)} = F\left(y_{(i)}\middle|\hat{\theta}_n\right)$ is the probability integral transformation of the order statistics of the exceedances $y_{(1)} \leq \ldots \leq y_{(n)}$, based on the maximum likelihood estimator of θ, $\hat{\theta}_n$, under the null hypothesis H_0. F denotes the cumulative distribution function of the GPD for each candidate threshold.

The methodology proposed by Silva Lomba and Fraga Alves (2020) is based on L-moments. For the random variable X with distribution function F, the theoretical L-moments λ_{r+1} with r=0, 1, .. are expressed as linear functions of the specific probability weighted moments (PWM):

$$a_r = M_{1,0,r} = \mathrm{E}\{X[1 - F(X)]^r\} \tag{6.6}$$

with the dimensionless L-moment ratios L-skewness, $\tau_3=\lambda_3/\lambda_2$, and L-kurtosis, $\tau_4=\lambda_4/\lambda_2$, calculated as functions of the L-scale, λ_2, and the third, λ_3, and fourth, λ_4, L-moments. Let a_r be the unbiased estimator of a_r for an ordered sample $x_{1:n}\leq\ldots\leq x_{n:n}$:

$$a_r = \frac{1}{n}\sum_{i=1}^{n}\binom{n-i}{r}x_{i:n}\binom{n-1}{r}^{-1}, r = 0, 1, \ldots, n-1 \tag{6.7}$$

with the unbiased sample L-skewness, $t_3=l_3/l_2$, and L-kurtosis, $t_4=l_4/l_2$, calculated as functions of the sample L-scale, l_2, and the third, l_3, and fourth, l_4, sample L-moments, respectively.

A set of candidate thresholds $\{u_i\}_{i=1}^{I}$ is first defined with I=10 or 20 sample quantiles. The minimum Euclidean distance is then defined between the sample L-skewness, τ_{3,u_i}, and L-kurtosis, τ_{4,u_i}, for each threshold value and the respective quantities of the theoretical GPD curve:

$$\mathrm{d}_{u_i} = \min_{\tau_3}\sqrt{\left(t_{3,u_i}-\tau_3\right)^2+\left(t_{4,u_i}-g(\tau_3)\right)^2}, \text{ for } i=1,.., I, \text{ with } g(\tau_3) = \tau_3\frac{1+5\tau_3}{5+\tau_3} \tag{6.8}$$

The best candidate threshold is then defined as:

$$u^* = \underset{u_i, 1\leq i\leq I}{argmin}\{d_{u_i}\} \tag{6.9}$$

characterized by L-moment statistics that fall closer to the respective values of the theoretical L-moment ratio curve.

6.2.2.2 *Scaling rainfall extremes*

Rainfall features of different temporal scales can be linked using scaling models, mainly based on the multifractal behaviour of rainfall. Temporal downscaling and temporal disaggregation methods are used to produce finer temporal scale rainfall data from coarser resolution observations. Temporal downscaling usually refers to the generation of data of high temporal resolution by means of statistical techniques, most commonly stochastic models, calibrated using information on the statics of data from lower resolution temporal scales. Temporal disaggregation indicates the generation of high-resolution temporal data based on coarser time scales, so that the former add-up to the totals of the second scale. This can be performed by means of a temporal partitioning of low temporal resolution amounts using a recursive rule or by repeatedly adjusting stochastic models to the generated high-resolution data. Within the general framework of temporal disaggregation, different methodologies have been developed in the literature. Some quite simple techniques, based on assumptions on the association of specific characteristics of the probability distribution functions of rainfall amounts at different time scales, have been developed by Liu et al. (2006), and Chen et al. (2011), among others. However, these techniques do not represent the basic statistics of the fine temporal scales of precipitation in a satisfactory way, nor the intermittency of precipitation events. Precipitation stochastic generators are also utilized for temporal disaggregation purposes of rainfall amounts. Methods based on point-process models for temporal disaggregation of hydro-meteorological data are quite spread, producing satisfactory results (Hanaish et al., 2011; Koutsoyiannis & Onof, 2001; Koutsoyiannis et al., 2003; Marani & Zanetti, 2007; Onof et al., 2005). Lee et al. (2010), Salas and Lee (2010) and Lee and Jeong (2014) introduced a nonparametric model for temporal disaggregation of hydro-meteorological variables, which incorporates a *k*-nearest neighbour resampling and a genetic algorithm. Temporal disaggregation of hydro-meteorological data is also performed by means of machine learning techniques (i.e. Kumar et al. (2012)).

The hypothesis of scale invariance (Veneziano et al., 2007) is usually applied to link rainfall intensities of different temporal scales. More specifically, the hypothesis of scale invariance states that annual maximum rainfall intensities, I_d and $I_{\lambda d}$, corresponding to durations d and λd, can be related by the following equation (Bara et al., 2010; Galiatsatou & Iliadis, 2022; Innocenti et al., 2017):

$$I_{\lambda d} = \lambda^{\beta} I_d \tag{6.10}$$

where equality corresponds to similarity of probability distributions. The coefficient λ is the ratio of scale invariance between the known duration D and the duration to be assessed, d, and β is the self-similarity index of the studied rainfall process. The q^{th} moments of rainfall intensity are obtained from Equation (6.10) as follows (Bara et al., 2010):

$$E\left(I_{\lambda d}^{q}\right) = \lambda^{\beta(q)} E\left(I_d^{q}\right) \tag{6.11}$$

where $\beta(q)$ is the scale exponent of order q, estimated by log-transforming Equation (6.11):

$$logE\left[I_{\lambda d}^{q}\right] = \beta(q) log\lambda + logE\left[I_d^{q}\right] \tag{6.12}$$

Therefore, the exponent β can be assessed as the slope of the linear relationship described by Equation (6.12). The abovementioned scaling behaviour can be also detected in quantiles of rainfall intensities corresponding to durations d and λd, considering that their cumulative distribution function (CDF) has a standardized form independent of the rainfall duration (Galiatsatou & Iliadis, 2022). In this chapter, a scaling procedure is applied to rainfall intensity quantiles corresponding to different durations, considering that their CDF has a standardized form independent of the rainfall duration. The scaling laws are assessed for all return periods for rainfall durations from 5min to 30min and from 30min to 24h, considering that rainfall dynamics change quite significantly in convective events.

Intensity-duration-frequency (IDF) and depth-duration-frequency (DDF) curves based on local precipitation measurements summarise the relationships between rainfall dynamics, namely rainfall intensity or depth, duration and frequency (return period), and are currently utilized for engineering design and management applications, such as flood risk protection structures and infrastructures or flood mitigation projects. The IDF (DDF) curves are constructed for different return periods representing the variation of rainfall intensity (depth) with duration. Theoretical probability distribution functions are fitted to annual maximum or POT rainfall intensities of particular durations ranging from shorter ones e.g. 5 min to daily events. When annual maximum rainfall intensities (or depths) are available, the GEV distribution (Eq. 6.1) is fitted to the samples of different duration and rainfall return levels are assessed as:

$$X_T = \begin{cases} \mu - \frac{\sigma}{\xi}\left\{1 - \left[-\ln\left(1 - \frac{1}{T}\right)\right]^{-\xi}\right\}, \ \xi \neq 0 \\ \mu - \sigma \ln\left[-\ln\left(1 - \frac{1}{T}\right)\right], \ \xi = 0 \end{cases} \quad (6.13)$$

for a defined return period, T. When the GPD (Eq. 6.2) is fitted to rainfall POTs, the return levels are given by (Coles et al., 2001):

$$X_T = \begin{cases} u + \frac{\sigma}{\xi}\left[\left(T n_y \zeta_u\right)^{\xi} - 1\right], \ \xi \neq 0 \\ u + \sigma \ln\left(T n_y \zeta_u\right), \ \xi = 0 \end{cases} \quad (6.14)$$

where n_y is the number of observations per year and ζ_u is the total exceedance rate of the threshold u.

6.2.3 Flood exposure

An efficient flood exposure tool, developed by Bertsch et al. (2022), was used to calculate the flood exposure likelihood to buildings. Figure 6.2 presents the schematic workflow of the flood exposure analysis tool. Each building was assessed for flood risk using simulated flood depths in a 3m buffer zone around its perimeter, where the mean and the 90th percentile values were calculated, the proposed value for the buffer zone (see Figure 6.3) depending on the resolution of the computational grid (2m in this study). A simple classification scheme shown in Table 6.1 was used to categorise buildings at low, medium and high flood risk.

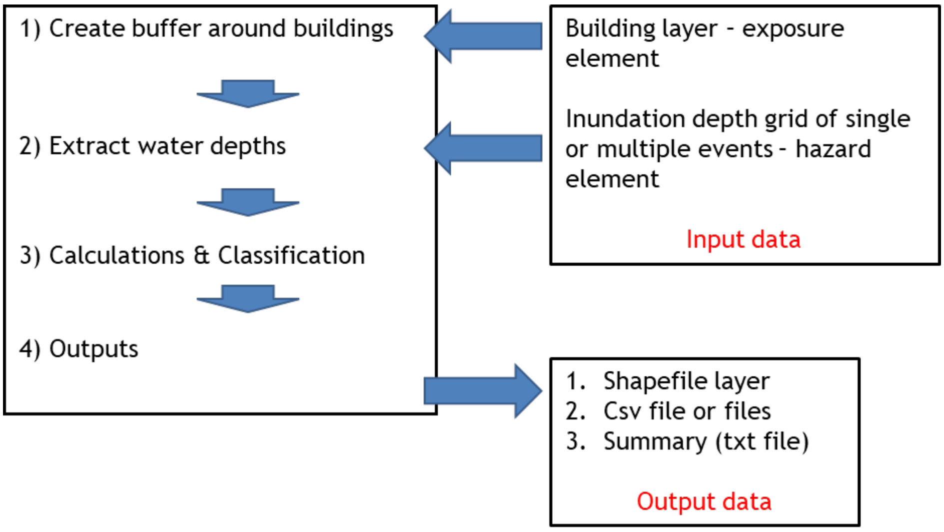

Figure 6.2 Schematic workflow of the flood exposure analysis tool for the classification of buildings to the water depth in the buffer zone (Bertsch et al., 2022).

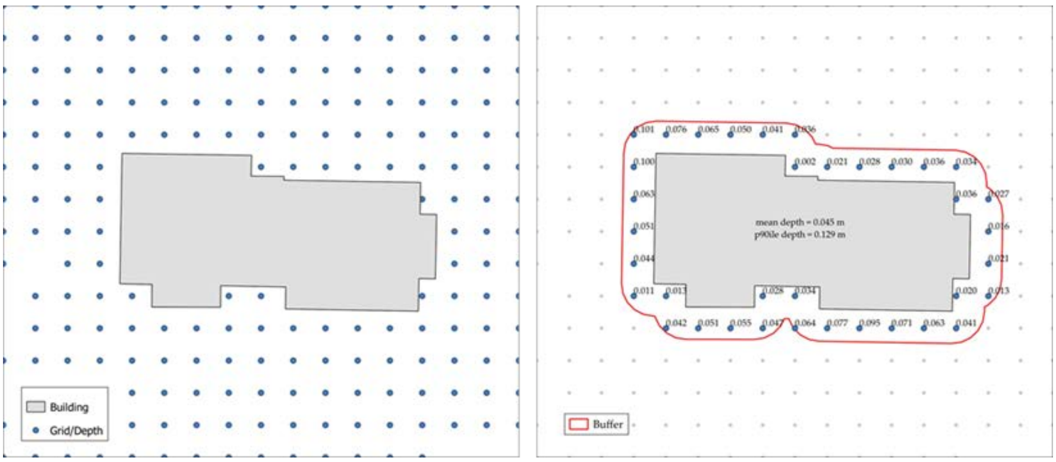

Figure 6.3 Example of the buffer zone to calculate inundation depth from grid squares (Bertsch et al., 2022).

Table 6.1 Classification scheme to calculate flood exposure likelihood for buildings.

Exposure Class	Mean depth (m)	90th percentile (m)
Low	<0.10	<0.30

Medium	<0.10	≥0.30
	≥0.10 - <0.30	<0.30
High	≥0.10	≥0.30

6.2.4 Modelling system and model set up

Over the last decade, many studies have reviewed hydraulic and hydrodynamic models which have been developed to simulate surface flows (K. Guo et al., 2021; Morales-Hernández et al., 2021; Sanders, 2017; Teng et al., 2017), and one of the most advanced and fully featured is the City Catchment Analysis Tool—CityCAT (for a full description, see Glenis et al. (2018)) developed at Newcastle University. CityCAT is a unique hydrodynamic model able to simulate fully coupled surface and pipe network flows, and it can represent natural drainage systems and built-up areas, with the explicit representation of buildings, where the buildings' footprint is excluded from the computational grid, and different types of blue-green infrastructure (BGI) (Bertsch et al., 2017; Glenis et al., 2018; Iliadis, Glenis, et al., 2023a; Kilsby et al., 2020) (such as blue/green roofs, water butts, swales, etc.), thus enabling the assessment of different alleviation measures. The model outputs include maps and time series of water depth, flow velocity, and the volume in and out of manholes, gully drains, buildings, etc. The required inputs are: (a) a high-resolution Digital Terrain Model (DTM) to unlock the full potential of the model, although depending on urban layouts, a lower resolution model may still be very functional; (b) the buildings' footprint; (c) green spaces to calculate the infiltration with the Green–Ampt method (Warrick, 2003); and (d) the IDF and DDF curves to generate storm profiles with the rainfall–runoff method (Kjeldsen, 2007a, 2007b), to be applied over the whole domain with a uniform assumption.

The flood domain studied here was modelled using CityCAT for two different design storm events, with a magnitude of 1 in 50 years and a duration of 1 h and 2 h. The buildings' footprint was extracted from the ONEGEO data (https://onegeo.co/data, accessed on 10 May 2023) and the permeable areas from OpenStreetMap (https://www.openstreetmap.org, accessed on 10 May 2023). The computational grid was constructed using the DTM provided by the Hellenic Cadastre (http://www.ktimatologio.gr/en, accessed on 10 May 2023) at a resolution of 2 m (each cell with an area of 4 m^2), so the total number of computational cells in the flow domain was 125,192, covering an area of 0.78 km^2. The representation of the buildings in the model was performed following the *'Building Hole'* approach where a non-flow boundary is generated around buildings to redistribute the rainfall to the nearest grid square (for a full description and performance relative to other methods, see Iliadis et al. (2023b)). Following the previously described approach, this chapter explored the likelihood of flood exposure for 1165 buildings. The roughness coefficient (Manning's n) was defined as 0.02 for impermeable areas and 0.035 for permeable areas. Due to the limitations in the Hellenic National regulations in urban flood modelling, and the intended design of the combined sewer system for storms with a return period of 10 years in the city centre of Thessaloniki (based on design cross-sections of existing combined sewers), a simple assumption was made in this work, that 20% of the rainfall enters the drainage system. In other countries, i.e., the UK, there is an instruction to flood modellers, when they do not combine the drainage system with the surface, to exclude specific rainfall from the model (e.g., 6 mm–15 mm).

6.3 Results

6.3.1 Extreme rainfall assessment

Threshold selection for the daily rainfall data was performed using both well-known threshold selection techniques, such as the mean residual life plot (MRL) and parameter stability plots, while also accounting for site-specific characteristics of extreme rainfall, together with the two new threshold selection techniques presented in Section 6.2.2.1. The MRL plot of the daily rainfall sample at AUTh station is presented in Figure 6.4.

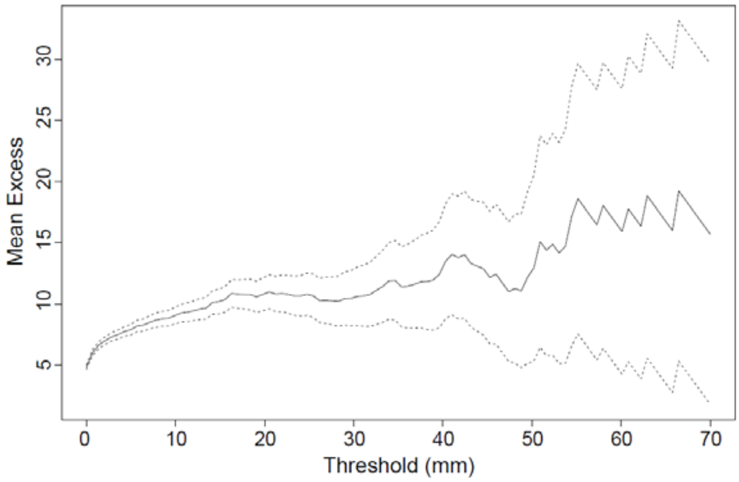

Figure 6.4 MRL plot of daily rainfall in Thessaloniki for the interval 1958-2021.

The MRL plot identifies a range of possible threshold values in the interval 10 mm ≤ u ≤ 30 mm. Figure 6.5 presents the GPD parameter stability plots for the modified scale (scale parameter of the GPD), and shape parameter, ξ, for thresholds in [10,30] mm. Based on stability characteristics of the GPD stability plots, while also considering the uncertainty of the parameters represented using 95% confidence intervals shown as vertical lines for each threshold, a threshold between 14 mm ≤ u ≤ 27 mm is considered to be a good candidate.

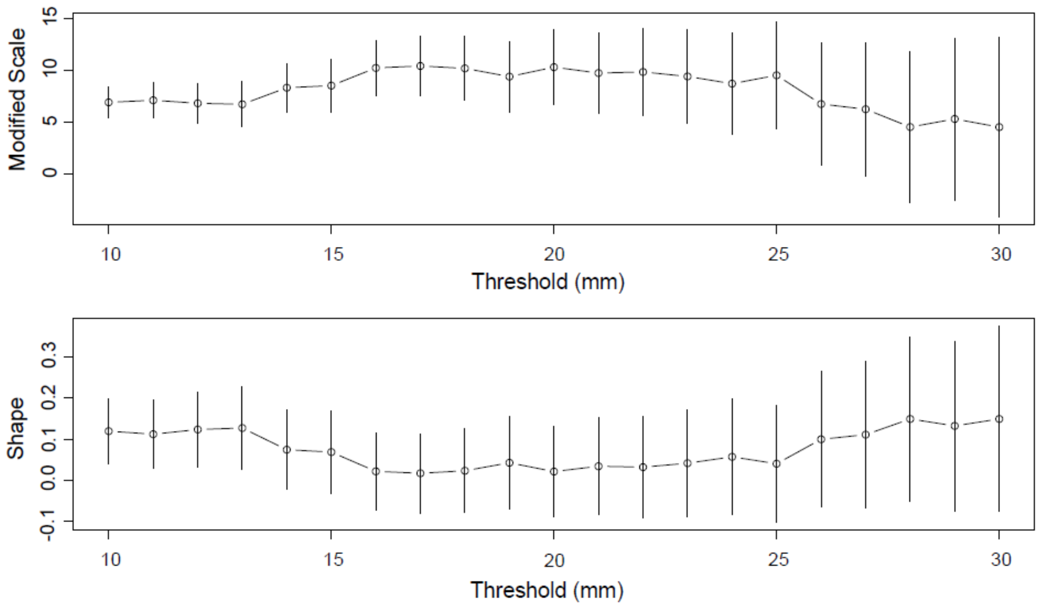

Figure 6.5 GPD parameter stability plots for daily rainfall in Thessaloniki for the interval 1958-2021.

The threshold selection method (a) was applied for threshold values in the entire range, 10 mm ≤ u ≤ 30 mm. The significance level selected was set at 5%. The forward stop rule applied did not explicitly identify a cutoff level. However, it has been observed that the threshold u = 22 mm was the only one giving a p-value of the AD statistic lower than 5%. The threshold selection method (b) provided clearer results, indicating u = 22 mm as the threshold providing a local minimum to the Euclidean distance criterion. The threshold u = 28 mm provided the global minimum of the distance d_{u_i} in the studied interval. However, this threshold level ended up with only 134 POT samples, corresponding to just λ = 2.09 exceedances per year. Therefore, the threshold u = 22 mm was selected to perform the extreme value analysis of the daily rainfall data, corresponding to 221 POT samples, with around λ = 3.45 exceedances per year.

Using a threshold u = 22 mm, the GPD was fitted to daily rainfall maxima (Equation (6.2)) using both MLE and the L-moments approach, with both approaches providing consistent results, with higher return level estimates assessed using MLE. Figure 6.6 presents rainfall return level estimates assessed using Equation (14), with the parameters of the GPD calculated using the MLE approach. The black line represents maximum likelihood rainfall return level estimates, while the blue lines represent the upper 97.5% and the lower 2.5% confidence limits (95% confidence interval). Round marks in the return level plot correspond to measured data from the available extreme rainfall sample. It should be noted that the most extreme 24-hourly rainfall measurement was 98 mm, and was observed in 1985 and 2014. The maximum likelihood return level estimate significantly underestimates this value, while the upper 97.5% confidence limit seems to better fit the most extreme part of the observed sample. More specifically, for a return period of 64 years, equal to the daily rainfall sample length, the maximum likelihood estimate of the rainfall return level is about 84 mm, and the respective 97.5% upper confidence limit is 100.5 mm. Based on this finding, the upper 97.5% confidence limit for daily rainfall return levels was used in the scaling methodology presented in Section 6.2.2.2 to extract rainfall return levels corresponding to finer temporal scales.

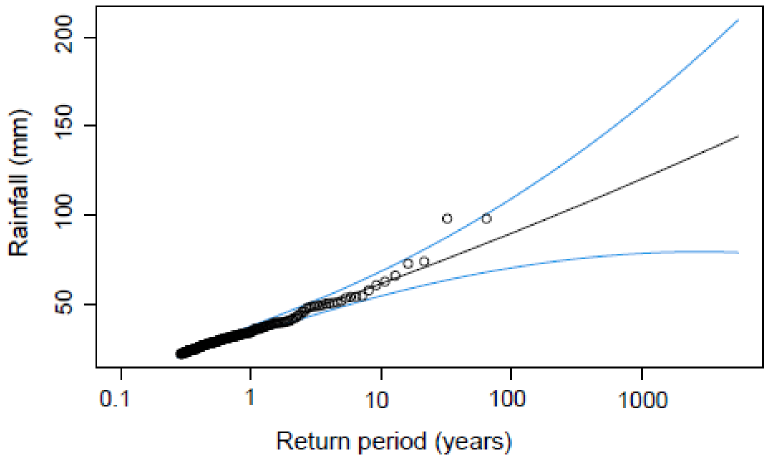

Figure 6.6 Rainfall ML return levels and 95% confidence interval (mm) assessed by fitting the GPD to daily rainfall in Thessaloniki for the period 1958-2021.

The GEV distribution (Equation (6.1)) is then fitted to annual maximum rainfall intensities for time periods of 5 min, 10 min, 15 min, 30 min, 1 h, 2 h, 6 h, 12 h and 24 h, available at Mikra station for the period 1963–1987 using L-moments (due to the small sample size of this dataset). Rainfall return levels for the different durations are assessed for return periods of 2, 5, 10, 20, 50, 100, 200 and 500 years using Equation (6.13). For each return period, plots of Log(i) and Log(λ) are created, and linear functions are then fitted, dividing the plots into two parts, the first one corresponding to rainfall durations from 5 min to 30 min, and the second one from 30 min to 24 h. To end up with two different rainfall duration groups, a number of trials were performed considering different duration groups, and finally we selected those providing the highest coefficients of determination, R^2, for all return periods. Figure 6.7 presents the linear relationships between the log-transformed quantiles (log-transformed return levels) of rainfall intensity and log-transformed scale factors of different durations, for return periods of 5 years (left panel) and 50 years (right panel). The plots include the linear function equations for rainfall durations in the intervals of 5 min to 30 min and

30 min to 24 h, and the respective coefficients of determination. Table 6.2 presents estimates of the self-similarity index (estimates of $-\beta$) assessed for all return periods and for the two groups of rainfall duration.

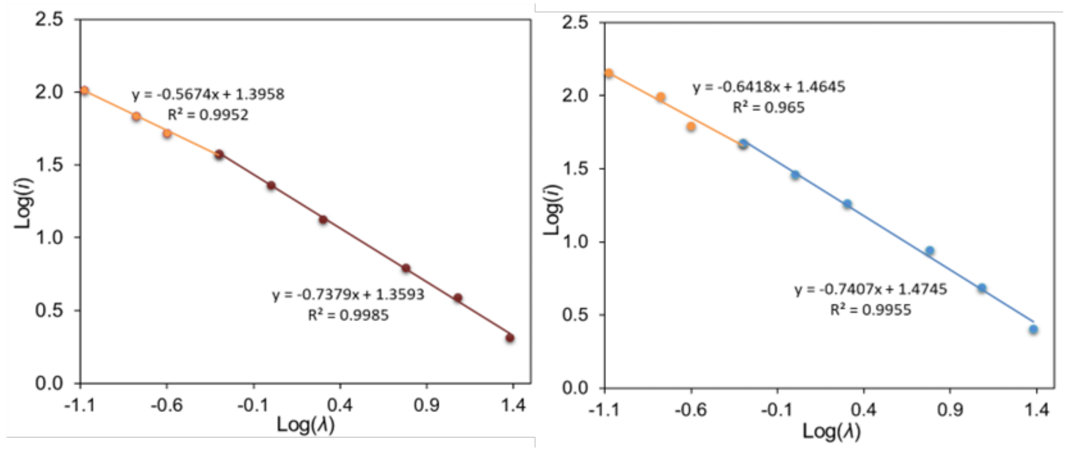

Figure 6.7 Scaling of rainfall return level estimates at the station of Mikra, in Thessaloniki, for return periods 5 (left panel) and 50 (right panel) years.

Table 6.2 Self-similarity indices, $-\beta$, for all return periods and rainfall durations in 5min-30min and 30min-24hr.

Return period (years)	**5min-30min**	**30min-24hr**
2	0.5415	0.7286
5	0.5674	0.7379
10	0.5908	0.7400
20	0.6136	0.7407
50	0.6418	0.7407
100	0.6614	0.7403
200	0.6794	0.7398
500	0.7008	0.7390

The self-similarity indices presented in Table 6.2 are then used in Equation (6.12) to temporally downscale daily rainfall return levels assessed from fitting the GPD to data from AUTh station (1958–2021). More specifically, daily rainfall return level estimates corresponding to the 97.5% upper confidence limit (see Figure 6.6) are used in the scaling process. Rainfall return level estimates extracted for durations of 5 min, 10 min, 15 min, 30 min, 1 h, 2 h, 6 h, and 12 h are used to construct IDF and DDF curves for the study site. The formulas extracted to describe the IDF and DDF curves are given below:

$$i\left(\frac{mm}{h}\right) = \frac{16.63T^{0.2152}}{t^{0.7116}} \text{ and } p\ (mm) = 17.47T^{0.2152}t^{0.2884} \quad (6.15)$$

where *T* is the return period (years) and *t* is the rainfall duration (h). Figure 6.8 presents IDF and DDF curves for Thessaloniki based on Equation (6.15) for return periods of 2, 5, 10, 20, 50, 100, 200, and 500 years.

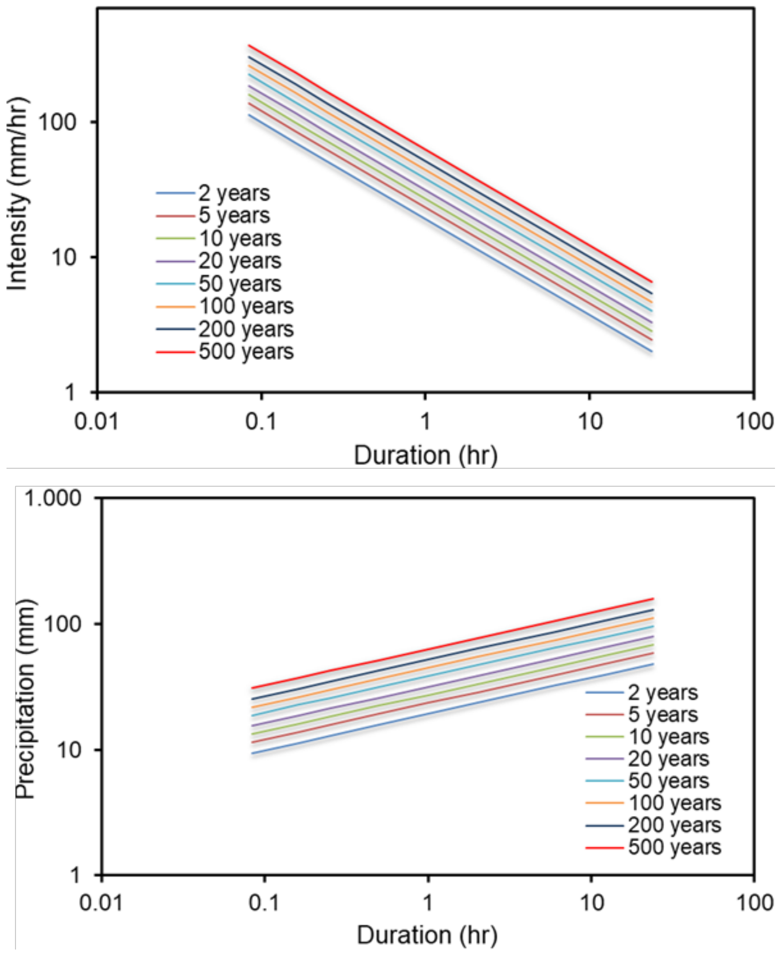

Figure 6.8 IDF (top panel) and DDF (bottom panel) curves for Thessaloniki for return periods 2, 5, 10, 20, 50, 100, 200, and 500 years.

6.3.2 Modelled flow depth

A detailed analysis of the areas where maximum water depths are highlighted and analysis identifying the critical roads during heavy rains will be presented in this section. The rainfall depth for 50-year events, specifically for durations of 1 h and 2 h, is evaluated. The findings indicate that the assessed rainfall depth is approximately 70% higher than the quantiles derived from the DDF curves extracted from the shorter-duration dataset spanning 25 years (1963–1987). This high difference is attributed to: (i) using the upper 97.5% confidence limit to assess daily rainfall return levels of the longer time series (1958–2021), (ii) fitting a POT model to the 64-year daily series to assess extreme quantiles, and (iii) missing observations in the shorter series perhaps leading to an underestimation of the extreme sample. To simulate these two storm events, the CityCAT model is employed. It should be noted that when selecting the duration for modelling purposes, it is essential to consider the critical duration that triggers the most significant flood response, taking into account factors such as time-to-peak and other relevant characteristics. In the case of a catchment area spanning only a few square kilometres, a duration of 1 or 2 h is often sufficient to adequately represent the hydrological processes and capture the flood dynamics effectively. These durations are typically suitable for encompassing the key rainfall patterns and associated runoff generation within the catchment, enabling accurate flood modelling and analysis. The application of the CityCAT model in simulating the two storm events (50-year events with durations of 1 h and 2 h, see Figure 6.9) provides valuable insights into flood depths and water flowpaths within the study area. Note that the simulated storm events here exhibit similarities to previously observed storms as reported by the Hellenic National Meteorological Service (HNMS).

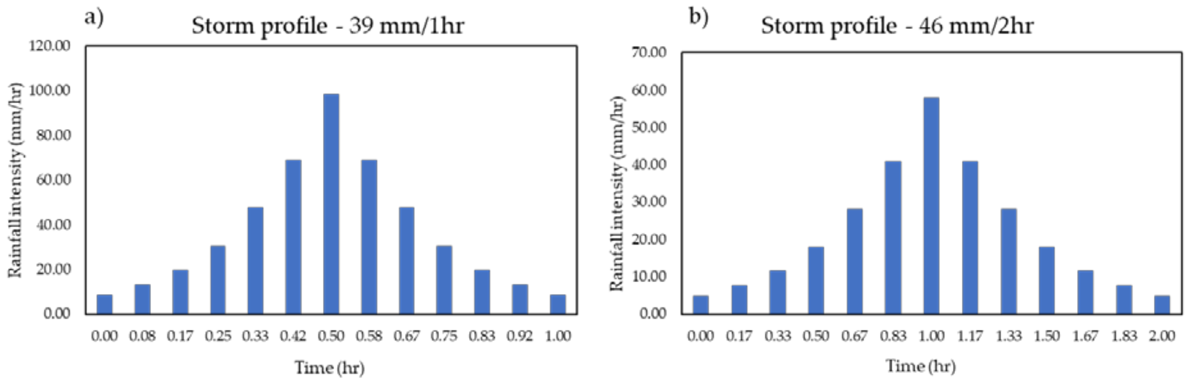

Figure 6.9 Storm profiles corresponding to the constructed DDF curves for Thessaloniki, Greece: a) a 39 mm rainfall of 1hr duration; and b) a 46 mm rainfall of 2hr duration.

The flood maps produced by the model outputs, depicted in Figure 6.10 (maximum flood depths), clearly identify a major water flowpath along Agias Sofias street (see Figure 1 to locate the street), where the darker blue illustrates water depths exceeding 30 cm. This indicates that the street is highly susceptible to flooding during intense rainfall events. Furthermore, the presence of small ponds in various parts of the catchment, attributed to the complex and dense topography of the area, highlights the potential for localised flooding. Identifying these ponding areas is crucial for understanding flood risk and implementing measures to minimise the impacts, such as sacrificial zones, the creation of retention ponds, the improvement of surface drainage in specific locations, or converting the impermeable pavements to permeable pavements.

The study area's locations and roads, discussed below, have experienced substantial water buildup during intense rainfall events in the past, as reported by local authorities and residents. However, additional efforts are required to compare and confirm these observed occurrences with the results obtained through modelling. The modelled water depths of this work were calculated to estimate the maximum levels on the following roads (see Figure 6.1 to locate the streets): (a) Palaion Patron Germanou and Pavlou Mela. This particular area demonstrates a significant propensity for water pooling, with estimated water depths exceeding 30 cm. (b) Notably, Proxenou

Koromila experiences frequent ponding, with estimated flood depths ranging from 25 cm to 41 cm. This road is particularly susceptible to water accumulation during storm events, which can lead to hazardous conditions. (c) In certain parts of Mitropoleos street, water depths exceeding 25 cm have been estimated. This poses a risk of localised flooding which would result in traffic disruption.

The estimated water depth and the flow direction for the two storms with 1 h and 2 h durations can be seen in Figures 6.11 – 6.13, where we zoom in on these areas. Overall, the contribution of a detailed flood model, such as CityCAT, is crucial to developing a better understanding of the flood dynamics, quantifying water depths with high accuracy, and locating areas at high flood risk to improve inundation resilience in dense cities.

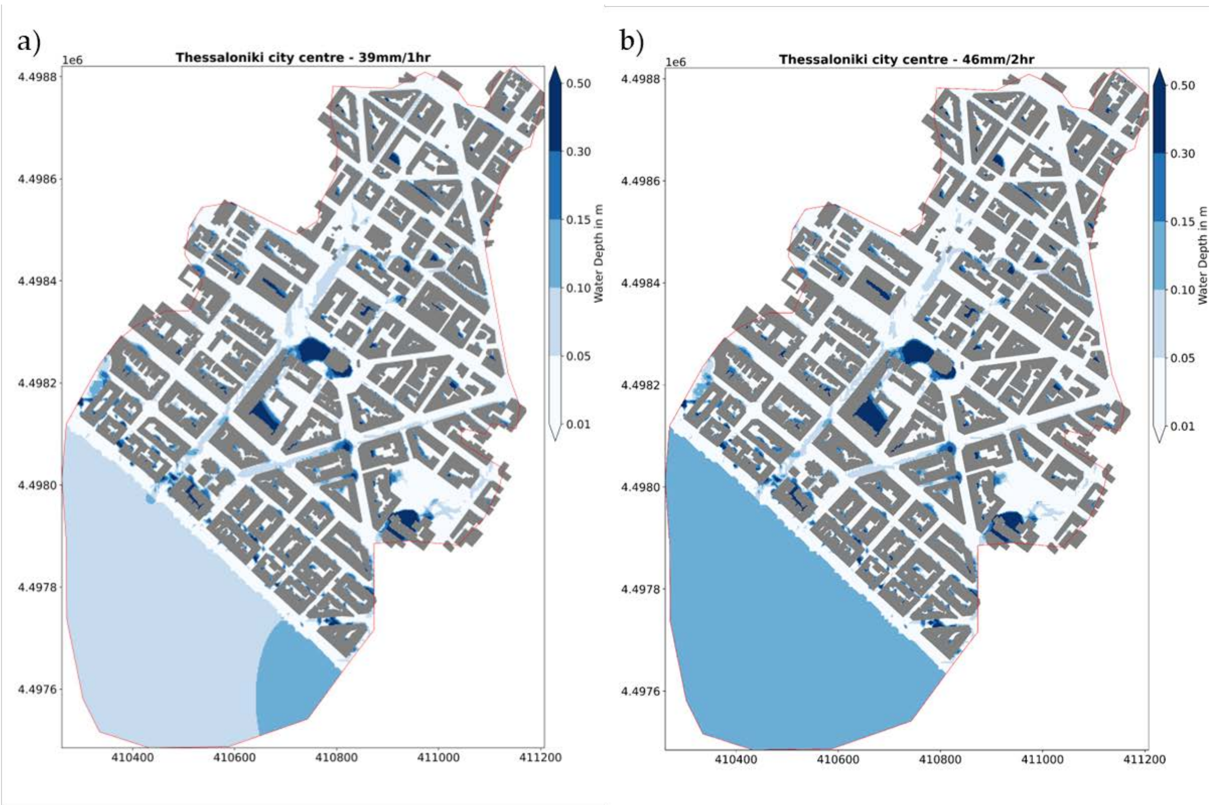

Figure 6.10 Example of maximum flood depths from a CityCAT simulation for a 50-year storm event with durations of (a) 1 h and (b) 2 h, for the centre of Thessaloniki.

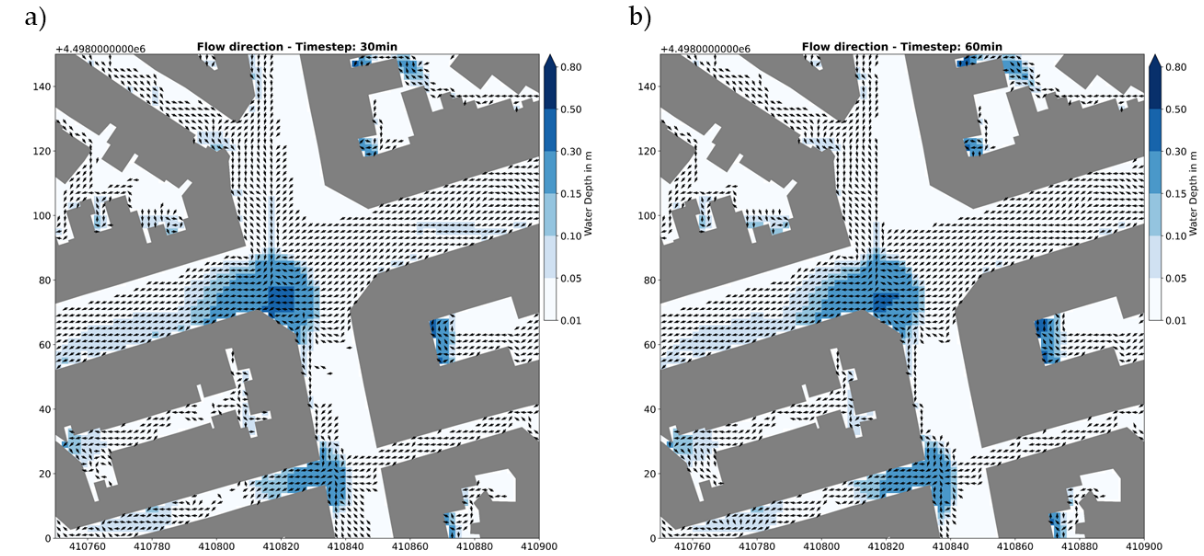

Figure 6.11 Flood depths and flow direction (black arrows) for a 50-year storm event with durations of (a) 1 h and (b) 2 h at Palaion Patron Germanou and Pavlou Mela streets (marked as (b) in Figure 6.1).

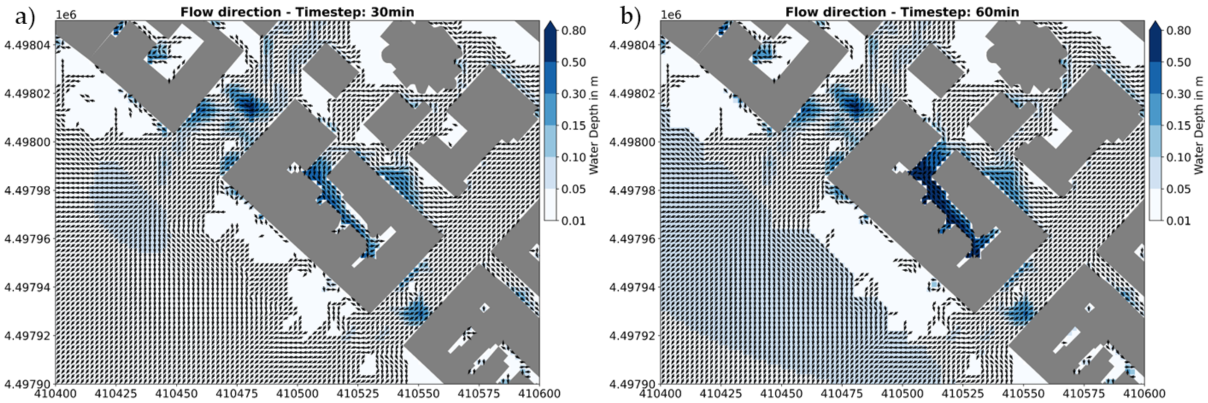

Figure 6.12 Flood depths and flow direction (black arrows) for a 50-year storm event with durations of (a) 1 h and (b) 2 h at Proxenou Koromila (marked as (c) in Figure 6.1).

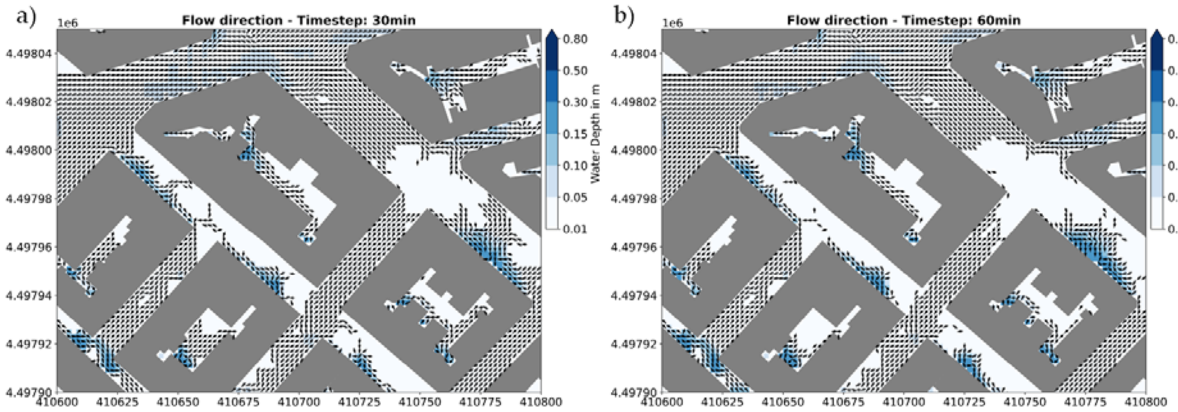

Figure 6.13 Flood depths and flow direction (black arrows) for a 50-year storm event with durations of (a) 1 h and (b) 2 h at a part of Mitropoleos street (marked as (d) in Figure 6.1).

6.3.3 Exposure likelihood to buildings

In order to identify the urban features exposed to flood risk, an innovative tool was used, as described in Section 6.2.3. The analysis of flood exposure to buildings in the study area provides valuable insights into the vulnerability of urban features to flood risk. Note that this area has faced inundation issues from extreme events in the past, for which no formal reports exist, but are well known by local people.

Table 6.3 provides the total number of inundated buildings per scenario in the study area. The number of buildings classified as being at high risk for the first storm event (1 h duration) is 165, and that for the second storm event (2 h duration) is 186. These values are nearly twice as high as for the buildings with medium flood exposure. Most of the high-risk buildings are located on the streets mentioned in Section 6.3.2, where the flood depth is more than 30 cm. Furthermore, in the studied area of the city centre, many buildings house businesses, particularly on their ground floor, often containing vulnerable assets, while there also exist numerous buildings of historical value.

Table 6.3 Total number of inundated buildings per scenario for the centre of Thessaloniki.

Storm Scenarios	Medium	High
50-years event of 1hr	90	165
50-years event of 2hr	99	186

Figure 6.14 illustrates the flood depths and the resulting flood exposure of buildings during the two generated storm events (50-year storm events with durations of 1 h and 2 h). The use of colour-coded zones helps to categorize buildings based on the flood depths in the buffer zone. The red-coloured buildings indicate high-risk, where the flood depth exceeds the 30 cm threshold. These buildings are estimated to be more vulnerable to damage from flooding, and it is crucial to prioritize them for adaptation measures and enhance their resilience to future flooding. Buildings depicted in orange indicate a medium risk of flooding, where damage from flooding is still significant. Lastly, a grey colour highlights the buildings at low risk, with minimal flood depths and lower vulnerability to flooding.

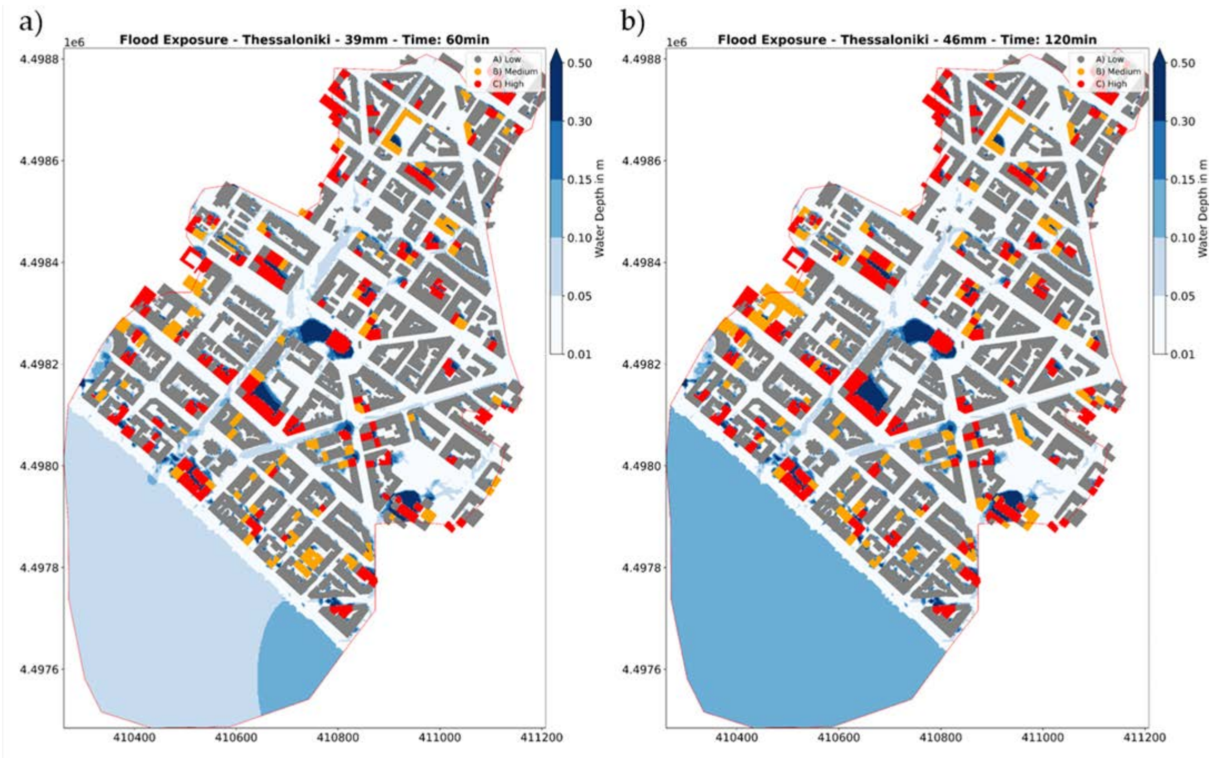

Figure 6.14 Maximum flood depths and flood exposure of buildings for a 50-year storm event with durations of (a) 1 h and (b) 2 h for the centre of Thessaloniki.

It should be noted that further investigation is needed into the 30 cm threshold to categorise buildings according to their flood risk, in order to provide more accurate estimations to understand the risk and the vulnerability profile of the city's buildings.

6.4 Conclusions

This chapter combines a detailed contemporary analysis of extreme rainfall events in Thessaloniki, Greece, with an advanced hydrodynamic model to simulate pluvial flooding, assisting in the reliable assessment of building exposure to flooding risks. A dual scheme is employed to assess extreme rainfall: (i) extreme daily rainfall, resulting from a long daily series, is analysed using a GPD. Two threshold detection methods are applied, to assist a less ambiguous selection of daily extreme rainfall events. (ii) Extreme rainfall of shorter annual maximum series ranging from sub-hourly to sub-daily durations is analysed using the GEV distribution. A scaling procedure is applied to rainfall return level estimates assessed from (ii), and the resulting scaling laws are applied to the more reliable daily rainfall return levels of (i), in order to finally derive storm profiles with durations of 1 h and 2 h. The resulting storm profiles are used to drive the hydrodynamic model CityCAT to simulate flooding, estimate the water depths, identify the critical water flowpaths and finally assess the total number of inundated buildings through a novel exposure analysis calculator per extreme rainfall scenario in the historic centre of Thessaloniki. Furthermore:

1. Typical storm events have durations spanning 1 h to 2 h, so both durations have been used here to see how sensitive the damages are to storm duration. For storms of the same return period, a modest increase is found for the 2 h storm relative to the 1 h storm.
2. The CityCAT model provides valuable insights into flood depths and water flowpaths, identifying a major water flowpath along Agias Sofias street, which is highly susceptible to flooding during intense rainfall events. The presence of small ponds in various parts of the studied catchment further highlights the potential for localised flooding.
3. The estimated likelihood of flood exposure to buildings reveals the vulnerability of urban features to flood risk. Due to the previous flood events in the area, the number of buildings at high risk for both storm events underscores the importance of addressing flood impacts on the built environment.

4. The modelling system is suitable for assessing the performance of flood-resilience strategies such as retention ponds, surface drainage improvements, and permeable pavements.

This chapter showcases the unique capabilities of CityCAT in its application to a country like Greece, which faces challenges of limited data availability. By leveraging globally accessible datasets, a high-resolution Digital Terrain Model (DTM, provided by the Hellenic Cadastre), and a detailed analysis of extreme rainfall events, this model facilitates a better understanding of the dynamics of urban flooding. It is noteworthy that in Greece, flood exposure analysis is conducted here for the first time at the level of individual buildings, moving away from the conventional approach of assessing flood risk in predefined zones. The identification of critical flow paths and the assessment of buildings at high flood risk serve as key considerations for future work. This includes expanding the catchment area, adding the current sub-surface drainage system or developing new synthetic methods to represent the system, implementing the model, and validating against historical storm events. These efforts are aimed at making informed decisions to develop flood-resilience solutions that safeguard people, assets, and infrastructure from future flood events.

Chapter 7. Conclusions and Future work

7.1 Conclusions

This thesis has made significant contributions to the field of flood risk management in urban areas by developing, demonstrating and critically assessing methods for simulation and analysis of flood exposure and adaptation using blue-green infrastructure .

It includes a comprehensive and direct comparison of two widely used approaches for modelling buildings and their associate flood exposure, providing valuable insights into their strengths and weaknesses. As well as showing the advantages of the "*Building Hole*" method, an improvement to the inferior but more widely used "*Stubby Building*" approach was developed, providing two alternative novel methods to link surface water flooding information with individual building exposure and flood damages. Moving on from assessing flood exposure in existing cities, the research focused on identifying optimal locations for implementing Blue-Green Infrastructure (BGI) to mitigate flood risks. By considering various factors such as land use, hydrological characteristics, and infrastructure suitability, it has provided valuable guidance to decision-makers for strategically placing nature-based solutions. This approach can contribute to reducing flood damages, improving urban resilience, and promoting sustainable development.

The critical role of Digital Terrain Model (DTM) resolution in large-scale hydrodynamic modelling was then explored using a real-life case study of the whole of London, and it was demonstrated that higher-resolution DTMs (better than 5m) significantly enhance the accuracy and reliability of flood simulations, emphasizing the importance of investing in high-quality elevation data for effective flood mapping and forecasting.

Furthermore, to enable high resolution modelling for very large domains such as Greater London, this thesis proposed a novel combination of cloud computing with the powerful hydrodynamic model CityCAT. By leveraging the scalability and computational resources of the cloud, this integration offers unprecedented opportunities for large-scale simulations in flood risk management with high accuracy. Achieving high-resolution flood simulations for large areas is possible, but it requires cloud computing resources. Even with cloud-based processing, the computations can still be time-intensive, particularly for intricate systems like pipe networks.

Further work demonstrated the portability of the modelling approach to cities where high resolution data are not so readily available, with a case study in Thessaloniki in Greece.

Through the research, this project has gained a better understanding of flood dynamics in urban areas, enabling the development of systematic and efficient flood risk management strategies. It identified highly vulnerable urban features and provided insights into effective mitigation measures. This knowledge can guide urban planners, policymakers, and emergency responders in developing comprehensive strategies to manage flood risks effectively.

Lastly, the developed modelling system proves to be suitable for assessing the performance of flood-resilient strategies, including retention ponds, surface drainage improvements, and permeable pavements. By simulating the implementation of these strategies under different flood scenarios, decision-makers can prioritize and optimise their investments based on cost-effectiveness and potential impact.

In summary, this thesis advances the understanding of flood risk management in urban areas by comparing different approaches, proposing novel methods, identifying optimal locations for BGI implementation, emphasizing the role of DTM resolution, exploring cloud integration, and enhancing the overall understanding of flood dynamics. The link between the novel aspects of this work and the research gaps identified in Chapter 2 are summarised in Table 7.1. These findings provide valuable insights for practitioners, enabling them to make informed decisions and develop effective strategies to mitigate flood risks in urban areas worldwide.

Table 7.1: Linking the developed methodologies with the research gaps identified in Chapter 2 (Section 2.5) in Table 2.1.

	Methods	Novel aspects	Research Gap
1	*'Building Hole'* approach	1) Demonstrated accuracy of method by validating against real storm events; 2) Demonstrated advantages for megacities as it reduces the number of active computational grid squares.	**1**
2	A *'cleaned'* Stubby Building approach	1) Identified and quantified errors of SB approach from two sources: (a) flow over buildings (b) DEM interpolation on building footprint 2) Developed *'cleaned'* approach for SB addressing type (b) error and identified where the method may be inaccurate to give advice to users.	**2**
3	A cost-benefit *'source-receptor' flood risk* framework	Linked flood depth maps to building level damages through an improved exposure method, and developed methods to identify locations to add cost-effective Blue-Green Infrastructure with any flood model.	**3, 4, 5**
4	A city-scale application in London by linking cloud computing with hydrodynamic models	1) The largest known application of a high-resolution flood model; 2) establishing minimum reliable DTM resolution; 3) providing an easily analysed list of exposed buildings and associated damages rather than a spatial map.	**6, 7**
5	An application presenting that the CityCAT model is powerful in areas with limited access to data and the construction of detailed IDF curves	Establishing that useful and informative results can be obtained with pragmatic use of limited spatial data.	**8, 9**

7.2 Limitations

While this research has made significant advances in addressing key aspects of flood modelling to achieve urban resilience, it is imperative to acknowledge the limitations that shape the scope of the outcomes. In this section, these limitations are discussed to provide a comprehensive perspective on the thesis's boundaries.

1. While current capabilities for representation of buildings within flood models are fully exploited here using high accuracy building outlines with high resolution surrounding terrain to capture water flow paths, no attempt has been made so far to account for openings that allow water ingress and egress from buildings. The CityCAT '*Building Hole*' approach allows partial opening of no flow boundaries around the building, but this has not been systematically implemented to represent e.g. doors or window openings which may be available from more detailed data sets such as Building Information Models (BIM) or from imagery.
2. Regarding the categorisation of flood risk to buildings based on the 30cm threshold assumption for significant flood risk, it's important to acknowledge the necessity for further investigation as the risk critically depends on door threshold heights. In the UK for various building types, and certainly in various other countries, the initial elevation of a building's entrance may differ from the standard 30cm used here, so there exists a need for further exploration and investigation of the impact of this simplification.
3. Challenges arise when seeking data on building types to calculate the estimated damages from flooding. While this study has assumed all urban features are either residential or commercial, a comprehensive coverage of these categories is needed as large differences and errors may arise from mis-classification. Additionally, the utilisation of damages values from the UK based on the Multi-Coloured Handbook by Priest et al. (2022) raises questions about global applicability.
4. While this work has carried out validation using observed data obtained by leveraging social media imagery for flood depth estimations during a flood event in London, this was limited to a modest number of locations due to time constraints. To obtain larger numbers of depth points, an automated approach such as presented by Chaudhary et al. (2019). According to their findings, automation methods that identify objects of known dimensions, such as

vehicles and individuals, could enhance accuracy as well as providing orders of magnitude larger data sets.

5. The adaptation portfolio here's introduces manually added ponds, but automation holds potential to streamline and enhance the process and include further classes of BGI. By automating the addition of BGI, simulations could optimise placement across different locations, exploring a range of interventions with varying footprints and cost-effectiveness, and ultimately improving feasibility and adaptability.
6. Global challenges in obtaining high-resolution DTMs hinder universal flood risk analysis. While some regions like the UK and the US benefit from DTMs with multiple resolutions, starting from 0.50m, global availability is currently coarser, typically 12m or 30m and above. This limitation restricts both accurate simulation of flowpaths, and the representation of small-scale flood risk management solutions in urban areas.
7. Storm or combined sewer networks can be an important component of urban drainage, especially in less intense storm events, but present a significant hurdle in simulation due to scarce network data. It is hard to imagine automatic and universal implementation of detailed real networks in flood models in the next few years due to restricted access to commercial information on pipe networks (UK), lack of formal records (developing countries) and difficulties in digitising and setting up network models (all cases). Modellers often resort to approximations, such as the UK practice of deducting 12mm/hr from observed rainfall. Improvements are possible by employing spatially variable pipe capacity datasets, following the approach demonstrated by Singh et al. (2023). A pressing need therefore exists to improve methodologies for accurately representing sewer systems, particularly in data-scarce urban areas. Synthetic storm drain generation that mirrors local conditions and adheres to design regulations of each country, as presented by Bertsch et al. (2017), offers a pioneering solution. This methodology holds promise in overcoming data

limitations and significantly advancing sewer system representation within flood models.

7.3 Future work

In terms of future work, there are several areas that can be explored to further enhance our understanding and management of flood risks in urban areas, addressing the limitations outlined above.

Firstly, the development of a methodology to represent the drainage system in cities with limited or no data presents an intriguing avenue for research. Many cities, especially in developing regions, lack comprehensive and up-to-date information on their drainage infrastructure. One approach is to exploit the limiting nature of the inlet drain capacity and simulate only the entry of water into the sewers system, assuming an infinite capacity once in the network. Inlet drain data sets can be surveyed or derived from remote sensing data (e.g. Google Street View), or innovative methodologies to generate synthetic but realistic layouts can be used, such as the Synthetic Storm Drains (SSD) QGIS routine, developed by Bertsch et al. (2017)

The SSD approach can be extended to create realistic representations of not only the storm drains, but also sewer networks and manholes. This can be done using physics-based rules for generating gravity drainage networks upstream of a "*pour point*", requiring only the already available DTM and street layout, together with design standards for spacing of drains and diameters of pipes. This approach could be extended by utilising remote sensing data, citizen science, or machine learning algorithms, enabling more accurate flood simulations and risk assessments.

Additionally, practical applications can be expanded to cover the exposure and vulnerability of buildings and assets by improving their resilience at property level as well as at strategic or city-wide scales. While previous studies have focused on assessing the vulnerability of structures to floods, future research can delve deeper into identifying and testing practical measures to enhance the resilience of buildings and critical infrastructure using either modified depth-damage curves, or explicitly modelling flooding within buildings. This can involve investigating the effectiveness of flood-resistant construction techniques, retrofitting existing buildings, or integrating smart technologies to enable real-time monitoring and adaptive flood management systems.

The vulnerability of underground assets in megacities, such as basements and metro systems, is an area that increasingly demands attention. Urban areas with extensive underground infrastructure face severe challenges during flood events, as water ingress into these spaces can lead to severe damage and disruptions as seen in recent years in London and China. Investigating the vulnerability of these underground assets, assessing their resilience, and developing targeted mitigation strategies can help in minimizing the impacts of flooding on critical urban infrastructure, ensuring the continuous functioning of essential services, and safeguarding public safety.

By addressing these future research areas, we can systematically advance and automate our capability for modelling and understanding of urban flood risks and contribute to the development of more effective and sustainable flood risk management strategies. These efforts will not only enable cities to mitigate the impacts of flooding but also enhance their overall resilience to future climate change and urbanisation challenges.

References

Al-Suhili, R., Cullen, C., & Khanbilvardi, R. (2019). An Urban Flash Flood Alert Tool for Megacities—Application for Manhattan, New York City, USA. *Hydrology*, *6*(2), 56. https://www.mdpi.com/2306-5338/6/2/56

Alcrudo, F. (2004). *Mathematical modelling techniques for flood propagation in urban areas* (IMPACT Project Technical Report, Issue. http://www.samui.co.uk/ impact-project/AnnexII_DetailedTechnicalReports/AnnexII_PartB_WP3/ Modelling_techniques_for_urban_flooding.pdf

Alonso, A. M., de Zea Bermudez, P., & Scotto, M. G. (2014). Comparing generalized Pareto models fitted to extreme observations: an application to the largest temperatures in Spain. *Stochastic Environmental Research and Risk Assessment*, *28*(5), 1221-1233. https://doi.org/10.1007/s00477-013-0809-8

Alonso, J., Orue-Echevarria, L., Casola, V., Torre, A. I., Huarte, M., Osaba, E., & Lobo, J. L. (2023). Understanding the challenges and novel architectural models of multi-cloud native applications – a systematic literature review. *Journal of Cloud Computing*, *12*(1), 6. https://doi.org/10.1186/s13677-022-00367-6

Alves, A., Sanchez, A., Gersonius, B., & Vojinovic, Z. (2016). A Model-based Framework for Selection and Development of Multi-functional and Adaptive Strategies to Cope with Urban Floods. *Procedia Engineering*, *154*, 877-884. https://doi.org/https://doi.org/10.1016/j.proeng.2016.07.463

Andjelkovic, I. (2001). *Guidelines on non-structural measures in urban flood management*.

Apel, H., Aronica, G. T., Kreibich, H., & Thieken, A. H. (2009). Flood risk analyses—how detailed do we need to be? *Natural Hazards*, *49*(1), 79-98. https://doi.org/10.1007/s11069-008-9277-8

Bach, P. M., Rauch, W., Mikkelsen, P. S., McCarthy, D. T., & Deletic, A. (2014). A critical review of integrated urban water modelling – Urban drainage and beyond. *Environmental Modelling and Software*, *54*, 88-107. https://doi.org/10.1016/j.envsoft.2013.12.018

Bader, B., Yan, J., & Zhang, X. (2018). Automated threshold selection for extreme value analysis via ordered goodness-of-fit tests with adjustment for false discovery rate. *The Annals of Applied Statistics*, *12*(1), 310-329, 320. https://doi.org/10.1214/17-AOAS1092

Bara, M., Gaal, L., Kohnova, S., Szolgay, J., & Hlavčová, K. (2010). On the use of the simple scaling of heavy rainfall in a regional estimation of IDF curves in Slovakia. *Journal of Hydrology and Hydromechanics*, *58*(1), 49-63.

Barredo, J. I., Saurí, D., & Llasat, M. C. (2012). Assessing trends in insured losses from floods in Spain 1971–2008. *Nat. Hazards Earth Syst. Sci.*, *12*(5), 1723-1729. https://doi.org/10.5194/nhess-12-1723-2012

Bates, P. D., Horritt, M. S., & Fewtrell, T. J. (2010). A simple inertial formulation of the shallow water equations for efficient two-dimensional flood inundation modelling. *Journal of Hydrology*, *387*(1), 33-45. https://doi.org/https://doi.org/10.1016/j.jhydrol.2010.03.027

Bellos, V., & Tsakiris, G. (2015). Comparing Various Methods of Building Representation for 2D Flood Modelling In Built-Up Areas. *Water Resources Management*, *29*(2), 379-397. https://doi.org/10.1007/s11269-014-0702-3

Bellos, V., & Tsakiris, G. (2016). A hybrid method for flood simulation in small catchments combining hydrodynamic and hydrological techniques. *Journal of Hydrology*, *540*, 331-339. https://doi.org/https://doi.org/10.1016/j.jhydrol.2016.06.040

Bentivoglio, R., Isufi, E., Jonkman, S. N., & Taormina, R. (2022). Deep learning methods for flood mapping: a review of existing applications and future research directions. *Hydrol. Earth Syst. Sci.*, *26*(16), 4345-4378. https://doi.org/10.5194/hess-26-4345-2022

Beretta, R., Ravazzani, G., Maiorano, C., & Mancini, M. (2018). Simulating the Influence of Buildings on Flood Inundation in Urban Areas. *Geosciences*, *8*(2), 77. https://doi.org/10.3390/geosciences8020077

Bertilsson, L., Wiklund, K., de Moura Tebaldi, I., Rezende, O. M., Veról, A. P., & Miguez, M. G. (2019). Urban flood resilience – A multi-criteria index to integrate flood resilience into urban planning. *Journal of Hydrology*, *573*. https://doi.org/10.1016/j.jhydrol.2018.06.052

Bertsch, R. (2019). *Exploring new technologies for simulation and analysis of urban flooding* Thesis (Eng. D.)--Newcastle University, 2019.]. Newcastle upon Tyne, England.

Bertsch, R., Glenis, V., & Kilsby, C. (2017). Urban flood simulation using synthetic storm drain networks. *Water (Switzerland)*, *9*(12). https://doi.org/10.3390/w9120925

Bertsch, R., Glenis, V., & Kilsby, C. (2022). Building level flood exposure analysis using a hydrodynamic model. *Environmental Modelling & Software*, *156*, 105490. https://doi.org/https://doi.org/10.1016/j.envsoft.2022.105490

Birkinshaw, S. J., & Krivtsov, V. (2022). Evaluating the Effect of the Location and Design of Retention Ponds on Flooding in a Peri-Urban River Catchment. *Land*, *11*(8).

Bisht, D., Chatterjee, C., Kalakoti, S., Upadhyay, P., Sahoo, M., & Panda, A. (2016). Modeling urban floods and drainage using SWMM and MIKE URBAN: a case study. *Natural Hazards*, *84*(2), 749-776. https://doi.org/10.1007/s11069-016-2455-1

Bourdarias, C., Ersoy, M., & Gerbi, S. (2012). A mathematical model for unsteady mixed flows in closed water pipes. *Science China Mathematics*, *55*(2), 221-244. https://doi.org/10.1007/s11425-011-4353-z

Bruwier, M., Maravat, C., Mustafa, A., Teller, J., Pirotton, M., Erpicum, S., Archambeau, P., & Dewals, B. (2020). Influence of urban forms on surface flow in urban pluvial flooding. *Journal of Hydrology*, *582*. https://doi.org/10.1016/j.jhydrol.2019.124493

Cabrera, J. S., & Lee, H. S. (2019). Flood-Prone Area Assessment Using GIS-Based Multi-Criteria Analysis: A Case Study in Davao Oriental, Philippines. *Water*, *11*(11), 2203. https://www.mdpi.com/2073-4441/11/11/2203

Carter, J. G., Cavan, G., Connelly, A., Guy, S., Handley, J., & Kazmierczak, A. (2015). Climate change and the city: Building capacity for urban adaptation. *Progress in Planning*, *95*, 1-66. https://doi.org/https://doi.org/10.1016/j.progress.2013.08.001

Casal-Campos, A., Fu, G., Butler, D., & Moore, A. (2015). An Integrated Environmental Assessment of Green and Gray Infrastructure Strategies for Robust Decision Making. *Environmental Science & Technology*, *49*(14), 8307-8314. https://doi.org/10.1021/es506144f

Cea, L., & Costabile, P. (2022a). Flood Risk in Urban Areas: Modelling, Management and Adaptation to Climate Change. A Review. *Hydrology*, *9*(3).

Cea, L., & Costabile, P. (2022b). Flood Risk in Urban Areas: Modelling, Management and Adaptation to Climate Change. A Review. *Hydrology*, *9*(3), 50. https://www.mdpi.com/2306-5338/9/3/50

CH2M. (2019). *Environmental Statement, Volume 4, Appendix 17.1, Flood Risk Assessment, Part 6 of 17* [Technical Note]. https://metrowestphase1.files.wordpress.com/2020/01/6.25-es-volume-4-appendix-17.1-fra-app-n-part-1-part-6-of-17.pdf

Chaudhary, P., D'Aronco, S., Moy de Vitry, M., Leitão, J. P., & Wegner, J. D. (2019). Flood-water level estimation from social media images. *ISPRS Annals of the Photogrammetry, Remote Sensing and Spatial Information Sciences*, *4*(2/W5), 5-12.

Chen, A. S., Djordjevic, S., Fowler, H. J., Burton, A., Walsh, C., Harvey, H., & Wood, G. (2009). Pluvial flood modelling of the South East London resilience zone in the community resilience to extreme weather (CREW) Project. Flood and Coastal Risk Management Conference. Telford, UK,

Chen, A. S., Evans, B., Djordjević, S., & Savić, D. A. (2012). A coarse-grid approach to representing building blockage effects in 2D urban flood modelling. *Journal of Hydrology*, *426-427*, 1-16. https://doi.org/https://doi.org/10.1016/j.jhydrol.2012.01.007

Chen, A. S., Leandro, J., & Djordjević, S. (2016). Modelling sewer discharge via displacement of manhole covers during flood events using 1D/2D SIPSON/P-DWave dual drainage simulations. *Urban Water Journal*, *13*(8), 830-840. https://doi.org/10.1080/1573062X.2015.1041991

Chen, G. F., Qin, D. Y., Ye, R., Guo, Y. X., & Wang, H. (2011). A new method of rainfall temporal downscaling: a case study on sanmenxia station in the Yellow River Basin. *Hydrol. Earth Syst. Sci. Discuss.*, *2011*, 2323-2344. https://doi.org/10.5194/hessd-8-2323-2011

Choley, C., Finaud-Guyot, P., Garambois, P.-A., & Mose, R. (2021). *AN EFFECTIVE URBAN FLOOD MODEL ACCOUNTING FOR STREET-BUILDING EXCHANGES* SimHydro 2021: Models for complex and global water issues - Practices and expectations, 16-18 June 2021, Sophia Antipolis.

Coles, S., Bawa, J., Trenner, L., & Dorazio, P. (2001). *An introduction to statistical modeling of extreme values* (Vol. 208). Springer.

Costabile, P., Costanzo, C., Kalogiros, J., & Bellos, V. (2023). Toward Street-Level Nowcasting of Flash Floods Impacts Based on HPC Hydrodynamic Modeling at the Watershed Scale and High-Resolution Weather Radar Data. *Water Resources Research*, *59*(10), e2023WR034599. https://doi.org/https://doi.org/10.1029/2023WR034599

Craig, R. (2021, 03/03/2021). *Flooding – can we turn the tide?* [Interview]. https://ww3.rics.org/uk/en/modus/built-environment/homes-and-communities/flooding---can-we-turn-the-tide-.html#:~:text=Every%20year%2C%20flooding%20in%20the%20UK%20causes%20damage,on%20their%20properties%20and%20their%20lives%20is%20vital

Da Silva, C. V. F., Schardong, A., Garcia, J. I. B., & Oliveira, C. d. P. M. (2018). Climate change impacts and flood control measures for highly developed urban watersheds. *Water*, *10*(7), 829.

Dasallas, L., An, H., & Lee, S. (2023). Developing synthetic sewer pipe system for data-scarce domains in application for urban flood modeling. *Hydrology Research*, nh2023066. https://doi.org/10.2166/nh.2023.066

Dawson, D. A., Vercruysse, K., & Wright, N. (2020). A spatial framework to explore needs and opportunities for interoperable urban flood management. *Philosophical Transactions of the Royal Society A: Mathematical, Physical and Engineering Sciences*, *378*(2168), 20190205. https://doi.org/10.1098/rsta.2019.0205

Di Paola, F., Ricciardelli, E., Cimini, D., Romano, F., Viggiano, M., & Cuomo, V. (2014). Analysis of Catania flash flood case study by using combined microwave and infrared technique [Article]. *Journal of hydrometeorology*, *15*(5), 1989-1998. https://doi.org/10.1175/JHM-D-13-092.1

Djordjević, S., Prodanović, D., & Maksimović, Č. (1999). An approach to simulation of dual drainage. *Water Science and Technology*, *39*(9), 95-103. https://doi.org/10.2166/wst.1999.0451

Djordjević, S., Prodanović, D., Maksimović, Č., Ivetić, M., & Savić, D. (2005). SIPSON – Simulation of Interaction between Pipe flow and Surface Overland flow in Networks. *Water Science and Technology*, *52*(5), 275-283. https://doi.org/10.2166/wst.2005.0143

Environment Agency. (2021, 10/11/2021). *Represent buildings and infrastructure (receptor)*. Retrieved 23/02/2022 from https://www.gov.uk/government/publications/river-modelling-technical-standards-and-assessment/represent-buildings-and-infrastructure-receptor

Environment Agency. (2022). *Flood and coastal erosion risk management report: 1 April to 31 March 2020* [Corporate report]. https://www.gov.uk/government/publications/flood-and-coastal-risk-management-national-report/flood-and-coastal-erosion-risk-management-report-1-april-2019-to-31-march-2020

Erduran, K. S., & Kutija, V. (2003). Quasi-three-dimensional numerical model for flow through flexible, rigid, submerged and non-submerged vegetation. *Journal of Hydroinformatics*, *5*(3), 189-202. https://doi.org/10.2166/hydro.2003.0015

Ernst, K. M., & Preston, B. L. (2017). Adaptation opportunities and constraints in coupled systems: Evidence from the U.S. energy-water nexus. *Environmental* *science & policy*, *70*, 38-45. https://doi.org/https://doi.org/10.1016/j.envsci.2017.01.001

Escobar-Silva, E. V., Almeida, C. M. d., Silva, G. B. L. d., Bursteinas, I., Rocha Filho, K. L. d., de Oliveira, C. G., Fagundes, M. R., & Paiva, R. C. D. d. (2023). Assessing the Extent of Flood-Prone Areas in a South-American Megacity Using Different High Resolution DTMs. *Water*, *15*(6), 1127. https://www.mdpi.com/2073-4441/15/6/1127

Eulogi, M., Ostojin, S., Skipworth, P., Kroll, S., Shucksmith, J. D., & Schellart, A. (2021). Comparing methods to place adaptive local RTC actuators for spill volume reduction from multiple CSOs. *Journal of Hydroinformatics*, *24*(1), 78-92. https://doi.org/10.2166/hydro.2021.085

Ewen, J., O'Donnell, G., Bulygina, N., Ballard, C., & O'Connell, E. (2013). Towards understanding links between rural land management and the catchment flood hydrograph. *Quarterly journal of the Royal Meteorological Society.*, *139*(671), 350-357. https://doi.org/doi/10.1002/qj.2026

Falconer, R. H., Cobby, D., Smyth, P., Astle, G., Dent, J., & Golding, B. (2009). Pluvial flooding: new approaches in flood warning, mapping and risk management. *Journal of Flood Risk Management*, *2*(3), 198-208. https://doi.org/https://doi.org/10.1111/j.1753-318X.2009.01034.x

Fenner, R., O'Donnell, E., Ahilan, S., Dawson, D., Kapetas, L., Krivtsov, V., Ncube, S., & Vercruysse, K. (2019). Achieving Urban Flood Resilience in an Uncertain Future. *Water*, *11*(5). https://doi.org/10.3390/w11051082

Fewtrell, T. J., Bates, P. D., Horritt, M., & Hunter, N. M. (2008). Evaluating the effect of scale in flood inundation modelling in urban environments [https://doi.org/10.1002/hyp.7148]. *Hydrological Processes*, *22*(26), 5107-5118. https://doi.org/https://doi.org/10.1002/hyp.7148

Fewtrell, T. J., Duncan, A., Sampson, C. C., Neal, J. C., & Bates, P. D. (2011a). Benchmarking urban flood models of varying complexity and scale using high resolution terrestrial LiDAR data. *Physics and Chemistry of the Earth*, *36*(7-8), 281-291. https://doi.org/10.1016/j.pce.2010.12.011

Fewtrell, T. J., Duncan, A., Sampson, C. C., Neal, J. C., & Bates, P. D. (2011b). Benchmarking urban flood models of varying complexity and scale using high resolution terrestrial LiDAR data. *Physics and Chemistry of the Earth, Parts A/B/C*, *36*(7), 281-291. https://doi.org/https://doi.org/10.1016/j.pce.2010.12.011

Fletcher, T. D., Shuster, W., Hunt, W. F., Ashley, R., Butler, D., Arthur, S., Trowsdale, S., Barraud, S., Semadeni-Davies, A., Bertrand-Krajewski, J.-L., Mikkelsen, P.

S., Rivard, G., Uhl, M., Dagenais, D., & Viklander, M. (2015). SUDS, LID, BMPs, WSUD and more – The evolution and application of terminology surrounding urban drainage. *Urban Water Journal*, *12*(7), 525-542. https://doi.org/10.1080/1573062X.2014.916314

Fuchs, S., Keiler, M., & Zischg, A. (2015). A spatiotemporal multi-hazard exposure assessment based on property data. *Nat. Hazards Earth Syst. Sci.*, *15*(9), 2127-2142. https://doi.org/10.5194/nhess-15-2127-2015

G'Sell, M. G., Wager, S., Chouldechova, A., & Tibshirani, R. (2016). Sequential selection procedures and false discovery rate control. *Journal of the Royal Statistical Society: Series B: Statistical Methodology*, 423-444.

Galiatsatou, P. (2009). *Statistical Methods for Simulation of Extremely Events, Rainfall & Wave/ ΕΠΙΜΕΡΟΥΣ ΕΦΑΡΜΟΓΕΣ ΣΕ ΜΕΤΕΩΡΟΛΟΓΙΚΗ ΠΑΛΙΡΡΟΙΑ,<div style="">ΒΡΟΧΟΠΤΩΣΗ ΚΑΙ ΚΥΜΑ* Aristotle University of Thessaloniki]. Thessaloniki.

Galiatsatou, P., & Iliadis, C. (2022). Intensity-Duration-Frequency Curves at Ungauged Sites in a Changing Climate for Sustainable Stormwater Networks. *Sustainability*, *14*(3). https://doi.org/10.3390/su14031229

Galiatsatou, P., & Prinos, P. (2011). Modeling non-stationary extreme waves using a point process approach and wavelets. *Stochastic Environmental Research and Risk Assessment*, *25*, 165-183. https://doi.org/10.1007/s00477-010-0448-2

Galland, J.-C., Goutal, N., & Hervouet, J.-M. (1991). TELEMAC: A new numerical model for solving shallow water equations. *Advances in Water Resources*, *14*(3), 138-148. https://doi.org/https://doi.org/10.1016/0309-1708(91)90006-A

Ghimire, B., Chen, A. S., Guidolin, M., Keedwell, E. C., Djordjević, S., & Savić, D. A. (2013). Formulation of a fast 2D urban pluvial flood model using a cellular automata approach. *Journal of Hydroinformatics*, *15*(3), 676-686.

Glenis, V., Kutija, V., & Kilsby, C. G. (2018). A fully hydrodynamic urban flood modelling system representing buildings, green space and interventions. *Environmental Modelling and Software*, *109*, 272-292. https://doi.org/10.1016/j.envsoft.2018.07.018

Glenis, V., McGough, A., Kutija, V., Kilsby, C., & Woodman, S. (2013). Flood modelling for cities using Cloud computing. *Journal of Cloud Computing*, *2*(1), 1-14. https://doi.org/10.1186/2192-113x-2-7

Great London Authority. (2022). *Surface Water Flooding in London - Roundtable progress report*. flooding_progress_report_final_1.pdf (london.gov.uk)

Guan, M., Sillanpää, N., & Koivusalo, H. (2015). Modelling and assessment of hydrological changes in a developing urban catchment. *Hydrological Processes*, *29*(13), 2880-2894. https://doi.org/https://doi.org/10.1002/hyp.10410

Guerreiro, S., Glenis, V., Dawson, R., & Kilsby, C. (2017). Pluvial Flooding in European Cities-A Continental Approach to Urban Flood Modelling. *Water*, *9*(4), 296. https://doi.org/10.3390/w9040296

Guidolin, M., Chen, A. S., Ghimire, B., Keedwell, E. C., Djordjević, S., & Savić, D. A. (2016). A weighted cellular automata 2D inundation model for rapid flood analysis [Article]. *Environmental Modelling and Software*, *84*, 378-394. https://doi.org/10.1016/j.envsoft.2016.07.008

Guo, K., Guan, M., & Yu, D. (2020). Urban surface water flood modelling – a comprehensive review of current models and future challenges. *Hydrol. Earth Syst. Sci. Discuss.*, *2020*, 1-27. https://doi.org/10.5194/hess-2020-655

Guo, K., Guan, M., & Yu, D. (2021). Urban surface water flood modelling – a comprehensive review of current models and future challenges. *Hydrol. Earth Syst. Sci.*, *25*(5), 2843-2860. https://doi.org/10.5194/hess-25-2843-2021

Guo, Z., Leitão, J. P., Simões, N. E., & Moosavi, V. (2021). Data-driven flood emulation: Speeding up urban flood predictions by deep convolutional neural networks. *Journal of Flood Risk Management*, *14*(1), e12684. https://doi.org/https://doi.org/10.1111/jfr3.12684

Hanaish, I. S., Ibrahim, K., & Jemain, A. A. (2011). Stochastic modeling of rainfall in Peninsular Malaysia using Bartlett Lewis rectangular pulses models. *Modelling and Simulation in Engineering*, *2011*, 37-37.

Hdeib, R., Abdallah, C., Colin, F., Brocca, L., & Moussa, R. (2018). Constraining coupled hydrological-hydraulic flood model by past storm events and post-event measurements in data-sparse regions. *Journal of Hydrology*, *565*, 160-176. https://doi.org/https://doi.org/10.1016/j.jhydrol.2018.08.008

Hewett, C. J. M., Wilkinson, M. E., Jonczyk, J., & Quinn, P. F. (2020). Catchment systems engineering: An holistic approach to catchment management [https://doi.org/10.1002/wat2.1417]. *WIREs Water*, *7*(3), e1417. https://doi.org/https://doi.org/10.1002/wat2.1417

Hoang, L., & Fenner, R. A. (2016). System interactions of stormwater management using sustainable urban drainage systems and green infrastructure. *Urban Water Journal*, *13*(7), 739-758. https://doi.org/10.1080/1573062X.2015.1036083

Hörnschemeyer, B., Henrichs, M., Dittmer, U., & Uhl, M. (2023). Parameterization for Modeling Blue–Green Infrastructures in Urban Settings Using SWMM-UrbanEVA. *Water*, *15*(15), 2840. https://www.mdpi.com/2073-4441/15/15/2840

Hou, J., Guo, K., Liu, F., Han, H., Liang, Q., Tong, Y., & Li, P. (2018). Assessing Slope Forest Effect on Flood Process Caused by a Short-Duration Storm in a Small Catchment. *Water*, *10*(9), 1256. https://www.mdpi.com/2073-4441/10/9/1256

Hu, H., Yang, H., Wen, J., Zhang, M., & Wu, Y. (2023). An Integrated Model of Pluvial Flood Risk and Adaptation Measure Evaluation in Shanghai City. *Water*, *15*(3), 602. https://www.mdpi.com/2073-4441/15/3/602

Huang, H., Liao, W., Lei, X., Wang, C., Cai, Z., & Wang, H. (2022). An urban DEM reconstruction method based on multisource data fusion for urban pluvial flooding simulation. *Journal of Hydrology*, 128825. https://doi.org/https://doi.org/10.1016/j.jhydrol.2022.128825

Huizinga, J., de Moel, H., & Szewczyk, W. (2017). Global flood depth-damage functions. Methodology and the database with guidelines. *Joint Research Centre (JRC)*, 1-108. https://doi.org/10.2760/16510

Hunter, N. M., Bates, P. D., Neelz, S., Pender, G., Villanueva, I., Wright, N. G., Liang, D., Falconer, R. A., Lin, B., Waller, S., Crossley, A. J., & Mason, D. C. (2008a). Benchmarking 2D hydraulic models for urban flooding. *Proceedings of the Institution of Civil Engineers - Water Management*, *161*(1), 13-30. https://doi.org/10.1680/wama.2008.161.1.13

Hunter, N. M., Bates, P. D., Neelz, S., Pender, G., Villanueva, I., Wright, N. G., Liang, D., Falconer, R. A., Lin, B., Waller, S., Crossley, A. J., & Mason, D. C. (2008b). Benchmarking 2D hydraulic models for urban flooding. *Proceedings of the ICE - Water Management*, *161*(1), 13-30. https://doi.org/10.1680/wama.2008.161.1.13

Iliadis, C., Galiatsatou, P., Glenis, V., Prinos, P., & Kilsby, C. (2023). Urban Flood Modelling under Extreme Rainfall Conditions for Building-Level Flood Exposure Analysis. *Hydrology*, *10*(8), 172. https://www.mdpi.com/2306-5338/10/8/172

Iliadis, C., Glenis, V., & Kilsby, C. (2023a). Cloud Modelling of Property-Level Flood Exposure in Megacities. *Water*, *15*(19), 3395. https://www.mdpi.com/2073-4441/15/19/3395

Iliadis, C., Glenis, V., & Kilsby, C. (2023a). A cost-benefit 'source-receptor' framework for implementation of Blue-Green flood risk management [under review]. *Journal of Hydrology*. https://doi.org/https://arxiv.org/abs/2311.00420

Iliadis, C., Glenis, V., & Kilsby, C. (2023b). Representing buildings and urban features in hydrodynamic flood models. *Journal of Flood Risk Management*, *n/a*(n/a), e12950. https://doi.org/https://doi.org/10.1111/jfr3.12950

Iliadis, C., Glenis, V., & Kilsby, C. (2023b). Representing buildings and urban features in hydrodynamic flood models. *Journal of Flood Risk Management*. https://doi.org/10.1111/JFR3.12950

Innocenti, S., Mailhot, A., & Frigon, A. (2017). Simple scaling of extreme precipitation in North America. *Hydrol. Earth Syst. Sci.*, *21*(11), 5823-5846. https://doi.org/10.5194/hess-21-5823-2017

IPCC, C. C. (2014). Synthesis report summary for policymakers. *An Assessment of the Intergovernmental Panel on Climate Change*.

Jamali, B., Löwe, R., Bach, P. M., Urich, C., Arnbjerg-Nielsen, K., & Deletic, A. (2018). A rapid urban flood inundation and damage assessment model [Article]. *Journal of Hydrology*, *564*, 1085-1098. https://doi.org/10.1016/j.jhydrol.2018.07.064

Jenkins, K., Hall, J., Glenis, V., & Kilsby, C. (2018). A Probabilistic Analysis of Surface Water Flood Risk in London [https://doi.org/10.1111/risa.12930]. *Risk Analysis*, *38*(6), 1169-1182. https://doi.org/https://doi.org/10.1111/risa.12930

Karim, F., Armin, M. A., Ahmedt-Aristizabal, D., Tychsen-Smith, L., & Petersson, L. (2023). A Review of Hydrodynamic and Machine Learning Approaches for Flood Inundation Modeling. *Water*, *15*(3).

Kilsby, C., Glenis, V., & Bertsch, R. (2020). Coupled surface/sub-surface modelling to investigate the potential for blue-green infrastructure to deliver urban flood risk reduction benefits. In C. Thorne (Ed.), *Blue-Green Cities: Integrating urban flood risk management with green infrastructure* (ICE Bookshop - civil engineering publications ed., pp. 37-50). ICE Publishing.

Kjeldsen, T. R. (2007a). *Flood Estimation Handbook - Supplementary Report No. 1*. Centre for Ecology & Hydrology.

Kjeldsen, T. R. (2007b). The revitalised FSR / FEH rainfall-runoff method. *FLOOD ESTIMATION HANDBOOK SUPPLEMENTARY REPORT No.1*, 1-64.

Koutsoyiannis, D., & Onof, C. (2001). Rainfall disaggregation using adjusting procedures on a Poisson cluster model. *Journal of Hydrology*, *246*(1), 109-122. https://doi.org/https://doi.org/10.1016/S0022-1694(01)00363-8

Koutsoyiannis, D., Onof, C., & Wheater, H. S. (2003). Multivariate rainfall disaggregation at a fine timescale. *Water Resources Research*, *39*(7). https://doi.org/https://doi.org/10.1029/2002WR001600

Kuller, M., Bach, P. M., Ramirez-Lovering, D., & Deletic, A. (2017). Framing water sensitive urban design as part of the urban form: A critical review of tools for best planning practice. *Environmental Modelling & Software*, *96*, 265-282. https://doi.org/https://doi.org/10.1016/j.envsoft.2017.07.003

Kumar, J., Brooks, B.-G. J., Thornton, P. E., & Dietze, M. C. (2012). Sub-daily statistical downscaling of meteorological variables using neural networks. *Procedia Computer Science*, *9*, 887-896.

Kutija, V., Bertsch, R., Glenis, V., Alderson, D., Parkin, G., Walsh, C., Robinson, J., & Kilsby, C. (2014). *Model Validation Using Crowd-Sourced Data From A Large Pluvial Flood* INTERNATIONAL CONFERENCE ON HYDROINFORMATICS, New York. https://academicworks.cuny.edu/cc_conf_hic/415

Kutija, V., & Murray, M. G. (2007). An object-oriented approach to the modelling of free-surface flows. *Journal of Hydroinformatics*, *9*(2), 81-94. https://doi.org/10.2166/hydro.2007.101

Lamb, R., Keef, C., Tawn, J., Laeger, S., Meadowcroft, I., Surendran, S., Dunning, P., & Batstone, C. (2010). A new method to assess the risk of local and widespread flooding on rivers and coasts. *Journal of Flood Risk Management*, *3*(4), 323-336. https://doi.org/https://doi.org/10.1111/j.1753-318X.2010.01081.x

Lazaridis, V., & Latinopoulos, D. (2023). Estimating urban vulnerability to flood and heat hazards: A case study in the municipality of Thessaloniki, Greece. *European Spatial Research and Policy*, *29*(2), 309-340. https://doi.org/10.18778/1231-1952.29.2.16

Leandro, J., Chen, A. S., Djordjević, S., & Savić, D. A. (2009). Comparison of 1D/1D and 1D/2D coupled (sewer/surface) hydraulic models for urban flood simulation. *Journal of Hydraulic Engineering*, *135*(6), 495-504. https://doi.org/10.1061/(asce)hy.1943-7900.0000037

Lee, S., & An, H. (2019). Evaluating the effect of grid size and type in integrated 1D/2D coupled urban inundation modelling on the interacting discharge between the surface and sewerage system. *Journal of Flood Risk Management*, *12*(S1), e12537. https://doi.org/https://doi.org/10.1111/jfr3.12537

Lee, T., & Jeong, C. (2014). Nonparametric statistical temporal downscaling of daily precipitation to hourly precipitation and implications for climate change scenarios. *Journal of Hydrology*, *510*, 182-196.

Lee, T., Salas, J. D., & Prairie, J. (2010). An enhanced nonparametric streamflow disaggregation model with genetic algorithm. *Water Resources Research*, *46*(8). https://doi.org/https://doi.org/10.1029/2009WR007761

Leitão, J. P., Boonya-aroonnet, S., Prodanović, D., & Maksimović, Č. (2009). The influence of digital elevation model resolution on overland flow networks for modelling urban pluvial flooding. *Water Science and Technology*, *60*(12), 3137-3149. https://doi.org/10.2166/wst.2009.754

Leitão, J. P., Moy de Vitry, M., Scheidegger, A., & Rieckermann, J. (2016). Assessing the quality of digital elevation models obtained from mini unmanned aerial vehicles for overland flow modelling in urban areas. *Hydrology and Earth System Sciences*, *20*(4), 1637-1653.

Leitão, J. P., Simões, N. E., Pina, R. D., Ochoa-Rodriguez, S., Onof, C., & Sá Marques, A. (2017). Stochastic evaluation of the impact of sewer inlets' hydraulic capacity on urban pluvial flooding. *Stochastic Environmental Research and Risk Assessment*, *31*(8), 1907-1922. https://doi.org/10.1007/s00477-016-1283-x

Li, Z., Dong, M., Wong, T., Wang, J., Kumar, A. J., & Singh, R. P. (2018). Objectives and Indexes for Implementation of Sponge Cities—A Case Study of Changzhou City, China. *Water*, *10*(5). https://doi.org/10.3390/w10050623

Lidar. (2016). *Composite Digital Terrain Model England 1m resolution [ASC geospatial data], Scale 1:4000, Updated: 5 January 2016, Open Government Licence, Using: EDINA LIDAR Digimap Service, https://digimap.edina.ac.uk/ (accesed on 1 December 2020).*

Liu, J., Wang, G., Li, T., Xue, H., & He, L. (2006). Sediment yield computation of the sandy and gritty area based on the digital watershed model. *Science in China Series E: Technological Sciences*, *49*, 752-763.

Liu, R., Wei, J., Ren, Y., Liu, Q., Wang, G., Shao, S., & Tang, S. (2017). HydroMP – a computing platform for hydrodynamic simulation based on cloud computing. *Journal of Hydroinformatics*, *19*(6), 953-972. https://doi.org/10.2166/hydro.2017.140

Liu, W., Chen, W., & Peng, C. (2014). Assessing the effectiveness of green infrastructures on urban flooding reduction: A community scale study. *Ecological Modelling*, *291*, 6-14.

Loftis, J. D., Wang, H., Forrest, D., Rhee, S., & Nguyen, C. (2017). *Emerging flood model validation frameworks for street-level inundation modeling with StormSense* Proceedings of the 2nd International Workshop on Science of Smart City Operations and Platforms Engineering, Pittsburgh, Pennsylvania. https://doi.org/10.1145/3063386.3063764

LONDON ASSEMBLY. (2016). *Oxford St – the busiest feet street in the world?* https://www.london.gov.uk/press-releases/assembly/oxford-st-the-busiest-feet-street-in-the-world

Mackay, E., & Jonathan, P. (2020). Assessment of return value estimates from stationary and non-stationary extreme value models. *Ocean Engineering*, *207*, 107406. https://doi.org/https://doi.org/10.1016/j.oceaneng.2020.107406

Mailhot, A., & Duchesne, S. (2010). Design criteria of urban drainage infrastructures under climate change. *Journal of Water Resources Planning and Management*, *136*, 201-208.

Maksimović, Č., Prodanović, D., Boonya-Aroonnet, S., Leitão, J. P., Djordjević, S., & Allitt, R. (2009). Overland flow and pathway analysis for modelling of urban pluvial flooding. *Journal of Hydraulic Research*, *47*(4), 512-523. https://doi.org/10.1080/00221686.2009.9522027

Malekpour, A., & Karney, B. W. (2016). Spurious Numerical Oscillations in the Preissmann Slot Method: Origin and Suppression. *Journal of Hydraulic Engineering*, *142*(3), 04015060. https://doi.org/doi:10.1061/(ASCE)HY.1943-7900.0001106

Marani, M., & Zanetti, S. (2007). Downscaling rainfall temporal variability. *Water Resources Research*, *43*(9). https://doi.org/https://doi.org/10.1029/2006WR005505

Martínez-Gomariz, E., Forero-Ortiz, E., Guerrero-Hidalga, M., Castán, S., & Gómez, M. (2020). Flood depth–damage curves for Spanish urban areas. *Sustainability*, *12*(7), 2666.

MasterMap, O. (2020). *Building Height Attribute [FileGeoDatabase geospatial data], Scale 1:2500, Updated: 11 March 2020, Ordnance Survey (GB), Using: EDINA Digimap Ordnance Survey Service, https://digimap.edina.ac.uk/ (accesed on 1 December 2020).*

McClean, F., Dawson, R., & Kilsby, C. (2020). Implications of Using Global Digital Elevation Models for Flood Risk Analysis in Cities. *Water Resources Research*, *56*(10), n/a. https://doi.org/10.1029/2020wr028241

McClean, F., Dawson, R., & Kilsby, C. (2023). Intercomparison of global reanalysis precipitation for flood risk modelling. *Hydrol. Earth Syst. Sci.*, *27*(2), 331-347. https://doi.org/10.5194/hess-27-331-2023

McKenna, J., Glenis, V., & Kilsby, C. (2023). A new riemann solver for modelling bridges in flood flows - Development and experimental validation. *Applied Mathematics and Computation*, *447*, 127870. https://doi.org/https://doi.org/10.1016/j.amc.2023.127870

Meselhe, E. A., & Holly, F. M. (1997). Invalidity of Preissmann Scheme for Transcritical Flow. *Journal of Hydraulic Engineering*, *123*(7), 652-655. https://doi.org/doi:10.1061/(ASCE)0733-9429(1997)123:7(652)

Microsoft. (2022). *Windows Azure Platform, Microsoft Cloud Services.* http://www.microsoft.com/windowsazure/

Mignot, E., Li, X., & Dewals, B. (2019). Experimental modelling of urban flooding: A review. *Journal of Hydrology*, *568*, 334-342. https://doi.org/https://doi.org/10.1016/j.jhydrol.2018.11.001

Mignot, E., Paquier, A., & Haider, S. (2006). Modeling floods in a dense urban area using 2D shallow water equations. *Journal of Hydrology*, *327*(1-2), 186-199. https://doi.org/10.1016/j.jhydrol.2005.11.026

Mokarram, M., & Khosravi, M. R. (2021). A cloud computing framework for analysis of agricultural big data based on Dempster–Shafer theory [Article]. *Journal of Supercomputing*, *77*(3), 2545-2565. https://doi.org/10.1007/s11227-020-03366-z

Morales-Hernández, M., Sharif, M. B., Kalyanapu, A., Ghafoor, S. K., Dullo, T. T., Gangrade, S., Kao, S. C., Norman, M. R., & Evans, K. J. (2021). TRITON: A Multi-GPU open source 2D hydrodynamic flood model. *Environmental Modelling & Software*, *141*, 105034. https://doi.org/https://doi.org/10.1016/j.envsoft.2021.105034

Morgan, M., & Fenner, R. (2019). Spatial evaluation of the multiple benefits of sustainable drainage systems. *Proceedings of the Institution of Civil Engineers - Water Management*, *172*(1), 39-52. https://doi.org/10.1680/jwama.16.00048

Muthusamy, M., Casado, M. R., Butler, D., & Leinster, P. (2021). Understanding the effects of Digital Elevation Model resolution in urban fluvial flood modelling. *Journal of Hydrology*, *596*, 126088. https://doi.org/https://doi.org/10.1016/j.jhydrol.2021.126088

Neal, J. C., Bates, P. D., Fewtrell, T. J., Hunter, N. M., Wilson, M. D., & Horritt, M. S. (2009). Distributed whole city water level measurements from the Carlisle 2005 urban flood event and comparison with hydraulic model simulations. *Journal of Hydrology*, *368*(1), 42-55. https://doi.org/https://doi.org/10.1016/j.jhydrol.2009.01.026

Néelz, S., & Pender, G. (2013). *Delivering Benefits Thorough Evidences: Benchmarking the Latest Generation of 2D Hydraulic Modelling Packages*. https://www.gov.uk/government/publications/benchmarking-the-latest-generation-of-2d-hydraulic-flood-modelling-packages

Ngo, H., Ranasinghe, R., Zevenbergen, C., Kirezci, E., Maheng, D., Radhakrishnan, M., & Pathirana, A. (2022). An Efficient Modeling Approach for Probabilistic Assessments of Present-Day and Future Fluvial Flooding [Article]. *Frontiers in Climate*, *4*, Article 798618. https://doi.org/10.3389/fclim.2022.798618

Noh, S. J., Lee, J.-H., Lee, S., Kawaike, K., & Seo, D.-J. (2018). Hyper-resolution 1D-2D urban flood modelling using LiDAR data and hybrid parallelization. *Environmental Modelling & Software*, *103*, 131-145. https://doi.org/https://doi.org/10.1016/j.envsoft.2018.02.008

Norbiato, D., Borga, M., Sangati, M., & Zanon, F. (2007). Regional frequency analysis of extreme precipitation in the eastern Italian Alps and the August 29, 2003 flash flood. *Journal of Hydrology*, *345*(3-4), 149-166.

Northrop, P. J., & Coleman, C. L. (2014). Improved threshold diagnostic plots for extreme value analyses. *Extremes*, *17*(2), 289-303. https://doi.org/10.1007/s10687-014-0183-z

O'Donnell, E., Thorne, C., Ahilan, S., Arthur, S., Birkinshaw, S., Butler, D., Dawson, D., Everett, G., Fenner, R., Glenis, V., Kapetas, L., Kilsby, C., Krivtsov, V., Lamond, J., Maskrey, S., O'Donnell, G., Potter, K., Vercruysse, K., Vilcan, T., & Wright, N. (2020). The blue-green path to urban flood resilience. *Blue-Green Systems*, *2*(1), 28-45. https://doi.org/10.2166/bgs.2019.199

O'Donnell, E. C., Lamond, J. E., & Thorne, C. R. (2017). Recognising barriers to implementation of Blue-Green Infrastructure: a Newcastle case study. *Urban Water Journal*, *14*(9), 964-971. https://doi.org/10.1080/1573062X.2017.1279190

O'Donnell, E. C., Netusil, N. R., Chan, F. K. S., Dolman, N. J., & Gosling, S. N. (2021). International Perceptions of Urban Blue-Green Infrastructure: A Comparison across Four Cities. *Water*, *13*(4), 544. https://www.mdpi.com/2073-4441/13/4/544

OECD. (2016). *Financial Management of Flood Risk*. https://www.oecd.org/finance/financial-management-of-flood-risk.htm

Ogden, F. L., Raj Pradhan, N., Downer, C. W., & Zahner, J. A. (2011). Relative importance of impervious area, drainage density, width function, and subsurface storm drainage on flood runoff from an urbanized catchment. *Water Resources Research*, *47*(12). https://doi.org/https://doi.org/10.1029/2011WR010550

Oladunjoye, O. P. D. X. H. R. S. U. D. S. A. C.-B. A. A. (2022). Retrofitting Sustainable Urban Drainage Systems (SuDS): A Cost-Benefit Analysis Appraisal. *Water*, *14*(16).

Onof, C., Townend, J., & Kee, R. (2005). Comparison of two hourly to 5-min rainfall disaggregators. *Atmospheric Research*, *77*(1), 176-187. https://doi.org/https://doi.org/10.1016/j.atmosres.2004.10.022

Oppenheimer, M., Campos, M., Warren, R., Birkmann, J., Luber, G., O'Neill, B., & Takahashi, K. (2014). IPCC-WGII-AR5-19. Emergent Risks and Key Vulnerabilities. *Climate Change 2014: Impacts, Adaptation, and Vulnerability. Part A: Global and Sectoral Aspects. Contribution of Working Group II to the Fifth Assessment Report of the Intergovernmental Panel on Climate Change*, 1039-1099.

Ordnance Survey. (2020). *OS MasterMap Topografy*. https://www.ordnancesurvey.co.uk/business-government/products/mastermap-topography

Papaioannou, G., Efstratiadis, A., Vasiliades, L., Loukas, A., Papalexiou, S. M., Koukouvinos, A., Tsoukalas, I., & Kossieris, P. (2018). An Operational Method for Flood Directive Implementation in Ungauged Urban Areas. *Hydrology*, *5*(2), 24. https://www.mdpi.com/2306-5338/5/2/24

Papaioannou, G., Varlas, G., Terti, G., Papadopoulos, A., Loukas, A., Panagopoulos, Y., & Dimitriou, E. (2019). Flood Inundation Mapping at Ungauged Basins Using Coupled Hydrometeorological–Hydraulic Modelling: The Catastrophic Case of the 2006 Flash Flood in Volos City, Greece. *Water*, *11*(11), 2328. https://www.mdpi.com/2073-4441/11/11/2328

Papaioannou, G., Vasiliades, L., Loukas, A., Alamanos, A., Efstratiadis, A., Koukouvinos, A., Tsoukalas, I., & Kossieris, P. (2021). A Flood Inundation Modeling Approach for Urban and Rural Areas in Lake and Large-Scale River Basins. *Water*, *13*(9), 1264. https://www.mdpi.com/2073-4441/13/9/1264

Pappenberger, F., Beven, K., Ratto, M., & Matgen, P. (2008). Multi-method global sensitivity analysis of flood inundation models. *Advances in Water Resources*, *31*(1), 1-14. https://doi.org/10.1016/j.advwatres.2007.04.009

Paquier, A., Mignot, E., & Bazin, P.-H. (2015). From Hydraulic Modelling to Urban Flood Risk. *Procedia Engineering*, *115*(C), 37-44. https://doi.org/10.1016/j.proeng.2015.07.352

Park, K., Choi, S.-H., & Yu, I. (2021). Risk Type Analysis of Building on Urban Flood Damage. *Water*, *13*(18), 2505. https://www.mdpi.com/2073-4441/13/18/2505

Paulik, R., Wild, A., Zorn, C., & Wotherspoon, L. (2022). Residential building flood damage: Insights on processes and implications for risk assessments [https://doi.org/10.1111/jfr3.12832]. *Journal of Flood Risk Management*, *15*(4), e12832. https://doi.org/https://doi.org/10.1111/jfr3.12832

Pettit, A. (2014). Assessing the Flood Risk Management Benefits of Property Level Protection, JBA Project Manager. In: JBA.

Pham, Q. B., Ali, S. A., Bielecka, E., Calka, B., Orych, A., Parvin, F., & Łupikasza, E. (2022). Flood vulnerability and buildings' flood exposure assessment in a densely urbanised city: comparative analysis of three scenarios using a neural network approach. *Natural Hazards*, *113*(2), 1043-1081. https://doi.org/10.1007/s11069-022-05336-5

Popescu, I. (2014). *Computational hydraulics : numerical methods and modelling*. London : IWA Publishing.

Potter, K., & Vilcan, T. (2020). Managing urban flood resilience through the English planning system: insights from the 'SuDS-face'. *Philosophical transactions. Series A, Mathematical, physical, and engineering sciences*, *378*(2168), 20190206. https://doi.org/10.1098/rsta.2019.0206

Preissmann, A., & Cunge, J. (1961). Calcul du mascaret sur machine électronique. *La Houille Blanche*(5), 588-596.

Preston, B. L., Mustelin, J., & Maloney, M. C. (2015). Climate adaptation heuristics and the science/policy divide. *Mitigation and Adaptation Strategies for Global Change*, *20*(3), 467-497. https://doi.org/10.1007/s11027-013-9503-x

Priest, S., Viavattene, C., Penning-Rowsell, E., Steinhausen, M., Dennis, P., Joyce, J., Morris, J., & Chatterton, J. (2022). *Flood and Coastal Erosion Risk Management*.

Radfar, S., & Galiatsatou, P. (2023). Influence of nonstationarity and dependence of extreme wave parameters on the reliability assessment of coastal structures - A case study. *Ocean Engineering*, *273*, 113862. https://doi.org/https://doi.org/10.1016/j.oceaneng.2023.113862

Rak, G., Grobljar, S., & Steinman, F. (2018). Flood Modelling in Urban Areas. *Acta hydrotechnica*(November), 21-33. https://doi.org/10.15292/acta.hydro.2018.02

Rehman, A. U., Glenis, V., Lewis, E., & Kilsby, C. (2023). CONFIGURE: An Optimisation Framework for the Cost-Effective Spatial Configuration of Blue-Green Infrastructure. *arXiv preprint arXiv:2310.13989*.

Rosenzweig, B. R., Herreros Cantis, P., Kim, Y., Cohn, A., Grove, K., Brock, J., Yesuf, J., Mistry, P., Welty, C., McPhearson, T., Sauer, J., & Chang, H. (2021). The Value of Urban Flood Modeling [https://doi.org/10.1029/2020EF001739]. *Earth's Future*, *9*(1), e2020EF001739. https://doi.org/https://doi.org/10.1029/2020EF001739

Rosenzweig, B. R., McPhillips, L., Chang, H., Cheng, C., Welty, C., Matsler, M., Iwaniec, D., & Davidson, C. I. (2018). Pluvial flood risk and opportunities for resilience [https://doi.org/10.1002/wat2.1302]. *WIREs Water*, *5*(6), e1302. https://doi.org/https://doi.org/10.1002/wat2.1302

Salas, J. D., & Lee, T. (2010). Nonparametric Simulation of Single-Site Seasonal Streamflows. *Journal of Hydrologic Engineering*, *15*, 284-296.

Sanders, B. F. (2017). Hydrodynamic Modeling of Urban Flood Flows and Disaster Risk Reduction. In: Oxford University Press.

Schmitt, T. G., Thomas, M., & Ettrich, N. (2004). Analysis and modeling of flooding in urban drainage systems. *Journal of Hydrology*, *299*(3), 300-311. https://doi.org/https://doi.org/10.1016/j.jhydrol.2004.08.012

Schubert, J. E., & Sanders, B. F. (2012). Building treatments for urban flood inundation models and implications for predictive skill and modeling efficiency. *Advances in Water Resources*, *41*, 49-64. https://doi.org/10.1016/j.advwatres.2012.02.012

Schubert, J. E., Sanders, B. F., Smith, M. J., & Wright, N. G. (2008). Unstructured mesh generation and landcover-based resistance for hydrodynamic modeling of urban flooding. *Advances in Water Resources*, *31*(12), 1603-1621. https://doi.org/10.1016/j.advwatres.2008.07.012

Schuch, G., Serrao-Neumann, S., Morgan, E., & Low Choy, D. (2017). Water in the city: Green open spaces, land use planning and flood management – An Australian case study. *Land Use Policy*, *63*, 539-550. https://doi.org/https://doi.org/10.1016/j.landusepol.2017.01.042

See, L. (2019). A review of citizen science and crowdsourcing in applications of pluvial flooding. *Frontiers in Earth Science*, *7*, 44.

SEPA. (2018). Flood Modelling Guidance for Responsible Authorities. Available at: https://www.sepa.org.uk/media/219653/flood_model_guidance_v2.pdf. In.

Shen, J., Tan, F., & Zhang, Y. (2018). Improved building treatment approach for urban inundation modeling: A case study in Wuhan, China. *Water (Switzerland)*, *10*(12). https://doi.org/10.3390/w10121760

Sillanpää, N., & Koivusalo, H. (2014). Measurements and data analysis of suburban development impacts on runoff event characteristics and unit hydrographs. EGU General Assembly Conference Abstracts,

Silva Lomba, J., & Fraga Alves, M. I. (2020). L-moments for automatic threshold selection in extreme value analysis. *Stochastic Environmental Research and Risk Assessment*, *34*(3), 465-491. https://doi.org/10.1007/s00477-020-01789-x

Simões, N. E., Leitão, J. P., Maksimović, Č., Sá Marques, A., & Pina, R. (2010). Sensitivity analysis of surface runoff generation in urban flood forecasting.

Water Science and Technology, *61*(10), 2595-2601. https://doi.org/10.2166/wst.2010.178

Singh, A., Dawson, D., Trigg, M., & Wright, N. (2021). A review of modelling methodologies for flood source area (FSA) identification. *Natural Hazards*, *107*(2), 1047-1068. https://doi.org/10.1007/s11069-021-04672-2

Singh, A., Dawson, D., Trigg, M. A., Wright, N., Seymour, C., & Ferriday, L. (2023). Drainage representation in flood models: Application and analysis of capacity assessment framework. *Journal of Hydrology*, *622*, 129718. https://doi.org/https://doi.org/10.1016/j.jhydrol.2023.129718

Smith, L. S., & Liang, Q. (2013). Towards a generalised GPU/CPU shallow-flow modelling tool. *Computers & Fluids*, *88*, 334-343. https://doi.org/https://doi.org/10.1016/j.compfluid.2013.09.018

SNIFFER. (2006). *Retrofitting Sustainable Urban Water Solutions - Final Report*. http://www.fwr.org/snifrprt.htm

Sörensen, J., & Emilsson, T. (2019). Evaluating Flood Risk Reduction by Urban Blue-Green Infrastructure Using Insurance Data. *Journal of Water Resources Planning and Management*, *145*(2), 04018099. https://doi.org/doi:10.1061/(ASCE)WR.1943-5452.0001037

Stefanidis, S., Alexandridis, V., & Theodoridou, T. (2022). Flood Exposure of Residential Areas and Infrastructure in Greece. *Hydrology*, *9*(8), 145. https://www.mdpi.com/2306-5338/9/8/145

Suriya, S., & Mudgal, B. V. (2012). Impact of urbanization on flooding: The Thirusoolam sub watershed – A case study. *Journal of Hydrology*, *412-413*, 210-219. https://doi.org/https://doi.org/10.1016/j.jhydrol.2011.05.008

Syme, W. J. (2008). *Flooding in Urban Areas - 2D Modelling Approaches for Buildings and Fences* 9th National Conference on Hydraulics in Water Engineering Darwin Convention Centre, http://support@tuflow.com

Szewrański, S., Chruściński, J., Kazak, J., Świąder, M., Tokarczyk-Dorociak, K., & Żmuda, R. (2018). Pluvial Flood Risk Assessment Tool (PFRA) for Rainwater Management and Adaptation to Climate Change in Newly Urbanised Areas. *Water*, *10*(4), 386. https://www.mdpi.com/2073-4441/10/4/386

Tan, W.-Y. (1992). *Shallow water hydrodynamics: Mathematical theory and numerical solution for a two-dimensional system of shallow-water equations*. Elsevier.

Teng, J., Jakeman, A. J., Vaze, J., Croke, B. F. W., Dutta, D., & Kim, S. (2017). Flood inundation modelling: A review of methods, recent advances and uncertainty analysis. *Environmental Modelling and Software*, *90*, 201-216. https://doi.org/10.1016/j.envsoft.2017.01.006

Teng, J., Vaze, J., Kim, S., Dutta, D., Jakeman, A. J., & Croke, B. F. W. (2019). Enhancing the Capability of a Simple, Computationally Efficient, Conceptual Flood Inundation Model in Hydrologically Complex Terrain. *Water Resources Management*, *33*(2), 831-845. https://doi.org/10.1007/s11269-018-2146-7

Thrysøe, C., Balstrøm, T., Borup, M., Löwe, R., Jamali, B., & Arnbjerg-Nielsen, K. (2021). FloodStroem: A fast dynamic GIS-based urban flood and damage model. *Journal of Hydrology*, *600*, 126521. https://doi.org/https://doi.org/10.1016/j.jhydrol.2021.126521

Torgersen, G., Rød, J. K., Kvaal, K., Bjerkholt, J. T., & Lindholm, O. G. (2017). Evaluating Flood Exposure for Properties in Urban Areas Using a Multivariate Modelling Technique. *Water*, *9*(5), 318. https://www.mdpi.com/2073-4441/9/5/318

Toro, E. F. (2001). Shock-Capturing Methods for Free-Surface Shallow Flows.

Toro, E. F. (2013). *Riemann solvers and numerical methods for fluid dynamics: a practical introduction*. Springer Science & Business Media.

TUFLOW. (2018). *TUFLOW Classic/HPC User Manual for the 2018-03 release*. https://downloads.tuflow.com/_archive/TUFLOW/Releases/2018-03/TUFLOW%20Manual.2018-03.pdf

UK Centre for Ecology & Hydrology. (2022). *Environmental science for a world where people and nature prosper*. Retrieved 25/04/2023 from https://www.ceh.ac.uk/

UK Government. (2016). *National Flood Resilience Review*. Retrieved from https://assets.publishing.service.gov.uk/government/uploads/system/uploads/attachment_data/file/551137/national-flood-resilience-review.pdf

United Nations Department of Economic and Social Affairs. (2019). *World Urbanization Prospects: The 2018 Revision*. United Nations. https://doi.org/https://doi.org/10.18356/b9e995fe-en

Vacondio, R., Dal Palù, A., & Mignosa, P. (2014). GPU-enhanced Finite Volume Shallow Water solver for fast flood simulations. *Environmental Modelling & Software*, *57*, 60-75. https://doi.org/https://doi.org/10.1016/j.envsoft.2014.02.003

Velasco, M., Cabello, À., & Russo, B. (2015). Flood damage assessment in urban areas. Application to the Raval district of Barcelona using synthetic depth damage curves. *Urban Water Journal*, *13*(4), 426-440. https://doi.org/10.1080/1573062x.2014.994005

Veneziano, D., Lepore, C., Langousis, A., & Furcolo, P. (2007). Marginal methods of intensity-duration-frequency estimation in scaling and nonscaling rainfall. *Water Resources Research*, *43*.

Vercruysse, K., Dawson, D. A., Glenis, V., Bertsch, R., Wright, N., & Kilsby, C. (2019). Developing spatial prioritization criteria for integrated urban flood management based on a source-to-impact flood analysis. *Journal of Hydrology*, *578*(June). https://doi.org/10.1016/j.jhydrol.2019.124038

Vesuviano, G. (2022). *The FEH22 rainfall depth duration-frequency (DDF) model*. UKCEH. https://fehwebdocs.hydrosolutions.co.uk/.attachments/The%20FEH22%20rainfall%20depth-duration-frequency%20(DDF)%20model-caa11347-4ff7-4c89-b707-bf5bb1c05d79.pdf

Wang, X., Cao, Z., Pender, G., & Neelz, S. (2010). Numerical modelling of flood flows over irregular topography. *Proceedings of the Institution of Civil Engineers - Water Management*, *163*(5), 255-265. https://doi.org/10.1680/wama.2010.163.5.255

Wang, Y., Chen, A. S., Fu, G., Djordjević, S., Zhang, C., & Savić, D. A. (2018). An integrated framework for high-resolution urban flood modelling considering multiple information sources and urban features [Article]. *Environmental Modelling and Software*, *107*, 85-95. https://doi.org/10.1016/j.envsoft.2018.06.010

Warrick, A. W. (2003). *Soil water dynamics*. Oxford ; New York : Oxford University Press.

Willis, T., Wright, N., & Sleigh, A. (2019). Systematic analysis of uncertainty in 2D flood inundation models. *Environmental Modelling and Software*, *122*(August 2018). https://doi.org/10.1016/j.envsoft.2019.104520

Woods Ballard, B., Wilson, S., Udale-Clarke, H., Illman, S., Scott, T., Ashley, R., & Kellagher, R. (2015). *The SuDS Manual (C753F)* [manual]. CIRIA (Construction Industry Research and Information Association). https://www.ciria.org/ItemDetail?iProductCode=C753F&Category=FREEPUBS

Wright, N. G., & Thorne, C. (2014). Delivering and evaluating multiple flood risk benefits in blue-green cities.

Xafoulis, N., Kontos, Y., Farsirotou, E., Kotsopoulos, S., Perifanos, K., Alamanis, N., Dedousis, D., & Katsifarakis, K. (2023). Evaluation of Various Resolution DEMs in Flood Risk Assessment and Practical Rules for Flood Mapping in Data-Scarce Geospatial Areas: A Case Study in Thessaly, Greece. *Hydrology*, *10*(4), 91. https://www.mdpi.com/2306-5338/10/4/91

Xia, X., Liang, Q., & Ming, X. (2019). A full-scale fluvial flood modelling framework based on a high-performance integrated hydrodynamic modelling system (HiPIMS). *Advances in Water Resources*, *132*, 103392. https://doi.org/https://doi.org/10.1016/j.advwatres.2019.103392

Xu, T., Xie, Z., Jiang, F., Yang, S., Deng, Z., Zhao, L., Wen, G., & Du, Q. (2023). Urban flooding resilience evaluation with coupled rainfall and flooding models: a small area in Kunming City, China as an example. *Water Science and Technology*. https://doi.org/10.2166/wst.2023.149

Yan, H., Sun, N., Wigmosta, M., Leung, L. R., Hou, Z., Coleman, A., & Skaggs, R. (2020). Evaluating next-generation intensity–duration–frequency curves for design flood estimates in the snow-dominated western United States. *Hydrological Processes*, *34*(5), 1255-1268.

Yang, L., Smith, J., Baeck, M. L., Smith, B., Tian, F., & Niyogi, D. (2016). Structure and evolution of flash flood producing storms in a small urban watershed [Article]. *Journal of Geophysical Research*, *121*(7), 3139-3152. https://doi.org/10.1002/2015JD024478

Zhao, L., Zhang, T., Fu, J., Li, J., Cao, Z., & Feng, P. (2021). Risk Assessment of Urban Floods Based on a SWMM-MIKE21-Coupled Model Using GF-2 Data. *Remote Sensing*, *13*(21), 4381. https://www.mdpi.com/2072-4292/13/21/4381

Zhou, Q., Yu, W., Chen, A. S., Jiang, C., & Fu, G. (2016). Experimental Assessment of Building Blockage Effects in a Simplified Urban District. *Procedia Engineering*, *154*(C), 844-852. https://doi.org/10.1016/j.proeng.2016.07.448

Zhu, S., Dai, Q., Zhao, B., & Shao, J. (2020). Assessment of Population Exposure to Urban Flood at the Building Scale. *Water*, *12*(11), 3253. https://www.mdpi.com/2073-4441/12/11/3253

Zischg, A. P., Mosimann, M., Bernet, D. B., & Röthlisberger, V. (2018). Validation of 2D flood models with insurance claims. *Journal of Hydrology*, *557*, 350-361. https://doi.org/https://doi.org/10.1016/j.jhydrol.2017.12.042

Appendix A

General files

The essential inputs needed for conducting a basic simulation using CityCAT in an urban area are as follows:

a. DTM for the topography;
b. Shape files of buildings and green areas (optional if not available);
c. Rainfall event – rainfall time series;
d. CityCAT Configuration file;
e. CityCAT executable;

The input data must be of a specific type with a specific name and must be in the same folder with CityCAT.exe.

Table 0.1 The format of the input data for CityCAT.

Data type	File type	File name	Comment
DTM	.asc	Domain_DEM.asc	
Buildings	.txt	Buildings.txt	
Green areas	.txt	GreenAreas.txt	
Rainfall event	.txt	Rainfall_Data_[i].txt	i is a positive integer
CityCAT Configuration file	.txt	CityCat_Config_[i].txt	i is a positive integer

To fully utilise the model's capabilities, a high-resolution DTM is essential. However, the model can still function with lower resolution DTMs. It has been observed that a 2m grid resolution adequately resolves streets and other flow paths between buildings, striking a good balance. On the other hand, using grid squares larger than 5m may lead to the closure of flow paths, resulting in unrealistic and inaccurate results.

Domain_DEM.asc

The DTM is the foundational input for CityCAT as it shapes the computational grid. The model generates a uniform rectangular grid based on the DTM. In certain scenarios, it may be necessary to clip the DTM from a larger area. This can be achieved by generating a catchment boundary using a shapefile or by identifying the specific catchment of interest and using the "*extract by mask*" tool in QGIS. This ensures that CityCAT operates within the relevant area of interest, allowing for more focused and accurate simulations. The procedure is: open QGIS and then '*Processing Toolbox -> Search -> then type extract by mask*'. Care must be taken to specify the correct coordinate system of the study area. The final file should have the format in Figure 0.1.

```
ncols        892
nrows        528
xllcorner    421557.500000000000
yllcorner    563557.500000000000
cellsize     5.000000000000
NODATA_value  -99999
 -99999.0 -99999 -99999 -99999 -99999 -99999 -99999 -99999 -99999 -99999
 -99999 -99999 -99999 -99999 -99999 -99999 -99999 -99999 -99999 -99999
 -99999 -99999 -99999 -99999 -99999 -99999 -99999 -99999 -99999 -99999
 -99999 -99999 -99999 -99999 -99999 -99999 -99999 -99999 -99999 -99999
 -99999 -99999 -99999 -99999 -99999 -99999 -99999 -99999 -99999 -99999
 -99999 -99999 -99999 -99999 -99999 -99999 -99999 -99999 -99999 -99999
 -99999 -99999 -99999 -99999 -99999 -99999 -99999 -99999 -99999 -99999
 -99999 -99999 -99999 -99999 -99999 -99999 -99999 -99999 -99999 -99999
 -99999 -99999 -99999 -99999 -99999 -99999 -99999 -99999 -99999 -99999
 -99999 -99999 -99999 -99999 -99999 -99999 -99999 -99999 -99999 -99999
 -99999 -99999 -99999 -99999 -99999 -99999 -99999 -99999 -99999 -99999
 -99999 -99999 -99999 -99999 -99999 -99999 -99999 -99999 -99999 -99999
 -99999 -99999 -99999 -99999 -99999 -99999 -99999 -99999 -99999 -99999
```

Figure 0.1 Example file of the Domain_DEM.asc with a 5 m resolution.

Buildings.txt & GreenAreas.txt

For buildings and green areas, the x and y coordinates should be extracted from a shape file to a txt file, which will allow the model to exclude the building's footprint from the computational grid and to locate the green spaces for infiltration. To extract the coordinates from buildings and green spaces and generate the txt file a Python script in *Spyder (Anaconda)* can be used (files of buildings and green areas are preferred to be in a shape file format):

The geopandas library and the citycatio library [citycatio · PyPI] need to be installed. More information about the citycatio library can be found at: [GitHub - nclwater/citycatio: Python package for creating CityCAT models and converting results]. Thus, the txt input files for CityCAT will be generated in the same folder with the scripts, and the final format is as shown in Figure 0.2.

To install the libraries:

Follow the steps:

1. Start Anaconda Prompt:

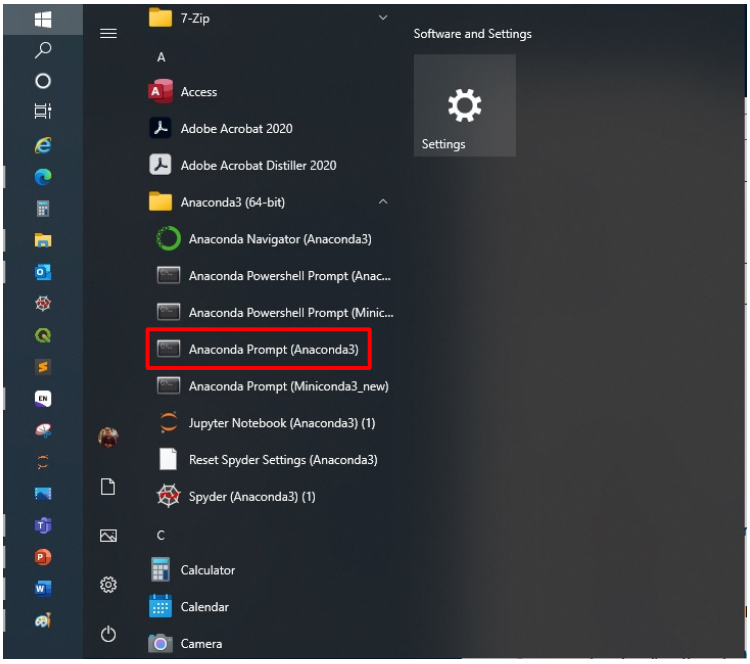

2. Type: 'conda create -n myenv rasterio geopandas' and press enter

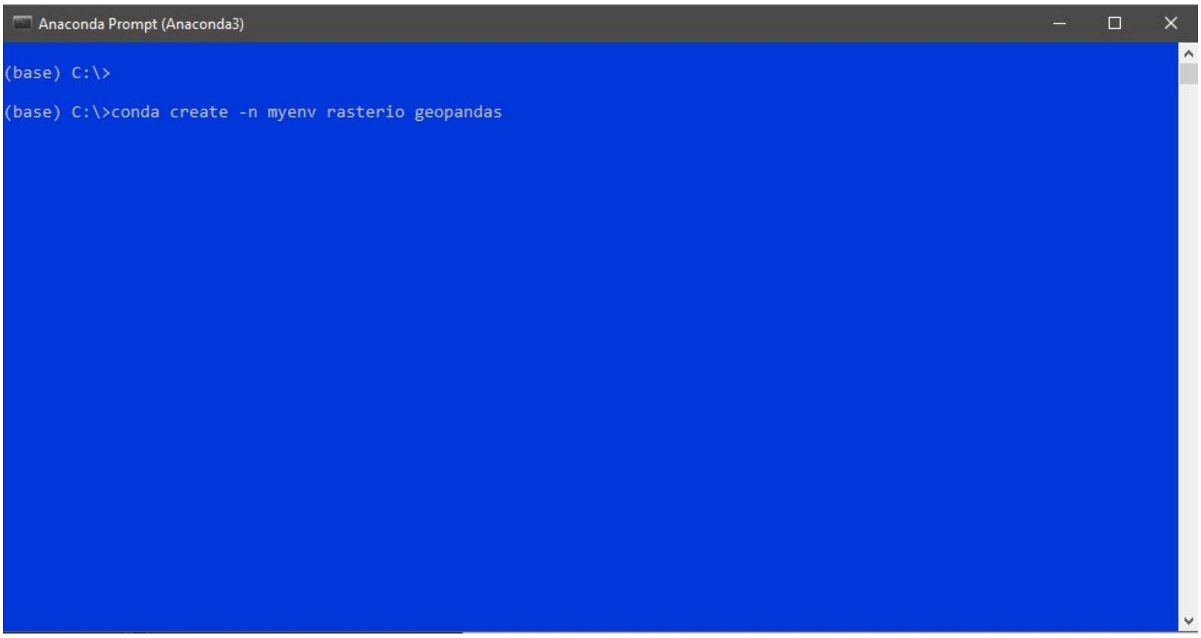

3. Type: 'conda activate myenv' and press enter

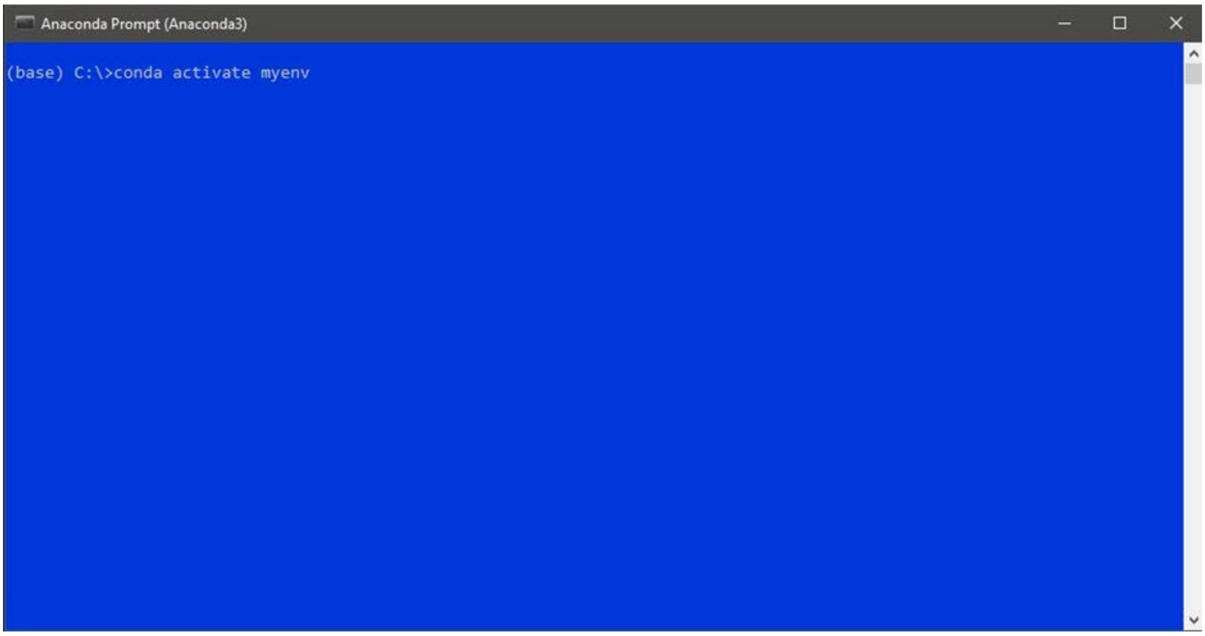

4. Type: 'pip install citycatio' and press enter

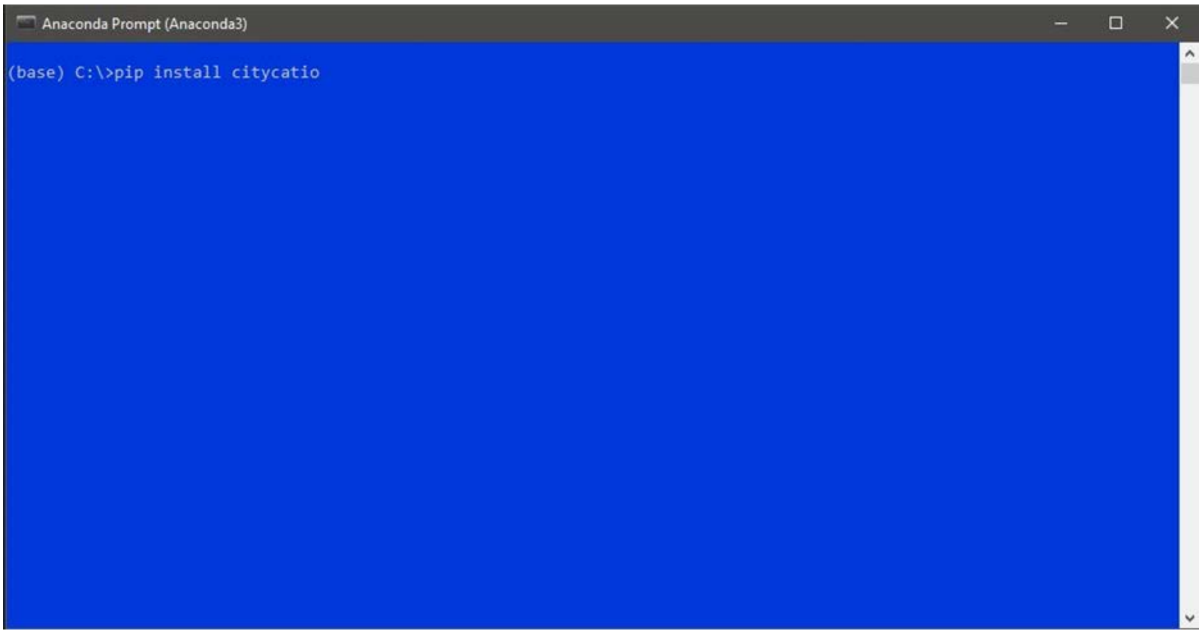

5. Type: 'conda update gdal'
6. Type: 'conda install -c anaconda ipywidgets' -> this library is for the exposure analysis
7. Type: 'pip install spyder'
8. Type: 'spyder'

Start *Spyder (Anaconda)* and write or copy the following python scripts for buildings and green areas:

For buildings:

```
#authors: Fergus Mcclean, Chris Iliadis
#host: Newcastle University
import geopandas as gpd
from citycatio.inputs import Buildings
```

```
input_folder = r'copy the folder path/'
name_shp_file = 'the name of the shp file'
```

```
gdf = gpd.read_file(input_folder + name_shp_file + '.shp')
Buildings(gdf).write('.')
```

```
# Just printing the output of the file to show what's in it
with open('Buildings.txt') as f:
  print(*f.readlines()[:10])
```

For Green Areas:

```
#authors: Fergus Mcclean, Chris Iliadis
#host: Newcastle University
import geopandas as gpd
from citycatio.inputs import GreenAreas
```

```
input_folder = r'copy the folder path/'
name_shp_file = 'the name of the shp file'
```

```
gdf = gpd.read_file(input_folder + name_shp_file + '.shp')
GreenAreas(gdf).write('.')
```

```
# Just printing the output of the file to show what's in it
with open('GreenAreas.txt') as f:
  print(*f.readlines()[:10])
```

Buildings.txt

```
9621
5 425934.921000038 425938.32800006866 425939.7800002098 425936.37300014496 425934.921000038 564627.8270001411 564629.6599998474 564626.9600000381 564625.126999855 564627.8270001411
5 425180.7399997711 425190.55000019073 425192.59999990463 425182.7600002289 425180.7399997711 564710.6900000572 564713.4000000954 564705.6500000954 564703.0100002289 564710.6900000572
5 425207.0100002289 425204.05000019073 425203.42999982834 425206.3600001335 425207.0100002289 564687.9699997902 564687.0999999046 564689.4400000572 564690.2699999809 564687.9699997902
4 425207.0100002289 425208.0 425204.05000019073 425207.0100002289 564687.9699997902 564684.4499998093 564687.0999999046 564687.9699997902
..........................................................................................................................
.............................................................
```

GreenAreas.txt

```
13573
9 425596.36 425596.9 425596.9100000003 425597.0 425592.389 425592.4 425584.491 425583.83 425596.36 564581.35 564575.9 564575.65 564573.75 564573.299 564573.109 564572.471 564580.67 564581.35
6 425592.55 425585.82 425585.75 425585.704 425592.55 425592.55 564477.67 564477.35 564479.05 564480.156 564480.41 564477.67
6 425592.9700000003 425593.15 425586.45 425586.25 425588.1000000003 425592.9700000003 564467.48 564463.25 564462.9500000001 564467.15 564467.25 564467.48
6 425603.64 425589.303 425589.072 425588.896 425603.261 425603.64 564500.773 564500.101 564504.694 564508.201 564508.927 564500.773
5 425592.55 425603.67 425603.78 425592.55 425592.55 564480.41 564480.9500000001 564478.1900000001 564477.67 564480.41
.......................................................................................................................
...........................................................
```

Figure 0.2 Example of txt files, where the first row defines the total number of buildings and green areas of the study area, the first column of the second row defines the number of points in that polygon/building/green space (the polygons must be closed, i.e. first and last point are the same) and then the x coordinates are listed first, and the y coordinates follow.

Rainfall_Data_[i].txt

The rainfall file is also compulsory, unless a boundary condition flow is being applied. The rainfall is usually applied over the whole domain (uniform assumption) for catchments or cities. Alternatively, spatially distributed rainfall can be used. The [i] in the file name corresponds to the index number (McClean et al., 2023) of rainfall event to be used in a simulation (see Figure 0.3(a)) and is specified in the command line when the run is initiated. In the case of no rainfall, this file should be specified, and the intensity of rainfall needs to have a zero value (see Figure 0.3(b)). To calculate the intensity of rainfall in a study area, Intensity-Duration-Frequency curves can be used, or the modeller can generate synthetic rainfall data e.g. with a python script.

The file format of <u>**Rainfall_Data_[i].txt**</u> is:

i. The first three lines are comments not used by the model but contain metadata giving information about the rainfall event;
ii. The fourth line is the number of data lines;
iii. Next line is also a comment and usually the modeller uses this line as a header for the lines below;
iv. In the first column of the sixth line the time is given in seconds from start of the simulation (s) and the second column defines the rate of rainfall in metres per second (m/s). These units will often be converted from mm/hr (conversion factor 2.7778e-7). The modeller could use as many lines are necessary for the study event;

It is possible to use spatially distributed rainfall by changing the following in the configuration file:

From uniform rainfall (<u>**Line 15**</u> in the configuration file, see Figure 0.5):

<RainfallData spatial="False" zones="1"/>

To:

<RainfallData spatial="True" zones="5"/>

The number of zones corresponds to the number of rainfall polygons. Two extra files are also needed:

i. Rainfall polygons file: "Rainfall_Polygons.txt' (see Figure 0.4)

ii. Rainfall time series: "Spatial_Rainfall_Data_[i].txt" (see Figure 0.3(c))

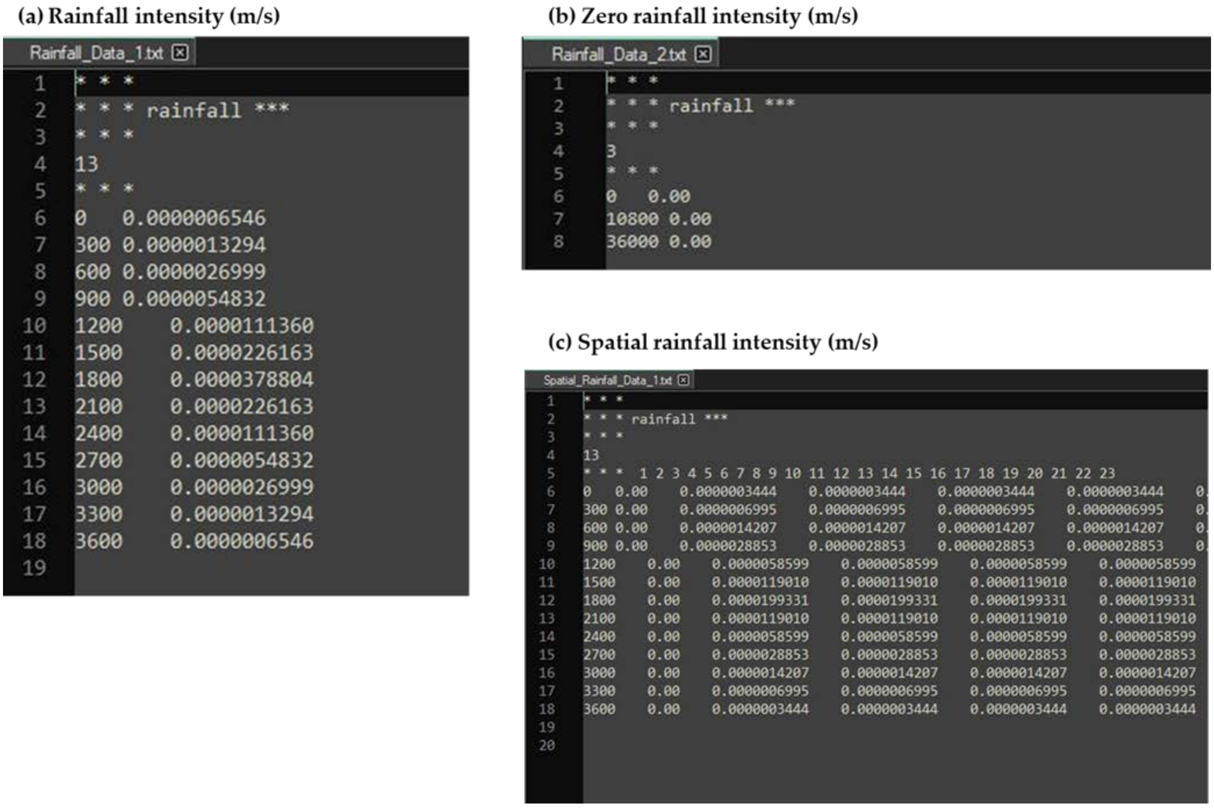

Figure 0.3 Examples of rainfall txt files: (a) File with rainfall in m/s; (b) File with zero rainfall rate; (c) Spatial rainfall file.

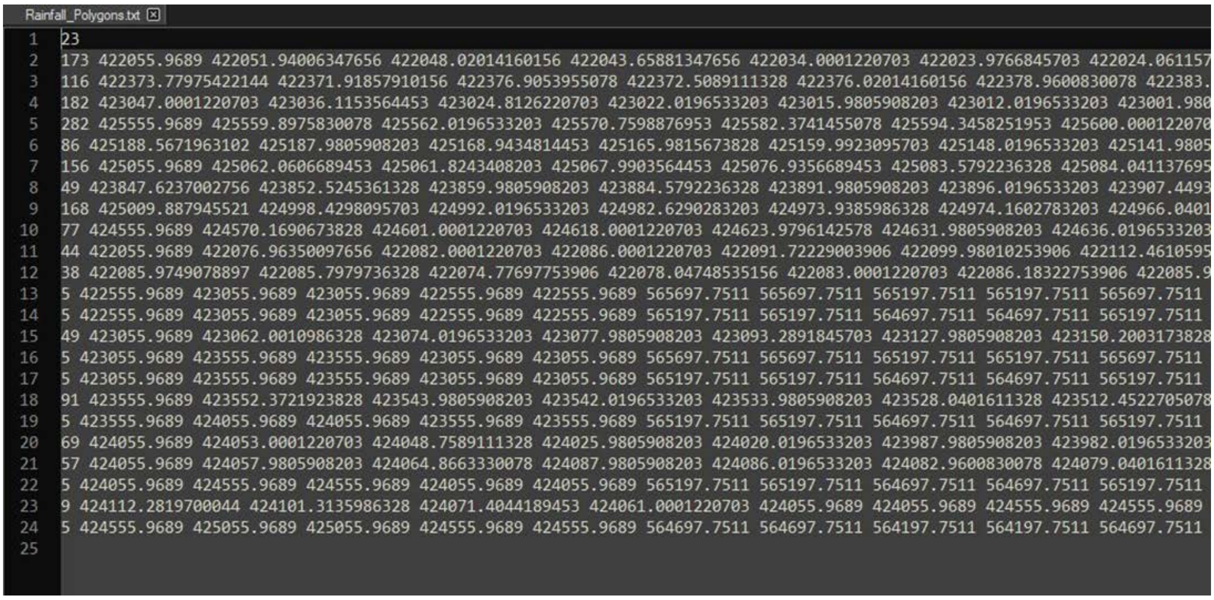

```
Rainfall_Polygons.txt
23
173 422055.9689 422051.94006347656 422048.02014160156 422043.65881347656 422034.0001220703 422023.9766845703 422024.061157
116 422373.77975422144 422371.91857910156 422376.9053955078 422372.5089111328 422376.02014160156 422378.9600830078 422383.
182 423047.0001220703 423036.1153564453 423024.8126220703 423022.0196533203 423015.9805908203 423012.0196533203 423001.980
282 425555.9689 425559.8975830078 425562.0196533203 425570.7598876953 425582.3741455078 425594.3458251953 425600.000122070
86 425188.5671963102 425187.9805908203 425168.9434814453 425165.9815673828 425159.9923095703 425148.0196533203 425141.9805
156 425055.9689 425062.0606689453 425061.8243408203 425067.9903564453 425076.9356689453 425083.5792236328 425084.041137695
49 423847.6237002756 423852.5245361328 423859.9805908203 423884.5792236328 423891.9805908203 423896.0196533203 423907.4493
168 425009.887945521 424998.4298095703 424992.0196533203 424982.6290283203 424973.9385986328 424974.1602783203 424966.0401
77 424555.9689 424570.1690673828 424601.0001220703 424618.0001220703 424623.9796142578 424631.9805908203 424636.0196533203
44 422055.9689 422076.96350097656 422082.0001220703 422086.0001220703 422091.72229003906 422099.98010253906 422112.4610595
38 422085.9749078897 422085.7979736328 422074.77697753906 422078.04748535156 422083.0001220703 422086.18322753906 422085.9
5 422555.9689 423055.9689 423055.9689 422555.9689 422555.9689 565697.7511 565697.7511 565197.7511 565197.7511 565697.7511
5 422555.9689 423055.9689 423055.9689 422555.9689 422555.9689 565197.7511 565197.7511 564697.7511 564697.7511 565197.7511
49 423055.9689 423062.0010986328 423074.0196533203 423077.9805908203 423093.2891845703 423127.9805908203 423150.2003173828
5 423055.9689 423555.9689 423555.9689 423055.9689 423055.9689 565697.7511 565697.7511 565197.7511 565197.7511 565697.7511
5 423055.9689 423555.9689 423555.9689 423055.9689 423055.9689 565197.7511 565197.7511 564697.7511 564697.7511 565197.7511
91 423555.9689 423552.3721923828 423543.9805908203 423542.0196533203 423533.9805908203 423528.0401611328 423512.4522705078
5 423555.9689 424055.9689 424055.9689 423555.9689 423555.9689 565197.7511 565197.7511 564697.7511 564697.7511 565197.7511
69 424055.9689 424053.0001220703 424048.7589111328 424025.9805908203 424020.0196533203 423987.9805908203 423982.0196533203
57 424055.9689 424057.9805908203 424064.8663330078 424087.9805908203 424086.0196533203 424082.9600830078 424079.0401611328
5 424055.9689 424555.9689 424555.9689 424055.9689 424055.9689 565197.7511 565197.7511 564697.7511 564697.7511 565197.7511
9 424112.2819700044 424101.3135986328 424071.4044189453 424061.0001220703 424055.9689 424055.9689 424555.9689 424555.9689
5 424555.9689 425055.9689 425055.9689 424555.9689 424555.9689 564697.7511 564697.7511 564197.7511 564197.7511 564697.7511
```

Figure 0.4 Example of the rainfall polygon file with 23 spatial zones.

CityCAT – Config_[i].txt

This file is compulsory to run CityCAT, as it defines the basic parameters to run the model. These are:

i. the total time of the simulation (in seconds)
ii. the initial time step (in seconds)
iii. the frequency of the outputs
iv. the friction coefficient for impervious and green areas
v. parameters for the Green-Ampt model.

The format of the configuration file can be seen in Figure 0.5 and the final files in Figure 0.6.

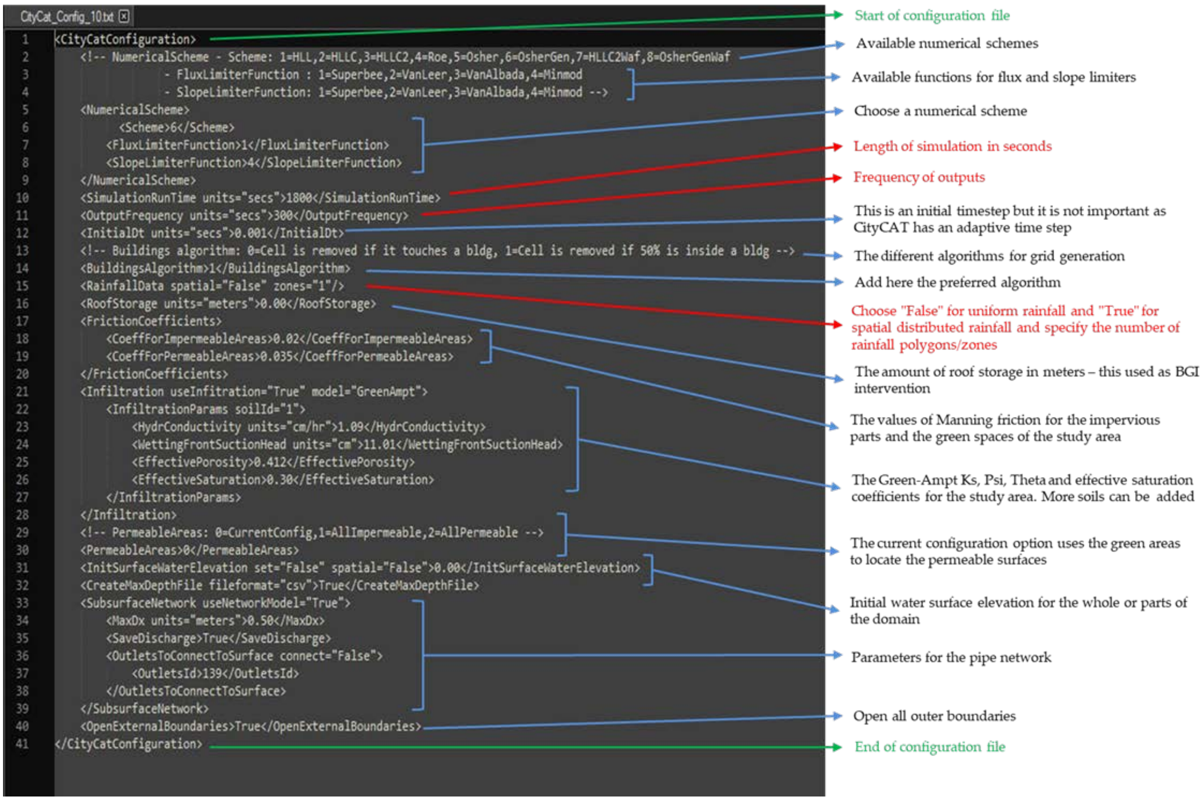

```
<CityCatConfiguration>
    <!-- NumericalScheme - Scheme: 1=HLL,2=HLLC,3=HLLC2,4=Roe,5=Osher,6=OsherGen,7=HLLC2Waf,8=OsherGenWaf
                - FluxLimiterFunction : 1=Superbee,2=VanLeer,3=VanAlbada,4=Minmod
                - SlopeLimiterFunction: 1=Superbee,2=VanLeer,3=VanAlbada,4=Minmod -->
    <NumericalScheme>
          <Scheme>6</Scheme>
        <FluxLimiterFunction>1</FluxLimiterFunction>
        <SlopeLimiterFunction>4</SlopeLimiterFunction>
    </NumericalScheme>
    <SimulationRunTime units="secs">1800</SimulationRunTime>
    <OutputFrequency units="secs">300</OutputFrequency>
    <InitialDt units="secs">0.001</InitialDt>
    <!-- Buildings algorithm: 0=Cell is removed if it touches a bldg, 1=Cell is removed if 50% is inside a bldg -->
    <BuildingsAlgorithm>1</BuildingsAlgorithm>
    <RainfallData spatial="False" zones="1"/>
    <RoofStorage units="meters">0.00</RoofStorage>
    <FrictionCoefficients>
        <CoeffForImpermeableAreas>0.02</CoeffForImpermeableAreas>
        <CoeffForPermeableAreas>0.035</CoeffForPermeableAreas>
    </FrictionCoefficients>
    <Infiltration useInfitration="True" model="GreenAmpt">
        <InfiltrationParams soilId="1">
            <HydrConductivity units="cm/hr">1.09</HydrConductivity>
            <WettingFrontSuctionHead units="cm">11.01</WettingFrontSuctionHead>
            <EffectivePorosity>0.412</EffectivePorosity>
            <EffectiveSaturation>0.30</EffectiveSaturation>
        </InfiltrationParams>
    </Infiltration>
    <!-- PermeableAreas: 0=CurrentConfig,1=AllImpermeable,2=AllPermeable -->
    <PermeableAreas>0</PermeableAreas>
    <InitSurfaceWaterElevation set="False" spatial="False">0.00</InitSurfaceWaterElevation>
    <CreateMaxDepthFile fileformat="csv">True</CreateMaxDepthFile>
    <SubsurfaceNetwork useNetworkModel="True">
        <MaxDx units="meters">0.50</MaxDx>
        <SaveDischarge>True</SaveDischarge>
        <OutletsToConnectToSurface connect="False">
            <OutletsId>139</OutletsId>
        </OutletsToConnectToSurface>
    </SubsurfaceNetwork>
    <OpenExternalBoundaries>True</OpenExternalBoundaries>
</CityCatConfiguration>
```


Figure 0.5 Example of the configuration file for a simulation in an urban area.

Name	Status	Date modified	Type	Size
CityCat.exe		03/10/2022 13:05	Application	4,744 KB
Domain_DEM.asc		15/10/2022 12:41	ASC File	537,845 KB
Buildings.txt		08/04/2022 13:14	TXT File	544,859 KB
CityCat_Config_1.txt		08/04/2022 13:12	TXT File	2 KB
GreenAreas.txt		08/04/2022 13:14	TXT File	577,666 KB
Rainfall_Data_45.txt		08/04/2022 13:14	TXT File	1 KB

Figure 0.6 Example of the final files to start a simulation in an urban area, all files should be in the same folder.

Other files

To configure CityCAT to simulate special cases such as river flows, dam break, and coastal flooding some extra files are required.

InitSurfaceWaterElev_Polygons.txt

This file can be used to simulate a dam break and it defines the reservoir and the water surface elevation in the reservoir (Figure 0.7). Also, some settings need to be changed in the configuration file (see Figure 0.8).

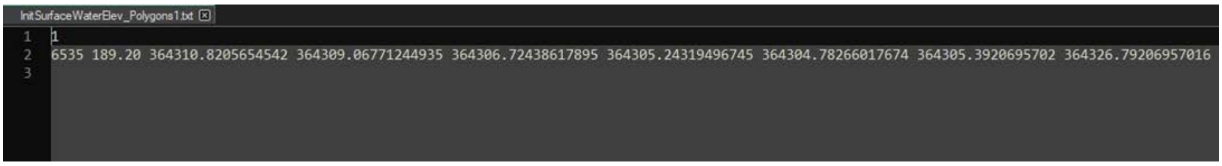

```
InitSurfaceWaterElev_Polygons1.txt
1
6535 189.20 364310.8205654542 364309.06771244935 364306.72438617895 364305.24319496745 364304.78266017674 364305.3920695702 364326.79206957016
```

Figure 0.7 Example of initial surface water elevation file, the first row defines the number of boundaries used, the first column of the second row refers to the total points of the boundary, the second column defines the water surface elevation in the reservoir and then the x coordinates are listed first, and the y coordinates are following as for the buildings/green areas/rainfall polygon.

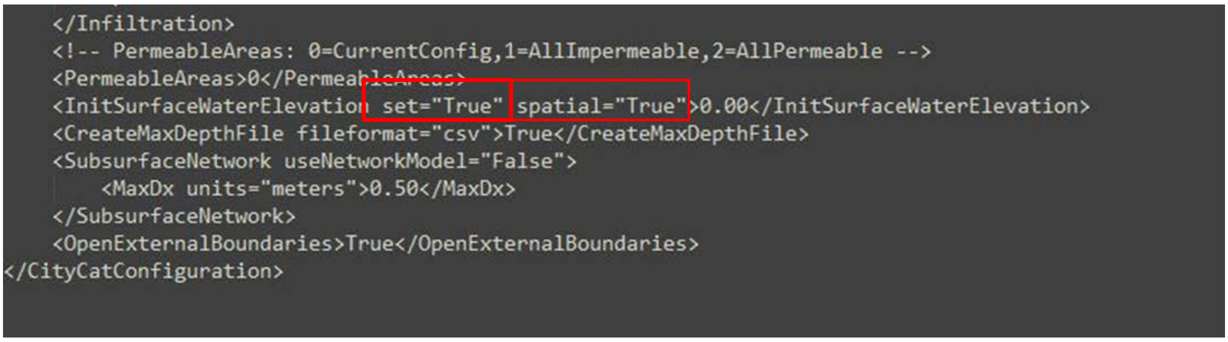

```
    </Infiltration>
    <!-- PermeableAreas: 0=CurrentConfig,1=AllImpermeable,2=AllPermeable -->
    <PermeableAreas>0</PermeableAreas>
    <InitSurfaceWaterElevation set="True" spatial="True">0.00</InitSurfaceWaterElevation>
    <CreateMaxDepthFile fileformat="csv">True</CreateMaxDepthFile>
    <SubsurfaceNetwork useNetworkModel="False">
        <MaxDx units="meters">0.50</MaxDx>
    </SubsurfaceNetwork>
    <OpenExternalBoundaries>True</OpenExternalBoundaries>
</CityCatConfiguration>
```

Figure 0.8 Red highlights the necessary settings in the configuration file that should be changed.

BCs_open.txt – Open boundary condition polygon

By default, all outer boundaries of the model are closed, so in many cases some open boundaries are needed to prevent the accumulation of water along the edges of the study area. If cell boundaries at the edge of the study area and those completely within the polygon are declared open, this allows surface water to leave the domain through that boundary. Polygons of such cell boundaries to be opened could be generated in QGIS, and their format can be seen in Figure 0.9. As previously, the first row is the number of polygons, the first column of the second row is the number of points of the polygon then the x coordinates are listed first, and the y coordinates are following.

```
BCs_Open.txt
1 1
2 5 424000.0 424000.0 426000.0 426000.0 424000.0 564000.0 566000.0 566000.0 564000.0 564000.0
3
```

Figure 0.9 Example of the open boundary condition polygon file.

Alternatively, all the outer boundaries can be opened by changing the following in the configuration file:

<OpenExternalBoundaries>True</OpenExternalBoundaries>

```
    </Infiltration>
    <!-- PermeableAreas: 0=CurrentConfig,1=AllImpermeable,2=AllPermeable -->
    <PermeableAreas>0</PermeableAreas>
    <InitSurfaceWaterElevation set="True" spatial="True">0.00</InitSurfaceWaterElevation>
    <CreateMaxDepthFile fileformat="csv">True</CreateMaxDepthFile>
    <SubsurfaceNetwork useNetworkModel="False">
        <MaxDx units="meters">0.50</MaxDx>
    </SubsurfaceNetwork>
    <OpenExternalBoundaries>True</OpenExternalBoundaries>
</CityCatConfiguration>
```

Figure 0.10 Red highlights the necessary settings in the configuration file that should be changed.

BCs_flow.txt – Flow boundary condition polygon

Flow boundary conditions can be defined at the outer boundaries of the domain using polygons and flow time series. The polygon and the format of the txt file follows the same procedure as with the Open boundary condition polygon.

```
BCs_flow.txt
1 1
2 5 419159.1945 419160.4864 419160.3907 419158.8595 419159.1945 586126.5029 586126.455 586113.5357 586113.6314 586126.5029
3
```

Figure 0.11 Example of flow boundary condition polygon file.

Flow_BC.flw - Flow time series

This file contains time series of flow data. The second column after the fifth row is the flow (q) per unit width (m3/s/m), see Figure 0.12. Note that the total flow Q = q × cell size × number of cell boundaries.

```
Flow_BC.flw
* * *
* * * discharge1 ***
* * *
97
* * *  sec -  m3/sec/m
0 2.375000
900 2.462500
1800 2.558333
2700 2.683333
3600 2.804167
4500 2.945833
5400 3.066667
6300 3.220833
7200 3.270833
8100 3.358333
9000 3.420833
9900 3.491667
10800 3.570833
11700 3.633333
12600 3.716667
13500 3.770833
14400 3.875000
15300 3.954167
16200 4.016667
17100 4.079167
```

Figure 0.12 Example of the flow time series, the first three rows and the fifth row are for comments, the fourth row defines the total number of data points, the first column after the fifth is the time (secs) and the second column is the flow (m3/s/m).

Spatial_GreenAreas.txt

Areas with different soil properties can be defined using polygons, see Figure 0.13. The Green-Ampt parameters for the infiltration for each soil should be added in the configuration file, see Figure 0.14.

```
2
1 5 423055.9689 423555.9689 423555.9689 423055.9689 423055.9689 565697.7511 565697.7511 565197.7511 565197.7511 565697.7511
2 5 423055.9689 423555.9689 423555.9689 423055.9689 423055.9689 565197.7511 565197.7511 564697.7511 564697.7511 565197.7511
```

Figure 0.13 Example of different soils in the catchment, the first row refers to the number of polygons used, the first column in the second row defines the soil id, the second column the total points of the polygon then the x coordinates are listed first, and the y coordinates follow.

```
<CityCatConfiguration>
    <!-- NumericalScheme - Scheme: 1=HLL,2=HLLC,3=HLLC2,4=Roe,5=Osher,6=OsherGen,7=HLLC2Waf,8=OsherGenWaf
                 - FluxLimiterFunction : 1=Superbee,2=VanLeer,3=VanAlbada,4=Minmod
                 - SlopeLimiterFunction: 1=Superbee,2=VanLeer,3=VanAlbada,4=Minmod -->
    <NumericalScheme>
          <Scheme>6</Scheme>
        <FluxLimiterFunction>1</FluxLimiterFunction>
        <SlopeLimiterFunction>4</SlopeLimiterFunction>
    </NumericalScheme>
    <SimulationRunTime units="secs">2678400</SimulationRunTime>
    <OutputFrequency units="secs">86400</OutputFrequency>
    <InitialDt units="secs">25</InitialDt>
    <RainfallData spatial="True" zones="2218"/>
    <RoofStorage units="meters">0.00</RoofStorage>
    <FrictionCoefficients>
        <CoeffForImpermeableAreas>0.02</CoeffForImpermeableAreas>
        <CoeffForPermeableAreas>0.5</CoeffForPermeableAreas>
    </FrictionCoefficients>
    <Infiltration useInfitration="True" model="GreenAmpt">
        <InfiltrationParams soilId="1">
            <HydrConductivity units="cm/hr">0.34</HydrConductivity>
            <WettingFrontSuctionHead units="cm">8.89</WettingFrontSuctionHead>
            <EffectivePorosity>0.434</EffectivePorosity>
            <EffectiveSaturation>0.99</EffectiveSaturation>
        </InfiltrationParams>
        <InfiltrationParams soilId="2">
            <HydrConductivity units="cm/hr">0.1</HydrConductivity>
            <WettingFrontSuctionHead units="cm">20.88</WettingFrontSuctionHead>
            <EffectivePorosity>0.390</EffectivePorosity>
            <EffectiveSaturation>0.99</EffectiveSaturation>
        </InfiltrationParams>
    </Infiltration>
    <!-- PermeableAreas: 0=CurrentConfig,1=AllImpermeable,2=AllPermeable -->
    <PermeableAreas>0</PermeableAreas>
    <InitSurfaceWaterElevation set="False" spatial="False">0.00</InitSurfaceWaterElevation>
    <CreateMaxDepthFile fileformat="csv">True</CreateMaxDepthFile>
    <SubsurfaceNetwork useNetworkModel="False">
        <MaxDx units="meters">0.50</MaxDx>
    </SubsurfaceNetwork>
</CityCatConfiguration>
```

Figure 0.14 Green-Ampt parameters for each soil.

FrictionCoeffs.txt

Areas with different Manning's n friction coefficient can be defined using polygon, see Figure 0.15.

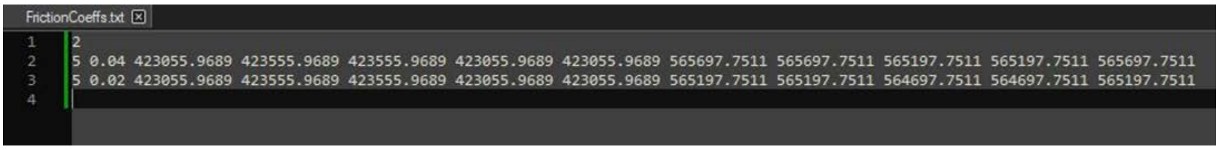

Figure 0.15 Example of areas with different friction coefficients, the first row refers the number of polygons, the first column in the second row defines the total points of the polygon, the second column refers to the coefficient then the x coordinates are listed first, and the y coordinates follow.

How to run CityCAT

<u>How to run the CityCAT model</u>

<u>**1st step**</u>: Check that the files have the correct format;

<u>**2nd step**</u>: Check that all files are in the same folder;

<u>**3rd step**</u>: Then select the folder (mouse left click) and click 'shift' on the keyboard plus right-click on the mouse and open the 'Open PowerShell window here' or 'Open command window here' (depending on the laptop or pc operating system);

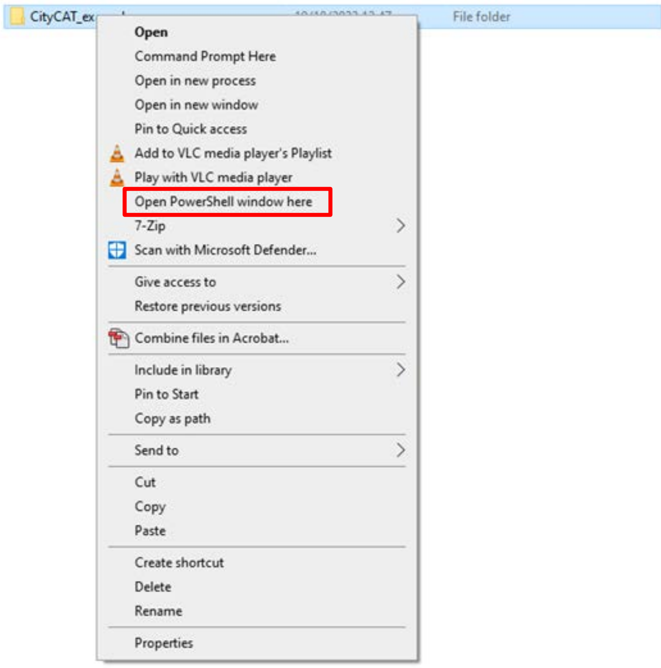

<u>**4th step**</u>: Type '*cmd*' to Windows PowerShell and press Enter;

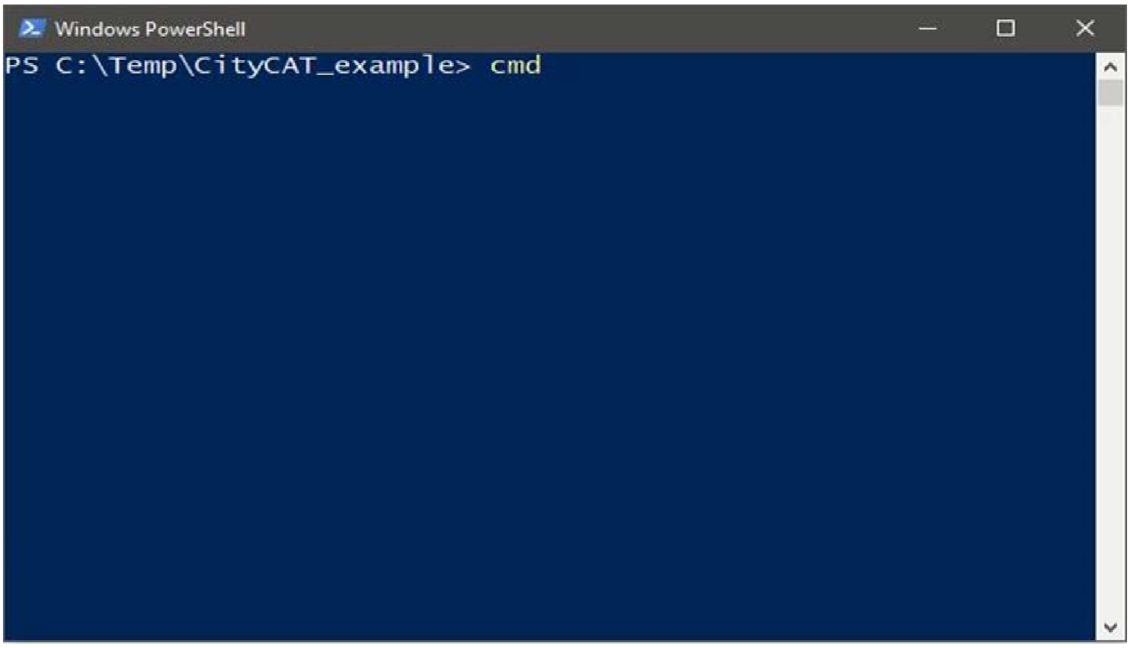

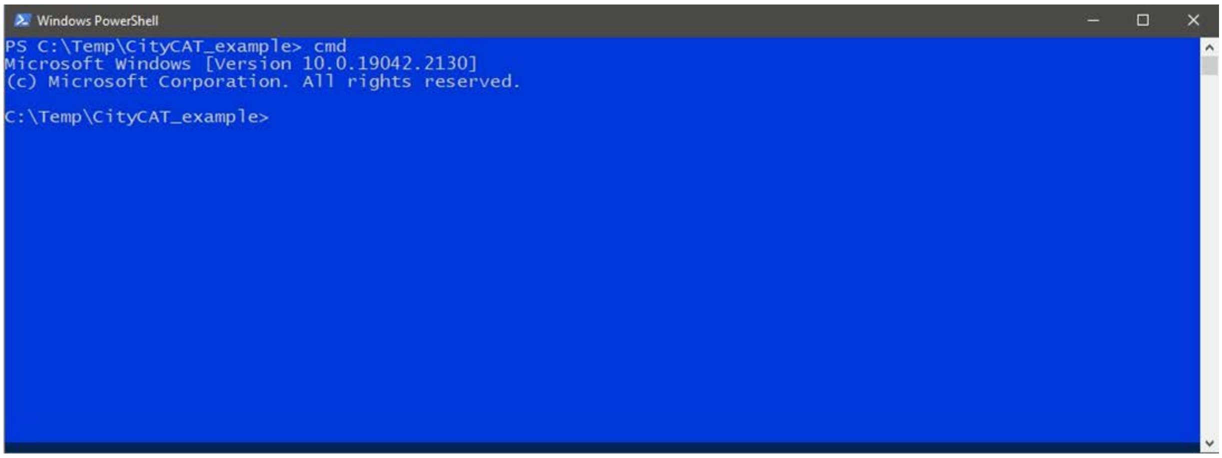

5th step: To run the simulation use the following command and then press Enter;

citycat -c [config file number] -r [rainfall file number]

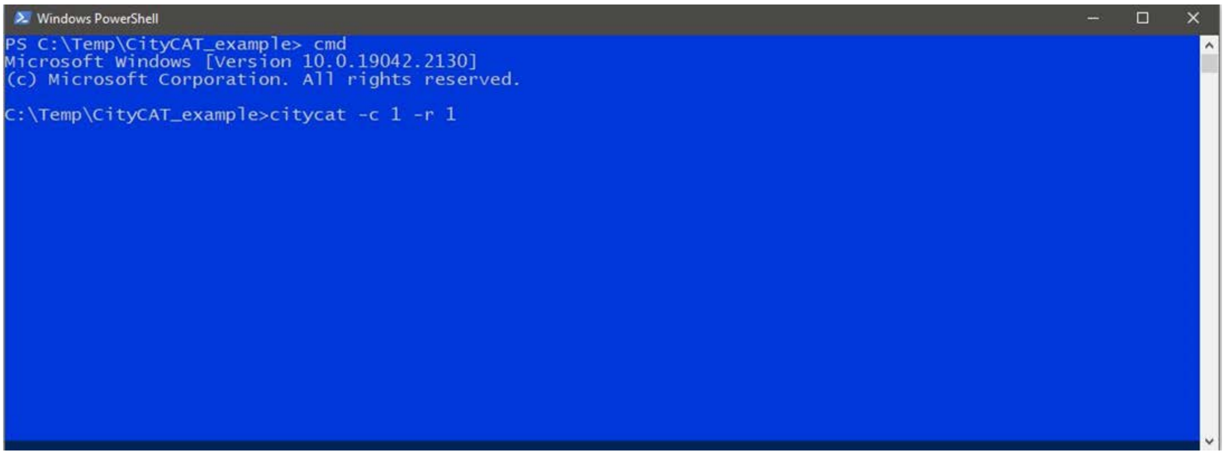

```
Windows PowerShell
PS C:\Temp\CityCAT_example> cmd
Microsoft Windows [Version 10.0.19042.2130]
(c) Microsoft Corporation. All rights reserved.

C:\Temp\CityCAT_example>citycat -c 1 -r 1
```

To stop the model run press simultaneously *'Ctrl'* and *'C'* buttons to the Windows PowerShell. To monitor the progress of the simulation open the file: CityCat_Log.txt. N.B. this file will not update itself and the modeller needs to close it and open it again.

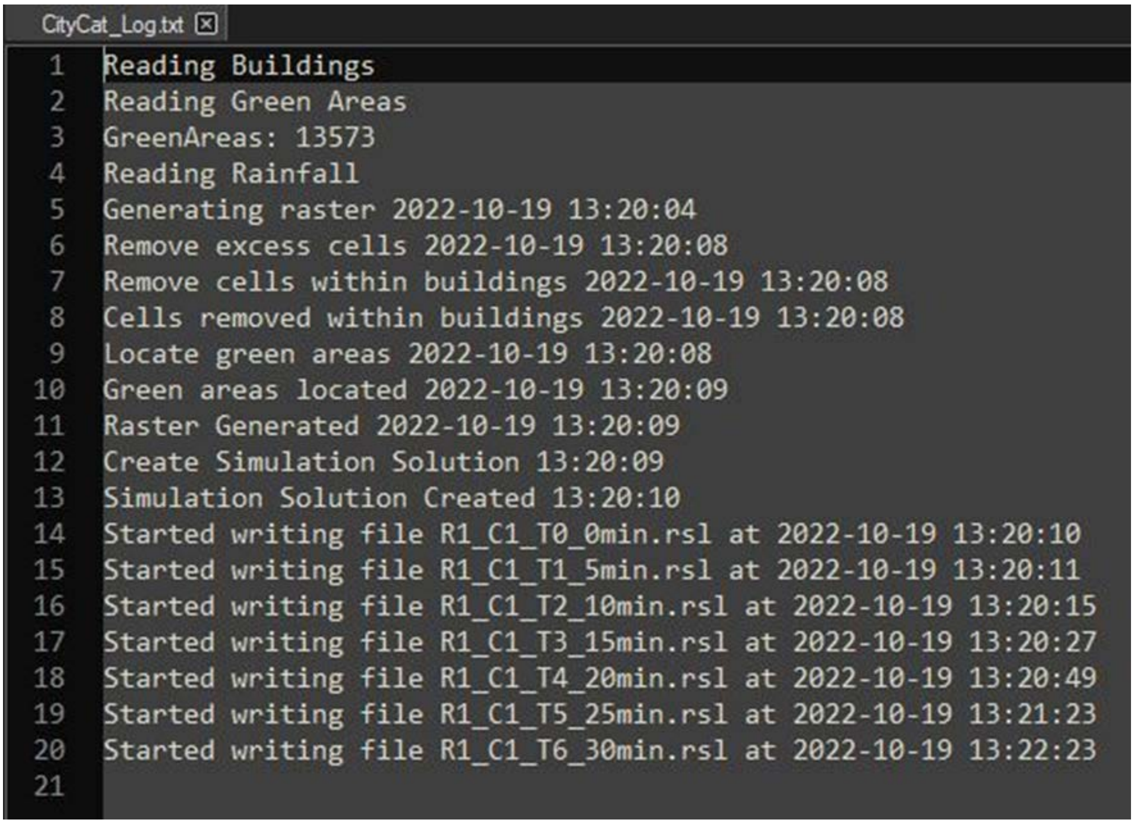

```
CityCat_Log.txt
1  Reading Buildings
2  Reading Green Areas
3  GreenAreas: 13573
4  Reading Rainfall
5  Generating raster 2022-10-19 13:20:04
6  Remove excess cells 2022-10-19 13:20:08
7  Remove cells within buildings 2022-10-19 13:20:08
8  Cells removed within buildings 2022-10-19 13:20:08
9  Locate green areas 2022-10-19 13:20:08
10 Green areas located 2022-10-19 13:20:09
11 Raster Generated 2022-10-19 13:20:09
12 Create Simulation Solution 13:20:09
13 Simulation Solution Created 13:20:10
14 Started writing file R1_C1_T0_0min.rsl at 2022-10-19 13:20:10
15 Started writing file R1_C1_T1_5min.rsl at 2022-10-19 13:20:11
16 Started writing file R1_C1_T2_10min.rsl at 2022-10-19 13:20:15
17 Started writing file R1_C1_T3_15min.rsl at 2022-10-19 13:20:27
18 Started writing file R1_C1_T4_20min.rsl at 2022-10-19 13:20:49
19 Started writing file R1_C1_T5_25min.rsl at 2022-10-19 13:21:23
20 Started writing file R1_C1_T6_30min.rsl at 2022-10-19 13:22:23
21
```

Hence, a new folder with the results will be generated. The output ASCII files (file extension: *.rsl) contain water depths and velocities at different times during the simulation. The files can be opened in any text editor, e.g. *Notepad++*, *Sublime Text*. Also in the folder will be the maximum flood depth map in csv format, i.e. a map showing for each cell the maximum depth recorded at any time in the whole simulation. Note this map is not a single '*snap shot*' in time – the maximum depth may occur at different times for different cells.

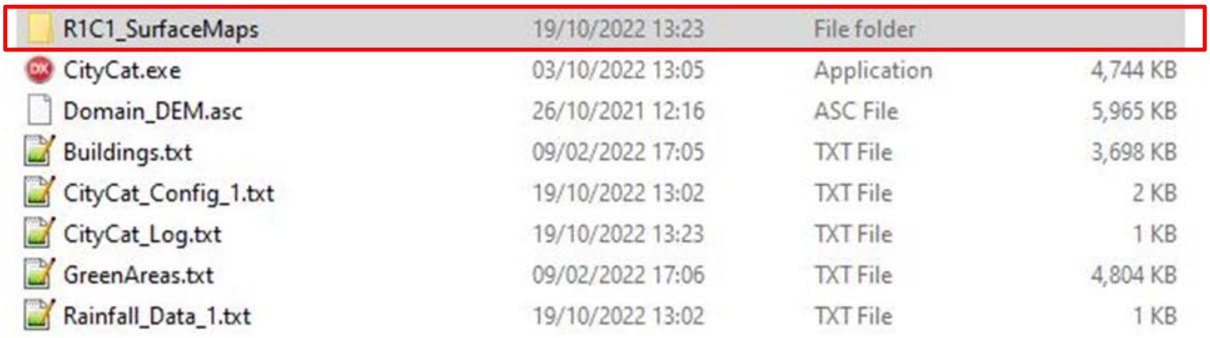

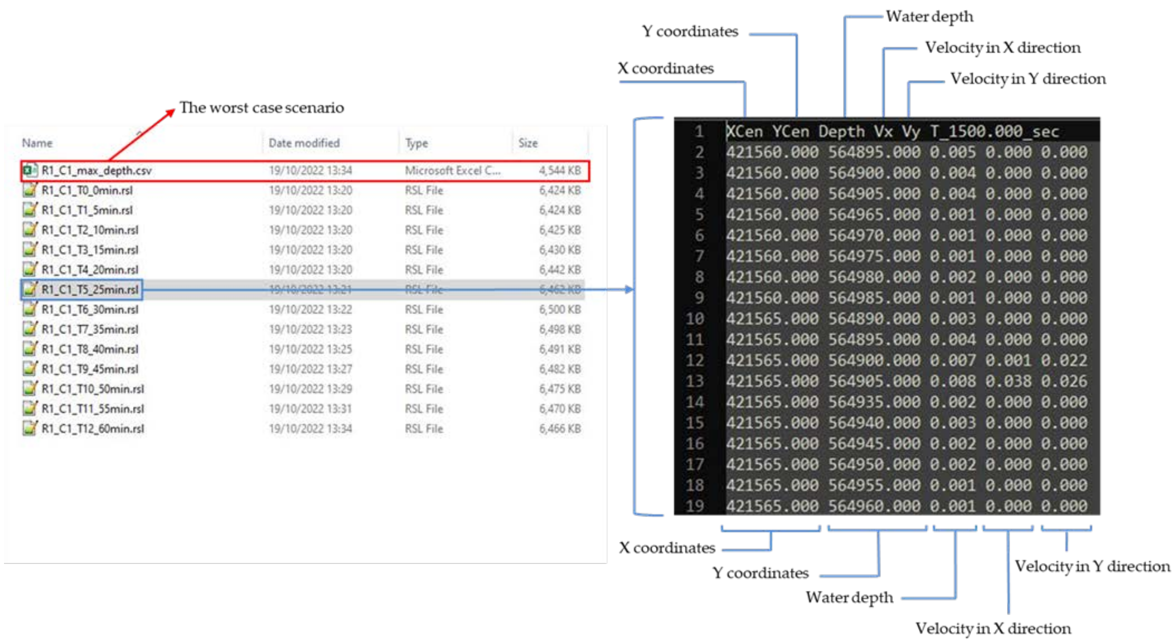

Figure 0.16 Example of an output folder from CityCAT, and explanation of every column on the results.

Plot the results

To analyse the outputs from CityCAT there are many options including :

1. Import the rsl files and the csv file into QGIS and rasterize them. These can then be used to generate tiff files which can be displayed in QGIS or ArcGIS (see the next section).
2. A python script to generate png files for water depths and velocities.

Rasterise csv files

Start QGIS and import the csv file (output from CityCAT):

Layer -> Add Layer -> Add Delimited Text Layer

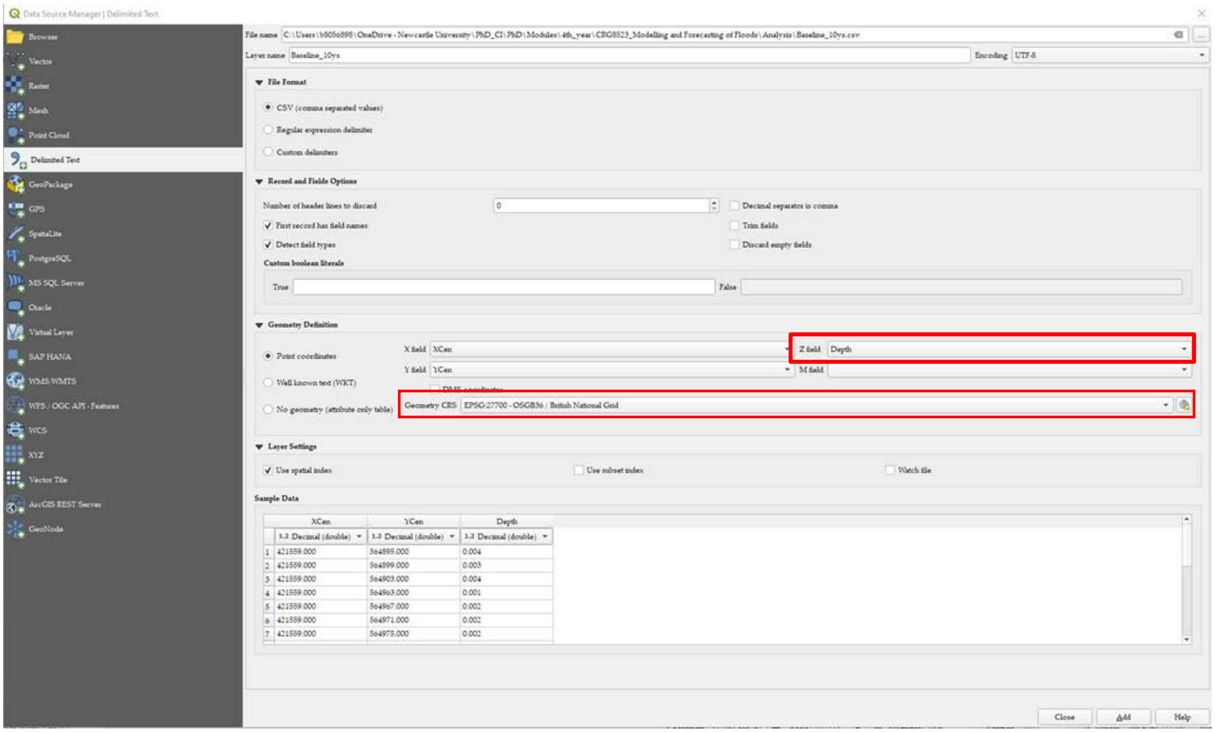

The important part of this step (highlighted with the red polygons) is to add the correct coordinate system (Geometry CRS) for the case study and for the Z field select the "*depth*". Then press <u>*Add*</u> in the bottom right corner.

The second step is to convert the csv file to tif file. For the latest version of QGIS go to *Processing Toolbox -> SAGA -> Raster – Rasterizing -> Features to Raster*, for older versions of QGIS go to *Processing Toolbox -> SAGA -> Raster creation tools -> Rasterize*.

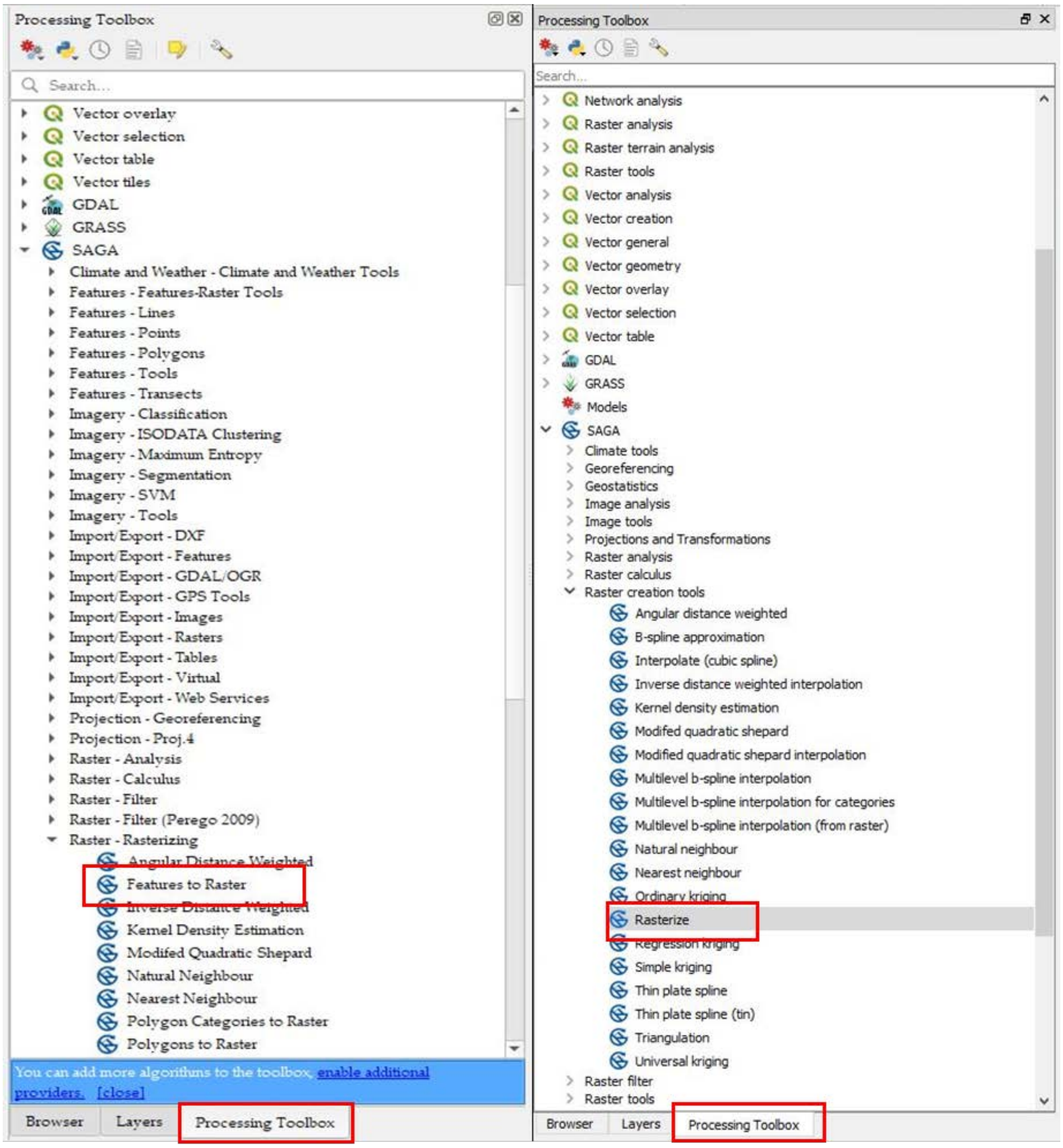

(a) (b)

To generate a raster layer from a csv file select the parameters/options shown in next figure. Then select the generated raster layer, right-click and <u>*Export -> Save As*</u> to save a tif file.

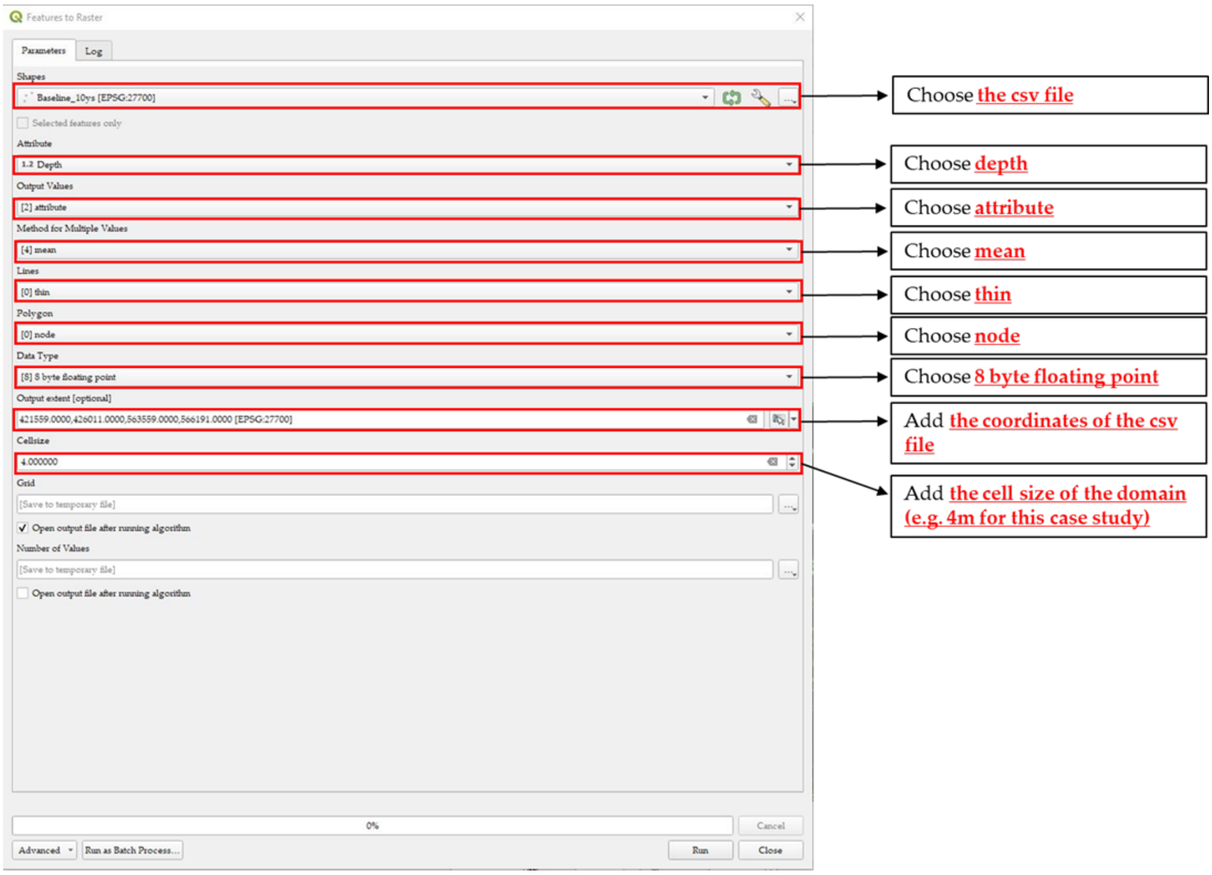

Features to Raster
Parameters
Log
Shapes
Baseline_10ys [EPSG:27700]
Selected features only
Attribute
1.2 Depth
Output Values
[2] attribute
Method for Multiple Values
[4] mean
Lines
[0] thin
Polygon
[0] node
Data Type
[8] 8 byte floating point
Output extent [optional]
421559.0000,426011.0000,563559.0000,566191.0000 [EPSG:27700]
Cellsize
4.000000
Grid
[Save to temporary file]
Open output file after running algorithm
Number of Values
[Save to temporary file]
Open output file after running algorithm
0%
Cancel
Advanced
Run as Batch Process...
Run
Close
Choose the csv file
Choose depth
Choose attribute
Choose mean
Choose thin
Choose node
Choose 8 byte floating point
Add the coordinates of the csv file
Add the cell size of the domain (e.g. 4m for this case study)

Appendix B

London flood maps

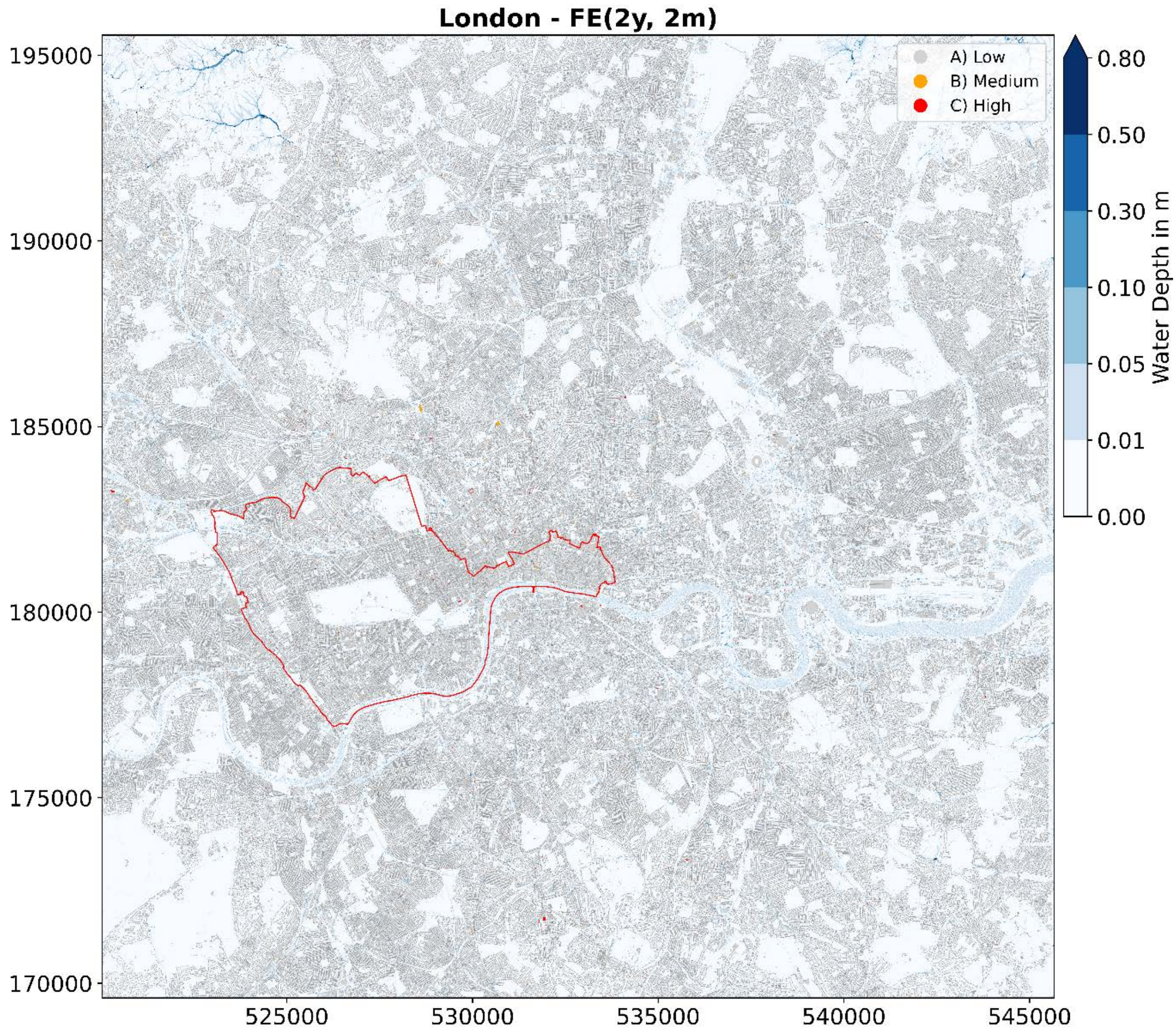

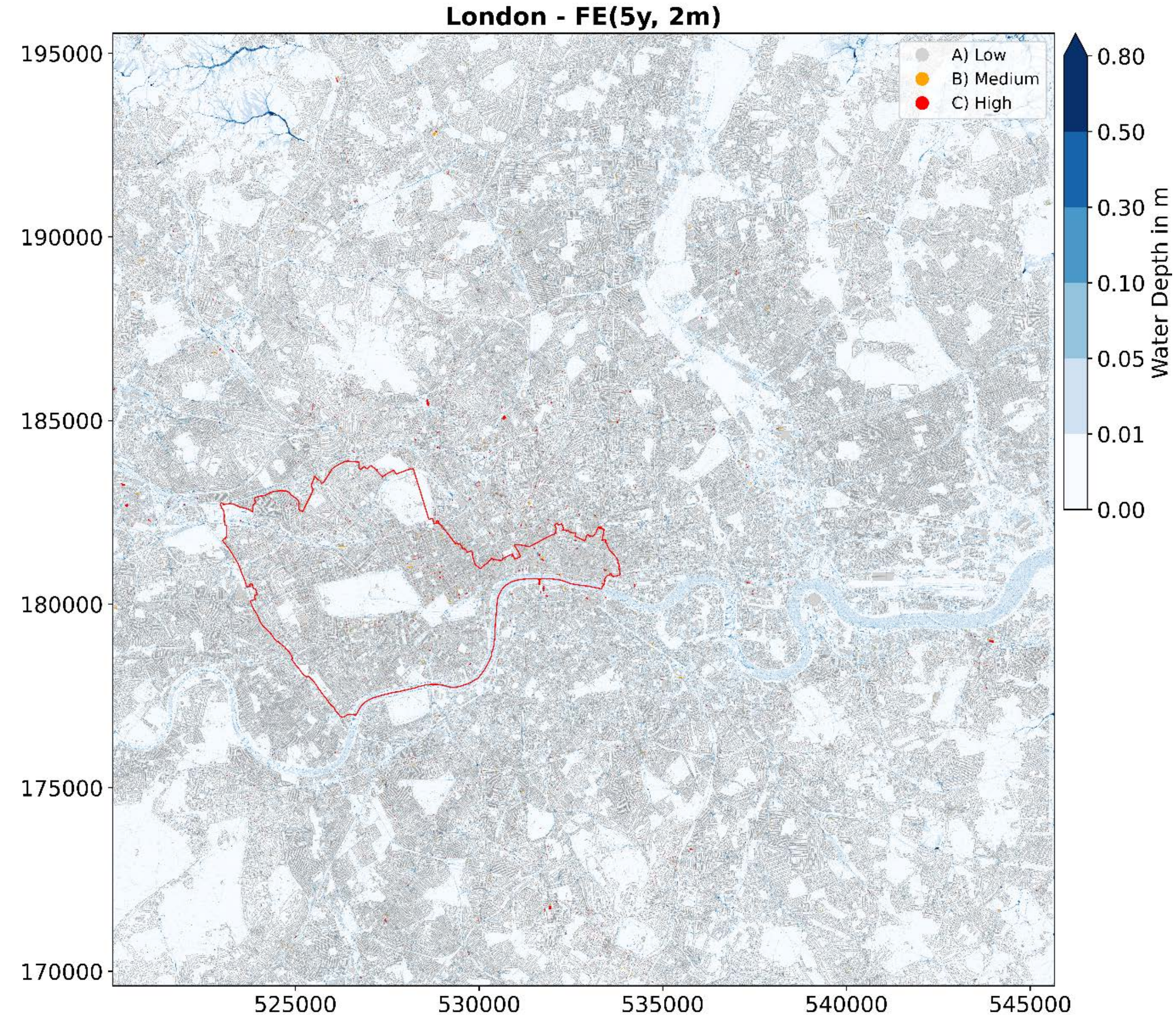
London - FE(5y, 2m)
195000
190000
185000
180000
175000
170000
525000
530000
535000
540000
545000
A) Low
B) Medium
C) High
0.80
0.50
0.30
0.10
0.05
0.01
0.00
Water Depth in m

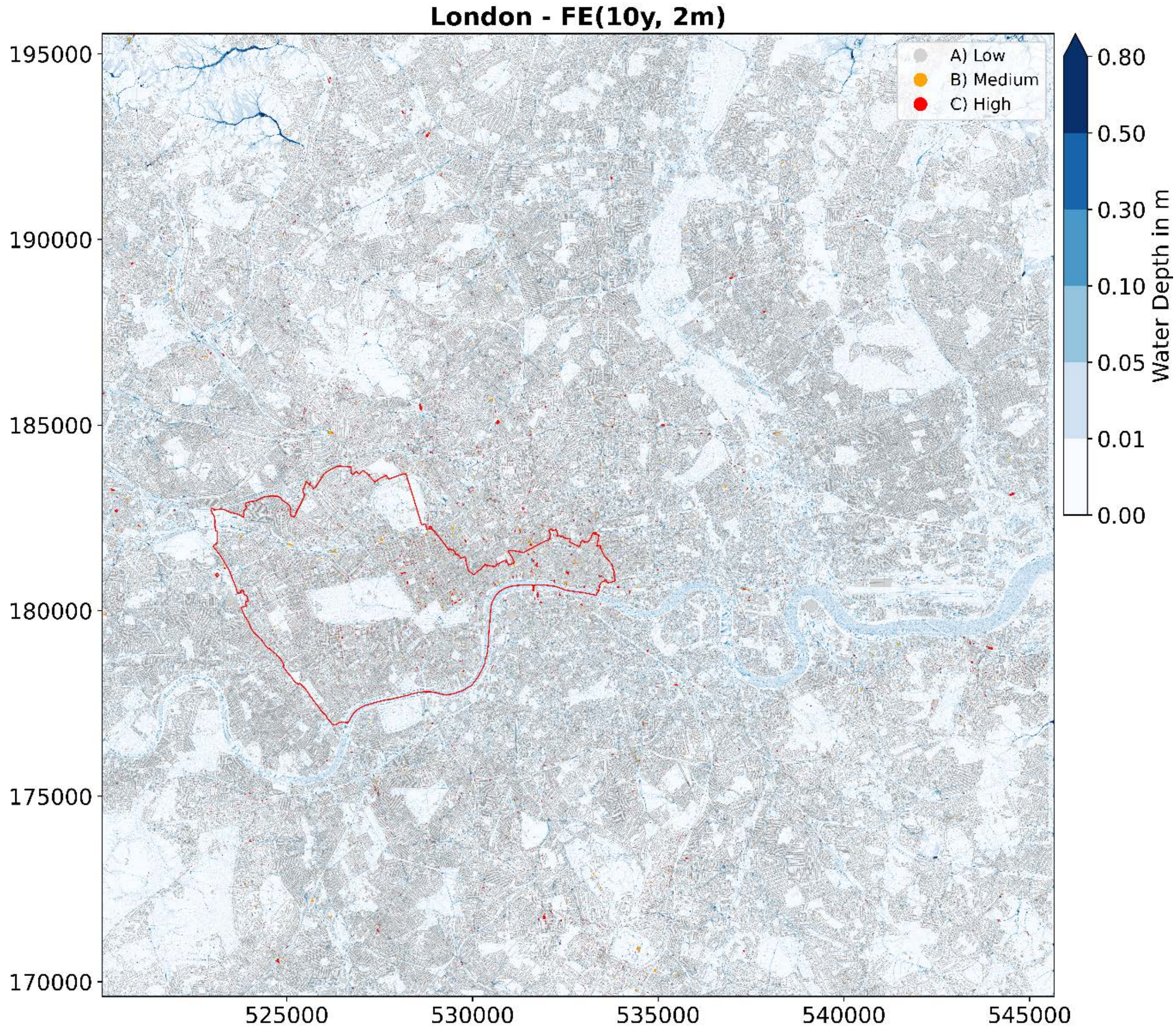
London - FE(10y, 2m)
A) Low
B) Medium
C) High
Water Depth in m
0.80
0.50
0.30
0.10
0.05
0.01
0.00
195000
190000
185000
180000
175000
170000
525000
530000
535000
540000
545000

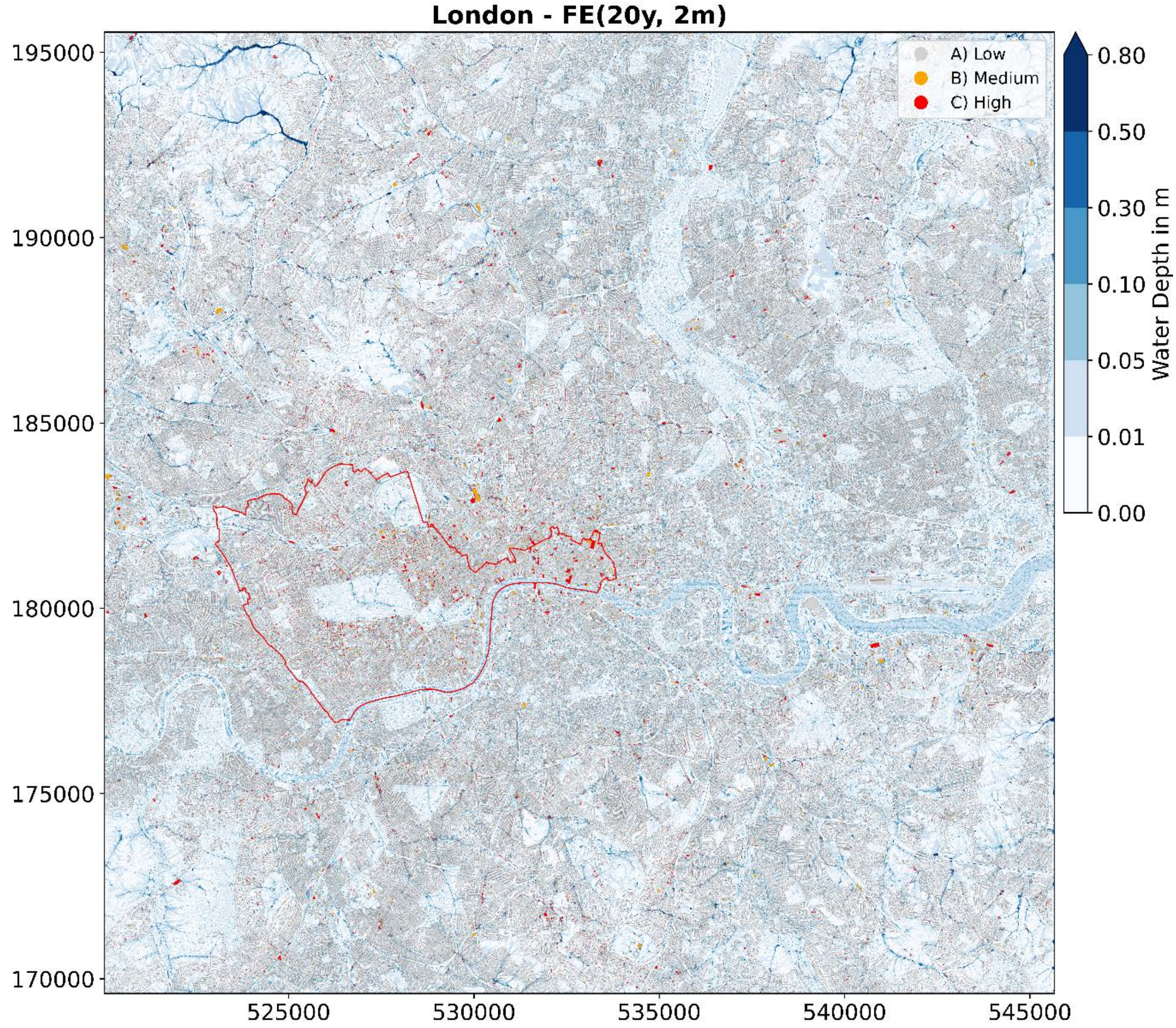
London - FE(20y, 2m)
A) Low
B) Medium
C) High
Water Depth in m
0.80
0.50
0.30
0.10
0.05
0.01
0.00
195000
190000
185000
180000
175000
170000
525000
530000
535000
540000
545000

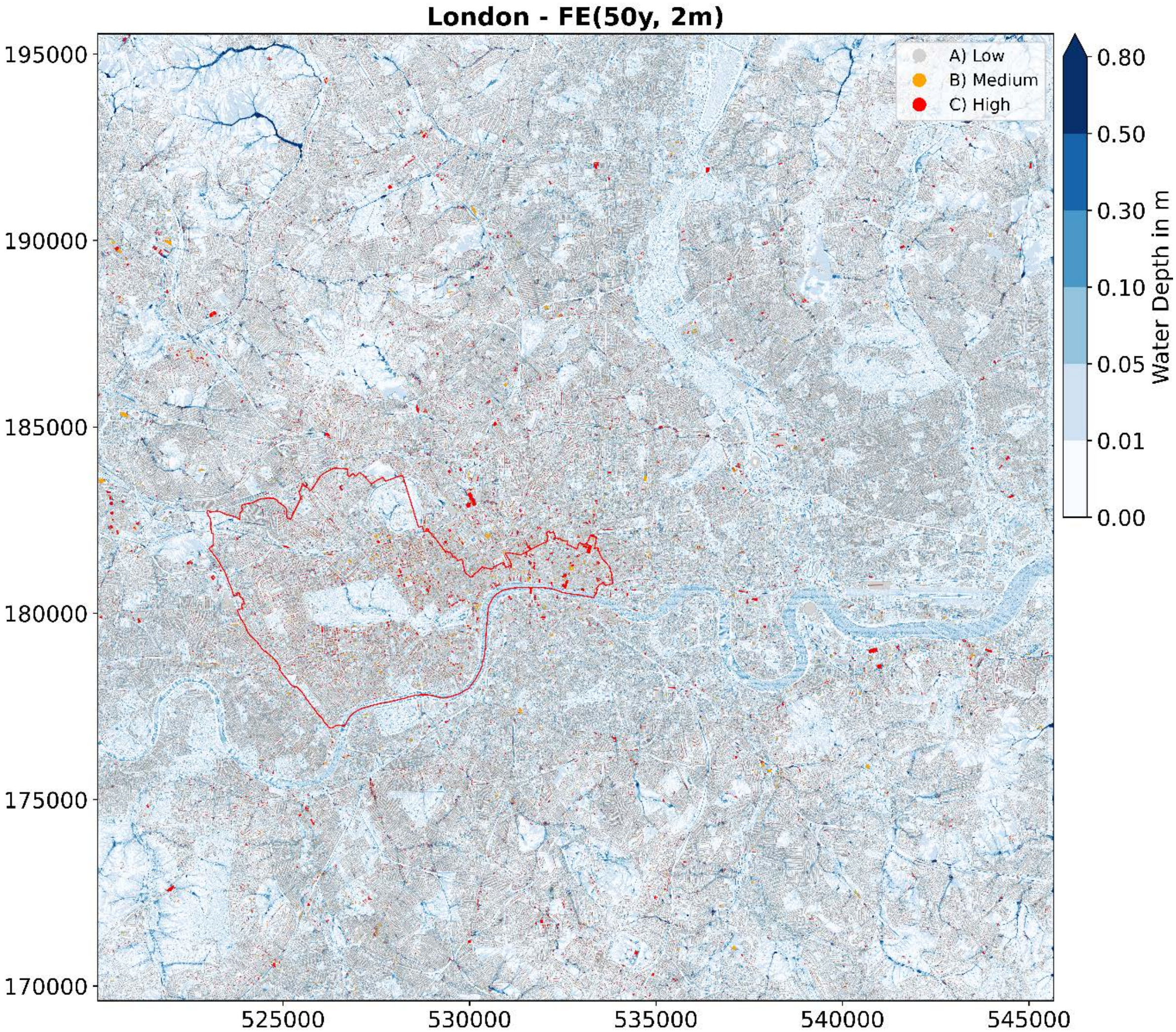
London - FE(50y, 2m)
195000
190000
185000
180000
175000
170000
525000
530000
535000
540000
545000
A) Low
B) Medium
C) High
0.80
0.50
0.30
0.10
0.05
0.01
0.00
Water Depth in m

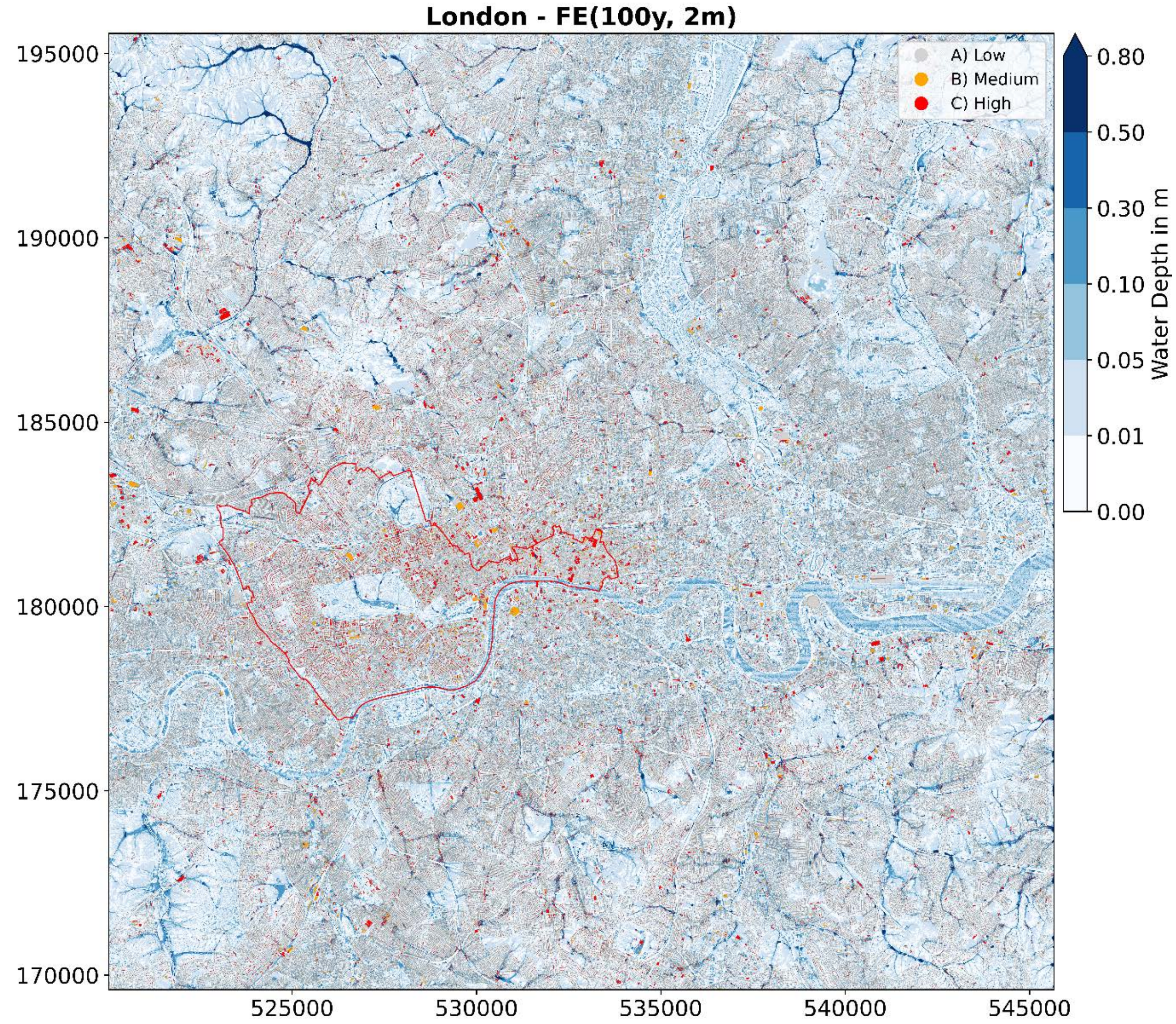
London - FE(100y, 2m)
A) Low
B) Medium
C) High
Water Depth in m
0.80
0.50
0.30
0.10
0.05
0.01
0.00
195000
190000
185000
180000
175000
170000
525000
530000
535000
540000
545000